

INFORMATION TO USERS

This manuscript has been reproduced from the microfilm master. UMI films the text directly from the original or copy submitted. Thus, some thesis and dissertation copies are in typewriter face, while others may be from any type of computer printer.

The quality of this reproduction is dependent upon the quality of the copy submitted. Broken or indistinct print, colored or poor quality illustrations and photographs, print bleedthrough, substandard margins, and improper alignment can adversely affect reproduction.

In the unlikely event that the author did not send UMI a complete manuscript and there are missing pages, these will be noted. Also, if unauthorized copyright material had to be removed, a note will indicate the deletion.

Oversize materials (e.g., maps, drawings, charts) are reproduced by sectioning the original, beginning at the upper left-hand corner and continuing from left to right in equal sections with small overlaps.

ProQuest Information and Learning
300 North Zeeb Road, Ann Arbor, MI 48106-1346 USA
800-521-0600

UMI[®]

**METAL SPECIATION IN NATURAL WATER: EVALUATING
KINETICS VERSUS EQUILIBRIUM**

by

Ismail Al-Fasfous

M.Sc. (University of Jordan)

A thesis submitted to the Faculty of Graduate Studies and Research

in partial fulfillment of the requirements for the degree of

Doctor of Philosophy

Department of Chemistry

Carleton University

Ottawa, Ontario

April 2005

Copyright © 2005

Ismail I. Al-Fasfous



Library and
Archives Canada

Bibliothèque et
Archives Canada

0-494-06730-6

Published Heritage
Branch

Direction du
Patrimoine de l'édition

395 Wellington Street
Ottawa ON K1A 0N4
Canada

395, rue Wellington
Ottawa ON K1A 0N4
Canada

NOTICE:

The author has granted a non-exclusive license allowing Library and Archives Canada to reproduce, publish, archive, preserve, conserve, communicate to the public by telecommunication or on the Internet, loan, distribute and sell theses worldwide, for commercial or non-commercial purposes, in microform, paper, electronic and/or any other formats.

The author retains copyright ownership and moral rights in this thesis. Neither the thesis nor substantial extracts from it may be printed or otherwise reproduced without the author's permission.

AVIS:

L'auteur a accordé une licence non exclusive permettant à la Bibliothèque et Archives Canada de reproduire, publier, archiver, sauvegarder, conserver, transmettre au public par télécommunication ou par l'Internet, prêter, distribuer et vendre des thèses partout dans le monde, à des fins commerciales ou autres, sur support microforme, papier, électronique et/ou autres formats.

L'auteur conserve la propriété du droit d'auteur et des droits moraux qui protègent cette thèse. Ni la thèse ni des extraits substantiels de celle-ci ne doivent être imprimés ou autrement reproduits sans son autorisation.

In compliance with the Canadian Privacy Act some supporting forms may have been removed from this thesis.

Conformément à la loi canadienne sur la protection de la vie privée, quelques formulaires secondaires ont été enlevés de cette thèse.

While these forms may be included in the document page count, their removal does not represent any loss of content from the thesis.

Bien que ces formulaires aient inclus dans la pagination, il n'y aura aucun contenu manquant.


Canada

Dedicated to Ebaa and Zeina

Abstract

Trace metals are essential micronutrients at low concentrations, but they may become toxic at elevated concentrations. Bioavailability of trace metals in freshwaters is known to be often correlated with free ion activity. The free metal ion activity is dependent on the dissociation of metal complexes of dissolved organic matter (DOC) in freshwaters. The objective of this research was to investigate trace metal competition in freshwaters and in model solutions of well-characterized fulvic and humic acids. Dissociation kinetics of metal-DOC complexes were investigated using Competing Ligand Exchange Method/Adsorptive Cathodic Stripping Voltammetry and Competing Ligand Exchange Method/Inductively Coupled Plasma-Mass Spectrometry. Three factors were found to influence the kinetics of trace metal competition in the freshwater environment: 1) metal-to-ligand mole ratio, 2) ionic potential (z^2/r), and 3) Ligand Field Stabilization Energy. The results show the importance of considering the valence-shell electron configuration in studying the kinetics of trace metal competition in the freshwater environment. The markedly slow dissociation kinetics of Ni(II)- and Cu(II)-complexes suggest that the usual equilibrium assumption for freshwater may not be valid. Exposure of the DOC in freshwaters to UV-B radiation of sunlight for 0, 10, 20, and 30 days resulted in photodegradation of the DOC, releasing the DOC-bound metals. The measured labile metal-complexes concentrations were compared with the predictions made by the applying widely-used computer speciation model, the Windermere Humic Aqueous Model (WHAM) and its improved version WHAM VI. For lake water samples studied, both versions of WHAM provided concentrations of free metal ions: Co^{2+} , Ni^{2+} , Zn^{2+} , and Cd^{2+} , which were in reasonably-close agreement (within one order of magnitude)

with the experimentally measured concentrations of labile metal complexes. The effect of metal competition on the stability constants of metal complexes, was investigated using an equilibrium approach. The heterogeneity of humic substances (humic acid and fulvic acid) in their metal complexation in model solutions, was investigated by using pseudopolarography, resulting in the determination of Differential Equilibrium Functions and Differential Kinetic Functions, which accounted for the heterogeneity of humic substances on the thermodynamic stability and kinetic lability of metal complexes.

Acknowledgements

First and foremost, I would like to thank my supervisor Professor C.L. Chakrabarti (“Chak”) for his supervision. I also wish to thank Dr. D.C. Grégoire and Dr. M.H. Back for their help, advice and expertise.

I would like also to thank Professor Ewa Dabek in Environment Canada, Ottawa, (Canada) for providing the use of an inductively-coupled plasma mass spectrometer.

I am especially grateful to Dr. John Murimboh for his invaluable discussion. I should also like to thank the following other members of Chak’s research group: Catherine Burroughs, Jeff Guthrie, Andrew Jian Fu Deng, Nouri Hassan, Min Yang, Mohamed Salam, Parthasarathi Chakraborty, Rong (Joya) Wang, and Tahir Yapici.

Last but not least, I wish to express my gratitude to my family and friends; in particular, to my parents and my wife for their unconditional love and devotion.

Financial support for a Postgraduate Scholarship for the Ph.D. program from The Hashemite University is gratefully acknowledged.

Table of Contents

Abstract		i
Acknowledgments		iii
List of Figures		ix
List of Tables		xviii
Chapter 1	Introduction	1
1.1	Introduction	2
1.2	Natural Organic Matter (NOM) and Humic Substances.....	4
1.2.1	<i>Metal complexation by humic Substances in freshwaters.....</i>	6
1.2.2	<i>Metal competition.....</i>	10
1.3	Solar Radiation and Metal Speciation.....	10
1.4	Speciation Techniques of Metals in Freshwaters.....	11
1.5	Objectives.....	12
1.6	Outline of the Organization of the Thesis.....	14
Chapter 2	Scientific Background	16
2.1	Current State of Knowledge.....	17
2.2	Scientific Background.....	19
2.2.1	<i>Kinetics of metal complexes in the bulk solution</i>	19
2.2.2	<i>Coupled diffusion of M and ML in the diffusion layer</i>	22
2.2.3	<i>The Differential Equilibrium Function.....</i>	25
2.2.4	<i>The Differential Kinetic Function.....</i>	27
2.3	Speciation Parameters.....	28
2.4	Hypothesis.....	29
2.5	Testing of the Hypothesis.....	30
Chapter 3	Kinetic Studies of Copper Speciation in Model Solutions of a Well-Characterized Humic Acid using Adsorptive Cathodic Stripping Voltammetry	32
3.1	Introduction.....	33
3.2	Theory.....	35
3.2.1	<i>Kinetic Model.....</i>	35
3.2.2	<i>Adsorptive Cathodic Stripping Voltammetry (AdCSV) of Cu(Ox)₂ Complex</i>	37
3.3	Experimental.....	39
3.3.1	<i>Materials and reagents</i>	39
3.3.2	<i>Humic acid model solutions.....</i>	40
3.3.3	<i>Containers and their cleaning procedure.....</i>	41
3.3.4	<i>Method optimization</i>	41
3.3.5	<i>Apparatus.....</i>	48
3.3.6	<i>Kinetic experiments.....</i>	50

3.3.7	<i>Data analysis</i>	50
3.4	Results and Discussion.....	51
3.4.1	<i>Effect of the [Cu(II)]/[HA] mole ratio on the dissociation rate coefficient of Cu(II)-HA complexes</i>	52
3.4.2	<i>The effect of pH on the dissociation rate coefficient of Cu(II)-HA complexes</i>	56
3.4.3	<i>Competitive binding of Ca(II), Mg(II) and Cu(II) by a well characterized HA</i>	59
3.5	Originality.....	68
Chapter 4	Kinetic Speciation of Nickel in Atmospheric Precipitation using Adsorptive Cathodic Stripping Voltammetry	69
4.1	Introduction	70
4.2	Theory.....	71
4.3	Experimental.....	72
4.3.1	<i>Materials and reagents</i>	72
4.3.2	<i>Containers and their cleaning procedure</i>	73
4.3.3	<i>Method optimization</i>	73
4.3.4	<i>Sampling sites and sampling protocol</i>	81
4.3.5	<i>Kinetic experiments</i>	84
4.3.6	<i>Apparatus</i>	84
4.3.7	<i>Data analysis</i>	84
4.4	Results and Discussion.....	84
Chapter 5	Kinetics of Trace Metal Competition in Freshwaters: Some Fundamental Chemical Characteristics	89
5.1	Introduction.....	90
5.2	The Kinetic Model.....	91
5.2.1	<i>Competing Ligand Exchange Method</i>	91
5.3	Experimental	93
5.3.1	<i>Materials and reagents</i>	93
5.3.2	<i>Containers and their Cleaning procedure</i>	93
5.3.3	<i>Model solutions and freshwater samples</i>	94
5.3.4	<i>Kinetic experiments and data analysis</i>	94
5.4	Results and Discussion.....	97
5.4.1	<i>Metal-to-Ligand Mole Ratio</i>	104
5.4.2	<i>Ligand Field Stabilization Energy</i>	110
5.4.3	<i>Ionic Potential</i>	116
5.5	Conclusion.....	127
Chapter 6	Influence of Solar Radiation on the Lability of Metal Complexes in Freshwaters	129
6.1	Introduction.....	130
6.2	The Kinetic Model	132
6.3	Experimental	132
6.3.1	<i>Materials and reagents</i>	132
6.3.2	<i>Containers and their cleaning procedure</i>	132
6.3.3	<i>Freshwater samples</i>	132
6.3.4	<i>Studies on solar irradiation of water samples</i>	133

6.3.5	<i>Kinetic experiments and data analysis</i>	133
6.4	Results and Discussion.....	134
6.4.1	<i>Chemical speciation</i>	134
6.4.2	<i>Influence of solar radiation</i>	137
6.5	Conclusions.....	148
Chapter 7	Kinetic Speciation of Ni, Cu and Pb in Lake Surface Waters. Comparison of Labile Metal Concentrations Obtained by Competing Ligand Exchange Method/Adsorptive Cathodic Stripping Voltammetry with those Predicted by a Computer Speciation Code, Windermere Humic Aqueous Model (WHAM), V and VI, for Free Metal Ion Concentrations	150
7.1	Introduction.....	151
7.2	Theory.....	153
7.3	Experimental.....	153
7.3.1	<i>Materials and reagents</i>	153
7.3.2	<i>Containers and their cleaning procedure</i>	155
7.3.3	<i>Method optimization</i>	156
7.3.4	<i>Sampling sites and sampling protocol</i>	162
7.3.5	<i>Apparatus</i>	165
7.3.6	<i>Kinetic experiments</i>	165
7.3.7	<i>Data analysis</i>	167
7.4	Results and Discussion.....	167
7.4.1	<i>Nickel speciation in freshwater samples collected form Rouyn Noranda, Québec in August 2002</i>	167
7.4.2	<i>Copper speciation in lake-water samples collected form Rouyn Noranda, Québec in July 2002 and August 2002</i>	171
7.4.3	<i>Lead speciation in lake-water samples collected form Rouyn Noranda, Québec in July 2002 and August 2002</i>	174
7.4.4	<i>A comparison of results of kinetic speciation method with those of the computer speciation code: WHAM V and VI</i>	177
7.5	Conclusions.....	187
Chapter 8	Kinetic Speciation of Trace Metals in Some Metal-Impacted Freshwater Lakes: a Comparison of Results of Distribution Analysis Method with those of a Non-linear Regression Method. Comparison of above results with the predictions of WHAM V and VI	189
8.1	Introduction.....	190
8.2	The Kinetic Model	192
8.3	Experimental.....	192
8.3.1	<i>Materials and reagents</i>	192
8.3.2	<i>Containers and their cleaning procedure</i>	193
8.3.3	<i>Freshwater samples</i>	193
8.3.4	<i>Kinetic experiments</i>	194
8.3.5	<i>Data analysis</i>	197
8.4	Results and Discussion.....	200
8.4.1	<i>Metal-To-Ligand Mole Ratio</i>	201
8.4.2	<i>Ligand Field Stabilization Energy</i>	202
8.4.3	<i>Ionic Potential</i>	203

8.4.4	WHAM modelling.....	204
8.5	Conclusion.....	239
Chapter 9	Heterogeneity of Humic Substances. Differential Equilibrium Functions of Pb(II)-Complexes in Model Solutions of a Well-Characterized Humic Acid Determined by Pseudopolarography using a Static Mercury Drop Electrode	243
9.1	Introduction.....	244
9.2	Theory.....	245
9.2.1	<i>Pseudopolarography.....</i>	245
9.2.2	<i>Differential Equilibrium Function.....</i>	248
9.2.3	<i>Diffusion coefficients.....</i>	249
9.3	Experimental.....	249
9.3.1	<i>Materials and reagents..</i>	249
9.3.2	<i>Containers and their cleaning procedure.....</i>	250
9.3.3	<i>Model solutions and pseudopolarography.....</i>	251
9.3.4	<i>Apparatus.....</i>	252
9.3.5	<i>Electrochemical parameters</i>	252
9.3.6	<i>Data analysis</i>	252
9.4	Results and Discussion	253
9.4.1	<i>The effect of [Pb(II)]/[HA] mole ratio on the Differential Equilibrium Function of Pb(II)-HA complexes.....</i>	257
9.4.2	<i>Kinetic lability of Pb(II)-HA complexes.....</i>	261
9.4.3	<i>Effect of various concentrations of other trace metals, Cu(II), Ni(II) and Zn(II), on the heterogeneity of Pb(II)-HA complexes....</i>	266
9.4.4	<i>Diffusion coefficients.....</i>	271
9.5	Conclusion.....	271
Chapter 10	Differential Equilibrium Functions and Differential Kinetic Functions of Heterogeneous Systems. Pseudopolarography of Cu(II), Zn(II), Cd(II) and Pb(II) complexes in Model Solutions of a Well-Characterized Fulvic Acid using a Static Mercury Drop Electrode: Kinetics versus Equilibrium	273
10.1	Theory	274
10.1.1	<i>Differential Equilibrium Function.....</i>	274
10.1.2	<i>Kinetic Differential Function.....</i>	274
10.3	Experimental.....	274
10.3.1	<i>Materials and reagents.....</i>	274
10.3.2	<i>Fulvic acid model solutions</i>	275
10.3.3	<i>Apparatus.....</i>	275
10.3.4	<i>Electrochemical parameters.....</i>	276
10.3.5	<i>Data analysis</i>	276
10.4	Results and Discussion.....	276
10.4.1	<i>Influence of metal loading on the Differential Equilibrium Functions (DEF).....</i>	277
10.4.2	<i>Ionic Potential.....</i>	282
10.4.3	<i>Differential Kinetic Functions.....</i>	285
10.4.3	<i>Linear Free Energy Relationship.....</i>	286
10.5	Conclusion.....	289

References	292
Glossary	310

List of Figures

Figure 1	Schematic representation of the reaction of a metal ion with different types of aquatic components [2].....	3
Figure 2	The structure of bis(8-hydroxyquinolinato)copper(II) used in CLEM/AdCSV [49].....	38
Figure 3	Effect of variation of the deposition time on the AdCSV/SWV peak-height current obtained (i_p , μA) in a model solution containing Cu(II) 7.9×10^{-8} M, Oxine 1×10^{-5} M, 0.01M HEPES, pH 7.5 ± 0.1 , ionic strength 1.5×10^{-2} M, temperature 23 ± 2 °C.	43
Figure 4	Effect of variation of the deposition potential on the AdCSV/SWV peak-height current obtained (i_p , μA) in a model solution containing Cu(II) 7.9×10^{-8} M, Oxine 1×10^{-5} M, 0.01M HEPES, pH 7.5 ± 0.1 , ionic strength 1.5×10^{-2} M, temperature 23 ± 2 °C.	44
Figure 5	Effect of SWV-frequency A) on the AdCSV/SWV peak-height current (i_p , μA); B) on the potential of peak (E_p , V) obtained in a model solution containing Cu(II) 7.9×10^{-8} M, Oxine 1×10^{-5} M, 0.01 M HEPES, pH 7.5 ± 0.1 , ionic strength 1.5×10^{-2} M, temperature 23 ± 2 °C.....	46
Figure 6	Effect of variation in the oxine concentration A) on the AdCSV/SWV peak-height current (i_p , μA); B) on the potential of peak (E_p , V) obtained in a model solution containing Cu(II) 7.9×10^{-8} M, Oxine 1×10^{-5} M, 0.01 M HEPES, pH 7.5 ± 0.1 , ionic strength 1.5×10^{-2} M, temperature 23 ± 2 °C.....	47
Figure 7	Effect of variation in pH A) on the AdCSV/SWV peak-height current (i_p , μA); B) on the potential of peak (E_p , V) obtained in a model solution containing Cu(II) 7.9×10^{-8} M, Oxine 1×10^{-5} M, 0.01 M HEPES, pH 7.5 ± 0.1 , ionic strength 1.5×10^{-2} M, temperature 23 ± 2 °C	49
Figure 8	Lability (i_p/i_o) of Cu(II)-HA complexes for three [Cu(II)]/[HA] mole ratios in model solutions at pH 8.0 ± 0.1 , studied by CLEM/AdCSV, using Oxine as the competing ligand.....	53
Figure 9	Lability (i_p/i_o) of Cu(II)-HA complexes for three [Cu(II)]/[HA] mole ratios in model solutions at pH 7.0 ± 0.1 , studied by CLEM/AdCSV, using Oxine as the competing ligand.....	57
Figure 10	Lability (i_p/i_o) of Cu(II)-HA complexes for three [Cu(II)]/[HA] mole ratios in model solutions at pH 6.0 ± 0.1 , studied by CLEM/AdCSV, using Oxine as the competing ligand.	58
Figure 11	Effect of various concentrations of Ca(II) on the lability (i_p/i_o) of Cu(II)-HA complexes in model solutions, determined by CLEM/AdCSV,	

	using Oxine as the competing ligand.....	60
Figure 12	Effect of various concentrations of Mg(II) on the liability (i_p/i_o) of Cu(II)-HA complexes in model solutions, determined by CLEM/AdCSV, using Oxine as the competing ligand.....	63
Figure 13	Effect of various concentrations of Mg(II) plus Ca(II) on the liability (i_p/i_o) of Cu(II)-HA complexes in model solutions, determined by CLEM/AdCSV, using Oxine as the competing ligand.....	66
Figure 14	The structure of bis(dimethylglyoximate)nickel(II) used in CLEM/AdCSV [148].....	75
Figure 15	Effect of variation of the deposition time on the AdCSV/SWV peak-height current (i_p , μA) obtained in a model solution containing Ni(II) 2.9×10^{-8} M, 0.02M HEPES, DMG 1×10^{-3} M, pH 7.5 ± 0.1 , ionic strength 2.0×10^{-2} M, temperature 23 ± 2 °C	76
Figure 16	Effect of variation of the deposition potential on the AdCSV/SWV peak-height current (i_p , μA) obtained in a model solution containing Ni(II) 7.5×10^{-7} M, 0.02M HEPES, DMG 1×10^{-3} M, pH 7.5 ± 0.1 , ionic strength 2.0×10^{-2} M, temperature 23 ± 2 °C	77
Figure 17	Effect of SWV-frequency (Hz) on the AdCSV/SWV peak- height current (i_p , μA) obtained in a model solution water containing Ni(II) 2.9×10^{-8} M, 0.02M HEPES, DMG 1×10^{-3} M, pH 7.5 ± 0.1 , ionic strength 2.0×10^{-2} M, temperature 23 ± 2 °C	79
Figure 18	Effect of variation in the DMG concentration on the AdCSV/SWV peak-height current (i_p , μA) obtained in a model solution containing Ni(II) 2.9×10^{-8} M, 0.02M HEPES, pH 7.5 ± 0.1 , ionic strength 2.0×10^{-2} M, temperature 23 ± 2 °C.....	80
Figure 19	Location of the sites for soil solutions (pore water) and through-fall precipitation samples collected from Sudbury Mining Area, Copper Cliff, Ontario.....	82
Figure 20	Liability (i_p/i_o) of Ni(II)-DOC complexes in soil solution (pore water) samples collected from Sudbury in May 2002 and June 2002, determined by CLEM/AdCSV, using DMG as the competing ligand ..	86
Figure 21	Map of the sampling area of the Grand River, Ontario. The star shows the location of the sampling site.....	95
Figure 22	Teflon reactor used in the CLEM/ICP-MS study.....	98
Figure 23	Dissociation kinetics of Zn(II)- and Cu(II)-FA complexes in a model solution of Laurentian fulvic acid, measured by ICP-MS, using Chelex 100 as the competing ligand.	100
Figure 24	Kinetic spectrum of lifetimes ($\tau \sim 1/k_d$) of Zn(II)- and Cu(II)-FA	

	complexes in a model solution of Laurentian fulvic acid, measured by ICP-MS, using Chelex 100 as the competing ligand.....	101
Figure 25	Influence of the metal-to-ligand ratio on the dissociation kinetics of Cd(II)-FA complexes in model solutions of Laurentian fulvic acid, measured by ICP-MS, using Chelex 100 as the competing ligand.....	107
Figure 26	Influence of the metal-to-ligand ratio on the mean dissociation rate constant of the slowest kinetically distinguishable component, $k_{d,slow}$ of Cd(II)-FA complexes in model solutions of Laurentian fulvic acid, measured by ICP-MS, using Chelex 100 as the competing ligand.....	108
Figure 27	Influence of the d-electron configuration on the dissociation kinetics of metal complexes in model solutions of Laurentian fulvic acid, measured by ICP-MS.	111
Figure 28	Influence of the d-electron configuration on the mean dissociation rate constant of the slowest kinetically distinguishable component $k_{d,slow}$ of metal complexes in model solutions of Laurentian fulvic acid, measured by ICP-MS.	115
Figure 29	Influence of the d-electron configuration in a freshwater sample collected from the Grand River on June 23, 2002 on dissociation kinetics of metal complexes, measured by ICP-MS using Chelex 100 as the competing ligand.....	117
Figure 30	Influence of the d-electron configuration in a freshwater sample collected from the Grand River on June 23, 2002, on mean dissociation rate coefficient of the slowest kinetically distinguishable component, $k_{d,slow}$ of metal complexes, measured by ICP-MS, using Chelex 100 as the competing ligand.....	118
Figure 31	Influence of the ionic potential (z^2/r) on the dissociation kinetics of metal complexes in model solutions of Laurentian fulvic acid, measured by ICP-MS, using Chelex 100 as the competing ligand.	121
Figure 32	Influence of the ionic potential (z^2/r) on mean dissociation rate constant of the slowest kinetically distinguishable component, $k_{d,slow}$ of metal complexes in model solutions of Laurentian fulvic acid, measured by ICP-MS, using Chelex 100 as the competing ligand.....	122
Figure 33	Influence of the ionic potential (z^2/r) on the dissociation kinetics of metal complexes in a freshwater sample collected from the Grand River on June 23, 2002, measured by ICP-MS, using Chelex 100 as the competing ligand.	124
Figure 34	Influence of the ionic potential (z^2/r) on the mean dissociation rate constant of the slowest kinetically distinguishable component, $k_{d,slow}$ of metal complexes in a freshwater sample collected from the Grand River on June 23, 2002, measured by ICP-MS, using Chelex 100 as the competing ligand.	125

Figure 35	Changes in the concentration of DOC as the function of the duration of the exposure to sunlight for the Grand River surface water sample.....	139
Figure 36	The influence of solar radiation on the lability of Cu(II)-DOC complexes in a freshwater sample collected from Grand River on June 23, 2002, determined by CLEM/ ICP-MS, using Chelex 100 as the competing ligand.	140
Figure 37	IC50 values at 95% confidence levels, determined from bioassays using Grand River water samples, which were spiked with Cu and exposed to solar radiation for 0, 10, and 30 days [184].....	141
Figure 38	The influence of solar radiation on the lability of Zn(II)-DOC complexes in a freshwater sample collected from Grand River on June 23, 2002, determined by CLEM/ ICP-MS, using Chelex 100 as the competing ligand.....	143
Figure 39	The influence of solar radiation on the lability of Pb(II)-DOC complexes in a freshwater sample collected from Grand River on June 23, 2002, determined by CLEM/ ICP-MS, using Chelex 100 as the competing ligand.	144
Figure 40	The influence of solar radiation on the lability of Ni(II)-DOC complexes in a freshwater sample collected from Grand River on June 23, 2002, determined by CLEM/ ICP-MS, using Chelex 100 as the competing ligand.	145
Figure 41	The influence of solar radiation on the lability of Cd(II)-DOC complexes in a freshwater sample collected from Grand River on June 23, 2002, determined by CLEM/ ICP-MS, using Chelex 100 as the competing ligand.	146
Figure 42	The influence of solar radiation on the lability of Co(II)-DOC complexes in a freshwater sample collected from Grand River on June 23, 2002, determined by CLEM/ ICP-MS, using Chelex 100 as the competing ligand.	147
Figure 43	The structure of bis(8-hydroxyquinolino)lead(II) used in CLEM/AdCSV.....	154
Figure 44	Effect of variation of the deposition time on the AdCSV/SWV peak-height current obtained (i_p , nA) in a model solution containing Pb(II) 4.8×10^{-9} M, oxine 1×10^{-6} M, 0.01M HEPES, pH 7.5 ± 0.1 , ionic strength 1×10^{-2} M, temperature 23 ± 2 °C.....	157
Figure 45	Effect of variation of the deposition potential on the AdCSV/SWV peak-height current obtained (i_p , μ A) in a model solution containing Pb(II) 4.8×10^{-9} M, oxine 1×10^{-6} M, 0.01M HEPES, pH 7.5 ± 0.1 , ionic strength 2×10^{-2} M, temperature 23 ± 2 °C.....	158

Figure 46	Effect of SWV-frequency on the AdCSV/SWV peak-height current (i_p , nA) obtained in a model solution containing Pb(II) 4.8×10^{-9} M, oxine 1×10^{-6} M, 0.01 M HEPES, pH 7.5 ± 0.1 , ionic strength 1×10^{-2} M, temperature 23 ± 2 °C.....	160
Figure 47	Effect of variation in the oxine concentration on the AdCSV/SWV peak-height current (i_p , nA) obtained in a model solutions containing Pb(II) 4.8×10^{-9} M, oxine 1×10^{-6} M, 0.01 M HEPES, pH 7.5 ± 0.1 , ionic strength 1×10^{-2} M, temperature 23 ± 2 °C.	161
Figure 48	Map of the sampling area of Rouyn-Noranda, Québec, and the lakes studied. The filled circle is the location of the smelter. Adapted from J.C. Brodeur [198].....	163
Figure 49	Lability (i_p/i_o) of Ni(II)-DOC complexes in complexes in freshwater samples collected from Rouyn-Noranda, Québec, in August 2002, determined by CLEM/AdCSV, using DMG as the competing ligand.....	168
Figure 50	... Lability (i_p/i_o) of Cu(II)-DOC complexes in complexes in lake-water samples collected from Rouyn-Noranda, Québec, in July 2002 and August 2002, determined by CLEM/AdCSV, using Oxine as the competing ligand.....	172
Figure 51	Lability (i_p/i_o) of Pb(II)-DOC complexes in complexes in lake-water samples collected from Rouyn-Noranda, Québec, in July 2002 and August 2002, determined by CLEM/AdCSV, using Oxine as the competing ligand	175
Figure 52	Comparison of WHAM predicted pNi with the measured concentrations of labile Ni(II)-complexes in lake-water samples collected from Rouyn-Noranda, Québec, in July 2002 and August 2002.....	182
Figure 53	Comparison of WHAM predicted pCu with the measured concentrations of labile Cu(II)-complexes in lake-water samples collected from Rouyn-Noranda, Québec, in July 2002 and August 2002.....	185
Figure 54	Comparison of WHAM predicted pPb with the measured concentrations of labile Pb(II)-complexes in lake-water samples collected from Rouyn-Noranda, Québec, in July 2002 and August 2002.	186
Figure 55	Example of an output file from distribution analysis method software [223].....	199
Figure 56	Dissociation kinetics of M(II)-DOC complexes in Lake Dufault water samples collected from the Rouyn-Noranda area, Québec, in June 2003, determined by CLEM/ICP-MS, using Chelex 100 as the	

	competing ligand. DOC = 15.7 ± 1.5 , pH 6.1 ± 0.1 , ionic strength 1.9×10^{-3} mol/L, temperature 23 ± 2 °C. (\diamond), Cu(II)-DOC; (\blacktriangledown), Ni(II)-DOC; (\square), Co(II)-DOC; (\bullet), Zn(II)-DOC complexes. Solid lines represent non-linear curve-fitting.....	205
Figure 57	Dissociation kinetics of M(II)-DOC complexes in Lake Osisko water samples collected from the Rouyn-Noranda area, Québec, in June 2003, determined by CLEM/ICP-MS, using Chelex 100 as the competing ligand. DOC = 6.0 ± 1.3 , pH 7.3 ± 0.1 , ionic strength 4.4×10^{-3} mol/L, temperature 23 ± 2 °C. (\diamond), Cu(II)-DOC; (\blacktriangledown), Ni(II)-DOC; (\square), Co(II)-DOC; (\bullet), Zn(II)-DOC complexes. Solid lines represent non-linear curve-fitting.....	206
Figure 58	Dissociation kinetics of M(II)-DOC complexes in Lake Opasatica water samples collected from the Rouyn-Noranda area, Québec, in June 2003, determined by CLEM/ICP-MS, using Chelex 100 as the competing ligand. DOC = 9.0 ± 0.4 , pH 6.9 ± 0.1 , ionic strength 1.5×10^{-3} mol/L, temperature 23 ± 2 °C. (\diamond), Cu(II)-DOC; (\blacktriangledown), Ni(II)-DOC; (\square), Co(II)-DOC; (\bullet), Zn(II)-DOC complexes. Solid lines represent non-linear curve-fitting.....	207
Figure 59	Dissociation kinetics of M(II)-DOC complexes in Lake Vaudray water samples collected from the Rouyn-Noranda area, Québec, in June 2003, determined by CLEM/ICP-MS, using Chelex 100 as the competing ligand. DOC = 11.0 ± 0.6 , pH 6.1 ± 0.1 , ionic strength 8.6×10^{-5} mol/L, temperature 23 ± 2 °C. (\diamond), Cu(II)-DOC; (\blacktriangledown), Ni(II)-DOC; (\square), Co(II)-DOC; (\bullet), Zn(II)-DOC complexes; complexes. Solid lines represent non-linear curve-fitting.....	208
Figure 60	Influence of the d-electron configuration on dissociation rate coefficient of the slowest kinetically distinguishable component, $k_{d,slow}$ in freshwater samples collected from the Rouyn-Noranda area, received on June 26, 2003, determined by CLEM/ICP-MS, using Chelex 100 as the competing ligand. (Tables 25-28).	209
Figure 61	Influence of the d-electron configuration on mean dissociation rate coefficient of the slowest kinetically distinguishable component, $k_{d,slow}$ in freshwater samples collected from the Rouyn-Noranda area, received on June 26, 2003, determined by CLEM/ICP-MS, using Chelex 100 as the competing ligand. (Tables 29-32).....	210
Figure 62	Dissociation kinetics of M(II)-DOC complexes in Lake Dufault water samples collected from the Rouyn-Noranda area, Québec, in June 2003, determined by CLEM/ICP-MS, using Chelex 100 as the competing ligand. DOC = 15.7 ± 2.9 , pH 6.1 ± 0.1 , ionic strength 1.9×10^{-3} mol/L, temperature 23 ± 2 °C. (\diamond), Pb(II)-DOC; (\bullet), Cd(II)-DOC; (\square), Zn(II)-DOC complexes. Solid lines represent non-linear curve-fitting.....	211
Figure 63	Dissociation kinetics of M(II)-DOC complexes in Lake Osisko water samples collected from the Rouyn-Noranda area, Québec, in June	

	2003, determined by CLEM/ICP-MS, using Chelex 100 as the competing ligand. DOC = 6.0 ± 1.3 ; pH 7.3 ± 0.1 ; ionic strength 4.4×10^{-3} mol/L, temperature 23 ± 2 °C. (\diamond), Pb(II)-DOC; (\square), Cd(II)-DOC; (\bullet), Zn(II)-DOC complexes. Solid lines respresent non-linear curve-fitting.....	212
Figure 64	Dissociation kinetics of M(II)-DOC complexes in Lake Opasatica water samples collected from the Rouyn-Noranda area, Québec, in June 2003, determined by CLEM/ICP-MS, using Chelex 100 as the competing ligand. DOC = 9.0 ± 0.4 , pH 6.9 ± 0.1 , ionic strength 1.5×10^{-3} mol/L, temperature 23 ± 2 °C. (\diamond), Pb(II)-DOC; (\bullet), Cd(II)-DOC; (\square), Zn(II)-DOC complexes. Solid lines respresent non-linear curve-fitting.....	213
Figure 65	Dissociation kinetics of M(II)-DOC complexes in Lake Vaudray water samples collected from the Rouyn-Noranda area, Québec, in June 2003, determined by CLEM/ICP-MS, using Chelex 100 as the competing ligand. DOC = 11.0 ± 0.6 , pH 6.1 ± 0.1 , ionic strength 8.6×10^{-3} mol/L, temperature 23 ± 2 °C. (\bullet), Cd(II)-DOC; (\diamond), Pb(II)-DOC; (\square) \blacktriangle , Zn(II)-DOC; (∇), Mn(II)-DOC complexes. Solid lines respresent non-linear curve-fitting.....	214
Figure 66	Influence of the ionic potential (z^2/r) on dissociation rate coefficient of the slowest kinetically distinguishable component, $k_{d,slow}$ in freshwater samples collected from the Rouyn-Noranda area, received on June 26, 2003, determined by CLEM/ICP-MS, using Chelex 100 as the competing ligand. (Tables 25-28).	223
Figure 67	Influence of the ionic potential (z^2/r) on mean dissociation rate coefficient of the slowest kinetically distinguishable component, $k_{d,slow}$ in freshwater samples collected from the Rouyn-Noranda area, received on June 26, 2003, determined by CLEM/ICP-MS, using Chelex 100 as the competing ligand. (Tables 22-32):	224
Figure 68	Comparison of the pNi predicted by WHAM V and WHAM VI, with the measured concentrations of labile Ni(II)-complexes in lake-water samples collected from the Rouyn-Noranda area, Québec, (received on June 26, 2003). (---) 1:1 line, (o) WHAM V predictions, (\square) WHAM VI predictions.	227
Figure 69	Comparison of the pCo predicted by WHAM V and WHAM VI, with the measured concentrations of labile Co(II)-complexes in lake-water samples collected from the Rouyn-Noranda area, Québec, (received on June 26, 2003). (---) 1:1 line, (o) WHAM V predictions, (\square) WHAM VI predictions.	231
Figure 70	Comparison of the pCu predicted by WHAM V and WHAM VI, with the measured concentrations of labile Cu(II)-complexes in lake-water samples collected from the Rouyn-Noranda area, Québec, (received on June 26, 2003). (---) 1:1 line, (o) WHAM V predictions, (\square) WHAM VI predictions.	233

Figure 71	Comparison of the pZn predicted by WHAM V and WHAM VI, with the measured concentrations of labile Zn(II)-complexes in lake-water samples collected from the Rouyn-Noranda area, Québec, (received on June 26, 2003). (---) 1:1 line, (o) WHAM V predictions, (□) WHAM VI predictions.	234
Figure 72	Comparison of the pCd predicted by WHAM V and WHAM VI, with the measured concentrations of labile Cd(II)-complexes in lake-water samples collected from the Rouyn-Noranda area, Québec, (received on June 26, 2003). (---) 1:1 line, (o) WHAM V predictions, (□) WHAM VI predictions.	236
Figure 73	Comparison of the pPb predicted by WHAM V and WHAM VI, with the measured concentrations of labile Pb(II)-complexes in lake-water samples collected from the Rouyn-Noranda area, Québec, (received on June 26, 2003). (---) 1:1 line, (o) WHAM V predictions, (□) WHAM VI predictions.	237
Figure 74	Simulated polarographic curves for the reduction of M a) under non-complexing conditions, b) in the presence of a simple, homogeneous ligand (equation 9.1), $\Gamma = 1$; c) in the presence of a heterogeneous complexant (equation 9.2), $\Gamma = 0.3$. [239].....	247
Figure 75	Typical pseudopolarogram for Pb(II)-HA in model solutions of humic acid.	255
Figure 76	Differential Equilibrium Function of Pb(II)-HA complex.	260
Figure 77	Numerical simulations on the influence of lability (i/i_{lim}) on the shape of the polarographic wave [84].....	262
Figure 78	Influence of the stirring rate (timescale of measurement) on the lability (i/i_{lim}) of the Pb(II)-HA complexes.	263
Figure 79	Effect of various concentrations of Cu(II) on the pseudopolarographic waves of Pb(II)-HA complexes in model solutions, using DPASV at a SMDE.....	267
Figure 80	Pseudopolarogram for Cu(II)-FA in model solutions of Laurentian fulvic acid.....	278
Figure 81	Pseudopolarogram for Zn(II)-FA in model solutions of Laurentian fulvic acid	279
Figure 82	Pseudopolarogram for Cd(II)-FA in model solutions of Laurentian fulvic acid	280
Figure 83	Pseudopolarogram for Pb(II)-FA in model solutions of Laurentian fulvic acid	281

Figure 84	Influence of the ionic potential (z^2/r) on the Differential Equilibrium Parameter, K^* , of metal (Pb(II), Zn(II), Cd(II)) complexes in model solutions of Laurentian fulvic acid, measured by pseudopolarography.....	284
Figure 85	Linear free energy relationship between the dissociation rate coefficient (k_d) of Zn(II), Cd(II), and Pb(II) complexes with Laurentian fulvic acid and Differential Equilibrium Parameter (K^*).....	290
Figure 86	Linear free energy relationship between the dissociation rate coefficient (k_d) of Zn(II), Cd(II), and Pb(II) complexes with Laurentian fulvic acid and Differential Equilibrium Parameter (K^*).....	291

List of Tables

Table 1	Ligand exchange kinetics of Cu(II)-HA in model solutions, determined by CLEM/AdCSV, using 8-hydroxyquinoline (Oxine) as the competing ligand. Oxine 1×10^{-5} M, HEPES 0.01 M, ionic strength 0.01 M, temperature 23 ± 2 °C.....	55
Table 2	Effect of various concentrations of Ca(II) on the ligand-exchange kinetics of Cu(II)-HA in model solutions, determined CLEM/AdCSV, using 8-hydroxyquinoline (Oxine) as the competing ligand.	61
Table 3	Effect of various concentrations of Mg(II) on the ligand-exchange kinetics of Cu(II)-HA in model solutions, determined by CLEM/AdCSV, using 8-hydroxyquinoline (Oxine) as the competing ligand.	64
Table 4	Effect of various concentrations of Ca(II) plus Mg(II) on the ligand-exchange kinetics of Cu(II)-HA in model solutions, determined by CLEM/AdCSV, using 8-hydroxyquinoline (Oxine) as competing ligand.....	67
Table 5	Some properties of the organic soil solutions and through-fall precipitation water samples collected from Sudbury Mining area (Site 1 and Site 2) in May 2002 and June 2002.....	83
Table 6	Kinetically distinguishable components of Ni-DOC complexes in organic soil solutions and through-fall precipitation samples collected from Sudbury area in (Site 1 and Site 2) in May 2002 and June 2002, determined by CLEM/AdCSV using DMG as the competing ligand.....	87
Table 7	Some properties of the surface-water samples collected from Grand River, Ontario in June 2002.....	96
Table 8	Kinetically distinguishable components of Zn(II)- and Cu(II)-FA species in model solutions of Laurentian fulvic acid. $c_M / c_{FA} = 0.056$, pH 5.0 ± 0.1 , ionic strength 6×10^{-6} mol/L, temperature 23 ± 2 °C	102
Table 9	Influence of the metal-to-ligand mole ratio on the kinetic speciation parameters of Cd(II) in model solutions of Laurentian fulvic acid. pH 5.0 ± 0.1 , ionic strength 6×10^{-6} mol/L, temperature 23 ± 2 °C.....	109
Table 10	Influence of the d-electron configuration on the kinetic speciation parameters in model solutions of Laurentian fulvic acid. $c_M / c_{FA} = 0.056$, pH 5.0 ± 0.1 , ionic strength 6×10^{-6} mol/L, temperature 23 ± 2 °C.....	112
Table 11	Rate constants for water exchange (k_w) of selected 3d transition metal ions (weak field). Adapted from Butler and Harrod [171].....	113
Table 12	Influence of the d-electron configuration on the kinetic speciation	

	parameters in a freshwater sample collected from the Grand River on June 23, 2002. DOC 14.9 ± 0.4 mg/L, pH 7.9 ± 0.1 , ionic strength 6×10^{-3} mol/L, temperature 23 ± 2 °C.....	119
Table 13	Influence of ionic potential (z^2/r) on the kinetic speciation parameters in model solutions of Laurentian fulvic acid. $c_M / c_{FA} = 0.056$, pH 5.0 ± 0.1 , ionic strength 6×10^{-6} mol/L, temperature 23 ± 2 °C.....	123
Table 14	Influence of ionic potential (z^2/r) on the kinetic speciation parameters in a freshwater sample collected from the Grand River on June 23, 2002. DOC 14.9 ± 0.4 mg/L, pH 7.9 ± 0.1 , ionic strength 6×10^{-3} mol/L, temperature 23 ± 2 °C.....	126
Table 15	Instrumental operating conditions and data acquisition protocol for ICP-MS.....	135
Table 16	Some properties of the surface-waters of the lakes in Rouyn-Noranda, Québec. Blank spaces refer to metals that were not determined.....	164
Table 17	Parameters of the electrochemical techniques used for the determination of metal speciation: nickel, copper, and lead in surface water samples from the in lakes in the area of Rouyn-Noranda, Québec.....	166
Table 18	Ligand exchange kinetics of Ni(II)-DOC in the lake-water samples, determined by CLEM/AdCSV, using DMG as the competing ligand.	169
Table 19	Ligand exchange kinetics of Cu(II)-DOC in lake-water samples from Rouyn-Noranda, Québec, determined by CLEM/AdCSV, using 8-hydroxyquinoline (oxine) as the competing ligand.	173
Table 20	Ligand exchange kinetics of Pb(II)-DOC in freshwaters, determined by CLEM/AdCSV, using 8-hydroxyquinoline (Oxine) as the competing ligand.....	176
Table 21	WHAM model predictions of the speciation of Ni, Cu, and Pb in the lake water samples based on 65% of the DOC as “active”, and the measured concentrations of labile Ni(II)-, Cu(II)-, and Pb(II)-complexes in the lake waters collected from Rouyn-Noranda, Quebec, in July 2002 and August 2002.....	180
Table 22	Default values of the constant $\log K_{MA}$ in Model V [192] and VI [193].....	183
Table 23	Some properties of the surface-water samples of the selected lakes in Rouyn-Noranda, Québec.....	195
Table 24	Instrumental operating conditions and data acquisition protocol for ICP-MS.....	196
Table 25	Ligand exchange kinetics of M(II)-DOC in Lake Dufault-water samples collected from the Rouyn-Noranda area, determined by CLEM/ICP-MS,	

	using Chelex 100 as the competing ligand. The water samples were received on June 26, 2003. Ionic strength 1.9×10^{-3} mol/L; temperature 23 ± 2 °C. The non-linear regression analysis was used to fit the kinetic data.....	215
Table 26	Ligand exchange kinetics of M(II)-DOC in Lake Opasatica-water samples collected from the Rouyn-Noranda area, determined by CLEM/ICP-MS, using Chelex 100 as the competing ligand. The water samples were received on June 26, 2003. Ionic strength 1.5×10^{-3} mol/L; temperature 23 ± 2 °C. The non-linear regression analysis was used to fit the kinetic data.....	216
Table 27	Ligand exchange kinetics of M(II)-DOC in Lake Osisko-water samples collected from the Rouyn-Noranda area, determined by CLEM/ICP-MS, using Chelex 100 as the competing ligand. The water samples were received on June 26, 2003. Ionic strength 4.4×10^{-3} mol/L; temperature 23 ± 2 °C. The non-linear regression analysis was used to fit the kinetic data.....	217
Table 28	Ligand exchange kinetics of M(II)-DOC in Lake Vaudray-water samples collected from the Rouyn-Noranda area, determined by CLEM/ICP-MS, using Chelex 100 as the competing ligand. The water samples were received on June 26, 2003. Ionic strength 8.6×10^{-3} mol/L; temperature 23 ± 2 °C. The non-linear regression analysis was used to fit the kinetic data.....	218
Table 29	Ligand exchange kinetics of M(II)-DOC in Lake Dufault-water samples collected from the Rouyn-Noranda area, determined by CLEM/ICP-MS, using Chelex 100 as the competing ligand. The water samples were received on June 26, 2003. Ionic strength 1.9×10^{-3} mol/L; temperature 23 ± 2 °C. The distribution analysis method was used to fit the kinetic data.....	219
Table 30	Ligand exchange kinetics of M(II)-DOC in Lake Opasatica-water samples collected from the Rouyn-Noranda area, determined by CLEM/ICP-MS, using Chelex 100 as the competing ligand. The water samples were received on June 26, 2003. Ionic strength 1.5×10^{-3} mol/L; temperature 23 ± 2 °C. The distribution analysis method was used to fit the kinetic data.....	220
Table 31	Ligand exchange kinetics of M(II)-DOC in Lake Osisko-water samples collected from the Rouyn-Noranda area, determined by CLEM/ICP-MS, using Chelex 100 as the competing ligand. The water samples were received on June 26, 2003. Ionic strength 4.4×10^{-3} mol/L; temperature 23 ± 2 °C. The distribution analysis method was used to fit the kinetic data.....	221
Table 32	Ligand exchange kinetics of M(II)-DOC in Lake Vaudray-water samples collected from the Rouyn-Noranda area, determined by CLEM/ICP-MS, using Chelex 100 as the competing ligand. The water samples were received on June 26, 2003. Ionic strength 8.6×10^{-3} mol/L; temperature	

	23 ± 2 °C. The distribution analysis method was used to fit the kinetic data.....	222
Table 33	WHAM model predictions of the speciation of Co, Ni, Cu, Zn, Cd, and Pb in the lake water samples based on 65% of the DOC as “active”, and the measured concentrations of labile Co(II)-, Ni(II)-, Cu(II)-, Zn(II)-, Cd(II)-, and Pb(II)-complexes in the lake water samples collected from the Rouyn-Noranda area, Quebec, in June 2003.....	228
Table 34	Effect of decreasing the mole ratio of [Pb(II)]/[HA] on the Differential Equilibrium Functions of Pb(II)-HA system in model solutions of humic acid (HA).....	258
Table 35	Influence of the stirring rate on Differential Equilibrium Functions of Pb(II)-HA complexes in model solutions of humic acid (HA).	265
Table 36	Differential Equilibrium Functions of Pb(II) in model solutions of humic acid in the presence of various concentrations of Ni(II), Cu(II), or Zn(II).....	269
Table 37	Differential Equilibrium Functions of Zn(II), Cd(II), Pb(II) and Cu(II) in model solutions of Laurentian fulvic acid. $c_M = 7.0 \times 10^{-7}$ mol/L, and the lability (i/i_{lim}) of these systems.....	283
Table 38	Differential Kinetic Functions for M(II)-FA complexes in model solutions of Laurentian fulvic acid.....	287

-- Chapter 1 --

Introduction

1.1 Introduction

A recent recommendation from the International Union of Pure and Applied Chemistry (IUPAC) defines “speciation” as the distribution of an element among defined chemical species in a system. A chemical species is defined as a specific form of an element defined as to isotopic composition, electronic or oxidation state, and/or complex or molecular structure [1]. This definition implies that chemical speciation reflects the differences from nuclear and electronic structure to the level of macromolecular complexation.

Chemical speciation of trace elements in natural waters is a major concern to many analytical and environmental chemists. This is due to presence of numerous complexing agents, some of which are unknown; also, concentrations of trace elements in natural waters are generally very low. Depending on the metal, typical concentrations may vary between several hundred $\mu\text{g/L}$ in highly polluted rivers to $0.001 \mu\text{g/L}$ in unpolluted, open ocean waters. In the aquatic environment, an element usually exists in a variety of physicochemical forms in both particulate and solution phases: free-metal ion (metal aqua complex), metal ions incorporated into colloids or adsorbed onto suspended particles, and various metal complexes of naturally-occurring inorganic and organic complexants (e.g. humic and fulvic acids), as shown in Figure 1 [2,3].

Trace metals participate in a wide variety of chemical reactions in the freshwater environment; many trace metals are essential micronutrients in biological systems at low levels, but they may become toxic at elevated levels [4]. Bioavailability or toxicity of the metals is not dependent on total metal concentration, but rather on the form in which the

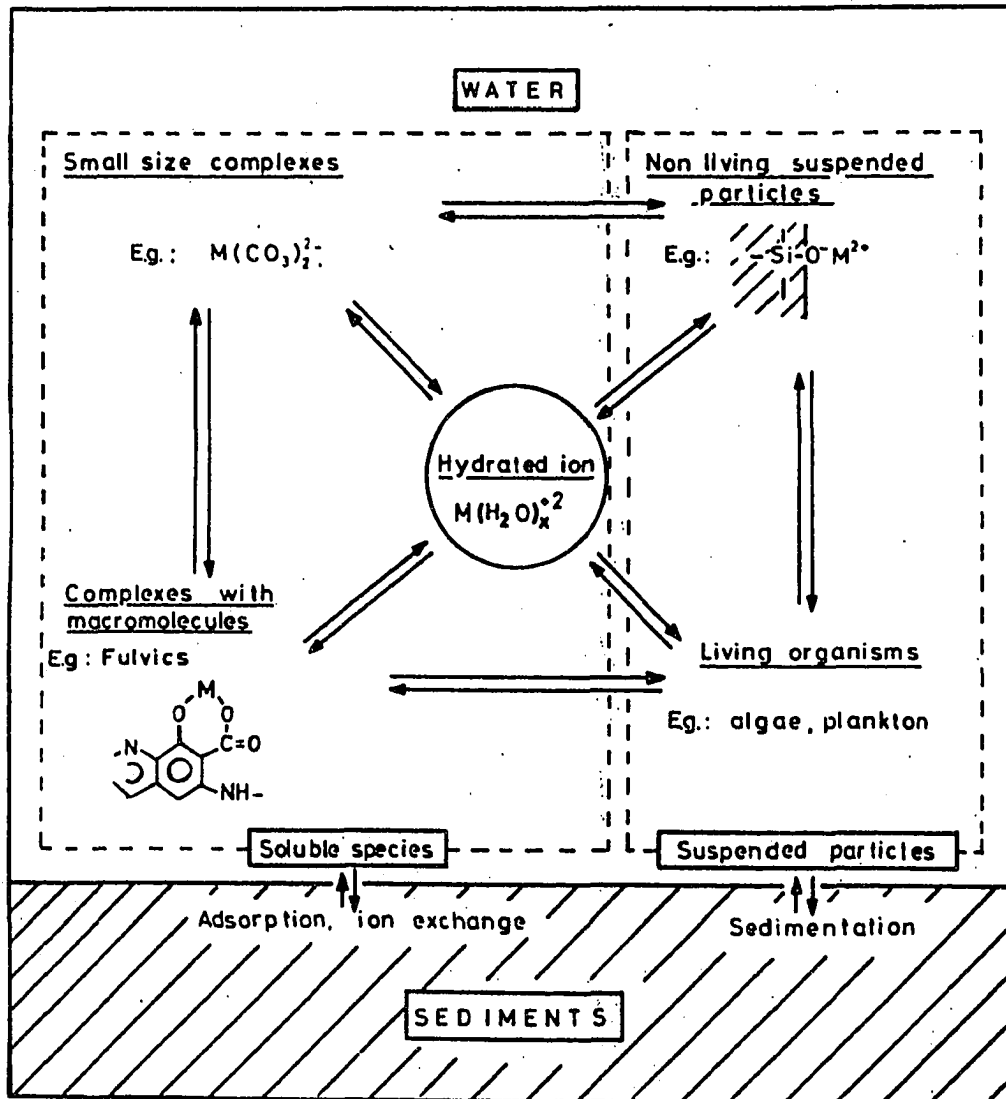


Figure 1 Schematic representation of the reaction of a metal ion with different types of aquatic components [2].

metal ion is present in the sample (i.e. its chemical speciation) [5]. Assessment of the impact of trace metals in the natural environment is ultimately concerned with how these metals directly or indirectly affect the health of biota. An understanding of the distribution of a metal among its different chemical forms (metal speciation) and the bioavailability of the metal species is essential for predicting the ecotoxicity of metal species and interpreting many biological and geochemical processes [6]. The overall goal of environmental metal speciation studies is to provide the data and information required for environmental impact assessment of metals by determining their chemical speciation, distribution, properties, and fluxes [7]. The interactions of trace metals with dissolved organic matter (DOM), which is ubiquitous in freshwaters, sediments and soils, play an important role in trace metal transport, fate and bioavailability. However, our knowledge of the metal speciation in freshwaters is severely limited by the inherent extreme complexity of naturally-occurring organic complexants.

1.2 Natural Organic Matter (NOM) and Humic Substances

Natural Organic Matter (NOM) plays an important role in the speciation of trace metals in natural waters. DOM content in aquatic systems is usually approximated by the more readily measurable dissolved organic carbon (DOC) concentrations. Concentrations of DOC in freshwater streams, rivers and lakes vary from less than 0.5 mg/L to as high as 100 mg/L, depending on the nature of the catchment, climate, trophic status of the water body, and pollutant inputs. The average value for DOC in the major rivers of the world is ca. 5 mg/L [8].

In aquatic systems, humic substances (HS), including humic acid (HA) and fulvic acid (FA), represent 70-90% of DOC in wetlands and 10-30% in seawater [9]. Humic substances are refractory (i.e. degradation-resistant), polydisperse, polyelectrolytic, and polyfunctional acids with molecular weights ranging from 500 to 500000 g/mol. Humic substances are formed by decomposition of plants, animals, and by microbial activity. Knowledge of humic concentrations in natural waters is needed to understand the environmental effects of cation-binding by humic substances. Because humic substances are mixtures, not defined by a single chemical characteristic, their concentrations are difficult to measure. Full-scale isolation of humic substances from their environments is impractical. The most useful humic-related determinant is DOC. Although not a very proper measure of humic matter, DOC concentrations provide a useful indication, since much of DOC is usually humic substance [8]. This thesis is primarily concerned with scientific investigation of the metal-complexation properties in aqueous environmental samples, including an in-depth, theoretical and experimental study of speciation of metals.

Traditionally, humic substances (HS) have been considered to comprise three main fractions, distinguished by their solubility and adsorption properties. Humic acid is soluble in base but insoluble in acid, whereas fulvic acid is soluble in both base and acid. A third fraction, humin, is not soluble in either acid or base. In general, humic acid and humin occur mostly in soils and sediments as part of the solid phase, whereas fulvic acid is more mobile and accounts for a major part of the dissolved organic matter in natural waters [8]. Humic substances are both chemically and physically heterogeneous, and this affects their metal complexation properties. Because of their inherent complexity,

heterogeneity, and structural variability, they have the ability to buffer a wide range of free metal ion concentrations in freshwaters following metal-pollution events [10]. This buffering process constitutes the basis for chemostasis in aquatic systems and is essential for the maintenance of aquatic life [2].

1.2.1 Metal complexation by humic substances in freshwaters

An abundance of experimental evidence suggests that in the aquatic environment, complexation of metal ions by dissolved organic ligands reduces their toxicity by decreasing the free metal ion concentration [11]. Most of earlier research efforts has been directed toward studying metal and proton binding by isolated humic substances, aimed both at elucidating mechanisms and providing quantitative information. The interactions of metal ions with humic substances can influence transport and bioavailability of the metals, acid-base balance, and humic solubility in waters, sediments and soils. Humic substances are a particularly important category of complexants because of their high concentrations, strong affinity for metals, and ubiquity in freshwaters, soil solutions (pore water), and in through-fall precipitation samples. Aqueous environmental samples, freshwaters, soil solutions (pore water), and through-fall precipitation, are complex media, in which competition between protons and metals for binding sites of the complexants is important. Competition of major cations with trace metals is an important phenomenon in freshwaters [12]. However, trace metals in freshwaters also compete with one another [13, 14].

It is impractical to study each individual binding site of humic acid independently. Metal-complexation by humic substances involves additional effects on the stability of metal complexes compared with simple ligand such as ethylenediaminetetraacetic acid (EDTA) [2]. These additional effects can be attributed to the following properties of HS [2].

- (a) **Polydispersity.** Humic substances represent a variety of different molecules with diverse molecular masses, which make them polydisperse.

- (b) **Polyfunctional Properties.** Each molecule of HS contains a number of different functional groups. Fulvic and humic acids primarily have carboxylic or phenolic groups, but moieties containing sulphur, nitrogen and phosphorus are also known. Metal-binding sites in humic substances can be divided into two categories [10,15-16]: major sites and minor sites. Major sites are carboxylate and phenolate-type functional groups, which represent 99-90 % of the total sites, and are considered to be chemically homogeneous, and are weak Lewis bases. Minor sites are those present in trace amounts (~ 1-10 % of the total sites present), but have more chemical diversity; they including N- and S-bearing functional groups. They can be considered to be chemically heterogeneous, and are strong Lewis bases. Carboxyl groups play a prominent role in the binding of metal ions by humic substances. Mixed complexes are probably formed, the most prominent one involving both phenolic and COOH groups i.e. a salicylate-type site [16-17]. Other possible combinations include two COOH e.g. a phthalate-type site, two phenolic OH, quinone groups, NH₂ groups, sulphydryl groups, and conjugated ketonic structures [17,19-20].

pH Effect

Acidic functional groups have diverse pK_a values such that some ionize at pH 6-7 and lower, whereas others ionize at pH 8-9 and higher. Therefore, pH has a significant effect on metal-binding by humic substances. At a given temperature, the total charge on the humate anion depends on the pH and the degree of site occupation by metals, and on the ionic strength of the medium [21-24].

(c) **Polyelectrolytic Properties.** Each individual molecule of humic substances contains a large number of acidic functional groups that ionize at characteristic pH values (hence, these are pH-dependent charges) to form anionic moieties, and thus impart electric charges (negative charges) to the surface (polyanion). It is more accurate to call them oligoelectrolytic properties because of the smaller charge densities compared to true polyelectrolytes, such as proteins [21-24]. When a cation reacts with a functional group of polyanions such as a humic acid, the binding of metal ions by polyanion can be greatly strengthened by the long-range, coulombic attraction from the neighboring, non-reacting, negative sites. This is called polyelectrolyte effect (properly called oligoelectrolyte effect in the case of humic substances) [25].

(d) **Conformational Properties.** Humic substances in aqueous media are water-swollen gels— they are macromolecular and naturally-occurring colloidal substances. Factors such as pH and ionic strength affect conformational

changes, degree of aggregation, coiling and uncoiling of the various molecules of humic substances and consequently their ability for metal ion binding. The metal ion bound to such sites must diffuse out of the cavernous gel of HS by a process called restrained diffusion instead of the normal process of free diffusion [26]. Hence, diffusion of the metal ions from within the interior of the colloid causes metals to appear to dissociate much more slowly than surface-bound metal species (this may become the limiting factor in metal-complex formation and dissociation). As C.H. Langford et al. [27-28] who pioneered the study of kinetic speciation of metals in the freshwater environment aptly pointed out, the effect of this slow diffusion results in a seeming paradox: thermodynamically equivalent sites appear kinetically different. Conformational changes in humic substances may result in changes in the accessibility of some ligand sites to metal ions [10,30]. In particular, conformation depends on hydration-dehydration process, formation of hydrogen bonds among the various functional groups on a single molecule, and formation of metallic bridges between two hydrodynamically separate molecules (pseudochelation), which themselves depend on the degree of occupation of the complexing sites [30]. In all cases, the relative importance of these properties varies with pH, ionic strength and degree of the metal loading.

As a result of chemical and steric differences of binding sites on humic substances, they have a continuous (Gaussian) range of metal binding constants.

1.2.2 Metal competition

In aqueous systems, protons (or hydroxyl ions) are by definition present. Since protons largely determine the state of the functional groups and the charge of the humic substances, a proton effect on the metal ion binding is the least that is to be expected. Additionally, Major cations (e.g. Ca(II), Mg(II)) are usually present in freshwaters in concentrations, which are several orders of magnitude greater than those of trace metal ions (e.g. Ni(II), Co(II), Zn(II)). Since all trace metals and major cations coexist and interact with all ligands, and each ligand interacts with all trace metals and major cations, competition between various cations and ligand anions [21] must be considered. Addition of any trace metal or major cations to freshwater systems produces significant impact in the interdependent 'web' of metals and ligands, and may lead to a redistribution of all trace metals and their surrounded ligands [3].

1.3 Solar Radiation and Metal Speciation

Photochemical reactions (caused by UV-B radiation of sunlight) play an important role in the biogeochemistry of the surface waters [32]. DOM contains chromophores that strongly absorb solar radiation over a broad spectral range [33], and is primarily responsible for regulating the transmission of solar radiation in freshwaters, from the surface towards the bottom of the water column. This property helps chromophoric DOM to shield the water column from direct effects of solar radiation; however, DOM can also be subjected to considerable photochemical degradation. Photochemical transformation of the chromophores can lead to photoisomerization, intramolecular decomposition, rearrangement, and electron transfer [323]. These sunlight-mediated processes can lead to transformation of DOM into low molecular weight aliphatic carbonyl compounds (e.g.

acetaldehyde, formaldehyde, malonate and pyruvate) [34-36] and release of carbon monoxide [34-39], carbon dioxide [40-41] and other forms of inorganic carbon [40,42-44] (i.e. photomineralization). Hence, photochemical modification of DOM affects the optical properties of water and influences the penetration of light [45], as these smaller compounds do not absorb UV radiation as strongly as the larger parent molecules [46]. This phenomenon, known as photobleaching, can substantially increase the penetration of UV radiation in lakes [33]. Solar radiation may promote degradation of DOM, either directly through complete photooxidation or indirectly through secondary reactions of photochemically produced free radicals with other organic compound. Although photodegradation of DOM has been widely studied, little information is available on the effects of solar radiation on the metal-binding properties of DOM, which may significantly affect the chemical speciation and bioavailability of trace metals in freshwaters.

1.4 Speciation Techniques of Metals in Freshwaters

Trace metal speciation in natural waters is usually done experimentally to determine reliable values of free metal ion concentrations and complexation parameters including stability constants and concentrations of natural metal-complexing ligands. A variety of analytical techniques has been developed to determine metal speciation of environmentally important metals: Cu, Cd, Co, Ni, Pb and Zn, in both marine and freshwaters, each technique having its own advantages and limitations [47-51].

The only analytical technique capable of direct (i.e. without pre-concentration) determination of free-metal ion activity is ion-selective electrode potentiometry [54]—all

other analytical techniques measure concentration, not activity, and they measure ‘total’ metal (not free-metal ion). However, the limit of detection of ion-selective electrode potentiometry is typically 10^{-5} M, which is inadequate for environmentally relevant concentrations, in which the free metal ions can be lower than 10^{-9} M. Traditional techniques for chemical speciation provide results that are operationally-defined, e.g.: “ASV-labile”, which is the amount of metal that is available using Anodic Stripping Voltammetry (ASV) [53], and “Chelex-labile”, which is the amount of metal that is taken up by Chelex 100 chelating resin. The major limitation of operationally-defined methods is that the results are inherently ill-defined. In operationally-defined methods, the results are “operationally-defined.” In the words of Nirel and Morel [54]: “to put it in another way, what is measured is defined by what is measured, a safe if not illuminating tautology.” The results of operationally-defined methods cannot be related to naturally-occurring processes in the environment. While the significance of all analytical results is limited by the analytical procedures used, it is precisely the degree to which the results are independent of the analytical methods that gives them meaning and usefulness. New concepts and approaches, and well-defined analytical methods, such as those for Speciation Parameters (e.g., dissociation rate coefficients), are needed to investigate metal speciation and bioavailability in freshwaters.

1.5 Objectives

Despite the variety of studies on metal complexation with DOM that have been reported, there remains a paucity of knowledge of the binding, including proton binding, metal binding, and effects of competition of other trace metals on the metal-DOM binding. Within the context of this need, the objectives of this research are as follows:

1. To investigate metal speciation in model solutions of two well-characterized, naturally-occurring, organic complexants: a fulvic acid and a humic acid.
2. To investigate metal speciation in freshwater samples from freshwater lakes in Canada that have been impacted by anthropogenic metal pollutants.
3. To investigate some factors that influence the kinetics of trace metal competition in the freshwater environment within the context of freshwater as a dynamic system.
4. To investigate the competition of major cations, Ca and Mg, with copper in a model solution of a well-characterized humic acid (HA) using an electrochemical technique.
5. To investigate the impact of solar radiation on the metal binding properties of DOM.
6. To test the ability of the computer speciation code, WHAM (Windermere Humic Aqueous Model), versions V and VI, to correctly predict the free metal ion concentrations in metal-impacted freshwater lakes: to compare the WHAM prediction of the free-metal-ion concentrations with the experimentally-measured concentrations
7. To investigate the heterogeneity in metal complexation by well characterized humic substances in model solutions and to study the influence of metal loading on the equilibrium and kinetic properties of these metal-complex systems.

1.6 Outline of the Organization of the Thesis

This thesis is divided into ten chapters as follows. Chapter 1 gives a brief introduction. Chapter 2 gives the scientific background of this thesis and describes the limitations of the existing knowledge of the subject and presents the hypothesis that drives this thesis. Chapter 3 deals with copper speciation in model solutions of a well-characterized humic acid (HA) by Competing Ligand Exchange Method, and presents a discussion on the importance of [metal]/[HA] mole ratio and pH for the metal speciation. It also discusses the competition of major cations (Ca(II) and Mg(II)) with Cu(II) for the binding sites of a well-characterized humic acid. Chapter 4 presents determination of Ni(II) speciation in through-fall precipitation samples and soil solutions (pore waters) by Competing Ligand Exchange Method/Adsorptive Cathodic stripping Voltammetry (CLEM/AdCSV). Chapter 5 presents a kinetic approach using Competing Ligand Exchange Method with Chelex 100 as the competing ligand and Inductively Coupled Plasma-Mass Spectrometry (ICP-MS) to determine the dissociation kinetics of metal complexes. Chapter 5 also presents the following factors that influence the kinetics of trace metal complexation in the freshwater environment within the context of freshwater as a dynamic system: 1) metal-to-ligand ratio, 2) ionic potential (z^2/r), and 3) Ligand Field Stabilization Energy. Chapter 6 describes the influence of solar irradiation on metal speciation in freshwaters. Chapter 7 presents and critically analyzes experimental results of dissociation kinetics of Ni(II)-, Cu(II)-, and Pb(II)-DOC complexes using Competing Ligand Exchange Method/Adsorptive Cathodic Stripping Voltammetry in metal-impacted freshwater lakes. Chapter 7 also presents a computer-based speciation code, WHAM, versions V and VI, and a critical comparison of the WHAM-predicted $[\text{Ni}^{2+}]$, $[\text{Cu}^{2+}]$, and $[\text{Pb}^{2+}]$, with the experimentally-measured free-metal-ion concentrations in lake-water samples. Chapter 8

presents dissociation kinetics of metal-DOC complexes in waters from metal-impacted freshwater lakes, investigated by CLEM/ICP-MS. This chapter also presents a critical comparison of the WHAM-predicted free metal ions: $[\text{Co}^{2+}]$, $[\text{Ni}^{2+}]$, $[\text{Cu}^{2+}]$, $[\text{Zn}^{2+}]$, $[\text{Cd}^{2+}]$, and $[\text{Pb}^{2+}]$, with the experimentally-measured concentrations. Chapters 9 and 10 present the all-important subject of heterogeneity of metal complexes of humic substances, which are ubiquitous, naturally-occurring organic complexants in freshwaters. These chapters deal with the theoretical background of the inadequacy of stability constants and kinetic lability of metal complexes of simple ligands, e.g. EDTA, to describe the thermodynamic stability and kinetic lability of metal complexes of heterogeneous complexants, e.g., humic substances. The above inadequacy is due to the heterogeneity of humic substances, which is addressed by Differential Equilibrium Functions (for thermodynamic stability) and Differential Kinetic Functions (for kinetic lability); these are measured by pseudopolarography using a Static Mercury Drop Electrode.

-- Chapter 2 --

Scientific Background

2.1 Current State of Knowledge

There are two approaches for studying chemical speciation: equilibrium and kinetic. The dominant approach for the analysis of metal ion speciation in aquatic systems has been the local equilibrium (or pseudo-equilibrium) assumption [28], which is that complexation reactions are fast relative to other reactions in freshwaters. The equilibrium distribution among dissolved organic and inorganic species is assumed despite the fact that the total metal concentration may vary as a result of some controlling biogeochemical process. All reactions that are considered to take place in the system are considered to have reached equilibrium and that their distribution is given by thermodynamic equilibrium constants. Examples of analytical techniques to study chemical speciation that use the local equilibrium assumption include Ion Selective Electrode Potentiometry, Voltammetry (e.g. Pseudopolarography, Anodic Stripping Voltammetry, and Cathodic Stripping Voltammetry), Ion-exchange and Hydrophobic Resin Chromatography [55]. In many cases, complexation of metals by ligands is indeed rapid relative to other processes of interest. Computer-based chemical speciation models also make the equilibrium assumption (equilibrium models) and often provide a good description of complexation phenomena in natural waters [56]. The freshwater environment is an extremely complex system that has defied many earlier attempts to study its various components by applying simple mathematical models. Mathematical models set the free energy of the system to a minimum, and then calculate the distribution of a given element between its different chemical forms or groups of chemical species using known thermodynamic constants [57].

However, natural systems are not equilibrium systems. They are dynamic and often far-removed from equilibrium [58-61]; hence, equilibrium speciation methods may not apply [62]. Heterogeneous ligand systems (e.g. humic substances, which are colloidal, polyelectrolyte ligands) can depart considerably in kinetic behaviour from simple ligands. In some instances, the rates of biogeochemical reactions may be influenced, or even controlled, by the rates of metal complexation reactions [61].

A quantitative description of chemical speciation of metal ions in freshwaters cannot be considered complete without proper characterization of the rates of chemical reactions [62-63]. Furthermore, coordination equilibrium of trace metal complexation of humic substances in soils and freshwaters are typically slow (especially those involved in double exchange reactions), making distributions of trace metals among various thermodynamically possible chemical species kinetically controlled [62].

There is a growing realization of the importance of a kinetic approach for chemical speciation. However, there is little information on the kinetics of reactions of metal complexes in freshwaters. This is mainly due to the inherent complexity, physical and chemical heterogeneity, and structural variability of naturally-occurring organic complexants in freshwaters. Rates of ligand exchange reactions involving such complexants are difficult to study and interpret, and few publications on estimation the rate constants were reported in the literature. Different data interpretation models have been used to extract the dissociation rate coefficients of metal exchange reactions in model solutions and freshwaters: simple dissociation constants [65], discrete

multicomponent models [27,66-68], discrete kinetic spectra [70], continuous kinetic spectra [71], and log normal distribution [69,71]. Hering and Morel [72] have reported on the rates of ligand exchange reactions of copper-nitrilotriacetic acid complexes and copper-humate complexes: rate coefficients of ligand exchange were pH-dependent, and depend not only on the properties of the humic substances but also on the experimental conditions (e.g., ionic strength, temperature)

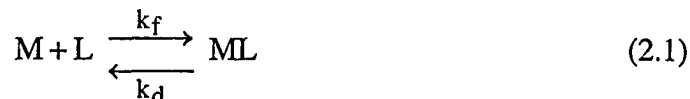
Kinetic approach reflects more correctly the realities of freshwaters, soil solutions (pore water), and through-fall precipitation samples, in which metal release is often kinetically controlled (equilibrium conditions may not be established during the time scale of the experiment). Kinetic studies of metal speciation can not only differentiate chemical species according to their kinetic parameters but can also give information on the distribution of the chemical species in the system at any time during biological process, hydrological process and geochemical process they may undergo. Current analytical techniques give an operationally-defined metal species since they do not take into their accounts the effect of analytical time scale of the measurement on chemical speciation and metal bioavailability. Hence, the results obtained from kinetic studies should be useful for estimating metal bioavailability if a kinetic model can be constructed to represent the process of biological uptake [73].

2.2 Scientific Background

2.2.1 Kinetics of metal complexes in the bulk solution

Reactions in the bulk solution can be approximated by a simple first order complexation

reaction between a metal ion, M, and ligand, L, to form a metal complex, ML (charges have been omitted for simplicity).

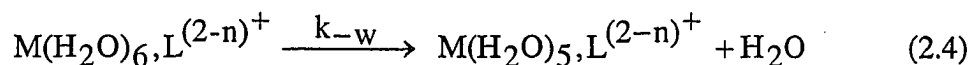
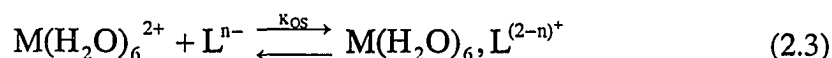


where k_f ($\text{mole}^{-1} \text{ L s}^{-1}$) and k_d (s^{-1}) represent the formation and dissociation rate coefficients, respectively. By the Principle of Microscopic Reversibility [74], k_f and k_d are related to the equilibrium constant (stability constant), K , by the equation

$$K = \frac{c_{ML}}{c_M c_L} = \frac{k_f}{k_d} \quad (2.2)$$

where c_{ML} , c_M and c_L are the concentrations of ML, M and L, respectively, in the bulk solution.

The Eigen-Wilkins [74-76] mechanism for complex formation is based on a rapid formation of an outer-sphere complex between a metal and a ligand, followed by the rate-limiting loss of water from the inner hydration sphere of the metal ion.



where K_{os} is the outer-sphere stability constant, and k_w is the water loss rate coefficient of $M(\text{aq})$. Because the water exchange rate of L is very fast in comparison to that of $M(\text{aq})$, we can neglect it. Based on the Eigen-Wilkins mechanism, the rate-determining step is the loss of water. The rate coefficient for the complex formation, k_f , is related to k_w as described below.

$$k_f = k_d K_{os} \quad (2.5)$$

but $k_d = k_{-w}$, therefore

$$k_f = k_{-w} K_{os} \quad (2.6)$$

K_{os} is dependent primarily on the charges of the reacting species and the ionic strength of the medium; values for K_{os} range from approximately 10 M^{-1} for ions with a single negative (-1) charge to $3 \times 10^3 \text{ M}^{-1}$ for ions with a triply-negative (-3) charge. k_{-w} is characteristic of the reacting metal, and its magnitude can be explained by the electrostatic interactions between the metal cation and the coordinated water molecules. Note that k_{-w} is related to the charge of the cation, and inversely related to the size of the metal. The value of k_{-w} has a large effect on how quickly the metal ions are able to react with the natural ligands.

K_{os} can be determined experimentally; k_d can be estimated by combining equations (2.2) and (2.6)

$$k_d = \frac{k_f}{K} = \frac{k_{-w} K_{os}}{K} \quad (2.7)$$

In the presence of an excess ligand,

$$k'_f = k_f c_L \text{ and } K' = K c_L = c_{ML} / c_M \quad (2.8)$$

The metal species in reaction 2.1 have characteristic lifetimes related to their association and dissociation rate coefficients (e.g. $\tau = 1/k'_f$ and $\tau = 1/k_d$). When the lifetimes of M and ML are much shorter than the timescale of measurement, t , (i.e. the interconversion

between M and ML in the bulk solution is rapid), the system is in *dynamic* equilibrium. The condition is given below by Eq . 2.9.

$$k'_f t \text{ and } k_d t \gg 1 \quad (2.9)$$

Dynamic complexes require rapid reactions to maintain dynamic equilibrium, whereas *inert* complexes are essentially frozen in time (static) relative to the analytical timescale of measurement. When the lifetimes of M and ML are much larger than the timescale of measurement, equilibrium is not maintained in the system. The system is termed static and the metal complex species, ML, are called *inert* [30]. The condition is given below by Eq . 2.10.

$$k'_f t \text{ and } k_d t \ll 1 \quad (2.10)$$

Conditions 2.9 and 2.10 can be used to define whether the metal complexes are dynamic or inert in the bulk solution in a given period of time.

2.2.2 Coupled diffusion of M and ML in the diffusion layer

Even when the association and dissociation kinetics in the bulk solution are rapid (i.e. condition 2.9 is fulfilled), the system may still be limited by the supply of free-metal ions to the interface, where the equilibrium is not maintained inside the reaction layer (interconversion of ML into M is not rapid).

The thickness of the Nernstian Diffusion Layer, δ , represents the layer between the bulk solution and an interface where mass transport of any species is controlled exclusively by diffusion due to the concentration gradient [77]. δ is related to the timescale, t , by

$$\delta = (t\bar{D})^{1/2} \quad (2.11)$$

where \bar{D} is the average diffusion coefficient of ML and M (i.e. D_{ML} and D_M , respectively). The reaction layer, μ , represents the distance adjacent to the biological interface over which a free metal ion can travel by diffusion and is given by Einstein's fundamental equation for diffusional mean displacement [78].

$$\mu = \left(\frac{D_M}{k_f} \right)^{1/2} \quad (2.12)$$

where D_M is the diffusion coefficient of the metal. μ is related to the timescale in that it is based on the finite lifetime of a free metal ion after dissociating from ML. This lifetime is given by $\frac{1}{k_f}$, which reflects the rate of re-association of M and L.

In a strongly complexed system, the purely kinetic flux, J_{kin} , [79] is described by,

$$J_{kin} = k_d c_{ML} \mu \quad (2.13)$$

The purely diffusion-controlled flux, J_{diff} , as described in Eq. 2.14 is [79]

$$J_{diff} = D_{ML} c_{ML} / \delta \quad (2.14)$$

The definition of *lability* requires that the kinetic flux from the dissociation of ML is much greater than the purely diffusional flux ($J_{kin}/J_{diff} \gg 1$). Combining Eqs 2.12, 2.13 and 2.14 gives the following:

$$J_{kin}/J_{diff} = (k_d/\varepsilon D_{ML} K')^{1/2} \delta_{ML} \gg 1 \quad (2.15)$$

where $\varepsilon = D_{ML}/D_M$ is the ratio of the diffusion coefficients of the metal complex ML and the metal ion, M, respectively. The time, t , is related to thickness of the Nernstian Diffusion Layer, δ , and the diffusion coefficient, D , by Eq. 2.21.

$$t = \delta^2/D \quad (2.16)$$

The lability condition may be obtained by combining Eqs. 2.12 and 2.14,

$$\Lambda t^{1/2} \gg 1 \quad (2.17)$$

where the lability parameter, Λ , is given by,

$$\Lambda = \frac{k_d^{1/2}}{D_{ML} (\varepsilon K')^{1/2}} t^{1/2} \quad (2.18)$$

Lability (Eq. 2.17) refers to the limiting condition where the association and dissociation kinetics are rapid enough to ensure the coupled diffusion of M and ML to the interface.

Eq. 2.18 has been derived for the condition of strong complexation ($\varepsilon K' \gg 1$). The general form for the lability parameter, Λ , has been derived by de Jong et al. [80-81].

$$\Lambda = \frac{k_d^{1/2} (\varepsilon^{-1} + K')}{\varepsilon^{-1} K' (1 + K')} \quad (2.19)$$

The *non-labile* case is defined by condition 2.20.

$$\Lambda t^{1/2} \ll 1 \quad (2.20)$$

The distinction between labile and non-labile systems is related to the nature of the flux towards the interface, not the dynamics in the bulk solution. If the association and dissociation kinetics are rapid relative to the diffusional transport, the flux is purely diffusion-controlled and the system is labile; if the kinetics are slow relative to the diffusional transport, the flux is controlled by the kinetics and the system is non-labile [82]. The systems that lie between those conditions are neither completely labile nor non-labile. That means formation and dissociation of metal species are approximately equivalent to each other. This kind of condition for metal species is termed quasi-labile.

“The fundamental distinction between static (inert) systems and non-labile systems is that static systems obey condition 2.10, whereas non-labile systems obey conditions 2.9 and 2.20” [82].

The earlier discussion illustrates the importance of investigating both 1) thermodynamic parameters, such as equilibrium constants, and 2) kinetic parameters, such as diffusion coefficients and the association/dissociation kinetics of metal complexes. However, determination thermodynamic and kinetic parameters in natural systems is complicated by the structural and physicochemical complexity and heterogeneity of naturally-occurring complexants, such as humic substances. As a consequence, the equilibrium constants and rate coefficients do not represent characteristic constants for the natural system, but must be described by some distribution that is a metal loading, such as humic substances [82].

2.2.3 The Differential Equilibrium Function

If the metal forms complexes with heterogeneous complexants such as fulvic acid, the average stability constant (*apparent* equilibrium constant), \bar{K} , which is defined by:

$$\bar{K} = \frac{\sum_i c_{ML_i}}{c_M \sum_i c_{L_i}} \quad (2.21)$$

where c represents the concentration of different species, and \bar{K} is an arithmetic mean of the true equilibrium constants, K_i , weighted by the corresponding free site concentrations.

Equation 2.1 can be rewritten as

$$\bar{K} = \frac{\sum_i K_i c_{L_i}}{\sum_i c_{L_i}} \quad (2.22)$$

The value of \bar{K} varies with the degree of site occupation, $\theta_i = c_{ML_i}/c_{L_i}$. Hence, \bar{K} decreases with increasing θ because \bar{K} is averaged over an increasing number of weak sites [82].

The lability of metal complexes has considered for the case of a Freundlich type of distribution function [83], for which

$$\theta = A c_M^\Gamma \quad (2.23)$$

where A is a constant and Γ is a measure of the heterogeneity of the system. Allowed values for Γ range between $0 < \Gamma \leq 1$, where $\Gamma = 1$ corresponds to the case for a simple, homogeneous complexant. Freundlich isotherm relation holds θ , when there is a large excess of binding sites, L_i , relative to the concentration of metal complexes, ML_i (i.e. $\theta \ll 1$ [83]).

Equation (2.23) is analogous to the Differential Equilibrium Function (DEF) [84-86]. DEF was first introduced by Gamble and Langford [85-86], and was further developed by Filella et al. [84] to describe complexing properties of heterogeneous complexants, such as humic substances.

$$\log \theta = \Gamma \log K_o^* - \Gamma \log K^* \quad (2.24)$$

where K^* is the Differential Equilibrium Parameter and K_o^* is a constant. K_o^* has no special significance other than the fact that it is the value of K^* when all the sites are

fully occupied (i.e. when $\theta = 1$). DEF has no prior assumption behind it, it can take any shape. As presented in Equation (2.24), it describes a log-log relationship between the degree of site occupation by the metals, θ , and the Differential Equilibrium Parameter, K^* [84].

As shown in equation (2.25), K^* is a well-defined, weighted average of equilibrium constants, K_i , for all the sites in the system [84].

$$K^* = \frac{\sum_i K_i \theta_i (1 - \theta_i) c_{L_i}}{\sum_i \theta_i (1 - \theta_i) c_{L_i}} \quad (2.25)$$

K^* is a measure of complexing ability of heterogeneous complexant that is analogous to a conditional equilibrium constant (i.e. valid at a given pH, temperature and ionic strength) [83]. The degree of occupation of each site determines the weighting factor, $\theta_i(1-\theta_i)$, in equation (2.25). Thus, K^* decreases as θ increases because K^* is averaged over an increasing number of weak sites (and also, because the strongest sites are saturated first).

2.2.4 The Differential Kinetic Function

The Differential Equilibrium Parameter [82], K^* , can be related to the association rate coefficient, k_a , and the Differential Kinetic Parameter, k_d^* , by analogy with equation (2.2)

$$K^* = \frac{k_a}{k_d^*} \quad (2.26)$$

Combining equations (2.24) and (2.26) yields the Differential Kinetic Function (DKF).

$$\log \theta = \Gamma \log K_o^* - \Gamma \log k_a + \Gamma \log k_d^* \quad (2.27)$$

As shown in equation (2.27), the Differential Kinetic Function also represents a log-log relationship between the degree of site occupation by the metals, θ , and the differential kinetic parameter [82], k_d^* .

2.3 Speciation Parameters

Speciation parameters are quantitative measures of speciation characteristics of chemical species, which are independent of the analytical methods that are used to measure them. It is often necessary to use several speciation parameters to characterize a system fully. Some important speciation parameters are given below:

- 1) *Free Metal Ion Concentration* ($[M^{n+}]$) is the most important parameter for the Free-Ion Activity Model (FIAM) [88-89], because under the FIAM free ion activity is often a good predictor of the bioavailability of the metal, and hence, its nutrient or toxic effect.
- 2) *Diffusion Coefficient* (D) is a direct measure of how quickly the chemical species can reach the biological membrane or the electrode surface. The mobility of a particular chemical species plays a crucial role in the biological impact in the natural environment [7]. The element must bind to the biological membrane surface or even penetrate to elicit a toxic response [90].
- 3) *Stability Constant* (K) is a measure of the availability of free metal ions at equilibrium. It is a very important property for characterizing the metal species in the aquatic and the terrestrial environment [91-93]. Determination of stability

constants requires equilibrium or pseudo-equilibrium condition to be established before the measurement can be made. The determination of the stability constants of metal complexes is strongly influenced by physical and chemical heterogeneity of naturally-occurring organic complexants. In such cases, instead of discrete values for stability constants, a large spectrum of stability constants is often observed and the interpretation becomes uncertain. Often, an average stability constant is estimated for a group of metal complexes having closely-spaced values of stability constants [7].

- 4) *Dissociation Rate Coefficients (k_d)* is a measure of the rate at which a metal complex dissociates to form free metal ion (i.e. the metal-aqua complex), and its surrounded ligand. Hence, it is a crucial speciation parameter, especially in the case where free metal ion is the bioavailability species [7].

A combination of both equilibrium and kinetic approaches [28, 94-95] are required to interpret the metal complexation data and assess their relation to the biological process. Since metal binding properties change with increasing metal to ligand mole ratio in the case of heterogeneous organic complexants [95-96]. Hence, there is a need for dissociation rate coefficients and stability constants to be experimentally determined in order to characterize metal species in model systems and in freshwaters.

2.4 Hypothesis

Within the framework outlined above, the hypothesis that drives this work is that the concentration of free metal ion in the freshwater environment, which is related to its bioavailability, is influenced both by the equilibria and kinetics of metal complexation

reactions. The key hypotheses to be tested is that 1) the release of target trace metal ions bound to humic substances, which are ubiquitous in the aquatic environment, is determined by competition of other trace metal ions and major cations (e.g. Ca^{2+} and Mg^{2+}) with target trace metal ions for the binding sites of organic complexants; 2) the speciation parameters can be tested for their chemical significance by metal-to-ligand mole ratio, the ionic potential of metal ion (its charge to radius ratio z^2/r), and Ligand Field Stabilization Energy; 3) for freshwater-systems a computer-based speciation code, WHAM, can model the $[\text{M}^{n+}]$, comparable to the experimentally measured concentrations of labile metal complexes; and 4) lability of metal complexes in freshwaters is influenced by solar irradiation of surface waters, which drastically affects the metal-binding properties of dissolved organic carbon (humic substances).

2.5 Testing of the Hypothesis

The above hypotheses were tested by making rigorous studies of metal competition for the binding sites of humic substances in three different types of water as follows: (1) laboratory model systems containing two well-characterized fulvic and humic acids in ultrapure water; (2) metal-impacted freshwaters from lakes in Rouyn-Noranda, PQ, Canada; and (3) metal-impacted freshwaters, soil solutions (pore water), and through-fall precipitation from Sudbury, Ontario, Canada. Two approaches were used in this study. The first approach was the kinetics-based approach in the bulk solution which involved the measurement of the dissociation kinetics of metal complexes of well-characterized fulvic and humic acids and in freshwaters, using the Competing Ligand Exchange Method (CLEM) with Chelex-100 as the competing ligand and Inductively Coupled

Plasma Mass-Spectrometry (ICP-MS); and dimethylglyoxime (DMG) and 8-hydroxyquinoline (oxine) as competing ligands with Adsorptive Cathodic Stripping Voltammetry (AdCSV) for the measurement of dissociation rate coefficients. The second approach was the equilibrium-based approach at the water-electrode interface that involves the measurement of stability constants of Cu(II)-, Zn(II)-, Cd(II)-, and Pb(II)-complexes of heterogeneous complexants, such as humic and fulvic acids. Pseudopolarography (stripping polarography) at a Static Mercury Drop Electrode was employed to determine the heterogeneity of the systems: the Differential Equilibrium Function (DEF) and the Differential Kinetic Function (DKF) of the metal complexes of humic substances.

-- Chapter 3 --

**Kinetic Studies of Copper Speciation in Model Solutions of a
Well-Characterized Humic Acid using Adsorptive Cathodic
Stripping Voltammetry**

3.1 Introduction

Copper is one of the most environmentally important metals in freshwaters. Bioavailability of metals depends on the metal speciation in the medium, and toxicity is often related to the activity of free metal ion under a local equilibrium (pseudo-equilibrium) assumption. Natural processes that determine the physical and chemical properties of the aquatic system are not in equilibrium [28]. Lack of equilibrium between metals and complexing agents in natural waters may result from changes that may arise from natural and anthropogenic inputs and from hydrological, geochemical and biological processes as well [97]. Speciation studies based on thermodynamic considerations alone do not give realistic information about the distribution of metal species and their bioavailability; information on kinetic speciation studies is needed in order to obtain a better approximation to the distribution of the species in natural waters [98].

An important kinetic parameter of metal speciation is usually referred to the lability of a metal complex, which is necessary in bioavailability and toxicity studies [99-101]. Especially in freshwaters, where environmental parameters change constantly or some reaction rates are slow, especially coordination equilibrium of transition metals [102], the dynamic character of metal speciation in freshwaters may become important.

Langford et al. [27] have reported that the speciation is controlled by the history of the sample prior to the initiation of the metal ion transfer but that the rate constants are specific to the experimental condition. This experimental limitation is not as serious for metal complexes as it might be in other circumstances, as six-coordinate metal complexes

tend to follow the adjunctive pathway (the observed rate coefficients are strongly influenced by the nature of the probe ligand such as steric and electrostatic factors, and protonation), and extrapolation from one condition to another is fairly simple and reliable; in particular, relative rates tend to remain the same [28].

Several analytical techniques have been used to characterize the lability of metal complexes in aqueous systems (each with a limited time scale and detection limit), including voltammetry [103-104], chromatography [105], and ion extraction [106,107]. Adsorptive Cathodic Stripping Voltammetry (AdCSV) with 8-hydroxyquinoline (oxine) has been used before for copper determination [108] and equilibrium speciation [49] in natural waters. Recent studies indicate that in seawater from all depths, 99% of total dissolved copper is organically complexed [109]. Olson et al. [70] have used the ligand exchange method for kinetic speciation of copper using the chromophore 4-(2-pyridylazo)resorcinol (PAR) as a competing ligand and spectrophotometric detection of the Cu(II)-PAR complex. Chakrabarti et al. [110-113] have studied the kinetic speciation of Cu(II)-FA complexes using Competing Ligand Exchange Method (CLEM) with Chelex-100 as the competing ligand and Graphite Furnace Atomic Absorption Spectrometry (GFAAS) or Inductively Coupled Plasma Mass Spectrometry (ICP-MS) for quantification of the copper that has remained bound to the fulvic acid complexes at different measurement times. However, CLEM/AdCSV method was used in this chapter to study kinetic speciation of copper in model systems containing a well-characterized humic acid as a model ligand and oxine as the competing ligand.

In freshwaters, alkaline and alkaline earth metal ions (e.g. calcium and magnesium), which are generally present at many orders of magnitude greater concentrations ($\sim 10^{-3}$ M) than trace metal ions ($\sim < 10^{-8}$ M), may outcompete trace metal ions for binding with ligands because the large excess of the former outweighs their weaker complexing power [7]. It is necessary to study the relative importance of covalent bonding and electrostatic bonding of trace metals by humic substances and the role of major ions (e.g. Ca^{2+} and Mg^{2+}).

The objectives of this research are (1) to determine the binding characteristics and speciation of Cu(II)-HA complexes (dissociation rate coefficients, concentrations of complexing sites) in model solutions using a Kinetic Model and Competing Ligand Exchange Method [19,20], (2) to study the competitive binding of Ca(II), Mg(II) and Cu(II) by a well-characterized HA in model aqueous solutions containing low concentration of copper (10^{-8} M) and high concentrations of calcium and magnesium ($\sim 10^{-3}$ M), typical of freshwaters.

3.2 Theory

3.2.1 Kinetic Model

The Kinetic Model proposed by Olson et al. [114], and has been developed further [12,110,111,115] to measure the dissociation kinetics of metal complex ML_i , where M is free metal ion (i.e. metal aqua complex) and L_i is a naturally occurring, heterogeneous complexant such as humic substances, which are ubiquitous in the aquatic environment (charges have been omitted for simplicity). The subscript, i , represents different binding sites on the naturally-occurring heterogeneous complexant.



where the formation and dissociation rate coefficients, $k_{f,i}$ and $k_{d,i}$, are coupled by the stability coefficient, $K = k_f/k_d$, through the principle of microscopic reversibility [116].

When a competing ligand, such as oxine (8-hydroxyquinoline), is added to the sample, M-oxine is formed, and with a large excess of oxine, reaction (3.2) is driven to the right.



If each complex, ML_i , dissociates simultaneously and independently (at a rate that depends on the nature of the functional group, its position on the macromolecule, and the residual charge), the total concentration of all complexes, c_{ML} , at any time, t , is given by a summation of exponentials (equation 3.3).

$$c_{\text{ML}}(t) = \sum_{i=1}^n c_{\text{ML},i}^{\circ} [1 - \exp(-k_{d,i} \cdot t)] \quad (3.3)$$

where $c_{\text{ML},i}^{\circ}$ is the initial concentration of ML_i and $c_{\text{ML},i}(t)$ is the concentration of ML_i at any time, t . The model assumes that (i) the reactions are first-order and pseudo-first-order; (ii) reaction (3.2) is much faster than reaction (3.1), so that reaction (3.1) is the rate-determining step, and the measured kinetics then represent the kinetics of the dissociation of the metal complex, ML_i ; (iii) ML does not directly (i.e. without predissociation) react with the oxine, and (iv) the ratio of the complexed metal's concentration to free metal's concentration is much larger than unity (i.e. $c_{\text{ML}}/c_{\text{M}} \gg 1$).

3.2.2 Adsorptive Cathodic Stripping Voltammetry (AdCSV) of $\text{Cu}(\text{Ox})_2$ Complex

AdCSV has attracted considerable attention for determination of trace and ultra trace metals [117] and speciation studies [49] because unlike ASV, which is restricted to only those metals, which are soluble in mercury, AdCSV is applicable to almost all metals. This is also due to its excellent sensitivity, accuracy, precision, low-cost and because it can be applied to virtually any element provided that a suitable ligand could be found for the element of interest.

Several sensitive AdCSV methods of Cu determination with oxine, catechol, tropolone, and salicylaldehyde have been developed by van den Berg and coworkers [118-119], which have found application in the analysis of seawater. Oxine (8-hydroxyquinoline) is one of the most employed ligands in analytical determinations of transition metal cations [120]. This ligand has two acid dissociation constants with $\text{pK}_{\text{a}1} = 5.16$ and $\text{pK}_{\text{a}2} = 9.63$ [121]. These values define the relative concentration of the cationic, neutral, and anionic species at a given pH indicated as H_2Ox^+ , HOx , and Ox^- . The Cu(II)-oxine complexes have 1:1 and 1:2 stoichiometries, $\text{Cu}(\text{ox})^+$ and $\text{Cu}(\text{ox})_2$, with stability constants $\beta_{\text{Cu}(\text{Ox})^+} = 3.2 \times 10^{13}$ and $\beta_{\text{Cu}(\text{Ox})_2} = 1.6 \times 10^{26}$, respectively [122]. The structure of the complex is shown in Figure 2 [49]. This system has been thoroughly studied for mechanistic processes of adsorption of Cu(II)-oxine species on mercury electrode [122-123]. Solis et al [123] reported that the 1:2 complex $[\text{Cu}(\text{Ox})_2]$ is the predominant species at $\text{pH} > 4$.

The kinetics of metal complex dissociation in freshwaters can be modeled by employing the CLEM using 8-hydroxyquinoline (oxine) as the competing ligand, eqn (3.3) can be

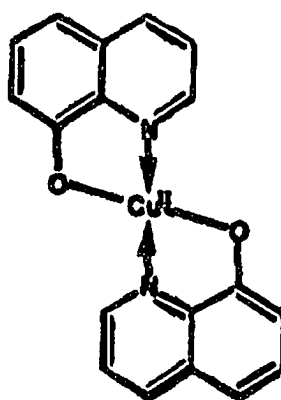


Figure 2 The structure of bis(8-hydroxyquinolinato)copper(II) used in CLEM/AdCSV [49].

rewritten as

$$[\text{Cu}^{2+}]_t = [\text{Cu(Ox)}_2]_t = \sum_{i=1}^n [\text{CuL}_i]_0 [1 - \exp(-k_i t)] \quad (3.4)$$

The concentration of “free” metal ion, $[\text{Cu}^{2+}]_t$, at any time, t , can be described by a function that rises exponentially to a limiting value.

3.3 Experimental

3.3.1 Materials and reagents

Standard solutions (1000 mg/mL) copper were purchased from SCP Science (ICP grade). Standard solutions (1000 $\mu\text{g} / \text{mL}$) of Ca^{2+} (from carbonate) and Mg^{2+} (from nitrate) were purchased from Fisher Scientific Company, NJ, USA. A 2 M stock solution of pure KNO_3 was prepared by dissolving an appropriate quantity of pure KNO_3 (Aldrich) in ultrapure water. Working standard solutions of the above metals were prepared daily by dilution of the standard solutions of the metals with ultrapure water containing 1% (v/v) ultrapure nitric acid (Seastar, Canada) to prevent metal loss by adsorption on the container wall. 0.01 M stock solution of 8-hydroxyquinoline (oxine) was prepared by dissolving an appropriate amount of the solid oxine (Fisher Scientific, certified) in pure methanol (HPLC grade). The HEPES [N-2-hydroxyethylpiperazine-N-2-ethanesulfonic acid] (BDH, ACS grade), PIPES (Piperazine-N,N'-bis[2-ethane-sulfonic acid] (SIGMA, ACS Grade), and sodium hydroxide (ACS reagent grade, BDH) were used to prepare the aqueous stock solutions of 2 M HEPES, 0.5 M PIPES, and 2 of M sodium hydroxide, respectively. Nitric acid and NaOH were used in order to adjust the pH to the desired value. The pH was checked before and after each experiment. Because the oxine

solutions can undergo photolytic decomposition, fresh solutions of oxine were prepared weekly. The HA was supplied by Dr. Les Evans (University of Guelph, Guelph, Ontario), who characterized and purified the HA according to the procedure recommended by the International Humic Substances Society [120]. The molar mass of the HA was estimated by using its bidentate complexing capacity of 4.88 mmol/g [120], since the actual molar mass was not directly ascertainable for such naturally-occurring, heterogeneous complexants as HA. A stock solution of approximately 1.00 g L⁻¹ HA was prepared by dissolving a suspension of approximately 0.100 g of the HA in 100 mL of ultrapure water in NaOH (electrolytically purified) – the pH of HA solution was 10. The pH of the HA solution was then adjusted to 8.0 with ultrapure HNO₃ [125]. Ultrapure water of resistivity 18.2 MΩ-cm, which was obtained direct from an ultrapure water system, Milli-Q-Academic (Millipore Corporation). The pH was measured with an Accumet 20 pH/conductivity meter (Fisher Scientific), fitted with an Accuplast combination glass electrode. The HA solution was stored in the dark at 4 °C until used.

3.3.2 Humic acid model solutions

A series of model solutions (100 mL volume) was prepared by adding known amounts of the HA stock solution to a 7.9×10^{-8} M copper solution to make the [Cu(II)]/[HA] mole ratios 0.1, 0.01, and 0.001. The [HA] in each solution was 0.32, 3.2, 32 mg/L, respectively, which was chosen to model a wide range of freshwater samples. The model solutions were buffered using HEPES for pH 7.0 and 8.0, or PIPES for pH 6.0, and NaOH or HNO₃ was added to the solutions depending on the pH required. A 20.00 g aliquot of the model solution was weighed and used as the test solution. A time study of a

7.9×10^{-8} M copper solution with a [Cu(II)]/[HA] mole ratio of 0.01 and a pH of 7.0 was done using Anodic Stripping Voltammetry (ASV) to determine the time required for equilibrium to be established. The results were recorded every 5 minutes. This study showed that the equilibration time between copper and HA under the above experimental conditions was about 1 hour. However, the solutions were equilibrated in the dark at room temperature for 24 hours prior to analysis. The pH of the model solution was again determined immediately prior to analysis.

3.3.3 Containers and their cleaning procedure

All containers used were made of Teflon. After cleaning with ultrapure water, they were filled to the top with 10% (v/v) nitric acid and allowed to stand at the room temperature for one week. They were then rinsed five times with ultrapure water, filled with ultrapure water, and allowed to stand until they were used. The filling water was renewed periodically to ensure continued contact with clean water.

3.3.4 Method optimization

Cyclic Voltammetry (CV) with Square Wave Voltammetry (SWV) gave evidence for the presence of two species, CuOx^+ and Cu(Ox)_2 , involved in the electrochemical reduction of the Cu(II)-oxine complexes. The presence of 1:1 complex was evident in unbuffered solutions, whereas Cu(Ox)_2 is the only one detected in the buffered solutions and is the predominant species at $\text{pH} > 4$, involves a direct transfer of two electrons in the reduction process [123]. In the presence of oxine and copper in model solutions at $\text{pH} 7.5 \pm 0.1$, a peak was observed in AdCSV at -0.56 V. The parameters of the AdCSV

method were optimized to study the dissociation kinetics of Cu(II)-HA complexes in model solutions.

3.3.4.1 Effect of adsorption time

Figure 3 shows the effect of increasing adsorption time on the AdCSV/SWV peak-height current. It was found that the peak-height current increased linearly with time up to 10 min. A further increase in the deposition time causes a decrease in the sensitivity (slope) of the peak-height current versus deposition time curve. Therefore, deposition time of less than 10 min. should be used for copper determination in freshwaters. The optimized deposition time 10 s was chosen to determine dissociation kinetics of copper in model solutions.

3.3.4.2 Effect of deposition potential

Copper-oxine complex accumulation onto mercury drop was studied as a function of potentials applied in the range between -0.2 and -1.2 V as shown in Figure 4. The reduction in the peak-height current with more negative deposition potential may be due to the saturation of the drop surface by the adsorbed copper-oxine complex [126-128]. The copper-oxine complex accumulation onto mercury drop was found to be optimum at a potential of -0.3 V.

3.3.4.3 Effect of SWV-frequency

The AdCSV/SWV peak-height current was measured as a function of the SWV frequency (Hz) as shown in Figure 5. The peak-height current increases with increasing

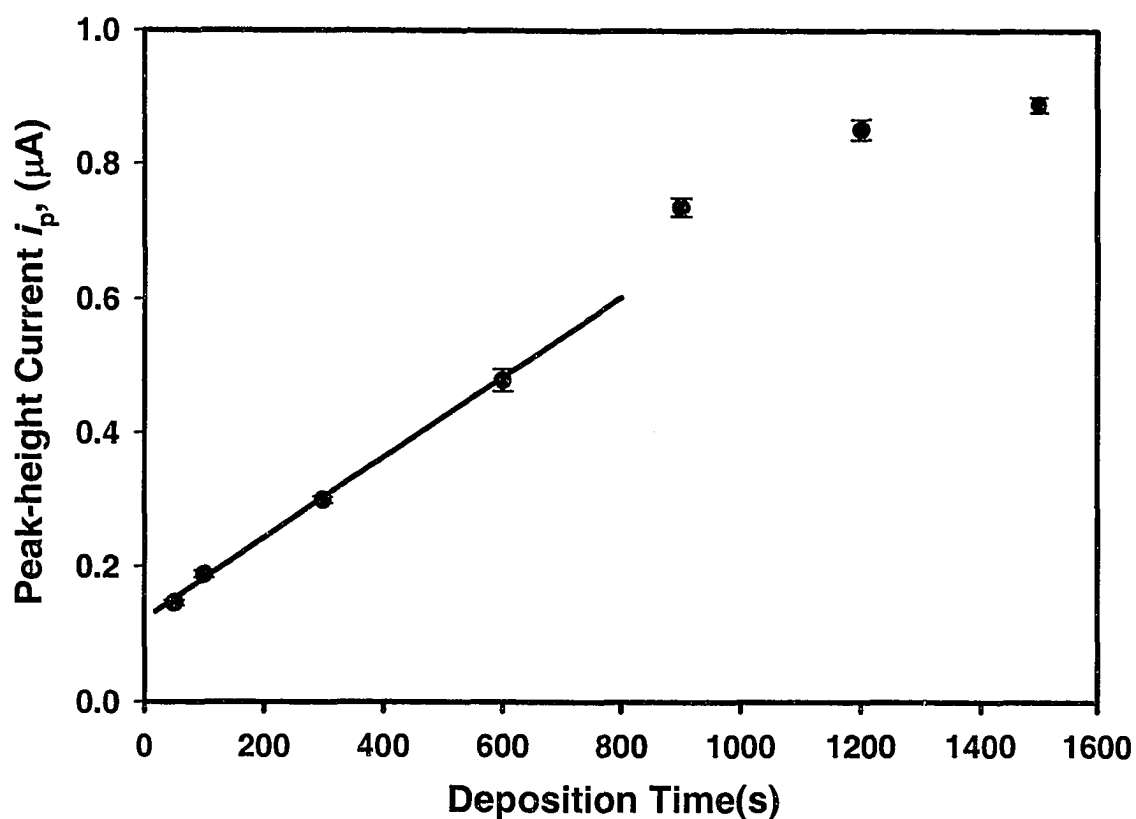


Figure 3 Effect of variation of the deposition time on the AdCSV/SWV peak-height current obtained (i_p , μA) in a model solution containing Cu(II) 7.9×10^{-8} M, oxine 1×10^{-5} M, 0.01M HEPES, pH 7.5 ± 0.1 , ionic strength 1.5×10^{-2} M, temperature 23 ± 2 °C. Error bars represent 2X standard deviation of three replicates.

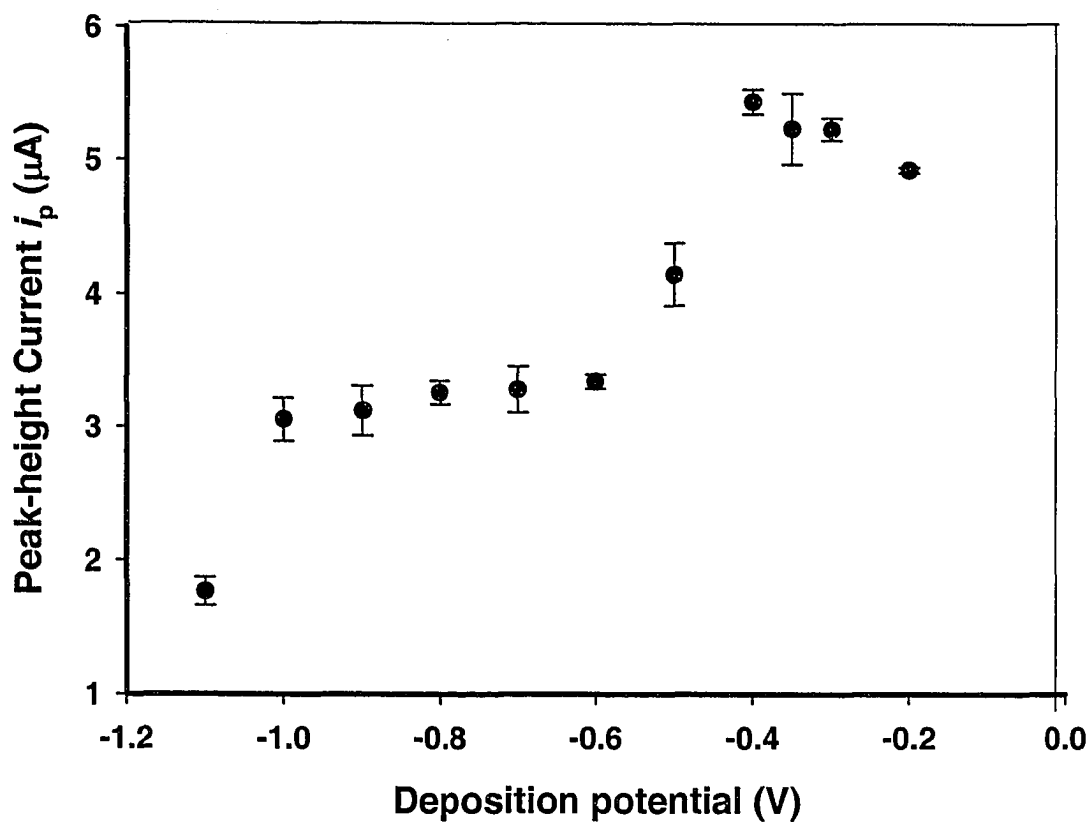


Figure 4 Effect of variation of the deposition potential on the AdCSV/SWV peak-height current obtained (i_p , μA) in a model solution containing Cu(II) 7.9×10^{-8} M, oxine 1×10^{-5} M, 0.01M HEPES, pH 7.5 ± 0.1 , ionic strength 1.5×10^{-2} M, temperature 23 ± 2 °C. Error bars represent 2X standard deviation of three replicates.

frequency; the background current of each scan also increases, but the peak-height current increases more rapidly. The background current can be subtracted as it is relatively smooth and constant during a scan. It was also found that the peak potential shifted in a negative direction with the SWV frequency. The increase of the peak-height current and negative shift in the peak potential with increasing oxine concentration were probably caused by increased stability of the adsorbed copper-oxine complex.

3.3.4.4 *Effect of oxine Concentration*

The effect of variation of oxine concentration on the AdCSV/SWV peak-height current is presented in Figure 6. Figure 6A shows that the height of reduction peak for copper increased with the oxine concentration and reached the maximum around 2.5×10^{-5} M, and then decreased at higher oxine concentrations, whereas the background current deteriorated probably because of competitive adsorption of free oxine. Weak interactions between adsorbed molecules at low oxine concentrations ($c_{\text{ox}} < 5 \times 10^{-5}$ M) have been described with a Frumkin type isotherm [128]. An oxine concentration of 1×10^{-5} M was selected as the optimum oxine concentration for the remaining optimization experiments and determination of dissociation kinetics of copper in model solutions. Shifting of the potential of the peak towards more negative direction coupled with increasing in peak-height current with increasing oxine concentrations, indicating higher stability of the adsorbed copper-oxine complex [129]. However, the decrease in the peak-height current at oxine concentrations higher than 2.5×10^{-5} M because of the competition between free oxine and copper-oxine complex on the surface of the mercury drop [129].

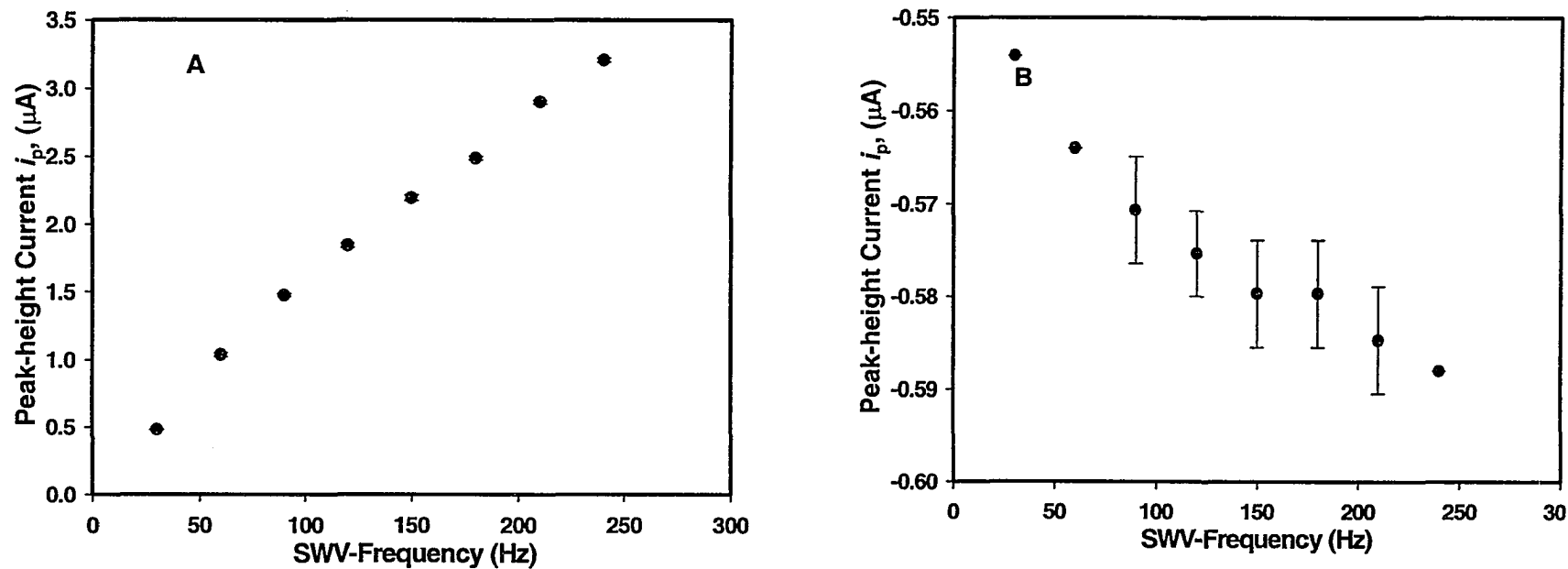


Figure 5 Effect of SWV-frequency A) on the AdCSV/SWV peak-height current (i_p , μA); B) on the potential of peak (E_p , V) obtained in a model solution containing Cu(II) 7.9×10^{-8} M, oxine 1×10^{-5} M, 0.01 M HEPES, pH 7.5 ± 0.1 , ionic strength 1.5×10^{-2} M, temperature 23 ± 2 °C. Error bars represent 2X standard deviation of three replicates. The data points without error bars have very small standard deviation of the three replicates, and hence, are not shown.

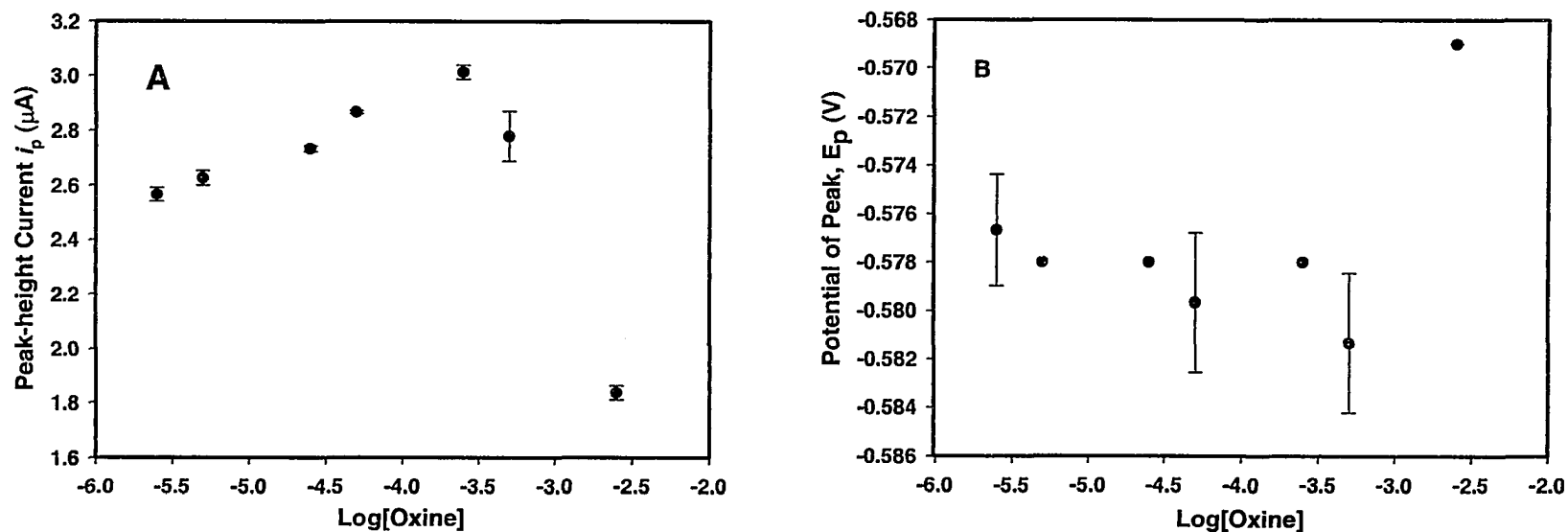


Figure 6 Effect of variation in the oxine concentration A) on the AdCSV/SWV peak-height current (i_p , μA); B) on the potential of peak (E_p , V) obtained in a model solution containing Cu(II) 7.9×10^{-8} M, oxine 1×10^{-5} M, 0.01 M HEPES, pH 7.5 ± 0.1 , ionic strength 1.5×10^{-2} M, temperature 23 ± 2 °C. Error bars represent 2X standard deviation of three replicates. The data points without error bars have very small standard deviation of the three replicates, and hence, are not shown.

3.3.4.5 *The pH effect*

The AdCSV/SWV peak-height current was measured as a function of pH in a model solution as shown in Figure 7. It was found that the peak-height current gradually increased with increasing pH up to pH 7.0; beyond pH 7.0, the peak-height current decreased with increasing pH. The potential of the peak is shifted towards a more negative direction with increasing pH, at the rate of ~ 0.05 V/pH unit at pH values between 5.5-8.0. This increase in the peak-height current as well as the negative shift in the potential of the peak with increasing pH may be the result of increased stability of copper-oxine complex, whereas the decrease in the peak-height current at a pH value above 7.0 may be caused by the hydrolysis of copper, which would increasingly affect the formation of Cu(II)-oxine complex. A similar discussion was given above for the effect of SWV-frequency on the AdCSV/SWV peak-height current. The peak-height currents obtained by this method were sufficiently sensitive to allow the labile copper determination to be performed at any pH between 6.0 and 8.0. There is no change in the pH of the model solutions before and after oxine was added to them.

3.3.5 *Apparatus*

Voltammetric measurements were carried out using a computer-controlled Autolab PGSTAT 30 potentiostat/galvanostat (Eco Chemie BV, The Netherlands). The working electrode was a static mercury drop electrode (medium drop size, "size 4") and the reference electrode was a Ag/AgCl electrode, held in a glass tube filled with a 3 M KCl solution and fitted with a porous Vycor tip (Bioanalytical Systems, USA). A platinum rod (Metrohm, Switzerland) was used as the counter electrode. Analysis of voltammetric

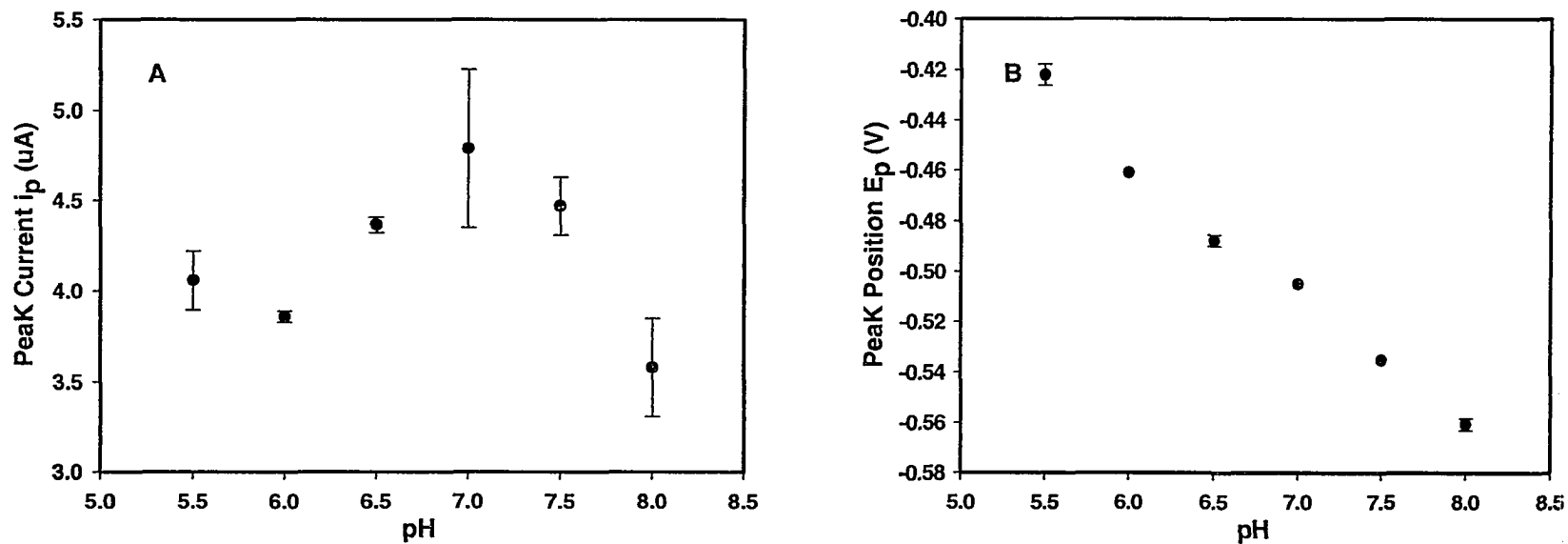


Figure 7 Effect of variation in pH A) on the AdCSV/SWV peak-height current (i_p , μA); B) on the potential of peak (E_p , V) obtained in a model solution containing Cu(II) 7.9×10^{-8} M, oxine 1×10^{-5} M, 0.01 M HEPES, pH 7.5 ± 0.1 , ionic strength 1.5×10^{-2} M, temperature 23 ± 2 °C. Error bars represent 2X standard deviation of three replicates. The data points without error bars have very small standard deviation of the three replicates, and hence, are not shown.

peaks was carried out using the General Purpose Electrochemical Software V 4.9 (Eco Chemie BV, The Netherlands). The data were transferred to and saved on a computer for subsequent data analysis.

3.3.6 Kinetic experiments

The kinetic experiments were started immediately upon addition of oxine to the test solution. The peak-height current was recorded every 22 s and the recording was continued until no further change in the signal was observed and the peak-height current achieved a maximum value. The reference solutions of no complexation, i.e. without HA, were prepared immediately prior to the test. The uptake of copper by oxine in the reference solution was sufficiently fast to complex all the copper within the first few seconds of the experiment. The sample was degassed with high-purity nitrogen (UHP, Praxair) for 15 min. prior to the measurements. Twenty microliters of 0.01M oxine were added to the sample and the adsorption of Cu(oxine)_2 on the SMDE was done for 10 s using a potential of -0.3 V (vs. $E_{\text{Ag}/\text{AgCl}}$). After a 5 s quiescent period, the adsorbed Cu(oxine)_2 complex was stripped using square-wave voltammetry. The stripping conditions were as follows: scan increment 5 mV s^{-1} , frequency 75 Hz, modulation amplitude 10 mV. The pH change in the test solution was found to be < 0.5 pH units between the beginning and the end of the experiment.

3.3.7 Data analysis

As discussed in the theoretical part, the overall reaction was treated as a pseudo-first-order and the dissociation rate coefficients and their associated kinetically distinguishable components were calculated by fitting the experimental data to a two-component

exponential-growth model by non-linear regression analysis using the Marquardt-Levenberg algorithm. The calculations were performed using SIGMAPLOT 8 computer program (SPSS Science).

3.4 Results and Discussion

It is important to highlight that there are many factors that may affect the rates of metal exchange reaction of Cu(II)-HA, such as the uncomplexed sites of HA, the deprotonation of HA at different pHs, the functional groups of the competing ligand and the hydrolysis kinetics of copper at different pH values [125]. The problem is over simplified by assuming that disjunctive pathway predominates. Hence, the dissociation of the Cu(II)-HA complex is the rate determining step.

The experimental data in Figures 8– 13 were fitted to the Kinetic Model (Eq. 3.4) to obtain the numerical values of the kinetically distinguishable components and the associated dissociation rate coefficients by non-linear regression analysis using the Marquardt-Levenberg algorithm (Tables 1- 4). It is important to realize that the two components are the minimum number of distinct components required to model the Cu(II)-HA system. Kinetic curves (Figures 8-13) of the model solutions show two kinetically distinguishable components: the rapidly rising section of the curve represents dissociation of copper aqua complex and highly labile Cu(II)-complexes (C_1) and the nearly-flat section of the curve represents slow dissociation of strong Cu(II)-HA complexes (C_2).

3.4.1 Effect of the [Cu(II)]/[HA] mole ratio on the dissociation rate coefficient of Cu(II)-HA complexes

The model system of humic acid, which has been characterized for the concentration of carboxylate and phenolate binding sites [130], allows for systematic tests of the chemical significance of the Kinetic Model over a wide range of [Cu(II)]/[HA] mole ratios. The symbol, i_o , stands for the peak-height current observed for reference solutions of Cu(II) with no humic acid; i_p stands for peak-height current observed with the sample containing Cu(II) and HA. Figure 8 presents the dissociation kinetics of Cu(II) complexes in model solutions of humic acid determined for three mole ratios of [Cu(II)]/[HA]: 0.1, 0.01 and 0.001, at pH 8.0. The [Cu(II)]/[HA] mole ratio required for saturation of the strong sites was estimated to be 0.01; to be on the safe side, a mole ratio of 0.001 was used as the lowest [Cu(II)]/[HA] mole ratio.

In Figure 8, the rapidly rising section at the beginning of the curves ($k_d \sim 10^{-2} \text{ s}^{-1}$) can be attributed to the Cu(II) aqua complex and/or rapidly-dissociating Cu(II)-HA complexes. The results suggest that Cu(II)-HA complexes with $k_d > 10^{-2} \text{ s}^{-1}$ cannot be experimentally resolved from the Cu(II) aqua complex. This represents the upper limit of the dissociation rate coefficients that can be experimentally determined within the experimental timescale of the method. The flat part (top of the curve) of all curves are probably due to the very slow dissociation rate coefficient ($k_d < 10^{-5} \text{ s}^{-1}$) of strong Cu(II)-HA complexes, which represents the lower limit of rate constants that can be measured under the experimental conditions used (i.e. an analytical window of 30 minutes) in this study. This flat part of

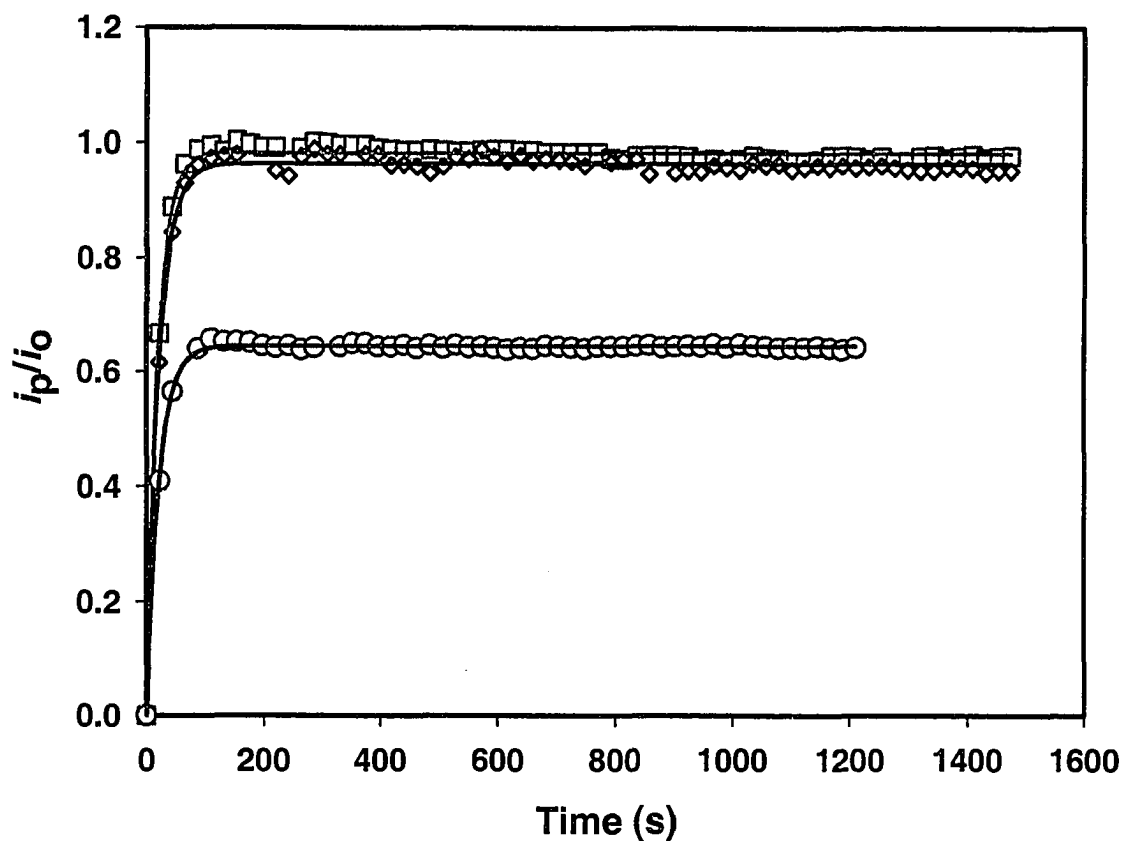


Figure 8 Lability (i_p/i_o) of Cu(II)-HA complexes for three [Cu(II)]/[HA] mole ratios in model solutions at $\text{pH } 8.0 \pm 0.1$, studied by CLEM/AdCSV, using oxine as the competing ligand. [Cu(II)] was 7.9×10^{-8} M for all solutions and [HA] was varied, [oxine] 1×10^{-5} M, HEPES 0.01 M, ionic strength 0.01 M, temperature 23 ± 2 °C. Curve A: (\square) mole ratio 0.1, [HA] = 7.9×10^{-7} M; curve B: (\diamond) mole ratio 0.01, [HA] = 7.9×10^{-6} M; curve C: (\circ) mole ratio 0.001, [HA] = 7.9×10^{-5} M. Solid lines represent non-linear curve-fitting.

the curve also represents the fraction of complexes that did not dissociate within the 30-min. measurement period. The kinetic parameters are presented in Table 1. The results indicate an increase in the dissociation rate coefficients with increasing $[\text{Cu(II)}]/[\text{HA}]$ mole ratio, suggesting that the observed dissociation rate constants are associated with weaker sites as the copper loading of the system is increased. Similar trends were also observed for dissociation of Cu(II)-HA complexes at pH 6 and 7 in Figures 9, and 10, respectively.

A unique property of naturally occurring complexants, such as humic acid, is that their metal binding properties change with the degree of metal loading of the system [84]. The decrease of the observed dissociation rate coefficients with decreasing $[\text{Cu(II)}]/[\text{HA}]$ mole ratio, can be attributed to the heterogeneous characteristics of humic acid, such as polyfunctional, polyelectrolytic and conformational properties. This suggests that humic acid has closely spaced binding energies that enable metals to be buffered over a large concentration range (several orders of magnitude) with only gradual changes in free metal ion concentration. The results are in agreement with the trend in complexation capacity observed by Town and Filella [131] for Cu(II), Zn(II), Cd(II) and Pb(II) complexes collected from a large dataset of published literature on natural waters.

Two kinetically distinguishable components were resolved for all the three mole ratios of $[\text{Cu(II)}]/[\text{HA}]$ studied (Table 1): the labile ($k \sim 10^{-2} \text{ s}^{-1}$) Cu(II)-HA complexes, which were the major fraction, and the inert ($1 < 10^{-5}$) Cu(II)-HA complexes. Other studies [70-71], however, have indicated that a large fraction (roughly 50–80%) of copper–humic

Table 1 Ligand exchange kinetics of Cu(II)-HA in model solutions, determined by CLEM/AdCSV, using 8-hydroxyquinoline (oxine) as the competing ligand. oxine 1×10^{-5} M, HEPES 0.01 M, ionic strength 0.01 M, temperature 23 ± 2 °C.

[Cu(II)]/[HA] mole ratio	pH ± 0.1	<u>Kinetically distinguishable</u>		<u>Dissociation rate</u>		R ² fitting
		<u>components</u>		<u>coefficients</u>		
		C ₁ (%)	C ₂ (%)	k ₁ , (s ⁻¹ 10 ⁻²)	k ₂ , (s ⁻¹ 10 ⁻⁵)	
0.1	8.0	98±5	2±1	5.3±0.3	<10 ⁻⁶ (inert)	0.992
0.01	8.0	96±2	4±1	4.7±0.3	<10 ⁻⁶ (inert)	0.993
0.001	8.0	67±1	33± 1	4.4± 1.7	<10 ⁻⁶ (inert)	0.998
0.1	7.0	99±2	1±1	6.0±0.2	1.6±6.2	0.997
0.01	7.0	95±2	5± 1	5.0±0.3	<10 ⁻⁶ (inert)	0.994
0.001	7.0	65±1	35± 1	4.7±1.0	<10 ⁻⁶ (inert)	0.995
0.1	6.0	100±3	---	5.3±0.4	--	0.988
0.01	6.0	90±4	10± 1	5.1±0.5	<10 ⁻⁶ (inert)	0.982
0.001	6.0	65±2	35±1	4.5± 2	<10 ⁻⁶ (inert)	0.998

Uncertainties represent 95.5% confidence limits in the non-linear regression analysis, for an individual measurement.

acid complexes is usually very labile. Cu(II)-HA complexes shows two complexing components with different dissociation kinetics [130]. Discrete dissociation rate constants are sometimes found for copper-humic acid complexes [15], but their identification and interpretation is rather difficult. Langford and Gutzman [27] found two complexing sites in Cu(II)-HA complexes with rate constants of 0.093 and 0.0078 s⁻¹, in agreement with the data obtained in present work.

3.4.2 The effect of pH on the dissociation rate coefficient of Cu(II)-HA complexes

Figures 8-10 and Table 1 present dissociation kinetics of Cu(II)-HA in model solutions determined for three [Cu(II)]/[HA] mole ratios at pH 6, 7 and 8. As the pH is decreased from 8.0 to 6.0, there is a slight increase in the percentage of the faster (C₁) component with a corresponding decrease in the slower (C₂) component; the dissociation rate coefficient (k₁) also slightly increases. This increase in C₁ and k₁ is very small, suggesting that the characteristics of the groups of the copper complexes represented collectively by C₁ and C₂ probably remain even though they have minute changes as shown in Table 1.

The observed difference in the lability is probably a reflection of their differences in the bonding involved in these Cu(II)-HA complexes: a phthalate-like structure is more probable for Cu(II)-HA complexes at pH 6.0 and 7.0 since carboxyl groups of the HA are being deprotonated, whereas a salicylate-like structure might be predominated at pH 8 since phenolic groups also being deprotonated [125]. The observed trend is consistent with more strong binding sites on the HA being available for binding by Cu²⁺ because of deprotonation of the functional group at higher pH values.

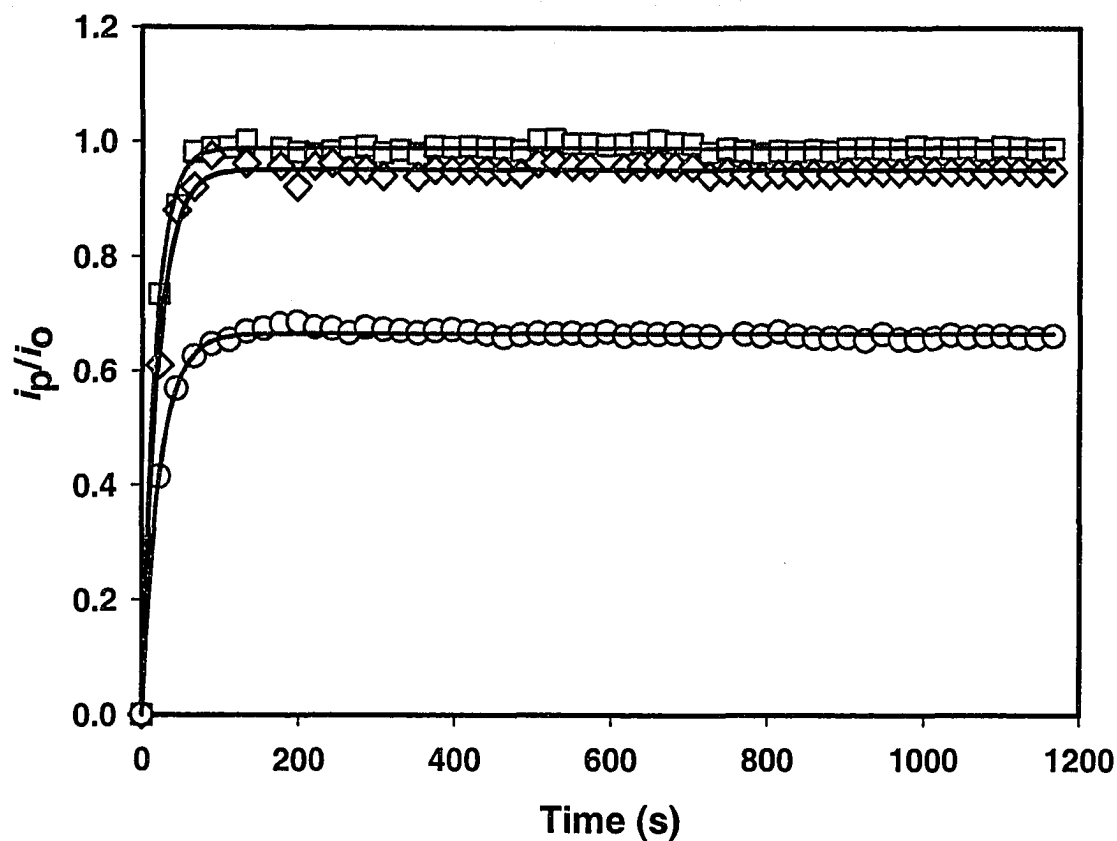


Figure 9 Lability (i_p/i_o) of Cu(II)-HA complexes for three [Cu(II)]/[HA] mole ratios in model solutions at $\text{pH } 7.0 \pm 0.1$, studied by CLEM/AdCSV, using oxine as the competing ligand. [Cu(II)] was 7.9×10^{-8} M for all solutions and [HA] was varied, [oxine] 1×10^{-5} M, HEPES 0.01 M, ionic strength 0.01 M, temperature 23 ± 2 °C. (\square) mole ratio 0.1, [HA] = 7.9×10^{-7} M; (\diamond) mole ratio 0.01, [HA] = 7.9×10^{-6} M; (\circ) mole ratio 0.001, [HA] = 7.9×10^{-5} M. Solid lines represent non-linear curve-fitting.

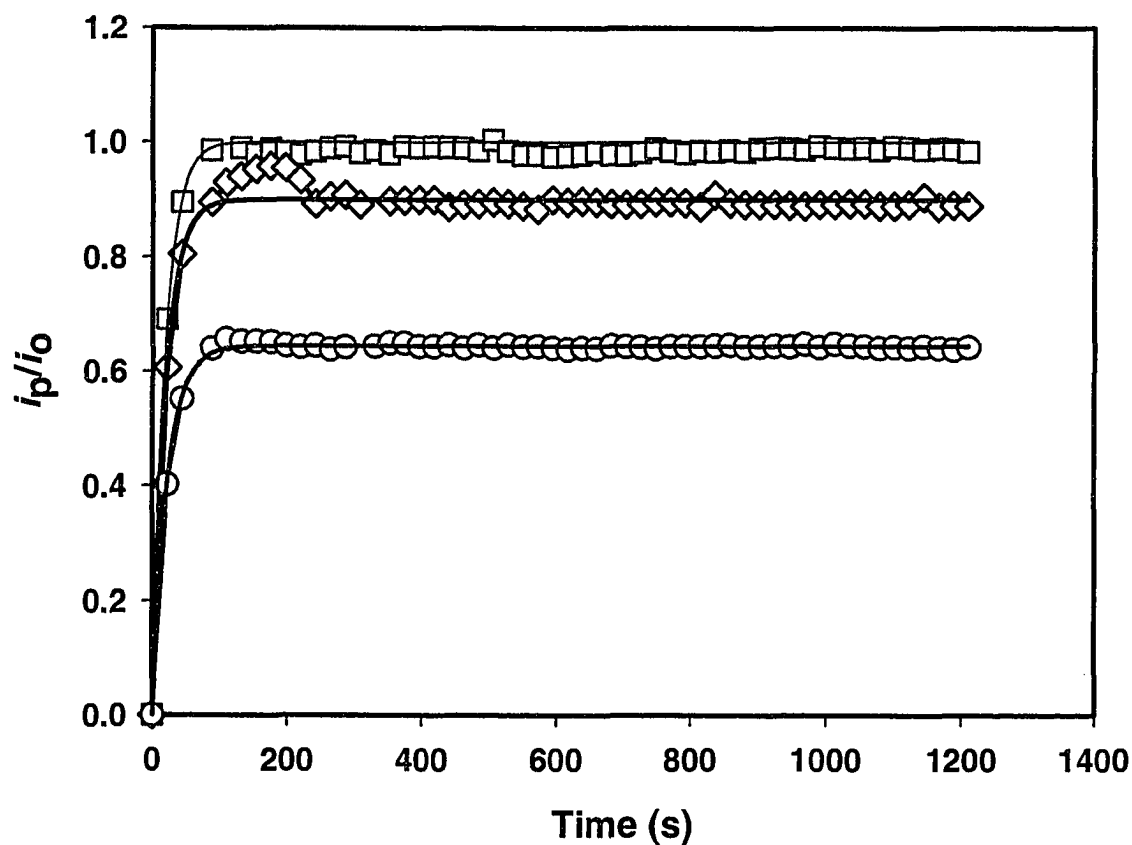


Figure 10 Lability (i_p/i_o) of Cu(II)-HA complexes for three [Cu(II)]/[HA] mole ratios in model solutions at pH 6.0 ± 0.1 , studied by CLEM/AdCSV, using oxine as the competing ligand. [Cu(II)] was 7.9×10^{-8} M for all solutions and [HA] was varied, [oxine] 1×10^{-5} M, PIPES 0.01 M, ionic strength 0.01 M, temperature 23 ± 2 °C. (□) mole ratio 0.1, [HA] = 7.9×10^{-7} M; (◇) mole ratio 0.01, [HA] = 7.9×10^{-6} M; (○) mole ratio 0.001, [HA] = 7.9×10^{-5} M. Solid lines represent non-linear curve-fitting.

3.4.3 Competitive binding of Ca(II), Mg(II) and Cu(II) by a well-characterized HA

There is a debt in the literature about the competition of major cations (Ca^{2+} and Mg^{2+}) with copper for the binding sites on humic substances [9, 132-137]. Most of these studies reported that there is a small effect of the competition of Ca and Mg on the binding of humic substances. Mandal et al. [12] have reported that overwhelming amounts of Ca^{2+} and Mg^{2+} promotes release of large fraction of the Ni(II)-FA complexes as free Ni^{2+} ions.

3.4.3.1 Effect of the concentrations of Ca(II) on the lability of the Cu(II)-HA complexes

The effect of varying concentrations of Ca(II) on the lability of the Cu(II)-HA complexes in the model aqueous solutions is shown in Figure 11. The results suggest that in the absence of Ca(II), the strong binding sites (which are few) of the HA are occupied by Cu(II), forming strong complexes, which are inert (bottom curve). However, in the presence of high and increasing concentrations of Ca(II) (1×10^{-4} – 1×10^{-3} M) (each curve from bottom to top), has a small effect on the lability of the Cu(II)-HA complexes. The values for kinetic parameters of the Cu(II)-HA complexes in the presence of various concentrations of Ca(II) and constant concentrations of Cu(II) and HA are presented in Table 2, which shows that the percentage of the fastest kinetically distinguishable component (%C₁), increased slightly, from 67 to 70% as the concentration of the Ca(II) was increased incrementally, from 0 to 1×10^{-3} M. Also, the dissociation rate coefficient (k_1) of the fastest kinetically distinguishable component (%C₁) increased, from $4.4 \times 10^{-2} \text{ s}^{-1}$ to $5.3 \times 10^{-2} \text{ s}^{-1}$ as the concentration of the calcium was increased incrementally.

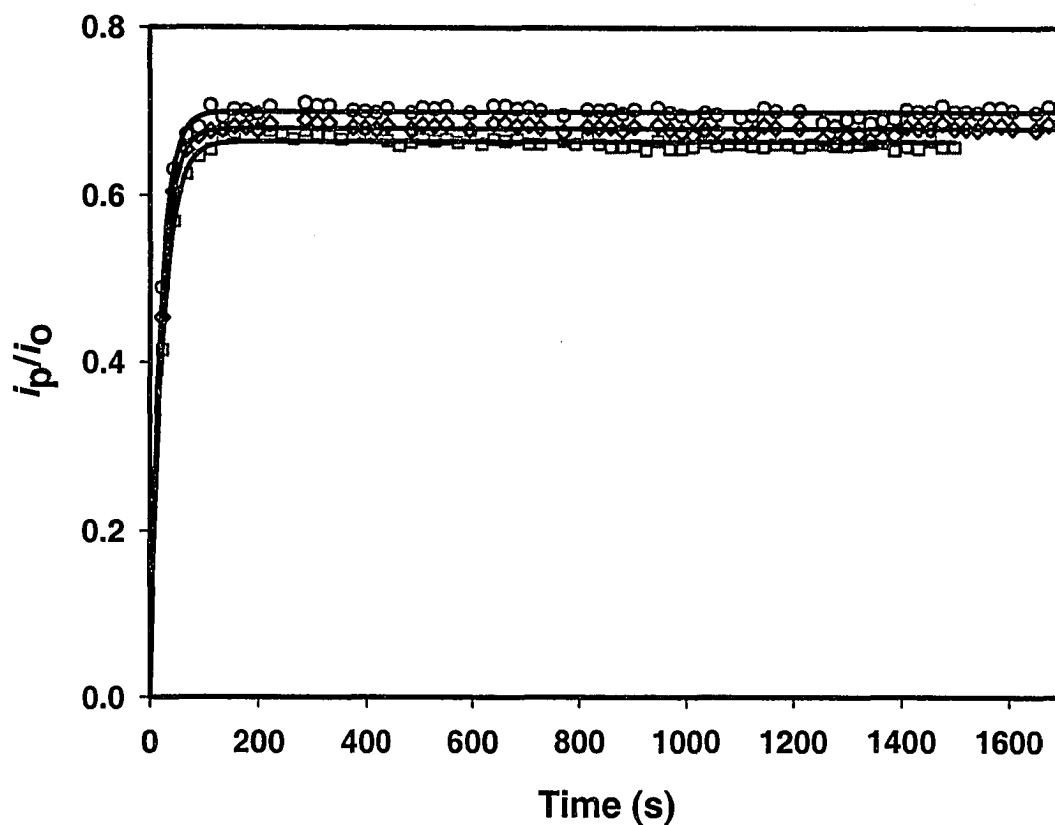


Figure 11 Effect of various concentrations of Ca(II) on the lability (i_p/i_o) of Cu(II)-HA complexes in model solutions, determined by CLEM/AdCSV, using oxine as the competing ligand. Concentrations of Cu(II) and the HA were same for all curves. Bidentate complexing capacity of the HA 4.88 mmole/g. pH 8.0 ± 0.1 , [oxine] 1×10^{-5} M, HEPES 0.01 M, ionic strength 0.01 M, temperature 23 ± 2 °C. (□), [Cu(II) 7.9×10^{-8} M] + [HA 7.9×10^{-5} M]; (○), [Cu(II) 7.9×10^{-8} M] + [Ca(II) 1×10^{-4} M] + [HA 7.9×10^{-5} M]; (◇), [Cu(II) 7.9×10^{-8} M] + [Ca(II) 1×10^{-3} M] [HA 7.9×10^{-5} M]. Solid lines respresent non-linear curve-fitting.

Table 2 Effect of various concentrations of Ca(II) on the ligand-exchange kinetics of Cu(II)-HA in model solutions, determined by CLEM/AdCSV, using 8-hydroxyquinoline (oxine) as the competing ligand. pH 8.0 ± 0.1 , [Cu(II)]/[HA] mole ratio 0.001, [oxine] 1×10^{-5} M, HEPES 0.01 M, ionic strength 0.01 M, temperature 23 ± 2 °C.

$$[[\text{Cu(II)} 7.9 \times 10^{-8} \text{ M}] + [\text{HA } 7.9 \times 10^{-5} \text{ M}] + [\text{Ca(II)}]]$$

Ca(II), M	<u>Kinetically distinguishable</u>		<u>Dissociation rate</u>		R ² fitting
	<u>components</u>		<u>coefficients</u>		
	C ₁ (%)	C ₂ (%)	k ₁ , (s ⁻¹ 10 ⁻²)	k ₂ , (s ⁻¹ 10 ⁻⁶)	
nil	67±1	33±1	4.4±0.2	<10 ⁻⁶ (inert)	0.995
1.0 X 10 ⁻⁴	68±2	32± 1	5.0±0.2	<10 ⁻⁶ (inert)	0.997
1.0 X 10 ⁻³	70±1	30± 3	5.3 ±0.3	<10 ⁻⁶ (inert)	0.966

Uncertainties represent 95.5% confidence limits in the non-linear regression analysis, for an individual measurement.

3.4.3.2 Effect of the concentrations of Mg(II) on the lability of the Cu(II)-HA complexes

Figure 12 presents the effect of the increasing concentrations of Mg(II) on the lability (i_p/i_o) of the Cu(II)-HA complexes in the model aqueous solutions and shows that almost the same behaviour as shown by Ca(II) (Figure 12). In the absence of Mg(II), the strong binding sites of HA (which are few) are occupied by Cu(II), forming strong Cu(II)-HA complexes, which are inert (bottom curve). However, the presence of high and increasing concentrations of Mg(II) ($1 \times 10^{-4} - 1 \times 10^{-3}$ M) (each curve from bottom to top) has a small effect on the lability (i_p/i_o) of the Cu(II)-HA complexes in the model aqueous solutions. The lability (i_p/i_o) of the Cu(II)-HA complexes increased slightly as the concentrations of the Mg(II) in the solution was increased. Table 3 shows the kinetic parameters of the dissociation of Cu(II)-HA complexes in presences of Mg(II). It is clear that the percentage of the fastest kinetically distinguishable component ($\%C_1$) increased slightly from 67 to 70% as the concentration of the magnesium was increased, from 0 to 1×10^{-3} M. Also, the dissociation rate coefficient (k_1) of the fastest kinetically distinguishable component (C_1) increased from $4.4 \times 10^{-2} \text{ s}^{-1}$ to $5.9 \times 10^{-2} \text{ s}^{-1}$ as the concentration of the magnesium was increased incrementally.

3.4.3.3 Effect of the concentrations of Ca(II) plus Mg(II) on the lability of the Cu(II)-HA complexes

Figure 13 presents the effect of the varying concentrations of Ca(II) plus Mg(II) on the lability (i_p/i_o) of the Cu(II)-HA complexes in model aqueous solutions and shows almost the same behaviour as shown in Figures 11 and 12. In the absence of Ca(II) and Mg(II), copper occupies strong binding sites (which are few) of the HA, forming strong Cu(II)-HA complexes, which are inert (bottom curve). However, the presence of high and

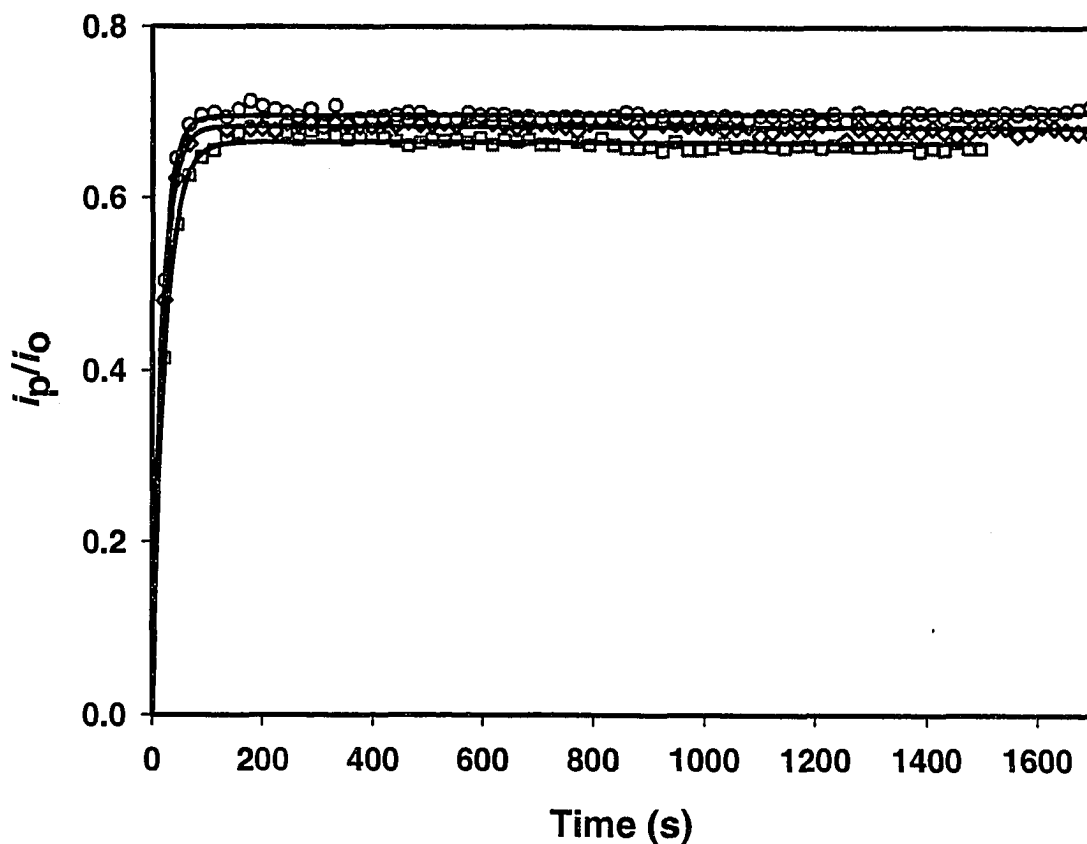


Figure 12 Effect of various concentrations of Mg(II) on the lability (i_p/i_o) of Cu(II)-HA complexes in model solutions, determined by CLEM/AdCSV, using oxine as the competing ligand. Concentrations of Cu(II) and the HA were same for all curves. Bidentate complexing capacity of the HA 4.88 mmole/g. pH 8.0 ± 0.1 , [oxine] 1×10^{-5} M, HEPES 0.01 M, ionic strength 0.01 M, temperature 23 ± 2 °C. (□), [Cu(II) 7.9×10^{-8} M] + [HA 7.9×10^{-5} M]; (○), [Cu(II) 7.9×10^{-8} M] + [Mg(II) 1.0×10^{-4} M] + [HA 7.9×10^{-5} M]; (Δ), [Cu(II) 7.9×10^{-8} M] + [Mg(II) 1.0×10^{-3} M] [HA 7.9×10^{-5} M]. Solid lines represent non-linear curve-fitting.

Table 3 Effect of various concentrations of Mg(II) on the ligand-exchange kinetics of Cu(II)-HA in model solutions, determined by CLEM/AdCSV, using 8-hydroxyquinoline (oxine) as the competing ligand. pH 8.0 ± 0.1 , [Cu(II)]/[HA] mole ratio 0.001, [oxine] 1×10^{-5} M, HEPES 0.01 M, ionic strength 0.01 M, temperature 23 ± 2 °C.



Mg(II), M	<u>Kinetically distinguishable</u>		<u>Dissociation rate</u>		R^2 fitting
	<u>components</u>		<u>coefficients</u>		
	$C_1(\%)$	$C_2(\%)$	$k_1, (s^{-1} 10^{-2})$	$k_2, (s^{-1} 10^{-6})$	
nil	67±2	33± 1	4.4±0.5	<10 ⁻⁶ (inert)	0.969
1.0 X 10 ⁻⁴	68±1	32±1	5.5±0.2	<10 ⁻⁶ (inert)	0.997
1.0 X 10 ⁻³	70±3	30± 1	5.9 ±0.2	<10 ⁻⁶ (inert)	0.870

Uncertainties represent 95.5% confidence limits in the non-linear regression analysis, for an individual measurement.

increasing concentrations of Ca(II) plus Mg(II) (1.0×10^{-4} – 1.0×10^{-3} M) (each curve from bottom to top) has a very small increase on the lability of the Cu(II)-HA complexes in model aqueous solutions (more copper released from the Cu(II)-HA complexes as the concentrations of the Ca(II) plus Mg(II) in the solution was increased). The values for kinetic parameters of Cu(II)-HA complexes in the presence of varying concentrations of Ca(II) plus Mg(II) and constant concentrations of Cu(II) and HA are presented in Table 4. Comparison of Figures 11 and 12 with Figure 13 shows that Cu(II)-HA complexes have the same lability in presence of Ca(II) and Mg(II) when they are together as compared with the lability of the Cu(II)-HA complexes when either Ca(II) or Mg(II) is present alone, which indicate that this behavior is due to a mass effect.

In Figures 12-14 and Tables 2-4, it is clear that the presence of high concentrations of Ca(II) and/or Mg(II) ($\sim 10^{-3}$ M) in model aqueous solutions has small effects on the binding of Cu(II) by the HA. The results have shown that in the presence of increasing concentrations of Ca(II) and Mg(II) release a little greater fraction of the Cu(II) in model aqueous samples as free Cu^{2+} ion (i.e. Cu-aqua complex).

The results described above are probably the composite effect of the following factors. The first factor is the competition: when Ca(II) and Mg(II) are present at high molar concentrations, they compensate for their relatively weak humic acid-binding affinities [12]. The second factor is polyelectrolyte effect, which can greatly strengthen the binding of metal ions (e.g., Cu(II)) by polyanions such as humic acid. Total binding energy metal between metal cation and its surrounded ligand consists of two components: covalent

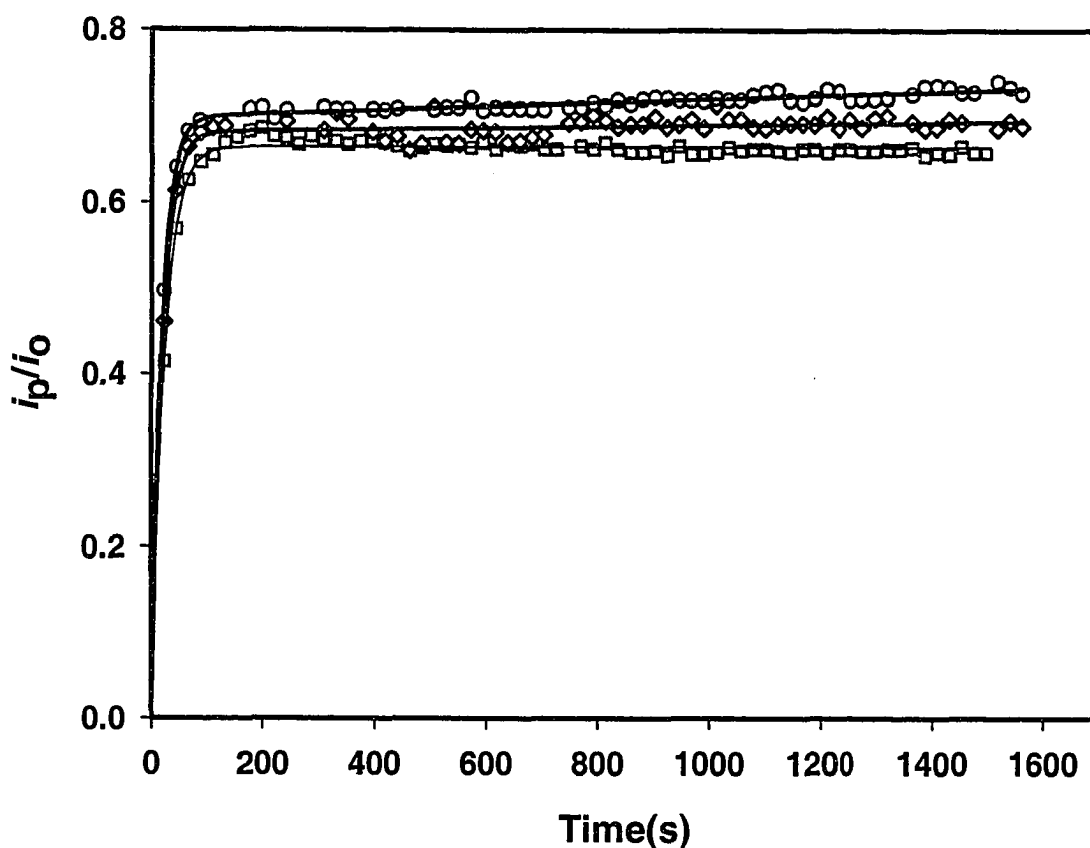


Figure 13 Effect of various concentrations of Mg(II) plus Ca(II) on the liability (i_p/i_o) of Cu(II)-HA complexes in model solutions, determined by CLEM/AdCSV, using oxine as the competing ligand. Concentrations of Cu(II) and the HA were same for all curves. Bidentate complexing capacity of the HA 4.88 mmole/g. pH 8.0 ± 0.1 , [oxine] 1×10^{-5} M, HEPES 0.01 M, ionic strength 0.01 M, temperature 23 ± 2 °C. (□), [Cu(II) 7.9×10^{-8} M] + [HA 7.9×10^{-5} M]; (○), [Cu(II) 7.9×10^{-8} M] + [Mg(II) 5.0×10^{-5} M] + [Ca(II) 5.0×10^{-5} M] + [HA 7.9×10^{-5} M]; (Δ), [Cu(II) 7.9×10^{-8} M] + [Mg(II) 5×10^{-4} M] + [Ca(II) 5.0×10^{-4} M] + [HA 7.9×10^{-5} M]. Solid lines represent non-linear curve-fitting.

Table 4 Effect of various concentrations of Ca(II) plus Mg(II) on the ligand-exchange kinetics of Cu(II)-HA in model solutions, determined by CLEM/AdCSV, using 8-hydroxyquinoline (oxine) as competing ligand. pH 8.0 ± 0.1 , [Cu(II)]/[HA] mole ratio 0.001, [oxine] 1×10^{-5} M, HEPES 0.01 M, ionic strength 0.01 M, temperature 23 ± 2 °C.



Ca(II), M	Mg(II), M	<u>Kinetically distinguishable</u>		<u>Dissociation rate</u>		R ² fitting
		<u>components</u>		<u>coefficients</u>		
		C ₁ (%)	C ₂ (%)	k ₁ , (s ⁻¹ 10 ⁻²)	k ₂ , (s ⁻¹ 10 ⁻⁵)	
nil	nil	67±1	33±1	4.4±0.5	4.2±0.7	0.995
5.0 X 10 ⁻⁵	5.0 X 10 ⁻⁵	68±2	32±1	5.2±0.4	2.7± 2.0	0.989
5.0 X 10 ⁻⁴	5.0 X 10 ⁻⁴	70±1	30 ±0	5.6 ±0.2	7.5±1.0	0.998

Uncertainties represent 95.5% confidence limits in the non-linear regression analysis, for an individual measurement.

component and electrostatic component (coulombic interaction). However, presence of high concentration of major cations reduces the coulombic part due to the screening effect and increasing the lability of Cu(II)-HA complexes leading to its release as free copper ion.

3.5 Originality

The trace-metal complexation properties of humic acid in freshwaters are much less known than those of fulvic acid because of their very different chemical and physical characteristics. This Chapter has presented the results of studies of complexation characteristics of Cu(II) with humic acid, which are radically different from those of Cu(II) with fulvic acid reported by other workers. Herein lies the originality of this work, which is presented for the first time.

-- Chapter 4 --

**Kinetic Speciation of Nickel in Atmospheric Precipitation using
Adsorptive Cathodic Stripping Voltammetry**

4.1 Introduction

Local equilibrium assumption for transition metal complexation in freshwaters is always hazardous, for Ni(II) complexation, especially risky. Slow coordination kinetics of *3d*-transition metals are most likely to be observed in systems containing mixtures of strong and weak ligands and high concentrations of alkaline earth metals or mixtures of competing transition metals, especially those involved in double exchange reaction [116]. The complexation kinetics of *3d*⁸ Ni(II) are known to be slow in water because of unfavourable changes in Ligand Field Stabilization Energy (LFSE) during complex formation [138]. Slow Ni(II) ligand exchange kinetics between DOM and dimethylglyoxime (half-life: 5 to 95 h) was observed by Xue et al. [139] in an oligotrophic lake, and in a small river affected by inputs from sewage effluents and agriculture in Switzerland.

Mandal et al. [12,14] have reported that *3d*-transition metals such as Cu(II) and Co(II) (especially Cu(II)) strongly affects the complexation reaction of Ni(II)-FA complexes in model solutions and in freshwaters. Trace concentrations Cu(II) and Co(II) have been found to successfully compete with Ni(II) in unpolluted freshwaters for the binding sites on DOC [10-11]. On the contrary, the comparable influence of major cations, Ca²⁺ and Mg²⁺, on the Ni(II)-DOC binding, was observed only when the Ca²⁺ and Mg²⁺ are present in large amounts ($\sim 10^{-3} - 10^{-5}$ M) over the nickel concentration ($\sim 10^{-8}$ M) [139].

Adsorptive Cathodic Stripping Voltammetry (AdCSV) with dimethylglyoxime (DMG) has been used for nickel determination [141-142] and equilibrium speciation [143-144] in natural waters. Recent voltammetric studies indicate that under marine conditions, more

than 95% of the total nickel is organically complexed [143]. The Dissociation Kinetics of Ni(II)-FA complexes has been studied using CLEM with Chelex 100 as the competing ligand and Graphite Furnace Atomic Absorption Spectrometry (GFAAS) or Inductively-Coupled Plasma - Mass Spectrometry (ICP-MS) to measure the dissociation rate coefficients [14,110-112]. However, the published literature on AdCSV of nickel reports on the kinetic speciation of nickel in natural waters [113,145]. In this work, Adsorptive Cathodic Stripping Voltammetry was applied to investigate the dissociation kinetics of nickel complexes in samples of soil solutions collected from the Sudbury (Ontario) area, using CLEM with DMG as the competing ligand.

This Chapter presents the results which show the effects of annual variations in the metal loadings and of seasonal changes on the freshwater environment that were impacted by industrial mining and metallurgical operations in Canada's Sudbury (Ontario) region. These effects had not been studied by an earlier worker from this laboratory [146]. Herein lies the originality of this work, which is presented for the first time.

4.2 Theory

As discussed in chapter 3, in the presence of a large excess of a competing ligand, such as DMG in the determination of Ni, eqn (3.3) can be rewritten as

$$[\text{Ni}^{2+}]_t = [\text{Ni}(\text{DMG})_2]_t = \sum_{i=1}^n [\text{NiL}_i]_0 [1 - \exp(-k_i t)] \quad (4.1)$$

The concentration of "free" metal ion at any time t , $[\text{Ni}^{2+}]_t$, can be described by an exponential function that rises to a limiting value.

4.3 Experimental

4.3.1 Materials and reagents

Standard solutions (1000 mg/mL) of nickel were purchased from SCP Science (ICP grade). A 2 M stock solution of pure KNO_3 was prepared by dissolving an appropriate quantity of pure KNO_3 (Aldrich) in ultrapure water. Working standard solutions were prepared daily by dilution of the stock standard solutions with ultrapure water; the solution was made to contain 1% (v/v) ultrapure nitric acid (Seastar, Canada) to prevent the metal loss by adsorption on the container wall. A stock solution of 0.1 M dimethylglyoxime (DMG) was prepared by dissolving an appropriate amount of the solid DMG (Fisher Scientific, certified reagent) in ethanol (Spectro grade). The pH buffer solution was 2 M sodium acetate (NaOAc) mixed with acetic acid. A 2 M stock solution of sodium acetate was prepared by dissolving an appropriate quantity of sodium acetate trihydrate (ACS grade/BDH) in ultrapure water. The sodium acetate solution was then purified of metals by electrolysis at -1.5 V vs. E_{SCE} for at least 48 h. immediately prior to its use. The electrolysis was continued while the sodium acetate aqueous solution was drained from the electrolysis cell in order to make sure that the impurity metals removed by electrolysis did not go back into the sodium acetate aqueous solution on the termination of electrolysis. A 2 M stock solution of acetic acid was prepared by diluting glacial acetic acid (ACS grade/Anachemia) with ultrapure water. 2 M aqueous NaOH (ACS reagent grade, BDH) was added to it to adjust the pH to 5.5. Ultrapure water of resistivity 18.2 $\text{M}\Omega\cdot\text{cm}$ was obtained direct from a Milli-Q-Plus water purification system (Millipore Corporation).

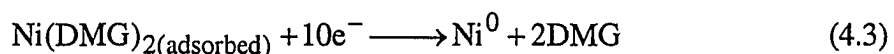
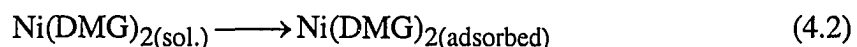
4.3.2 Containers and their cleaning procedure

Containers and their cleaning procedures were the same as presented in section 3.3.3 (chapter 3).

4.3.3 Method optimization

The high selectivity of dimethylglyoxime (DMG) for complexation and the great stability of the $\text{Ni}(\text{DMG})_2$ precipitate are due to the unusual structure of the solid $\text{Ni}(\text{DMG})_2$ complex. DMG forms a red, square-planar, strong chelate, $\text{Ni}(\text{DMG})_2$, with Ni(II). The square-planar bis(dimethylglyoximate)Ni(II) complex has two planar units stacked one on another so that the nickel “atoms” are bonded [147] with the structure shown in Figure 14 [148].

”The electrochemical measurements are done after the adsorption of the $\text{Ni}(\text{DMG})_2$ complex on the mercury electrode [143-144] and the reduction of the adsorbed complex, which according to Ma et al. [141], proceeds by a stepwise reduction involving 10 electrons.



Pihlar et al. [140] have reported that the reaction of $\text{Ni}(\text{DMG})_2$ reduction on a hanging mercury drop electrode is first-order with respect to the concentration of Ni^{2+} . The peak current as measured by AdCSV is proportional to the concentration of $\text{Ni}(\text{DMG})_2$ adsorbed on the mercury electrode surface [141,149]. Provided that both adsorption of the $\text{Ni}(\text{DMG})_2$ complex from the aqueous solution on the mercury electrode surface

(equation 4.2) [150], and reduction of the adsorbed complex (equation 4.3) are fast, the increasing rate of the measured peak current corresponds to the rate of formation of $\text{Ni}(\text{DMG})_{2(\text{sol.})}$ [151]. In the presence of DMG and Ni in ultrapure water at $\text{pH } 5.0 \pm 0.1$, a peak (current) was obtained by AdCSV at -0.84 V . The parameters of the AdCSV method were varied to optimize the analytical conditions to study the dissociation kinetics of Ni(II)-DOC complexes in the samples of soil solutions described later in section 4.3.4.

4.3.3.1 Effect of duration of adsorption (to be called adsorption time)

The effect of increasing adsorption time on the peak-height current of Adsorptive Cathodic Stripping Voltammetry/Square Wave Voltammetry (AdCSV/SWV) in a model solution is presented Figure 15, which shows that the peak-height current increased linearly with time up to 3 min. Further increase in the deposition time causes a decrease of the sensitivity (slope) of the peak-height current versus deposition time curves. This is probably caused saturation of the Hg drop surface. Deposition time of 10 seconds was employed for the kinetic studies of the nickel complexes in soil solutions using CLEM/AdCSV.

4.3.3.2 Effect of deposition potential

In the AdCSV/SWV method, the applied potential on the Static Mercury Drop Electrode (SMDE) affects the efficiency of the deposition during the deposition step. A series of the potentials ranging between -0.1 and -1.1 V were applied to determine the optimum

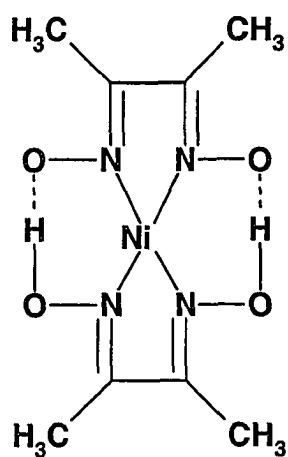


Figure 14 The structure of bis(dimethylglyoximate)nickel(II) used in CLEM/AdCSV [148].

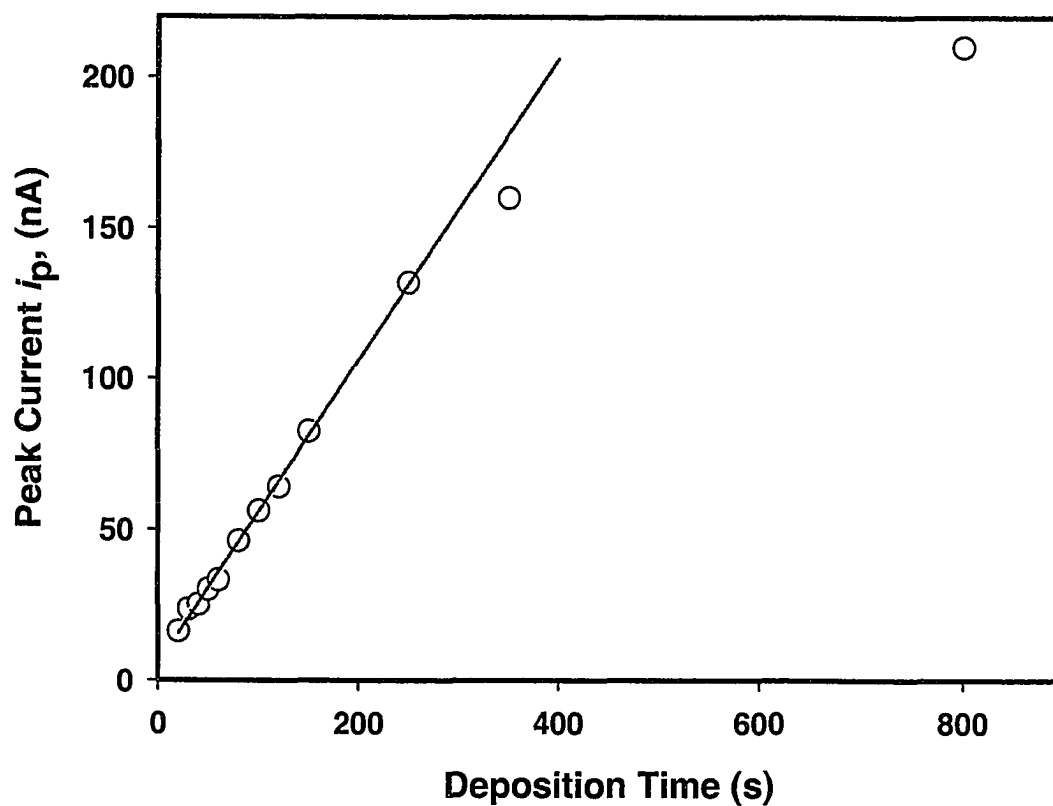


Figure 15 Effect of variation of the deposition time on the AdCSV/SWV peak-height current (i_p , μA) obtained in a model solution containing Ni(II) 2.9×10^{-8} M, 0.02M HEPES, DMG 1×10^{-3} M, pH 7.5 ± 0.1 , ionic strength 2.0×10^{-2} M, temperature 23 ± 2 °C.

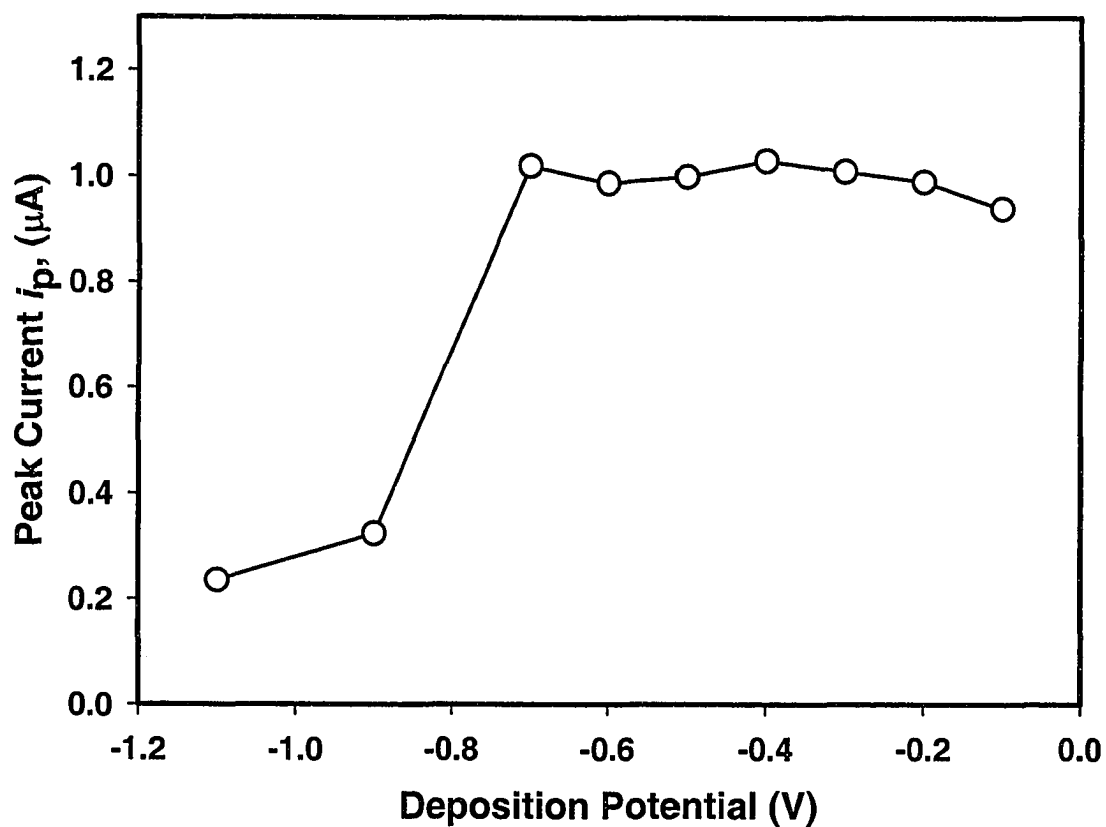


Figure 16 Effect of variation of the deposition potential on the AdCSV/SWV peak-height current (i_p , μA) obtained in a model solution containing Ni(II) 7.5×10^{-7} M, 0.02M HEPES, DMG 1×10^{-3} M, pH 7.5 ± 0.1 , ionic strength 2.0×10^{-2} M, temperature 23 ± 2 °C.

potential as shown in Figure 16. A large reduction of the peak-height current with more negative deposition potential may be due to the saturation of the mercury drop surface by nickel-DMG complex. The nickel accumulation onto mercury drop was found to be optimum at a potential of -0.6 V.

4.3.3.3 *Effect of SWV-frequency*

The AdCSV/SWV peak-current height was measured as a function of measurement-frequency (Hz) as shown in Figure 17. It was found that the peak current linearly increased with increasing frequencies up to 150 Hz. Above this frequency, ill-defined peaks and very high background currents were obtained. According to van den Berg [152], for short pulse widths, the total measured current is strongly influenced by the capacitive background component; consequently, sensitivity decreases. A frequency of 100 Hz was selected to be the optimum frequency. With increasing frequency, the potentials corresponding to peak currents were shifted to more negative values, indicating irreversible nature of the reduction process [153].

4.3.3.6 *Effect of DMG concentration*

The effect of the variation of DMG concentration on AdCSV/SWV peak-height current is presented in Figure 18. The peak height increased with increasing DMG concentrations up to 1.0×10^{-4} M and became nearly constant at DMG concentration higher than 1.0×10^{-4} M. DMG concentration of 1.0×10^{-3} M was therefore used as the optimum experimental condition for determination of nickel speciation in freshwaters

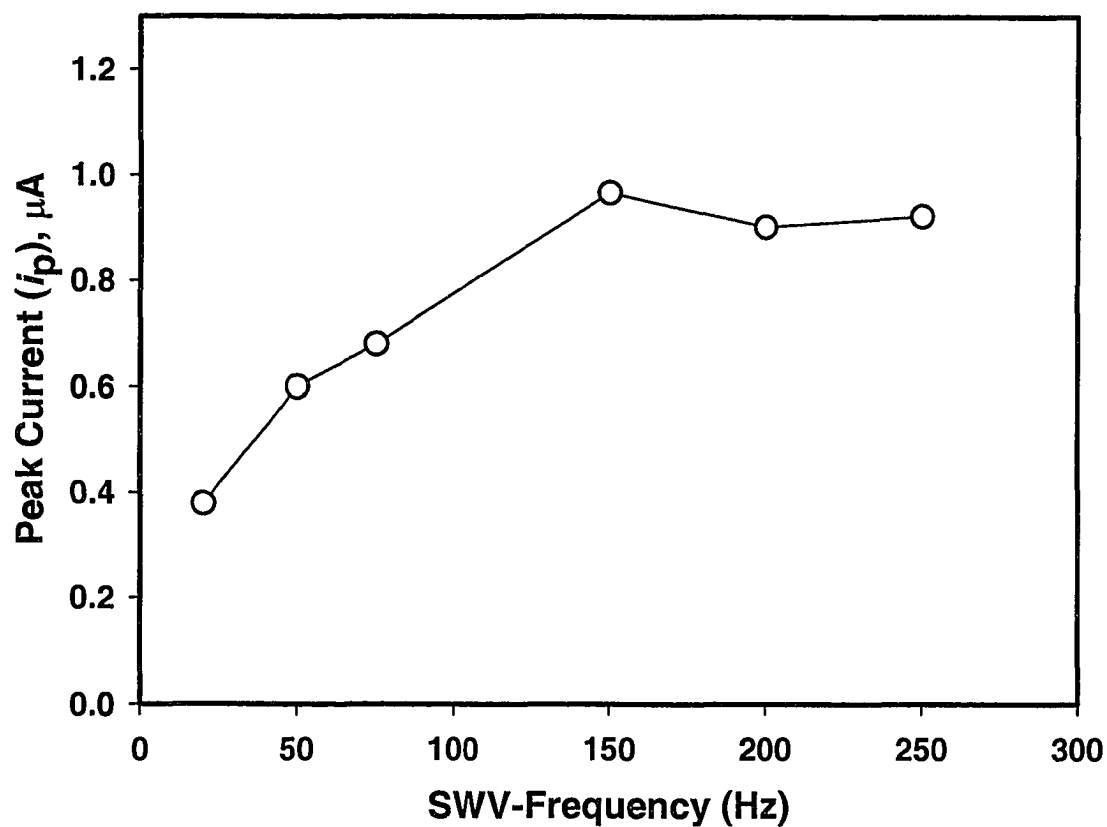


Figure 17 Effect of SWV-frequency (Hz) on the AdCSV/SWV peak- height current (i_p , μA) obtained in a model solution containing Ni(II) 2.9×10^{-8} M, 0.02M HEPES, DMG 1×10^{-3} M, pH 7.5 ± 0.1 , ionic strength 2.0×10^{-2} M, temperature 23 ± 2 °C.

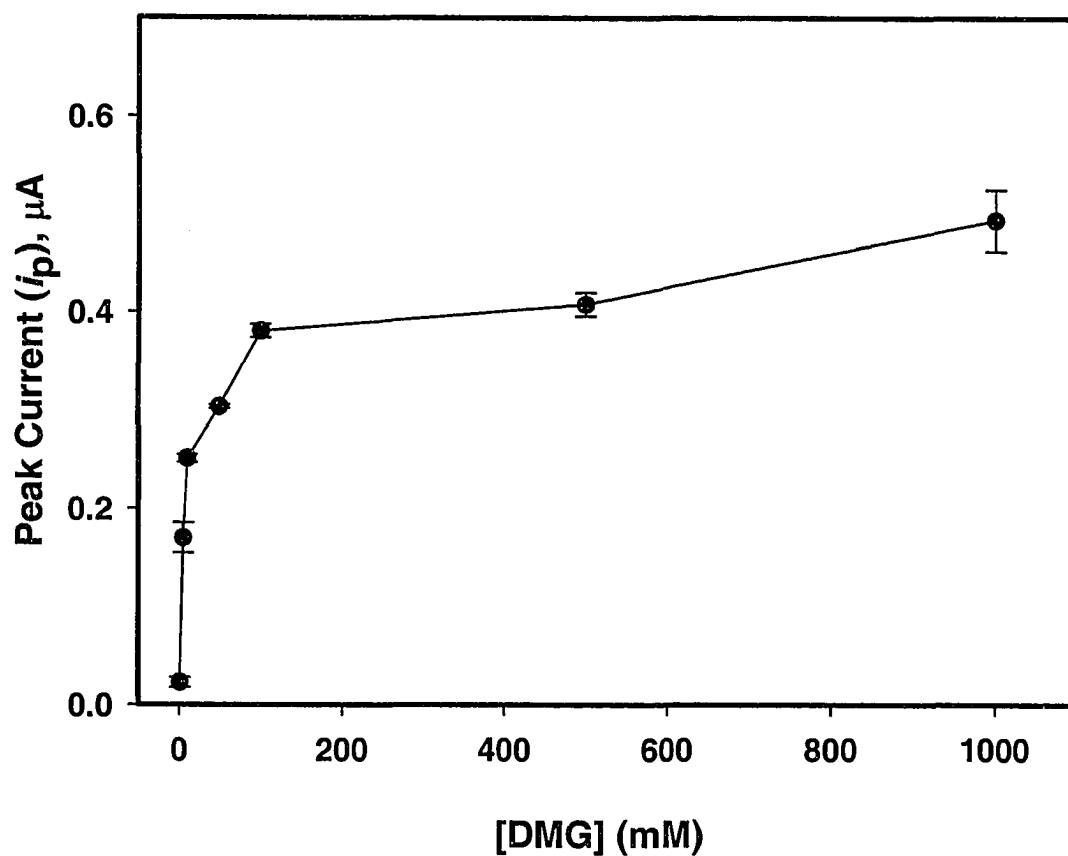


Figure 18 Effect of variation in the DMG concentration on the AdCSV/SWV peak-height current (i_p , μA) obtained in a model solution containing Ni(II) 2.9×10^{-8} M, 0.02M HEPES, pH 7.5 ± 0.1 , ionic strength 2.0×10^{-2} M, temperature 23 ± 2 °C.

4.3.4 *Sampling sites and sampling protocol*

Figure 19 shows the Sudbury mining area sites, where soil solution samples were collected in May 2002 and June 2002 from the lysimeters installed at sites. Through-fall precipitation samples and organic soil solutions were collected from transects that radiated from the Sudbury smelter's flue-stack in the direction of the prevailing wind, at distances of 10 and 24 km, respectively, from the flue-stack. Some properties of the organic soil solutions and through-fall precipitation water samples collected from Sudbury Mining area (Site 1 and Site 2) in May 2002 and June 2002 are shown in Table 5. Organic soil solutions were used for monitoring the metal output (through the use of zero-tension lysimeters installed below the forest floor at 30 cm). The DOC concentration of the filtered water samples was measured using a Total Organic Carbon Analyzer (OI Analytical Model 1010). The samples were filtered through 0.45 μm membrane filters (C.N-6 Metrical, 47 mm diameter, Gelman, Ann Arbor, MI) in our laboratory within 24 h of the sample collection to filter out the particulate matter. These filters, made of mixed cellulose esters, had the advantage of providing filtrates having low blanks for the metals. Each 0.45 μm filter was able to filter approximately 500 mL of water sample before it was clogged and discarded. A subsample (30 mL) of the filtered samples was acidified with nitric acid (Seastar, Canada) to pH 1.5 (to prevent metal loss by adsorption on the container walls). The acidified sample was used to determine the total nickel concentrations using ICP-MS. The remaining filtered samples were stored in the dark at 4 °C until the kinetic experiments, which were done within 72 h of filtration.

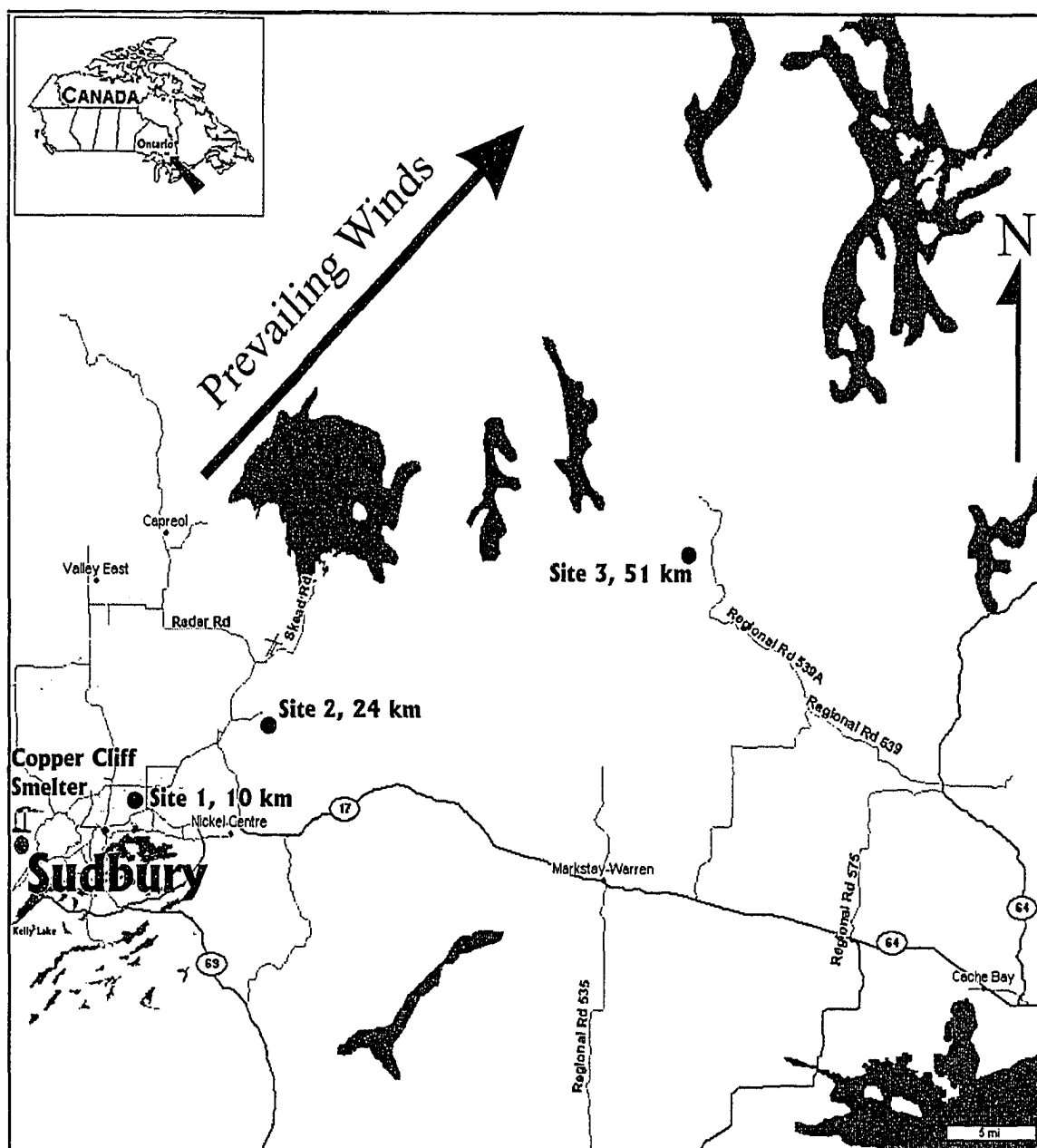


Figure 19 Location of the sites for soil solutions (pore water) and through-fall precipitation collected from Sudbury Mining Area, Copper Cliff, Ontario.

Table 5 Some properties of the organic soil solutions and through-fall precipitation water samples collected from Sudbury Mining area (Site 1 and Site 2) in May 2002 and June 2002.

Sample	pH ± 0.1	Conductivity (mS/m)	DOC (mg/L) ^c	Al (µg/L) ^d	Fe (µg/L) ^d	Ni (µg/L) ^d	Cu (µg/L) ^d	Zn (µg/L) ^d	Cd (µg/L) ^d	Pb (µg/L) ^d	Ca (µg/L) ^e	Mg (µg/L) ^e
Sudbury Site 1, Organic^a	4.2	2.4	18.1	2.9	498.0	34.6	60.8	21.0	0.2	10.3	--	--
Sudbury Site 2, Organic^a	5.5	2.3	12.9	245.0	471.0	28.3	48.3	13.3	0.1	2.4	--	--
Sudbury Site 1, Through-fall^b	6.1	3.4	11.2	71.1	511.5	25.5	21.6	111.9	0.5	2.0	800	190
Sudbury Site 2, Through-fall^b	5.8	2.5	8.4	11.5	1.0	2.2	3.1	184.9	0.1	0.4	268	50.4

All samples were filtered through 0.45mm mixed cellulose ester filters (Gelman Material No. 63077) before analysis

^a samples were received on May 16, 2002.

^b samples were received on June 19, 2002.

^c determined by OI Analytical Model 1010 Total Organic Carbon Analyzer.

^d determined by ICP-MS.

^e determined by Inductively Coupled Plasma Emission Atomic Spectroscopy (ICP-EAS).

-- not enough samples.

4.3.5 Kinetic experiments

Briefly, a 10 mL model solution buffered to pH 5.5 with 2 M sodium acetate/acetic acid, was de-gassed with ultra high-purity nitrogen (UHP, Praxair) for 15 min. prior to the measurements. 100 μ L of 0.1M DMG was added to soil solutions. The instrumental parameters in using square-wave voltammetry (SWV) experiment were the following: the stirring rate 2000 rpm, step potential (scan rate) 5.0 mVs⁻¹, deposition time 10 s, equilibration time 5 s, frequency 100 Hz, modulation amplitude 0.15 V.

4.3.6 Apparatus

The apparatus was the same as presented in section 3.3.6 (chapter 3).

4.3.7 Data analysis

As discussed in chapter three, the overall reaction is treated as pseudo-first-order and the dissociation rate coefficients and their associated distinguishable components were calculated by fitting the experimental data to a two-component exponential growth model by non-linear regression analysis using the Marquardt-Levenberg algorithm. The calculations were performed using SIGMAPLOT 8 computer program (SPSS Science).

4.4 Results and Discussion

Figure 20 presents the dissociation kinetics of Ni(II)-DOC complexes in soil solution samples collected from Sudbury Mining area (Site 1 and Site 2) in May 2002 and June 2002. The quickly rising section at the beginning of each curve (C_1 in Table 6) is due to dissociation of $[\text{Ni}(\text{H}_2\text{O})_6]^{2+}$ and highly labile Ni(II)-DOC complexes. The slowly-rising section of each curve (C_2 in Table 6) is probably due to slow dissociation of strong Ni(II)-

DOC complexes. The limiting value at the top of the each curve represents the total concentration of labile Ni(II)-DOC complexes plus nickel aqua complex. The lability of nickel species increases from bottom curve to top curve. The solid lines in Figure 20 represent data that were fitted to equation (4.1) by non-linear regression analysis. The results are presented in Table 6. Under the experimental measurement timescale ($t = 1$ h), complexes with $k_d \gg 10^{-3} \text{ s}^{-1}$ have been defined as dynamic ($k_d t \gg 1$, condition 2.9 of chapter 2), and complexes with $k_d \ll 10^{-3} \text{ s}^{-1}$ have been defined as inert ($k_d t \ll 1$, condition 2.10 of chapter 2). Two kinetically distinguishable components were identified: dynamic complexes ($k_d \approx 10^{-1} \text{ s}^{-1}$) that dissociate rapidly and *inert* complexes ($k_d < 10^{-4} \text{ s}^{-1}$) that dissociate slowly relative to the analytical timescale of measurement. As discussed in Chapter 3, the measured rate coefficients do not correspond to two precisely discrete binding sites [154-155]; rather, they probably represent averages over distribution of similar sites that remain kinetically defined over the full range of conditions [139]. The lability increases in soil solution samples from Sudbury Site 2, organic solution to Sudbury Site 1, organic solution, to Sudbury Site 2, through-fall precipitation sample to Sudbury Site 1, through-fall precipitation sample. Total binding sites in humic substances present in freshwater is not known. However, a rough estimate can be obtained from the concentration of DOC, which was in the range of 8.4-18.1 mg/L as shown in Table 6.

The lability of the Ni(II)-complexes increases with increasing [Ni]/[DOC] mole ratio because the less abundant strong binding sites were first occupied, and after they are saturated, then numerous weaker binding sites were occupied. Thus, through-fall precipitation sample collected from Sudbury site 1 had the highest labile Ni(II)-DOC

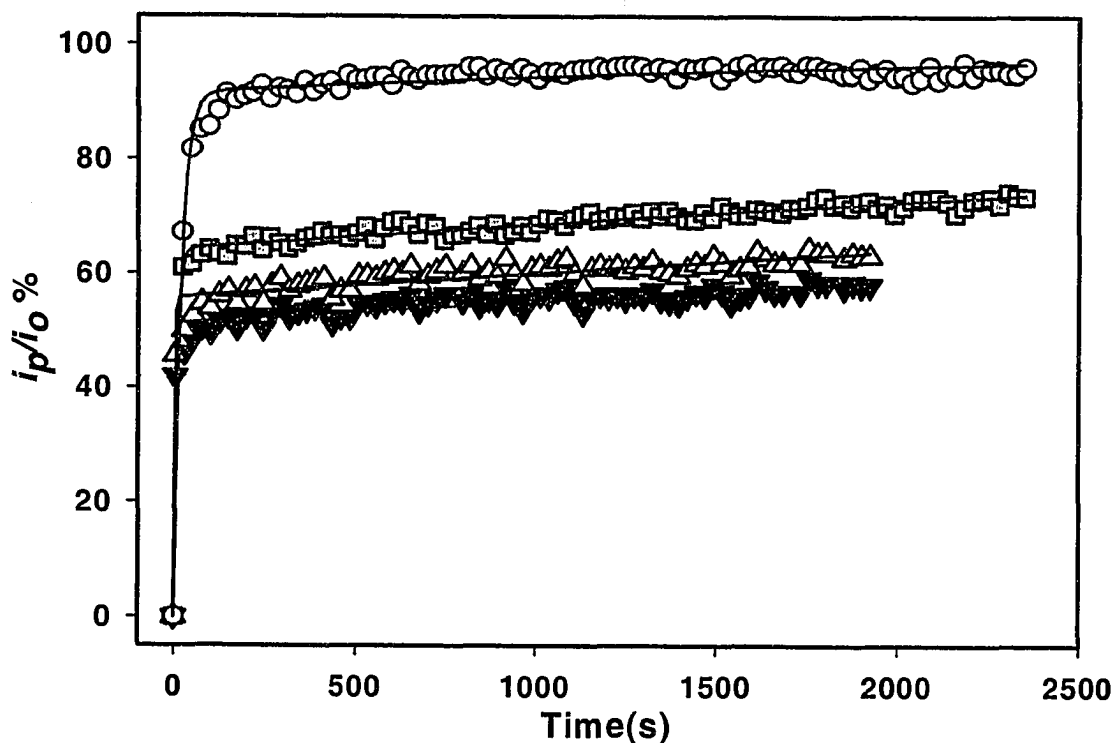


Figure 20 Lability (i_p/i_o) of Ni(II)-DOC complexes in soil solution (pore water) samples collected from Sudbury in May 2002 and June 2002, determined by CLEM/AdCSV, using DMG as the competing ligand; (▲), Sudbury Site 2, Organic, [Ni(II) 4.8×10^{-7} M] + [DOC 12.9 ± 0.2 mg/L], pH 5.5 ± 0.1 , ionic strength $\sim 2 \times 10^{-2}$ M, temperature 23 ± 2 °C; (Δ), Sudbury Site 1, Organic, [Ni(II) 5.9×10^{-7} M] + [DOC 18.1 ± 0.1 mg/L], pH 4.2 ± 0.1 , ionic strength $\sim 3.54 \times 10^{-4}$ M, ionic strength $\sim 2 \times 10^{-2}$ M, temperature 23 ± 2 °C; (O), Sudbury Site 1, through-fall, [Ni(II) 3.5×10^{-6} M] + [DOC 8.4 ± 0.1 mg/L], pH 5.8 ± 0.1 , ionic strength $\sim 2 \times 10^{-2}$ M, temperature 23 ± 2 °C; (■), Sudbury Site 2, through-fall, [Ni(II) 3.7×10^{-8} M] + [DOC 11.2 ± 0.1 mg/L], pH, 6.2 ± 0.1 , ionic strength $\sim 2 \times 10^{-2}$ M, temperature 23 ± 2 °C. Solid lines represent non-linear curve-fitting.

Table 6 Kinetically distinguishable components of Ni-DOC complexes in organic soil solutions and through-fall precipitation samples collected from Sudbury area in (Site 1 and Site 2) in May 2002 and June 2002, determined by CLEM/AdCSV, using DMG as the competing ligand.

Sample	^c [Ni] _t (M)	^d DOC (mg/L)	^c [Ni] _t / ^d DOC (mol/g)	C ₁ (%)	C ₂ (%)	k ₁ , (s ⁻¹ , 10 ⁻¹)	k ₂ , (s ⁻¹ , 10 ⁻⁴)	R ²
Sudbury Site1, Organic ^a	5.9 X 10 ⁻⁷	18.1	3.3 x 10 ⁻⁵	56±6	44±1	4.3 ± 1.4	1.0±0.3	0.959
Sudbury Site 2, Organic ^a	4.8 X 10 ⁻⁷	12.9	3.7 x 10 ⁻⁵	44±3	49±1	4.3 ±1.4	0.8±0.3	0.967
Sudbury Site 1, Through-fall ^b	4.2 X 10 ⁻⁷	11.2	3.8 x 10 ⁻⁵	91±4	9±1	9.3 ± 1.8	1.0±0.0	0.942
Sudbury Site 2, Through-fall ^b	3.7 X 10 ⁻⁸	8.4	4.4 x 10 ⁻⁶	65±2	35±1	11.5 ± 1.0	1.0±0.0	0.981

k₁ and k₂ are dissociation rate coefficients of the kinetically distinguishable components. %C₁ and %C₂ are the percentage concentrations of the first and second components, respectively. The uncertainties represent 95.5% confidence limits of non-linear regression analysis, for an individual value.

^a samples were received on May 16, 2002.

^b samples were received on June 19, 2002.

^c [Ni]_t is the total dissolved nickel, determined by ICP-MS.

^d determined by OI Analytical Model 1010 Total Organic Carbon Analyzer.

complexes ($[\text{Ni}]/[\text{DOC}] = 3.8 \times 10^{-5}$ mol/g) since it was located close (about 10 km) to the Inco smelter and hence, most likely received the highest amount of atmospheric deposition of nickel. Similar trend was also observed in organic solution samples, where the lability increased from Sudbury Site 2, organic solution to Sudbury Site 1, organic solution as shown in Figure 20 and Table 6.

The competition of trace metals as well as major cations with Ni(II) for the binding sites on DOC, plays an important role in nickel bioavailability. Mandal et al. [12, 14] have reported that trace metals can compete effectively with Ni(II) for the binding sites FA while large concentrations of major cations (Ca^{2+} and Mg^{2+}) only promote release of large fractions of the Ni(II)-FA as free Ni^{2+} ions. Therefore, it is expected that high concentration of major cation in through-fall precipitation samples at site 1 would significantly increase the lability of Ni(II)-DOC complexes.

-- Chapter 5 --

**Kinetics of Trace Metal Competition in the Freshwaters: Some
Fundamental Chemical Characteristics**

5.1 Introduction

Trace metals are natural components of the freshwater environment. Because of their participation in a wide variety of biochemical reactions, many trace metals are essential micronutrients in biological systems, but they may become toxic at elevated levels [4]. The interactions of trace metals with Dissolved Organic Matter (DOM), which is ubiquitous in freshwaters, sediments and soils, play an important role in trace metal transport, fate and bioavailability. The competition of major cations with trace metals is a well-known phenomenon in freshwaters. However, trace metals also compete with one another [13,14].

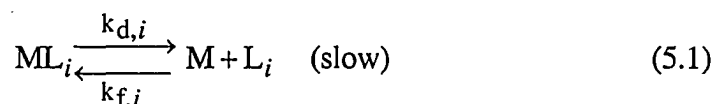
Free metal ion activity has been recognized as a universal factor for determining metal uptake, nutrition and toxicity [5,88]. In a system at equilibrium, the Free Ion Activity Model [5,88] and the Biotic Ligand Model [89] postulate that physiological effects, such as enzyme inhibition, are correlated to free metal ion activity in the bulk solution, regardless of particular species (e.g. free metal ions or other metal complexes) present, or the mechanisms of the reactions with the various sites on the biological surface. This is the local equilibrium approximation [28]. Under this equilibrium (or pseudoequilibrium) assumption, the correlation of biological response with free metal ion activity arises because all labile complexes are equally bioavailable. However, freshwaters contain a complex mixture of metals, and physically and chemically heterogeneous complexants, which often result in systems that are dynamic and far removed from equilibrium [28,61]. In many instances, the rates of biogeochemical reactions are controlled by the rates of metal complexation reactions [61]. The importance of considering dynamic processes for estimating metal bioavailability to aquatic organisms has been emphasized by van

Leeuwen [101] and Jansen et al. [156]. Hence, kinetic approaches for chemical speciation are required to reflect more correctly the realities of freshwater systems, in which metal release is often kinetically controlled. The objective of this work was to investigate some of the factors that influence the kinetics of the competition of Mn(II), Co(II), Ni(II), Cu(II), Zn(II), Cd(II) and Pb(II) in model solutions and in freshwater samples from Grand River (Ontario, Canada) within the context of freshwaters as dynamic systems.

5.2 The Kinetic Model

5.2.1 Competing Ligand Exchange Method [88,157]

Consider a freshwater sample of n components, in which each component, ML_i , exists in equilibrium with its dissociation products: the free metal ion (i.e. metal aqua complex), M , and a naturally occurring, heterogeneous complexant, L_i , such as humic substances, which are ubiquitous in the aquatic environment (charges have been omitted for simplicity). The subscript, i , represents different binding sites on the naturally-occurring heterogeneous complexant.



where the formation and dissociation rate coefficients, $k_{f,i}$ and $k_{d,i}$, are coupled by the stability coefficient, $K = k_f/k_d$, through the principle of microscopic reversibility [116].

When a competing ligand, such as Chelex 100 chelating resin, is added to the sample, M -Chelex is formed, and with a large excess of Chelex 100, reaction (5.1) is driven to the right.



If each complex, ML_i , dissociates simultaneously and independently (at a rate that depends on the nature of the functional group, its position on the macromolecule, and the residual charge), the total concentration of all complexes, c_{ML} , at any time, t , is given by a summation of exponentials (equation 5.3).

$$c_{ML}(t) = \sum_{i=1}^n c_{ML_i}^{\circ} \cdot \exp(-k_{d,i} \cdot t) \quad (5.3)$$

where $c_{ML_i}^{\circ}$ is the initial concentration of ML_i and $c_{ML_i}(t)$ is the concentration of ML_i at any time, t . The model assumes that (i) the reactions are first-order and pseudo-first-order; (ii) reaction (5.2) is much faster than reaction (5.1), so that reaction (5.1) is the rate-determining step, and the measured kinetics then represent the kinetics of the dissociation of the metal complex, ML_i , (iii) ML does not directly (i.e. without predissociation) react with the Chelex resin, and (iv) the ratio of the complexed metal's concentration to free metal's concentration is much larger than unity (i.e. $c_{ML} / c_M \gg 1$).

For complexants that are both physically and chemically heterogeneous, such as humic and fulvic acids, which have been reported to have a continuous distribution of binding sites [28,155], the summation can be approximated by an integral [158]:

$$c_{ML}(t) = \int_0^{+\infty} c_{ML_i}^{\circ} \exp(-k_{d,i} \cdot t) f_{\log}(k_{d,i}) d \log k_{d,i} \quad (5.4)$$

Equation (5.4) is a member of the general class of Fredholm integral equations of the first kind [159].

The rate coefficients obtained from the scheme outlined above arise from a fundamental process in natural systems: dissociation of the natural metal complex (reaction 5.1), which has been designated the disjunctive pathway [72,97] (not to be confused with the dissociative mechanism). By contrast, information from the adjunctive pathway [28] is difficult to interpret since the observed rate coefficients are strongly influenced by the nature (e.g. steric and electrostatic factors, and protonation) of the probe ligand.

5.3 Experimental

5.3.1 Materials and reagents

Stock solutions (1000 mg/mL) of manganese, cobalt, nickel, copper, zinc, cadmium and lead were purchased from SCP Science (Montreal, Canada). Working standard solutions were prepared daily by dilution of the stock solutions with ultrapure water (of resistivity 18.2 M Ω -cm) acidified to contain 1% (v/v) ultrapure nitric acid (Seastar, Canada). Analytical grade (minimum 99% pure) Chelex 100 resin, 100-200 mesh, sodium form, (Bio-Rad) was cleaned following the method of Morel et al. [160]. The wet capacity of Chelex 100 resin is 0.61 meq/g [161]. Freeze-dried Laurentian fulvic acid (FA), which is derived from a podzol collected from the Laurentian Forest Preserve of Laval University, Québec, Canada, was purchased from Fredriks Research Products (The Netherlands). The concentration of carboxylate and phenolate groups in the Laurentian fulvic acid is 11.6 mmol/g [162]. A 1.0000 g/L stock solution was prepared by dissolving 1.0000 g of freeze-dried Laurentian fulvic acid in ultrapure water.

5.3.2 Containers and their cleaning procedure

All containers used were made of Teflon. After cleaning with ultrapure water, they were

filled to the top with 10% (v/v) nitric acid and allowed to stand at the room temperature for one week. They were then rinsed five times with ultrapure water, filled with ultrapure water, and allowed to stand until they were used. The filling water was renewed periodically to ensure continued contact with clean water.

5.3.3 Model solutions and freshwater samples

A series of three model solutions was prepared in ultrapure water to contain varying concentrations of Laurentian fulvic acid (4.00×10^{-3} g/L, 4.00×10^{-2} g/L or 1.00×10^{-1} g/L) and equimolar concentrations of Mn(II), Co(II), Ni(II), Cu(II), Zn(II), Cd(II) and Pb(II). The concentration of each metal was 7.0×10^{-7} mol/L. The pH of the fulvic acid model solutions was adjusted to 5.0 ± 0.1 with 2 mol/L ultrapure nitric acid and/or 2 mol/L purified sodium hydroxide, and the samples left to equilibrate overnight (12 h). Surface water samples were collected from Grand River (44°05.791'N, 80°22.431'W) in south-western Ontario (Canada), as shown in Figure 21, using pre-cleaned 2.2-L Teflon bottles, and were brought to our laboratory without any delay. The samples were immediately filtered through 0.45 μ m Versapore membrane capsule filters (Pall) using a peristaltic pump. The pH and conductivity of the samples were measured using an Accumet 20 pH/conductivity meter (Fisher). The conductivity measurements were used to calculate the ionic strength of the samples. Table 7 presents some properties of the surface-water samples collected from Grand River in June 2002.

5.3.4 Kinetic experiments and data analysis

The simultaneous (rapid sequential) dissociation kinetics of Mn(II), Co(II), Ni(II), Cu(II),

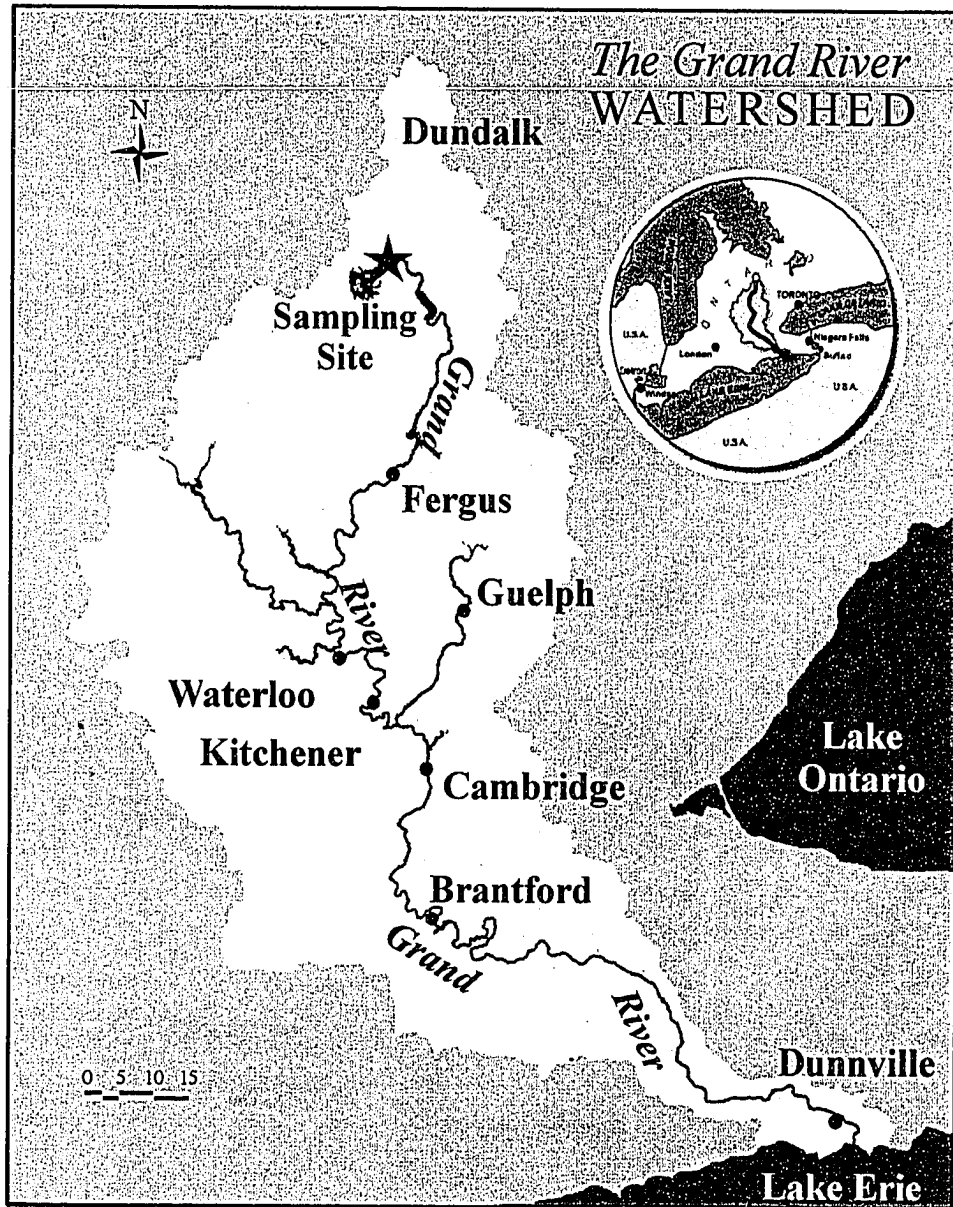


Figure 21 Map of the sampling area of Grand River, Ontario. The star shows the location of the sampling site.

Table 7 Some properties of the surface-water samples collected from Grand River, Ontario, in June 2002.

Grand River	
pH	7.9 ± 0.1
DOC (mg/L)	14.9 ± 0.4
Conductivity (mS/m)	16
[M] ^a	
Pb	$(1.5 \pm 0.3) \times 10^{-10}$
Cd	$(2.9 \pm 0.1) \times 10^{-10}$
Zn	$(4.5 \pm 0.1) \times 10^{-8}$
Cu	$(2.0 \pm 0.8) \times 10^{-8}$
Al	$(3.7 \pm 0.3) \times 10^{-7}$
Fe	$(4.6 \pm 0.1) \times 10^{-6}$
Ni	$(5.7 \pm 0.2) \times 10^{-8}$
Major Cations (M) ^b	
Ca	$(1.2 \pm 0.0) \times 10^{-3}$
Mg	$(6.2 \pm 0.1) \times 10^{-4}$
K	$(1.1 \pm 0.2) \times 10^{-5}$
Na	$(2.2 \pm 0.1) \times 10^{-4}$
Major Anions (M) ^c	
F	$(7.3 \pm 0.0) \times 10^{-5}$
Cl	$(4.0 \pm 0.0) \times 10^{-4}$
NO ₃	$(4.3 \pm 0.0) \times 10^{-5}$
SO ₄	$(6.7 \pm 0.0) \times 10^{-5}$
PO ₄	N/D

^a Determined by ICP-MS

^b Determined by ICP-OES

^c Determined by Ion Chromatography

N/D: Not Detectable

Zn(II), Cd(II) and Pb(II) complexes was studied using Chelex 100 as the competing ligand and an ELAN 6100 DRC ICP-MS (PerkinElmer SCIEX). Three grams (1% w/v, w stands for the wet weight) of Chelex 100 were added to 300 mL of the sample solution in a cylindrical Teflon Reactor (500 mL volume); the sample solution was stirred continuously with a Teflon-coated magnetic stirring bar, and was filtered with an online 0.40 μm polycarbonate membrane filter (Corning) to separate the Chelex 100 resin before introducing the filtrate into the plasma torch by solution nebulization at a flow rate of approximately 1 mL/min, as shown in Figure 22. Kinetic spectra were obtained by fitting the kinetic data to equation (5.4) using the distribution analysis feature (Level 2) of the FLA-900 (Edinburgh Analytical Instruments, UK) fluorescence lifetime analysis program, as reported in earlier publications from this laboratory [14,15]. Under the experimental conditions used in the work, the analytical time scale of measurement is 20 s to 7000 s, which corresponds to $k_d \sim 10^{-2} \text{ s}^{-1}$ to 10^{-5} s^{-1} . Complexes with $k_d > 10^{-2} \text{ s}^{-1}$ cannot be experimentally resolved from the metal aqua complex because the latter has very nearly the same dissociation rate coefficients. This represents the upper limit of the dissociation rate coefficients that can be experimentally determined within the experimental time scale of the method. This limitation arises from the time required for Chelex 100 to mix with the sample solution. The lower limit is simply defined by the time taken to complete the kinetic run. Metal species with $k_d < 10^{-5}$ (i.e., k_{ft} and $k_{dt} \ll 1$) are defined as inert [163].

5.4 Results and Discussion

Kinetic data for the dissociation of Zn(II) and Cu(II) complexes in model solutions of the Laurentian fulvic acid, at the metal-to-fulvic acid mole ratio $c_M/c_{FA} = 0.056$, are presented

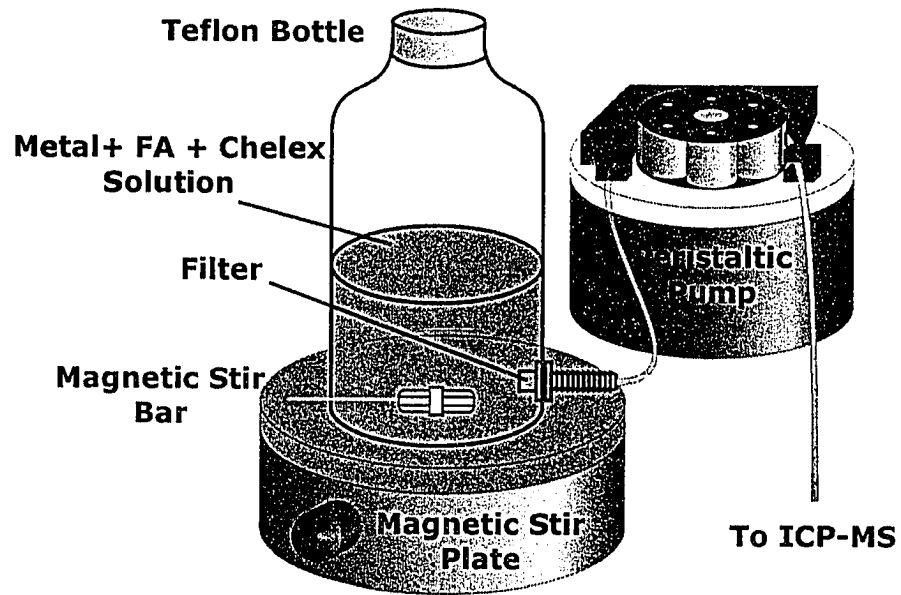


Figure 22 Teflon reactor used in the CLEM/ICP-MS study.

in Table 8 and Figure 23. The steep section at the beginning of the curve for the Zn(II)-FA system corresponds to a dissociation rate coefficient of approximately 10^{-2} s^{-1} , which is similar to the dissociation rate coefficient for uptake of the Zn^{2+} aqua complex by Chelex (data not shown). Hence, the results suggest that the steep section can be attributed to uptake of the Zn^{2+} aqua complex and/or rapidly-dissociating Zn(II)-FA complexes that cannot be experimentally distinguished from the aqua complex. The very slowly-falling section of the Cu(II)-FA curve is probably due to the very slow rate of dissociation ($k_d < 10^{-6} \text{ s}^{-1}$) of strong metal complexes, which represent the lower limit of dissociation rate coefficients that can be measured under the experimental conditions (i.e. an analytical window of 2 h) used in this study. Although the dissociation rate coefficients reported here are specific to the experimental conditions (e.g. pH, ionic strength and temperature), this limitation is not overly restrictive as results based on the disjunctive pathway can be extrapolated relatively easily and reliably to related rate processes in the natural environment [28]. Table 8 indicates that the slow component typically comprises more than 95% of the total metal concentration, suggesting that $c_{\text{ML}} / c_{\text{M}} \gg 1$ (i.e. assumption iv is satisfied).

Naturally occurring complexants such as fulvic acid consist of heterogeneous ligands. Since individual sites cannot be studied independently [27], estimating the number of kinetically distinguishable components and their associated dissociation rate coefficients through direct application of equation (5.3) poses a difficult problem. A kinetic spectrum of the dissociation rate coefficients for the Zn(II) and Cu(II) species based on equation (5.4) is presented in Figure 24. Each kinetically distinguishable component probably

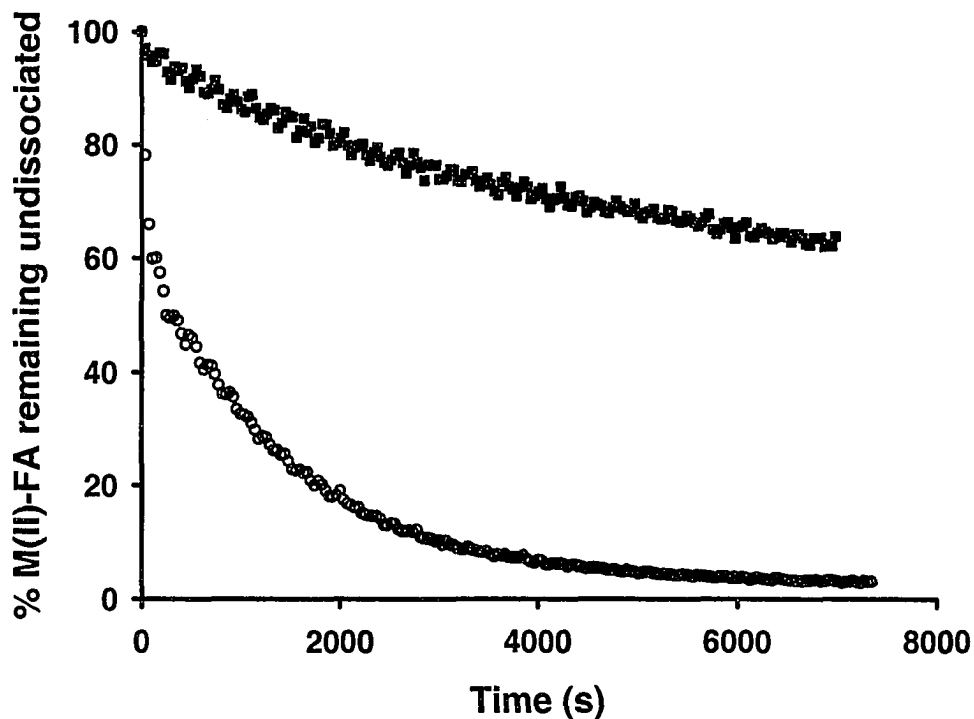


Figure 23 Dissociation kinetics of Zn(II)- and Cu(II)-FA complexes in a model solution of Laurentian fulvic acid, measured by ICP-MS, using Chelex 100 as the competing ligand. $c_M / c_{FA} = 0.056$, pH 5.0 ± 0.1 , ionic strength 6×10^{-6} mol/L, temperature 23 ± 2 °C. (O), Zn(II)-FA; (■), Cu(II)-FA.

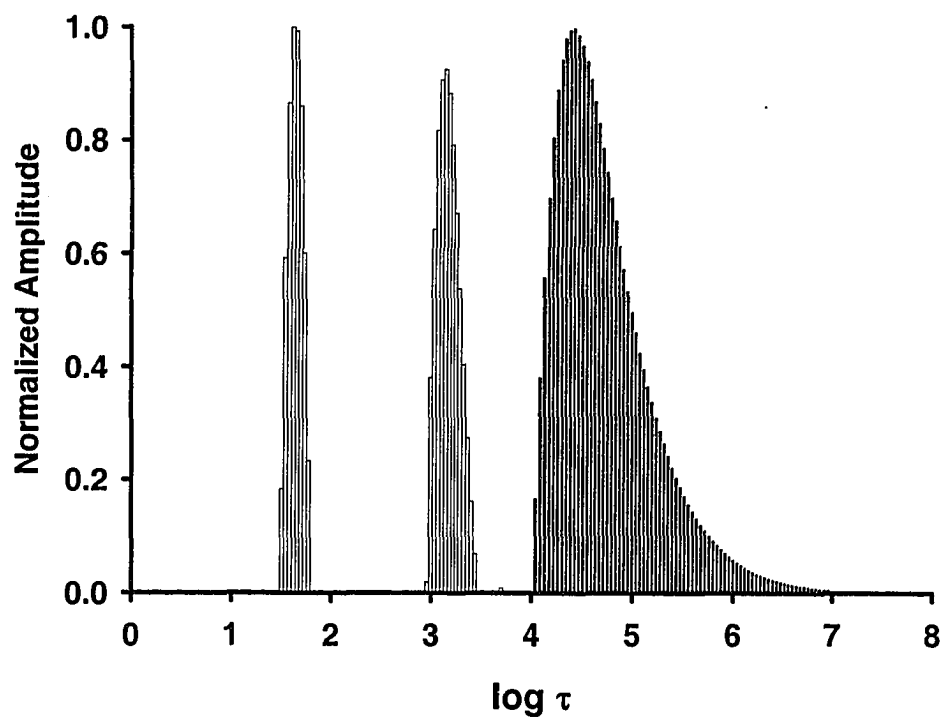


Figure 24 Kinetic spectrum of lifetimes ($\tau \sim 1/k_d$) of Zn(II)- and Cu(II)-FA complexes in a model solution of Laurentian fulvic acid, measured by ICP-MS, using Chelex 100 as the competing ligand. $c_M / c_{FA} = 0.056$, pH 5.0 ± 0.1 , ionic strength 6×10^{-6} mol/L, temperature 23 ± 2 °C. (□), Zn(II)-FA; (■), Cu(II)-FA.

Table 8 Kinetically distinguishable components of Zn(II)- and Cu(II)-FA complexes in model solutions of Laurentian fulvic acid. $c_M / c_{FA} = 0.056$, pH 5.0 ± 0.1 , ionic strength 6×10^{-6} mol/L, temperature 23 ± 2 °C.

Metal	%C ₁	k ₁ (10 ⁻¹ s ⁻¹)	%C ₂	k ₂ (10 ⁻³ s ⁻¹)	%C ₃	k ₃ (10 ⁻⁵ s ⁻¹)	χ ²
Cu(II)	---	---	0.2	0.80 ± 0.13	99.8	1.3 ± 4.0	0.017
Zn(II)	2.1	0.23 ± 0.04	97.9	0.68 ± 0.18	---	---	0.012

--- Not observed from the distribution analysis.

χ² is the goodness of fit test.

k₁, k₂ and k₃ are dissociation rate coefficients of the kinetically distinguishable components. %C₁, %C₂ and %C₃ are the percentage concentrations of the first, second and third components, respectively. The values after the ± sign are measures of the widths of the distributions.

reflects a range of chemically related, but not identical, metal complexes with similar dissociation rate coefficients [27]. As shown in Table 8, the observed dissociation rate coefficients from the distribution analysis range from 10^{-2} to 10^{-5} s^{-1} . The uncertainties, which represent the standard deviations of the distributions, are simply measures of the width of the distributions. The widest range of dissociation rate coefficients was observed for the slowest kinetically distinguishable component. This is reflected in the relatively high concentration (> 90%) of this component. The shape and size of the distribution probably arises from the colloidal nature of humic substances, in which steric hindrance and diffusion from within the interior of the colloid cause metals to appear to dissociate much more slowly than surface-bound metal species. Restrained diffusion of Cu(II) binding by hydrous iron oxide colloids has also been observed by Gutzman and Langford [96]. This phenomenon can be attributed to entropy effects, such as coiling and uncoiling, and conformational changes and aggregation of the colloidal ligands.

An important limitation of distribution analyses based on numerical methods, such as equation (5.4), is that they are sensitive to artefacts, which result in peak broadening [115,25]. This effect makes it difficult to distinguish a distribution of similar sites from one or more well-defined sites in the presence of experimental noise [27,155,158]. The importance of testing the observed speciation parameters for their chemical significance [28] is therefore emphasized in order to determine whether the results are simply a mathematical solution to the time-dependent concentration data, or if the complex chemistry of trace metal speciation in natural systems can be approximated by a small set of rate coefficients. The theory for metal complexation in aqueous solutions suggests that

three factors are expected to influence metal exchange reactions with DOM: (i) metal-to-ligand mole ratio, (ii) Ligand Field Stabilization Energy (LFSE) for transition metals, and (iii) ionic potential (z^2/r).

5.4.1 Metal-to-Ligand Mole Ratio

The model system of Laurentian fulvic acid, which has been characterized for the concentration of carboxylate and phenolate binding sites [162], allows for systematic tests of the chemical significance of the Kinetic Model over a wide range of metal-to-ligand mole ratios. The dissociation kinetics of Cd(II)-FA complexes in model solutions of Laurentian fulvic acid at $c_M/c_{FA} = 0.056, 0.0056$ and 0.0024 are presented in Figure 25. Speciation parameters for the Cd(II)-FA system are presented in Table 9. The results indicate a progressive increase in the dissociation rate coefficients with increasing metal-to-FA mole ratio, suggesting that the observed dissociation rate coefficients are associated with progressively weaker sites as the metal loading of the system is increased. The results presented in Figure 26 show similar trends for the Cu(II)- and Zn(II)-FA systems. The correlation coefficients for the Cu(II)-, Zn(II)- and Cd(II)-FA systems were $R^2 = 0.97$, $R^2 = 0.99$ and $R^2 = 0.99$, respectively. Similar trends (not shown) were also observed for Mn(II) ($R^2 = 0.94$), Co(II) ($R^2 = 0.99$), Ni(II) ($R^2 = 0.91$) and Pb(II) ($R^2 = 0.99$).

A unique property of naturally occurring complexants, such as fulvic acid, is that their metal binding properties change with the degree of metal loading of the system [84]. The progressive increase in the observed dissociation rate coefficients with increasing metal-

to-FA mole ratio arises from the chemical and physical heterogeneity [84] of fulvic acid. The results suggest that fulvic acid has sites of closely spaced binding energies, the cooperative metal-binding activity of which enable metals to be buffered over a large concentration range (several orders of magnitude) with only gradual changes in free metal ion concentration [164]. The results are in agreement with the trend in complexation capacity observed by Town and Filella [131] for the speciation of Cu(II), Zn(II), Cd(II) and Pb(II) complexes collected from a large dataset of published literature on natural waters. However, the different slopes observed for the Zn(II)-, Cd(II)- and Cu(II)-FA systems shown in Figure 26 suggest that the intrinsic binding properties of fulvic acid may vary considerably from one metal to another. The results at $c_M/c_{FA} = 0.0024$ probably approach the geochemical limit [28], where the site occupation of the fulvic acid is so small that only the strongest binding sites contribute significantly to metal complexation.

Kinetic data on metal-complex dissociation reactions in natural systems are scarce. Despite the absence of any universal relationship between the thermodynamics and kinetics of reactions, Linear Free Energy Relationships (LFERs) between the energetics and rates of reactions for many sets of related compounds have been established [165]. Although they began as empirical relationships, most have an underlying theoretical basis. For reactions based on the disjunctive pathway, Hammond's postulate [166] suggests that the LFER between the standard Gibbs free energy change (ΔG°) and the free energy of activation (ΔG^\ddagger) results from a transition state and an intermediate near on the energy surface having similar energies. Hence, a simple inverse relationship between

$\log k_d$ and $\log K$ is expected for a series of complexes of a particular metal. Here it is important to consider the contributions of both enthalpy and entropy to stability coefficients and rate coefficients, as shown in equation (5.5) and the Eyring Equation (equation 5.6).

$$-RT \ln K = \Delta G^\circ = \Delta H^\circ - T\Delta S^\circ \quad (5.5)$$

where ΔH° is the change in the standard enthalpy of reaction, ΔS° is the change in the standard entropy of reaction, R is the gas coefficient, and T is the thermodynamic temperature.

$$\ln k = \ln \frac{\kappa T}{h} - \frac{\Delta G^\ddagger}{RT} = \left(\ln \frac{\kappa T}{h} + \frac{\Delta S^\ddagger}{R} \right) - \frac{\Delta H^\ddagger}{RT} \quad (5.6)$$

where ΔH^\ddagger is the enthalpy change of activation, ΔS^\ddagger is the entropy change of activation, h is the planks constant and κ is the Boltzmann constant.

Hydrolysis of metal cations has been found to result in the formation of polynuclear, μ -hydroxyl bridged metal colloids in systems with partial covalent bonding [167]. This phenomenon probably results in the formation of water-swollen gels (colloids) with increasing fulvic acid concentration. Since oxygen-bearing functional groups, such as carboxylate and phenolate [162,168], account for over 90% of the binding sites in fulvic acid [10], only small changes in enthalpy are expected for oxygen bonds with a given metal. The progressive decrease in the dissociation rate coefficients with decreasing metal-to-FA mole ratio can be attributed to the heterogeneous characteristics of fulvic acid, such as polyfunctional, polyelectrolytic and conformational properties [169]. Equations (5.5) and (5.6) suggest that these heterogeneous properties of NOM are

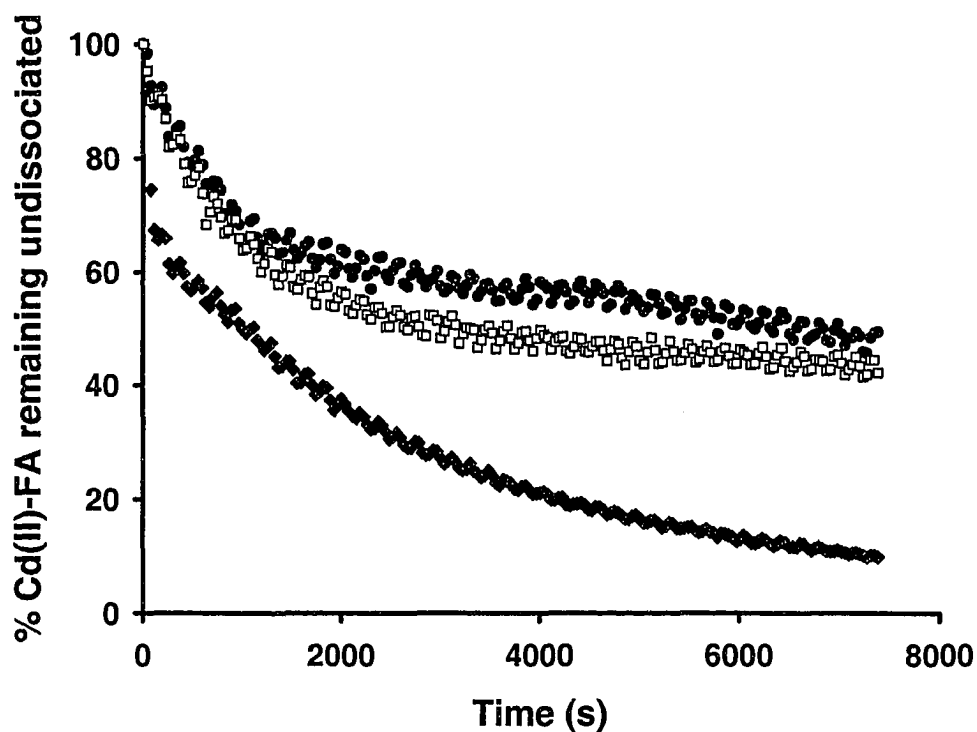


Figure 25 Influence of the metal-to-ligand mole ratio on the dissociation kinetics of Cd(II)-FA complexes in model solutions of Laurentian fulvic acid, measured by ICP-MS, using Chelex 100 as the competing ligand. pH 5.0 ± 0.1 , ionic strength 6×10^{-6} mol/L, temperature 23 ± 2 °C. (●), $c_M / c_{FA} = 0.056$; (□), $c_M / c_{FA} = 0.0056$; (◆), $c_M / c_{FA} = 0.0024$.

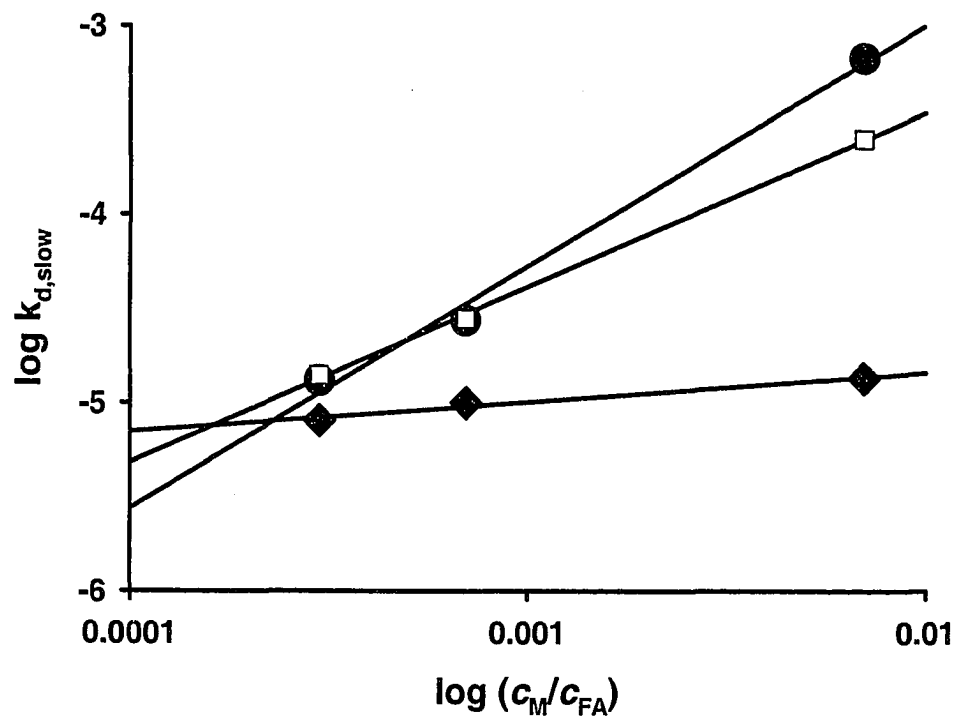


Figure 26 Influence of the metal-to-ligand mole ratio on the mean dissociation rate coefficient of the slowest kinetically distinguishable component, $k_{d,slow}$ of Cd(II)-FA complexes in model solutions of Laurentian fulvic acid, measured by ICP-MS, using Chelex 100 as the competing ligand. pH 5.0 ± 0.1 , ionic strength 6×10^{-6} mol/L, temperature 23 ± 2 °C. (●), Zn(II)-FA, $R^2 = 0.99$; (□), Cd(II)-FA, $R^2 = 0.99$; (◆), Cu(II)-FA, $R^2 = 0.97$.

Table 9 Influence of the metal-to-ligand mole ratio on the kinetic speciation parameters of Cd(II) in model solutions of Laurentian fulvic acid. pH 5.0 \pm 0.1, ionic strength 6×10^{-6} mol/L, temperature 23 ± 2 °C.

c_M / c_{FA}	%C ₁	k ₁ (10 ⁻¹ s ⁻¹)	%C ₂	k ₂ (10 ⁻³ s ⁻¹)	%C ₃	k ₃ (10 ⁻⁴ s ⁻¹)	%C ₄	k ₄ (10 ⁻⁵ s ⁻¹)	χ^2
0.0024	< 0.01	4.1 \pm 1.2	0.85	1.2 \pm 0.3	---	---	99.2	1.4 \pm 2.6	0.044
0.0056	---	---	0.37	2.5 \pm 0.5	---	---	99.6	2.8 \pm 7.0	0.058
0.056	0.75	0.21 \pm 0.02	---	---	99.3	2.5 \pm 1.8	---	---	0.020

--- Not observed from the distribution analysis.

χ^2 is the goodness of fit test.

k₁, k₂, k₃ and k₄ are dissociation rate coefficients of the kinetically distinguishable components. %C₁, %C₂, %C₃ and %C₄ are the percentage concentrations of the first, second, third and fourth components, respectively. The values after the \pm sign are measures of the widths of the distributions.

probably related to entropy effects, which are known to play an important role in many natural systems [116]. Structural changes (conformational) in fulvic acid following an increase in bound metal have been observed in light scattering measurements by Langford et al. [170].

5.4.2 Ligand Field Stabilization Energy

The effects of Ligand Field Stabilization Energy (LFSE) are usually significant in the chemistry of the first-row transition metals. Results for the dissociation kinetics of the metal complexes of equimolar concentrations of Mn(II) d^5 , Co(II) d^7 , Ni(II) d^8 , Cu(II) d^9 , and Zn(II) d^{10} in a model solution of Laurentian fulvic acid at $c_M/c_{FA} = 0.056$ are presented in Figure 27 and Table 10. The influence of the d -electron configuration on the dissociation rate coefficients of Mn(II) d^5 , Co(II) d^7 , Ni(II) d^8 , Cu(II) d^9 , and Zn(II) d^{10} in the model solutions of Laurentian fulvic acid at $c_M/c_{FA} = 0.056$ and $c_M/c_{FA} = 0.0024$ is presented in Figure 28. The results suggest that, with the exception of Cu(II), the dissociation rate coefficients fall into the familiar trend predicted from the LFSEs (weak field) (i.e. $k_{d,Mn(II) d^5} > k_{d,Co(II) d^7} > k_{d,Ni(II) d^8} > k_{d,Cu(II) d^9} < k_{d,Zn(II) d^{10}}$), and indicate that inert complexes are those with large LFSEs. A similar trend was reported by Sekaly et al. [116] for the dissociation rate coefficients of Ni(II) d^8 , Cu(II) d^9 and Zn(II) d^{10} in model solutions of Laurentian fulvic acid. Returning to the concept of a LFER, this effect is related to unfavourable changes in LFSE [171] on going to the transition state—the larger the LFSE, the larger the sacrifice in Ligand Field Activation Energy [37]. The unfavourable changes in LFSE for some metals during complex formation is illustrated by the data for one of the simplest substitution processes, the substitution of an

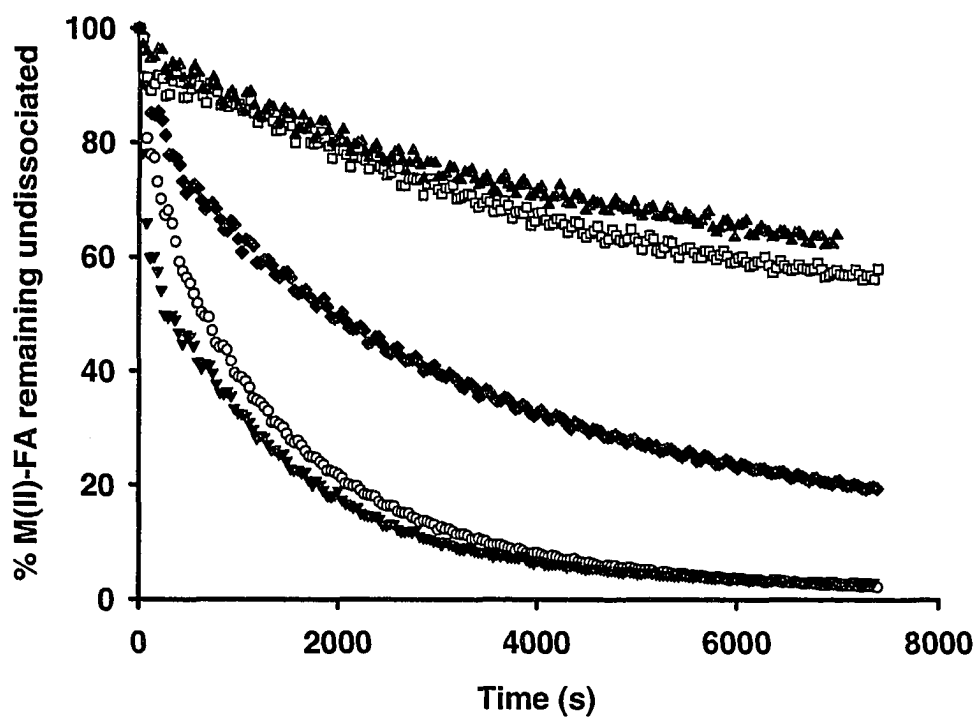


Figure 27 Influence of the *d*-electron configuration on the dissociation kinetics of metal complexes in model solutions of Laurentian fulvic acid, measured by ICP-MS, using Chelex 100 as the competing ligand. $c_M / c_{FA} = 0.056$. pH 5.0 ± 0.1 , ionic strength 6×10^{-6} mol/L, temperature 23 ± 2 °C. (O), Mn(II); (◆), Co(II); (□), Ni(II); (▲), Cu(II); (▼), Zn(II).

Table 10 Influence of the *d*-electron configuration on the kinetic speciation parameters in model solutions of Laurentian fulvic acid. $c_M / c_{FA} = 0.056$, pH 5.0 ± 0.1 , ionic strength 6×10^{-6} mol/L, temperature 23 ± 2 °C.

Metal	<i>d</i> -electron configuration	%C ₁	k ₁ (10 ⁻² s ⁻¹)	%C ₂	k ₂ (10 ⁻³ s ⁻¹)	%C ₃	k ₃ (10 ⁻⁴ s ⁻¹)	%C ₄	k ₄ (10 ⁻⁵ s ⁻¹)	χ ²
Mn(II)	<i>d</i> ⁵	0.6	2.3 ± 0.3	1.6	4.0 ± 0.7	97.8	6.1 ± 3.0	---	---	0.006
Co(II)	<i>d</i> ⁷	---	---	0.4	7.6 ± 1.3	99.6	1.3 ± 2.5	---	---	0.010
Ni(II)	<i>d</i> ⁸	---	---	---	---	0.3	5.0 ± 0.9	99.7	1.6 ± 4.8	0.019
Cu(II)	<i>d</i> ⁹	---	---	---	---	0.2	8.0 ± 1.3	99.8	1.3 ± 3.9	0.017
Zn(II)	<i>d</i> ¹⁰	2.1	2.3 ± 0.4	---	---	97.3	6.8 ± 1.8	---	---	0.012

--- Not observed from the distribution analysis.

χ² is the goodness of fit test.

k₁, k₂, k₃ and k₄ are dissociation rate coefficients of the kinetically distinguishable components. %C₁, %C₂, %C₃ and %C₄ are the percentage concentrations of the first, second, third and fourth components, respectively. The values after the ± sign are measures of the widths of the distributions.

Table 11 Rate constants for water exchange (k_w) of selected 3d transition metal ions (weak field). Adapted from Butler and Harrod [171].

Metal	Mn ²⁺	Fe ²⁺	Co ²⁺	Ni ²⁺	Cu ²⁺	Zn ²⁺ *
d^n	d^5	d^6	d^7	d^8	d^9	d^{10}
k_w (s ⁻¹)	3×10^7	3×10^6	1×10^6	3×10^4	8×10^9	7×10^7
LFSE (Dq)	0	4	8	12	6	0

LFSE – Ligand Field Stabilization Energy

* The data for Zn²⁺ are from Morel and Herring [116].

octahedrally coordinated water molecule in the divalent $3d$ transition metal ions with another water molecule in the bulk solvent in the absence of other ligands. With the exception of Cu(II), the rate coefficients of water exchange fall into the familiar order of LFSEs (weak field) as shown in Table 11, and indicate that inert complexes are those with large LFSEs. The anomalous behaviour of Cu(II), which has a large LFSE, is known to form thermodynamically stable metal complexes, and yet has a high rate coefficient of water exchange, $k_w = 1 \times 10^9 \text{ s}^{-1}$ [116], can be attributed to the Jahn-Teller effect, which results in the axial bonds becoming elongated and kinetically labile, and the equatorial bonds becoming shortened and kinetically inert.

Although curves at $c_M/c_{FA} = 0.056$ and $c_M/c_{FA} = 0.0024$ shown in Figure 28 have the same general shape, the dissociation rate coefficients were shifted towards lower values at the lowest metal-to-fulvic acid mole ratio ($c_M/c_{FA} = 0.0024$), which is consistent with the progressive increase in the dissociation rate coefficients with increasing metal-to-fulvic acid mole ratio described previously. However, Figure 28 also shows a reversal of the trend in the dissociation rate coefficients of Ni(II)- and Cu(II)-FA complexes at $c_M/c_{FA} = 0.0024$. Once again, an analogy can be drawn from coordination chemistry. A reversal in the relative stabilities of Ni(II) d^8 and Cu(II) d^9 complexes often occurs when the equatorial positions of Cu(II) are saturated and the axial positions become occupied [172]. Occupation of the kinetically labile (weak) axial positions balances the influence of the kinetically inert (strong) equatorial positions, and the trend predicted only by the LFSE is observed. The progressive saturation of the metals through the formation of polynuclear metal colloids suggests that the gradual influence of stronger (and hence, more inert) sites

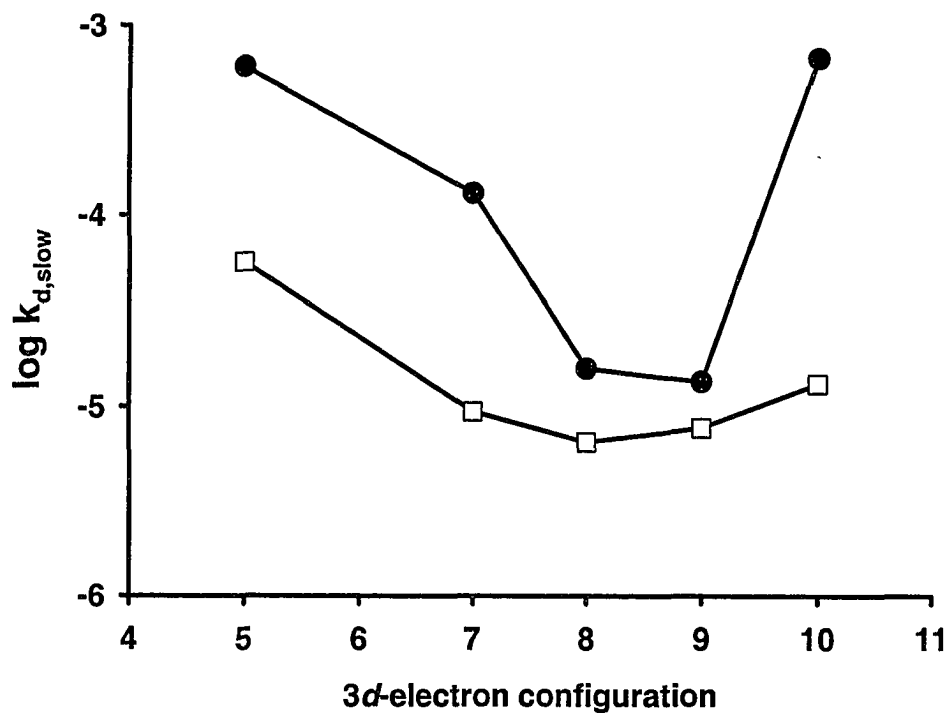


Figure 28 Influence of the d -electron configuration on the mean dissociation rate coefficient of the slowest kinetically distinguishable component $k_{d,slow}$ of metal complexes in model solutions of Laurentian fulvic acid, measured by ICP-MS, using Chelex 100 as the competing ligand. $c_M / c_{FA} = 0.056$. pH 5.0 ± 0.1 , ionic strength 6×10^{-6} mol/L, temperature 23 ± 2 °C. (●), $c_M / c_{FA} = 0.056$; (□), $c_M / c_{FA} = 0.0024$.

with decreasing metal-to-fulvic acid mole ratios primarily arises from the chelate effect, which results from the displacement of a large number of ordered water molecules coordinated around the metal. The results suggest that the heterogeneous properties (e.g. polyfunctional, polyelectrolytic and conformational) of DOM are related to entropy effects.

Results for the dissociation kinetics of metal complexes in freshwaters collected from Grand River are presented in Figure 29 and Table 12. Figure 30 shows a similar trend in the dissociation rate coefficients (i.e. $k_{d,Mn(II)} d^5 \sim k_{d,Co(II)} d^7 > k_{d,Ni(II)} d^8 < k_{d,Cu(II)} d^9 < k_{d,Zn(II)} d^{10}$) even though the metals in the freshwater sample were not present at equimolar concentrations. A similar trend in LFSE was observed by Sekaly et al. [173] for dissociation rate coefficients of Co(II), Ni(II), Cu(II) and Zn(II) complexes in freshwaters collected from the Sudbury (Canada) area. Slow Ni(II) ligand exchange kinetics between DOM and dimethylglyoxime (half-life: 5 to 95 h) was observed by Xue et al. [138] in an oligotrophic lake, and in a small river affected by inputs from sewage effluents and agriculture in Switzerland. Our results on the slow dissociation kinetics of Cu(II) complexes also agree with those of Achterberg et al. [174], who reported that equilibrium between organically complexed copper and suspended particulate matter was only reached after 4 to 15 h. The particularly slow dissociation kinetics of Ni(II) and Cu(II) complexes suggest that the usual equilibrium assumption for freshwaters may not be valid for these metals.

5.4.3 Ionic Potential

The metals for which the binding energy is expected to be dominated by only ionic

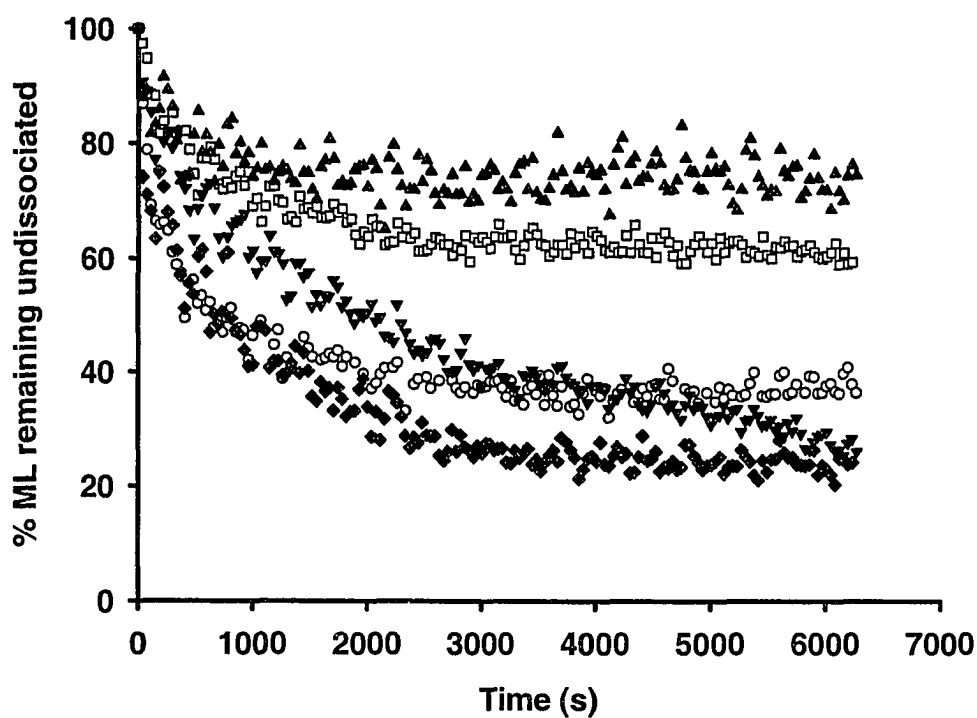


Figure 29 Influence of the *d*-electron configuration in a freshwater sample collected from Grand River on June 23, 2002 on dissociation kinetics of metal complexes, measured by ICP-MS, using Chelex 100 as the competing ligand. DOC 14.9 ± 0.4 mg/L, pH 7.9 ± 0.1 , ionic strength 6×10^{-3} mol/L, temperature 23 ± 2 °C. (O), Mn(II); (◆), Co(II); (□), Ni(II); (▲), Cu(II); (▼), Zn(II).

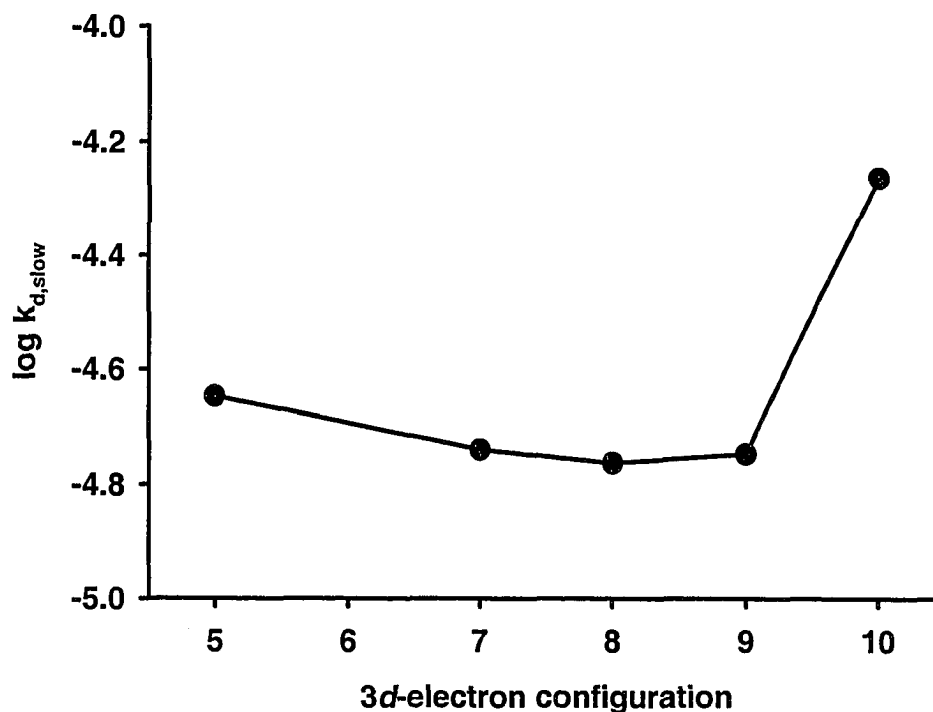


Figure 30 Influence of the d -electron configuration in a freshwater sample collected from Grand River on June 23, 2002, on mean dissociation rate coefficient of the slowest kinetically distinguishable component, $k_{d,slow}$ of metal complexes, measured by ICP-MS, using Chelex 100 as the competing ligand. DOC 14.9 ± 0.4 mg/L, pH 7.9 ± 0.1 , ionic strength 6×10^{-3} mol/L, temperature 23 ± 2 °C.

Table 12 Influence of the *d*-electron configuration on the kinetic speciation parameters in a freshwater sample collected from Grand River on June 23, 2002. DOC 14.9 ± 0.4 mg/L, pH 7.9 ± 0.1 , ionic strength 6×10^{-3} mol/L, temperature 23 ± 2 °C.

Metal	<i>d</i> -electron configuration	%C ₁	k ₁ (10 ⁻¹ s ⁻¹)	%C ₂	k ₂ (10 ⁻³ s ⁻¹)	%C ₃	k ₃ (10 ⁻⁴ s ⁻¹)	%C ₄	k ₄ (10 ⁻⁵ s ⁻¹)	χ ²
Mn(II)	<i>d</i> ⁵	0.05	0.15 ± 0.03	0.44	3.1 ± 0.8	0.17	11 ± 2	99.3	1.8 ± 2.7	0.20
Co(II)	<i>d</i> ⁷	0.02	0.60 ± 0.12	0.01	8.9 ± 1.0	2.7	11 ± 3	97.3	1.8 ± 3.1	0.18
Ni(II)	<i>d</i> ⁸	0.01	4.0 ± 1.1	0.1	5.2 ± 1.1	0.06	19 ± 4	99.8	1.7 ± 2.9	0.13
Cu(II)	<i>d</i> ⁹	0.01	3.6 ± 0.1	<0.01	41 ± 4	0.01	83 ± 9	100	1.8 ± 2.7	0.42
Zn(II)	<i>d</i> ¹⁰	---	---	0.1	8.2 ± 4.9	---	---	99.9	5.5 ± 18	0.11

--- Not observed from the distribution analysis.

χ² is the goodness of fit test.

k₁, k₂, k₃ and k₄ are dissociation rate coefficients of the kinetically distinguishable components. %C₁, %C₂, %C₃ and %C₄ are the percentage concentrations of the first, second, third and fourth components, respectively. The values after the ± sign are measures of the widths of the distributions.

potential ($\Delta H = z^2/r$) [27] include Mn(II) $3d^5$, Zn(II) $3d^{10}$, Cd(II) $4d^{10}$ and the post-transition metal, Pb(II). Figures 25 and 26 show that the relative labilities of Mn(II) and Zn(II) are consistent with the trend predicted from the electrostatic attraction between the metal cation and the coordinated ligands. Using NMR relaxation time measurements, Deczky and Langford [175] have demonstrated that Mn(II) forms outer-sphere complexes with Armadale fulvic acid. Kinetic results from model solutions of Laurentian fulvic acid containing equimolar concentrations of Pb(II) ($z^2/r = 0.030 \text{ pm}^{-1}$), Cd(II) ($z^2/r = 0.037 \text{ pm}^{-1}$), Mn(II) ($z^2/r = 0.041 \text{ pm}^{-1}$) and Zn(II) ($z^2/r = 0.046 \text{ pm}^{-1}$) at $c_M/c_{FA} = 0.056$ are presented in Figure 31. The kinetic distributions of the dissociation rate coefficients are presented in Table 13. Interestingly, the results for Zn(II), Cd(II) and Pb(II) indicate a reversal in the trend predicted from electrostatic effects, suggesting that for Zn(II), Cd(II) and Pb(II) the primary contribution to metal binding is not electrostatic. The same trend was observed at all three metal-to-fulvic acid mole ratios, i.e. $c_M/c_{FA} = 0.056$, 0.0056 and 0.0024, as shown in Figure 32. Mattock [167] attributed a reversal in the trend expected from electrostatic effects to greater metal-ligand bond stabilization in systems with partial covalent character. This effect probably results from mutual cation and anion polarization, which favours combination with larger, negatively-charged, polarizable ligands, such as carboxylate and phenolate. The covalent character was found to decrease with increasing ionic potential of the metal cation. An inverse relationship between the dissociation rate coefficients and the ionic potential was also observed in a freshwater sample collected from Grand River, as shown in Figures 33-34 and Table 14.

Although the results suggest a mechanistic relationship between the equilibria and kinetics

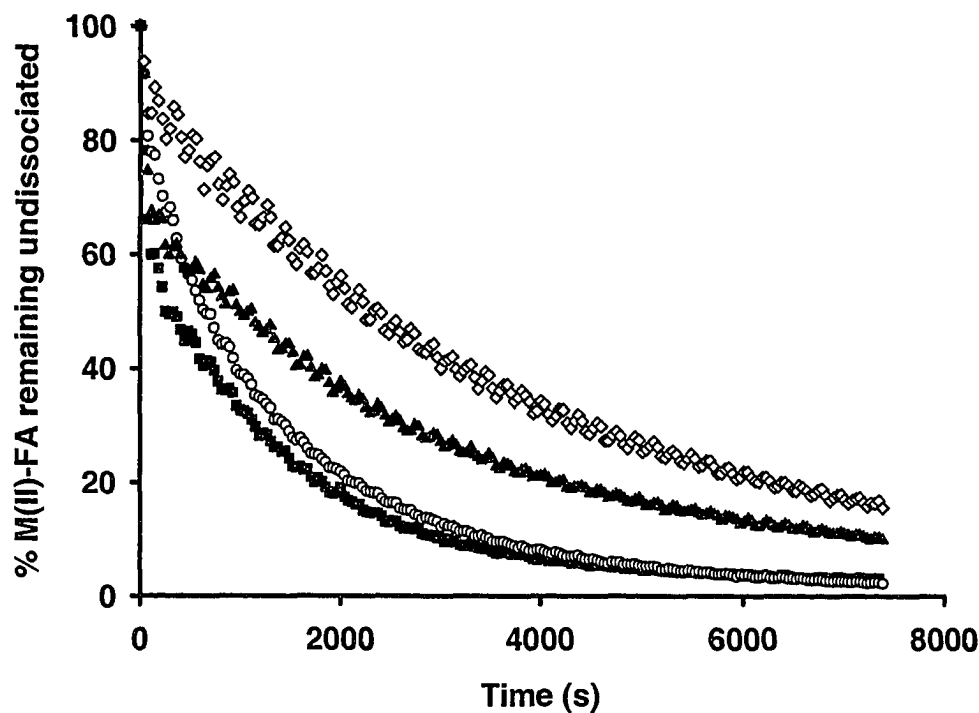


Figure 31 Influence of the ionic potential (z^2/r) on the dissociation kinetics of metal complexes in model solutions of Laurentian fulvic acid, measured by ICP-MS, using Chelex 100 as the competing ligand. pH 5.0 ± 0.1 , ionic strength 6×10^{-6} mol/L, temperature 23 ± 2 °C, $c_M / c_{FA} = 0.056$. (O), Mn(II); (■), Zn(II); (▲), Cd(II); (◇), Pb(II).

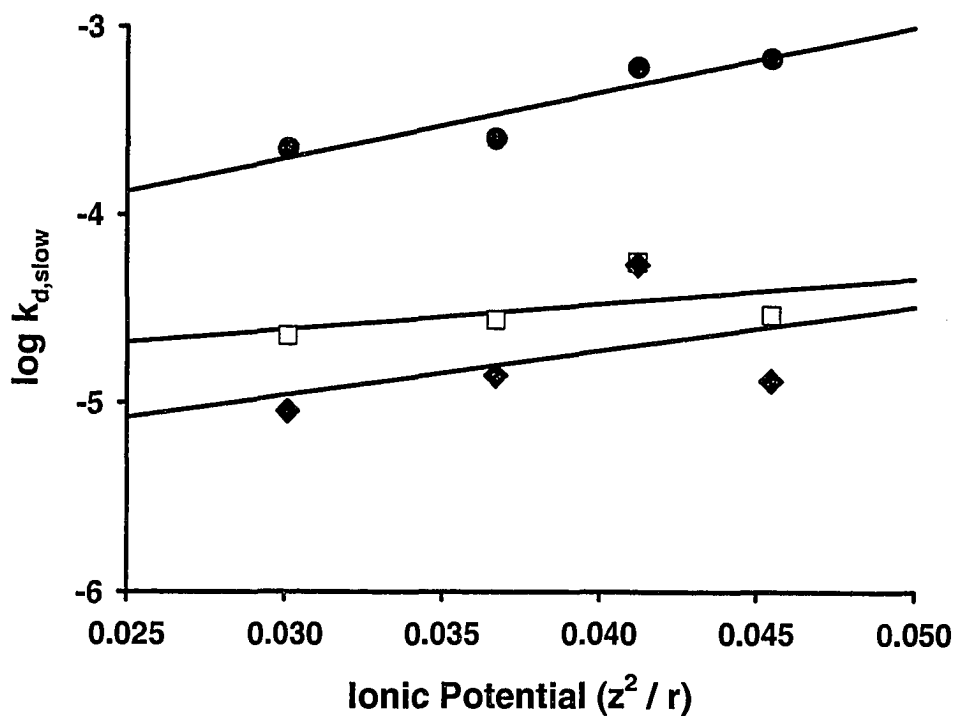


Figure 32 Influence of the ionic potential (z^2/r) on mean dissociation rate coefficient of the slowest kinetically distinguishable component, $k_{d,slow}$ of metal complexes in model solutions of Laurentian fulvic acid, measured by ICP-MS, using Chelex 100 as the competing ligand. pH 5.0 ± 0.1 , ionic strength 6×10^{-6} mol/L, temperature 23 ± 2 °C. (●), $c_M / c_{FA} = 0.056$; (□), $c_M / c_{FA} = 0.0056$; (◆), $c_M / c_{FA} = 0.0024$.

Table 13 Influence of ionic potential (z^2/r) on the kinetic speciation parameters in model solutions of Laurentian fulvic acid. $c_M / c_{FA} = 0.056$, pH 5.0 ± 0.1 , ionic strength 6×10^{-6} mol/L, temperature 23 ± 2 °C.

Metal	z^2/r (μm^{-1})	%C ₁	k ₁ (10^{-2} s ⁻¹)	%C ₂	k ₂ (10^{-3} s ⁻¹)	%C ₃	k ₃ (10^{-4} s ⁻¹)	χ^2
Pb(II)	0.030	---	---	---	---	100	2.2 ± 1.3	0.040
Cd(II)	0.037	0.8	2.1 ± 0.4	---	---	99.3	2.5 ± 1.8	0.020
Mn(II)	0.041	0.6	2.3 ± 0.3	1.6	4.0 ± 0.7	97.8	6.1 ± 3.0	0.006
Zn(II)	0.046	2.1	2.3 ± 0.4	---	---	97.9	6.8 ± 1.8	0.012

--- Not observed from the distribution analysis.

χ^2 is the goodness of fit test.

k₁, k₂ and k₃ are dissociation rate coefficients of the kinetically distinguishable components. %C₁, %C₂ and %C₃ are the percentage concentrations of the first, second and third components, respectively. The values after the \pm sign are measures of the widths of the distributions.

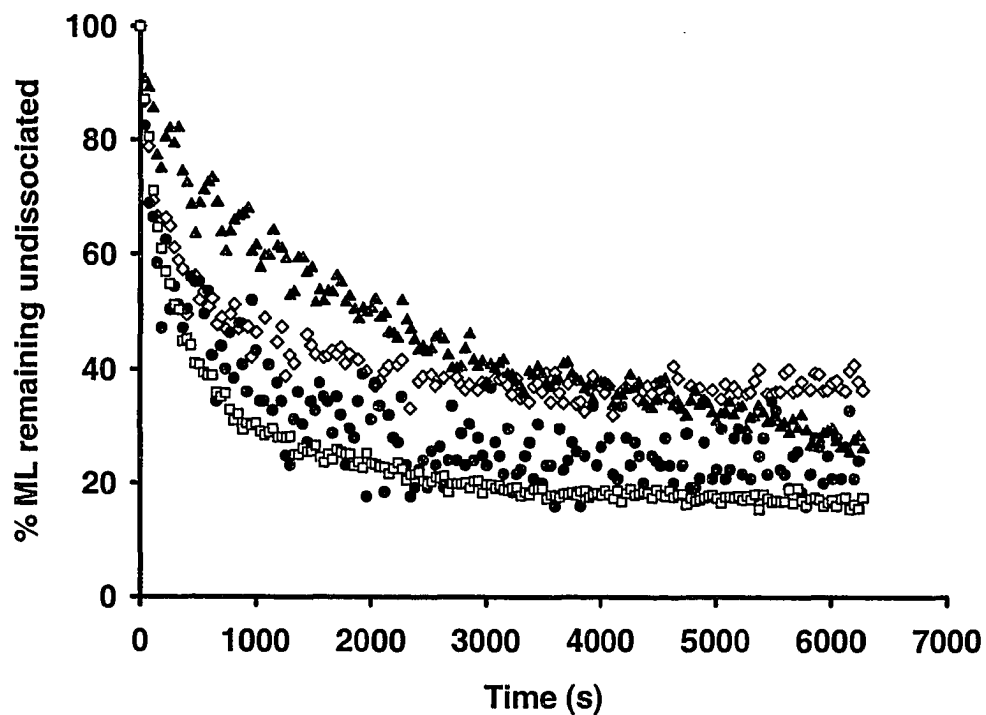


Figure 33 Influence of the ionic potential (z^2/r) on the dissociation kinetics of metal complexes in a freshwater sample collected from Grand River on June 23, 2002, measured by ICP-MS, using Chelex 100 as the competing ligand. DOC 14.9 ± 0.4 mg/L, pH 7.9 ± 0.1 , ionic strength 6×10^{-3} mol/L, temperature 23 ± 2 °C. (\diamond), Mn(II); (\blacktriangle), Zn(II); (\bullet), Cd(II); (\square), Pb(II).

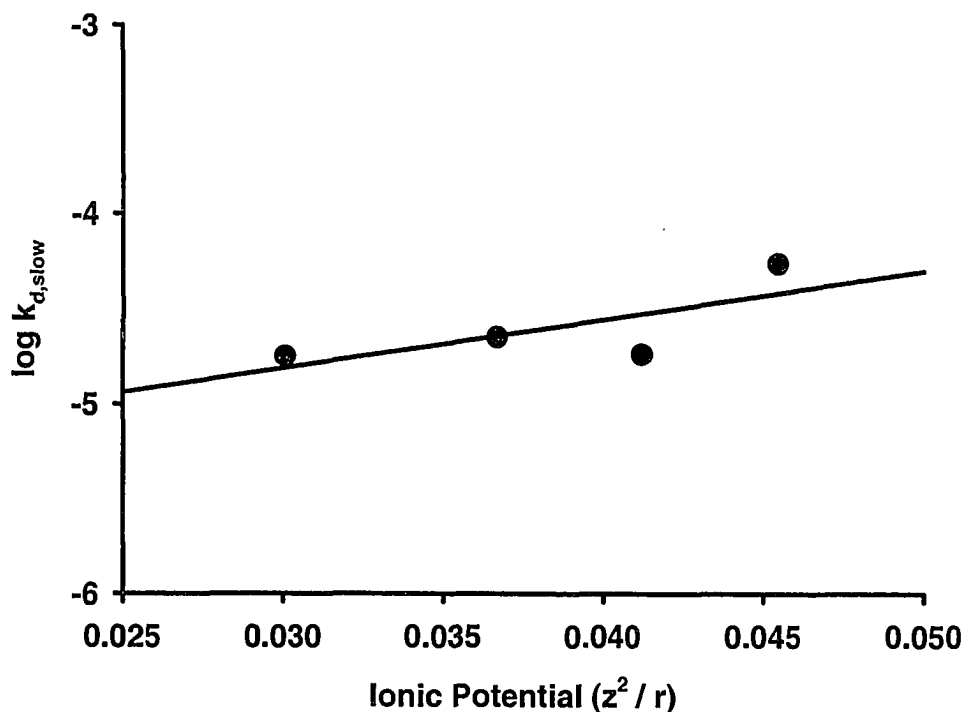


Figure 34 Influence of the ionic potential (z^2/r) on the mean dissociation rate coefficient of the slowest kinetically distinguishable component, $k_{d,slow}$ of metal complexes in a freshwater sample collected from Grand River on June 23, 2002, measured by ICP-MS, using Chelex 100 as the competing ligand. DOC 14.9 ± 0.4 mg/L, pH 7.9 ± 0.1 , ionic strength 6×10^{-3} mol/L, temperature 23 ± 2 °C.

Table 14 Influence of ionic potential (z^2/r) on the kinetic speciation parameters in a freshwater sample collected from Grand River on June 23, 2002. DOC 14.9 ± 0.4 mg/L, pH 7.9 ± 0.1 , ionic strength 6×10^{-3} mol/L, temperature 23 ± 2 °C.

Metal	z^2/r (pm ⁻¹)	%C ₁	k_1 (10 ⁻¹ s ⁻¹)	%C ₂	K_2 (10 ⁻³ s ⁻¹)	%C ₃	k_3 (10 ⁻⁴ s ⁻¹)	%C ₄	k_4 (10 ⁻⁵ s ⁻¹)	χ^2
Pb(II)	0.030	0.01	3.5 ± 1.1	2.3	1.3 ± 0.5	0.6	0.58 ± 0.19	97.1	1.8 ± 2.5	0.034
Cd(II)	0.037	0.05	0.94 ± 0.30	0.02	12 ± 2	2.3	14 ± 5	97.7	2.3 ± 3.6	0.855
Mn(II)	0.041	---	---	0.5	4.3 ± 0.5	0.3	13 ± 2	99.2	2.3 ± 2.8	0.212
Zn(II)	0.046	---	---	---	---	0.1	8.2 ± 4.9	99.9	5.5 ± 18	0.106

--- Not observed from the distribution analysis.

χ^2 is the goodness of fit test.

k_1 , k_2 , k_3 and k_4 are dissociation rate coefficients of the kinetically distinguishable components. %C₁, %C₂, %C₃ and %C₄ are the percentage concentrations of the first, second, third and fourth components, respectively. The values after the \pm sign are measures of the widths of the distributions.

of trace metal complexation, this interpretation is complicated by a number of factors. The kinetic inertness of Cu(II) complexes in both the fulvic acid model solutions and the freshwater sample collected from Grand River highlights the important distinction between interpretations based on the disjunctive pathway [97], which is based on complete dissociation of ML [116], and the dissociative mechanism, which is based on ligand substitution. This misunderstanding regarding their essential difference has been a source of confusion regarding the lability of Cu(II) complexes in freshwater systems. Whereas interpretations based on the dissociative mechanism use the high rate coefficient for water exchange of Cu^{2+} to incorrectly predict very rapid kinetics [27], the disjunctive pathway correctly predicts that Cu(II) complexes undergo slow dissociation kinetics. Hence, the rate coefficient of water exchange for Cu^{2+} is probably not a good predictor of the kinetic behaviour of Cu(II) in natural systems. Furthermore, the results also suggest that the rate coefficient of water exchange may not be a good predictor of the kinetic behaviour of Cd(II) and Pb(II) complexes, as they are found to exhibit a significant degree of covalent character.

5.5 Conclusion

The main advantage of the kinetic distribution approach is that it provides an objective approach for fitting the kinetic data to a set of rate coefficient, $k_{d,i}$, and concentration, $c_{\text{ML},i}^{\circ}$ parameters without any *a priori* knowledge about the total number of binding sites present in the system. The ability of the Kinetic Model to correctly predict the influence of the metal-to-ligand mole ratio, ionic potential and LFSE on the relative rates of metal complex dissociation supports the conclusion that the Kinetic Model provides a chemically significant description of the kinetics of metal-DOM interactions in

freshwaters. The observed trends in the ionic potential and the LFSE suggest that these trace metals compete for the same binding sites of DOM and emphasize the importance of considering the valence-shell electron configuration for predicting the competition of trace metals in the freshwater environment.

-- Chapter 6 --

Influence of Solar Radiation on the Lability of Metal

Complexes in Freshwaters

6.1 Introduction

Dissolved Organic Matter (DOM), which is formed from decomposition of plant and animal materials, is ubiquitous in the aquatic environment. The wide variety of organic matter and various degradation and transformation pathways for formation of DOM result in a complex structure and mixture. The complexity of DOM leads to a number of environmentally important properties such as serving as an electron donor (ligand) in metal complexation, sorption of xenobiotic material and adsorption onto mineral phases. Some typical properties of DOM include polydispersity, high molar mass (10^3 to 10^5 g/mol), polyfunctionality, and intense absorption of the UV radiation of the solar spectrum, which results in the complementary colour of DOM being yellow; the water containing DOM is therefore coloured yellow [176].

Photochemical reactions play an important role in the biogeochemistry of the upper water column [31]. DOM contains chromophores that strongly absorb solar radiation over a broad spectral range [32], and is primarily responsible for regulating the transmission of solar radiation in freshwaters. This property helps chromophoric DOM to shield the water column from the direct effects of solar radiation; however, DOM can also be subjected to considerable photochemical degradation. Most of the solar energy absorbed by DOM occurs between 300 and 500 nm, which corresponds to an excitation energy of 95 to 58 kcal/mol [177]. Absorption of sunlight can result in excitation of DOM and the production of reactive intermediates, such as singlet oxygen ($^1\text{O}_2$), OH radicals ($\cdot\text{OH}$), DOM-derived peroxy radicals ($\text{ROO}\cdot$), solvated electrons (e_{aq}^-), superoxide anions (O_2^-), triplet states of humic compounds and hydrogen peroxide.

Photochemical transformation of the chromophores can lead to photoisomerization, intramolecular decomposition, rearrangement, and electron transfer [33]. These sunlight-mediated processes can lead to transformation of DOM into low molecular weight aliphatic carbonyl compounds (i.e. acetaldehyde, formaldehyde, malonate and pyruvate) [34-36] and release of carbon monoxide [36-39], carbon dioxide [40,41] and other forms of dissolved inorganic carbon [40,42-44] (i.e. photomineralization). Photochemical modification of DOM thus affects the optical properties of water and influences the penetration of light [45], as these smaller compounds do not absorb UV radiation as strongly as the larger parent molecules [34]. This phenomenon, known as photobleaching, can substantially increase the penetration of UV radiation in lakes [46].

Solar radiation may promote the degradation of DOM, either directly through complete photooxidation or indirectly through secondary reactions of photochemically produced free radicals with other organic compounds in the water [33], which may significantly alter the metal binding properties of DOM. DOM plays a key role in the transport, fate and bioavailability of metals in the freshwater environment.

Although the photodegradation of DOM has been widely studied, little information is available on the influence of solar radiation on the chemical speciation and bioavailability of trace metals in freshwaters. The objectives of this research were to investigate the impact of solar radiation on the metal binding properties of DOM, and its effect on the metal bioavailability in freshwaters.

6.2 The Kinetic Model

The Kinetic Model was the same as presented in section 5.2 (chapter 5).

6.3 Experimental

6.3.1 Materials and reagents

Stock solutions (1000 µg/mL) of cobalt, nickel, copper, zinc, cadmium and lead were purchased from SCP Science (Montreal, Canada). Working standard solutions were prepared daily by dilution of the stock solutions with ultrapure water acidified to contain 1% (v/v) with ultrapure nitric acid (Seastar, Canada). Analytical grade (minimum 99% pure) Chelex 100 resin, 100-200 mesh, sodium form (Bio-Rad), was cleaned following the method of Morel et al. [160]. The wet capacity of Chelex 100 resin was 0.61 meq/g [161]. All standards and test solutions were prepared using ultrapure water of resistivity 18.2 MΩ cm, which was obtained direct from a Nanopure Diamond water purification system (Barnstead).

6.3.2 Containers and their cleaning procedure

Containers and their cleaning procedure were the same as presented in section 5.3.2 (chapter 5).

6.3.3 Freshwater samples

Surface water samples were collected near the headwaters of Grand River (44° 05.791' N, 80° 22.431' W) in the southwestern Ontario (Canada) using acid-pre-cleaned 2.2-L Teflon bottles, and were brought to our laboratory without any delay. The samples were immediately filtered through 0.45 µm Versapore membrane capsule filters (Pall) using a

peristaltic pump. The pH and conductivity of the samples were measured using an Accumet 20 pH/conductivity meter (Fisher).

6.3.4 Studies on solar irradiation of water samples

The water samples after filtration were delivered to our collaborating laboratory at the Department of Biology, University of Ottawa (Ottawa, Ontario) for UV irradiation. The samples were irradiated in 2.2 L Teflon bottles (11.5 cm diameter) under sunlight conditions for 0, 10, 20 and 30 days. OL754 spectroradiometer with dual monochromator was used to measure the UV irradiation dose at the outside surface of the bottle (in air) (Optronics Ltd) [73]. Nonirradiated water bottles were used as controls. The bottles of irradiated and non-irradiated water samples were stored in the dark at 4 °C. The pH of the water samples was measured with an Accumet 925 pH/ion meter using a combination glass electrode containing an internal calomel reference electrode. The DOC content of all samples was determined using an IO Analytical 1010 Total Organic Carbon Analyzer (persulfate oxidation method).

6.3.5 Kinetic experiments and data analysis

The dissociation kinetics of DOC-complexes of Co(II), Ni(II), Cu(II), Zn(II), Cd(II) and Pb(II) in fresh waters was studied with Chelex 100 as the competing ligand, using an ELAN 6100 DRC ICP-MS (PerkinElmer SCIEX). The instrument operating conditions and the data acquisition protocol are presented in Table 15. Three grams (1%, w/v) of Chelex 100 was added to 300 mL of the sample solution in a cylindrical Teflon Reactor (500 mL volume), which was stirred continuously with a Teflon-coated stirring bar. The sample solution was filtered with an online 0.40 µm polycarbonate membrane filter

(Corning) to filter out the Chelex 100 resin before introducing the filtrate into the plasma torch by the solution nebulization technique at a flow rate of approximately 1 mL/min. Distributions of dissociation rate coefficients were obtained by fitting the kinetic data to equation (5.4) using the Distribution Analysis Feature (Level 2) of the FLA-900 (Edinburgh Analytical Instruments, UK) fluorescence lifetime analysis program, as described previously [154-155].

6.4 Results and Discussion

6.4.1 Chemical speciation

The water samples were collected near the headwaters of Grand River, which drained a nearby marsh that was the major source of relatively “fresh”, unaltered DOM for the system. As a consequence, the water samples were relatively rich in Dissolved Organic Carbon (DOC = 14.9 ± 0.4 mg/L). Kinetic data for the dissociation kinetics of complexes of Co(II), Ni(II), Cu(II), Zn(II), Cd(II) and Pb(II) in the unirradiated sample are presented in Figures 29 and 33 (chapter 5). The steep section at the beginning of the curve ($k_d \sim 10^{-2} \text{ s}^{-1}$) can be attributed to the Zn(II) aqua complex and/or rapidly-dissociating Zn(II)-FA complexes. The very slowly-falling sections of both curves are probably due to the very slow dissociation ($k_d < 10^{-6} \text{ s}^{-1}$) of strong metal complexes, which represents the lower limit of dissociation rate coefficients that can be measured under the experimental conditions used (i.e. an analytical window of 2 h) in this study.

The theory for metal complexation in aqueous solutions suggests that two factors are expected to dominate metal exchange reactions with DOM: i) ionic potential (z^2/r), and ii) Ligand Field Stabilization Energy (LFSE) for the transition metals [178].

Table 15 Instrumental operating conditions and data acquisition protocol for ICP-MS

ICP-MS	
RF power (kW)	1.1
cooling argon flow rate (L min ⁻¹)	16
carrier argon flow rate (L min ⁻¹)	0.9
auxiliary argon flow rate (L min ⁻¹)	1.1
Data acquisition parameters	
dwell time (ms)	50
scan mode	peak hop
signal measurement	counts s ⁻¹
points/spectral peak	1
resolution	Normal

The results in Figure 34 (chapter 5) show an increase in the dissociation rate constants with increasing ionic potential (z^2/r). The same trend was observed by Fasfous et al. [178] in model solution of Laurentian fulvic acid. Mattock [167] attributed this trend to greater metal-ligand bond stabilization in systems with partial covalent character. This effect probably results from mutual cation and anion polarization, which favours combination with larger, more polarizable ligands, such as carboxylate and phenolate. The covalent character was found to decrease with increasing ionic potential (z^2/r) of the metal cation.

Results for the dissociation kinetics of DOC complexes of Co(II) d^7 , Ni(II) d^8 , Cu(II) d^9 , and Zn(II) d^{10} are presented in Figure 34 and Table 12 (chapter 5). The results suggest that, with the exception of Cu(II), the dissociation rate coefficients fall into the familiar trend predicted from the LFSEs (weak field) (i.e. Co(II) $d^7 >$ Ni(II) $d^8 >$ Cu(II) $d^9 <$ Zn(II) d^{10}), and indicate that inert complexes are those with large LFSEs. This effect is related to unfavourable changes in LFSE [116] on going to the transition state—the larger the LFSE, the larger the sacrifice in the Ligand Field Activation Energy [171]. The behaviour of Cu(II), which has a large LFSE, and is known to form thermodynamically stable metal complexes, can be attributed to the Jahn-Teller effect, which results in the axial bonds becoming elongated, and hence weaker and kinetically labile, and the equatorial bonds becoming shortened, and hence stronger and kinetically inert. A similar trend was reported by Fasfous et al. [178] and Sekaly et al. [172] for the dissociation rate coefficients of some first-row transition metals in model solutions of Laurentian fulvic acid.

The ability of the Kinetic Model to correctly predict the influence of the ionic potential (z^2/r) and LFSE on the relative rates of metal complex dissociation suggests that the speciation model provides a chemically significant description of the kinetic processes in fresh waters.

6.4.2 Influence of solar radiation

The samples were incubated in natural sunlight for periods varying from 0, 10, 20 to 30 days. A significant decrease (20%) in the DOC concentration was observed at the end of the 30-day irradiation period, as shown in Figure 35. The DOC concentration was reported by other workers to decrease following irradiation with UV radiation or simulated sunlight [179-180]. Kieber et al. [181] attributed this effect to a shift from high molecular weight to low molecular weight DOM.

Humic and fulvic substances have been reported to undergo photolytic decomposition to smaller molecular size fractions upon exposure to UV radiation [182,183]. Keiber et al. [181] reported the formation of formaldehyde and acetaldehyde upon irradiation of a variety of natural waters with sunlight.

Results of the solar irradiation experiments on the Cu(II)-DOC complexes show no significant change in the lability of Cu(II)-DOC complexes before 10 days of exposure to sunlight, but a large increase in the lability occurred after 10 days of exposure, as shown in Figure 36. Interestingly, an unexpected decrease in the lability was observed after 30 days of exposure to sunlight. All the kinetic experiments were performed in duplicate, and the same effect was observed in duplicate experiments. One possible explanation for

the decrease in the lability of the Cu(II)-DOC complex was an explosive growth of algae and other microorganisms within the containers between 20 and 30 days of exposure to sunlight. Practically all aquatic microorganisms, such as algae, release metabolites into their growth medium; such metabolites are biogenic ligands and may include strong chelating ligands [184]. Hence, the decrease in the lability might have resulted from the copper forming strong complexes with these strong chelating ligands.

Bioassay toxicity tests using the algae *Pseudokirchneriella subcapitata* (commonly known as *Selenastrum capricornutum*) were done in our collaborating laboratory at Department of Biology, University of Ottawa [185] in parallel with the metal speciation studies. Algae are environmentally important because they are part of the base of the food chain. The water samples were spiked with increasing concentrations of Ni, Cu, Zn, Cd and Pb, and the algae were incubated in the spiked water samples for 72h.

The endpoint for toxicity test was taken as the concentration of the metal required to inhibit 50% of the algal growth (IC_{50}). Interestingly, the toxicity results of Figure 38 after 30 days of exposure of the spiked water samples to sunlight did not reflect the decreased availability of the free metal ion expected from biogenic, strong chelating ligands which might be released in the growth medium of the algae. However, this is probably due to the fact that the algal bioassay studies require the sample to be spiked, which may mask the presence of the exudates present at low concentrations. Figure 33 presents the results of the solar irradiation experiments on the Zn(II)-DOC complex in a freshwater sample. The results suggest a gradual increase in lability from 0 to 10 to 20 days of exposure to sunlight, but a decrease in lability after 30 days of exposure—just as was observed for

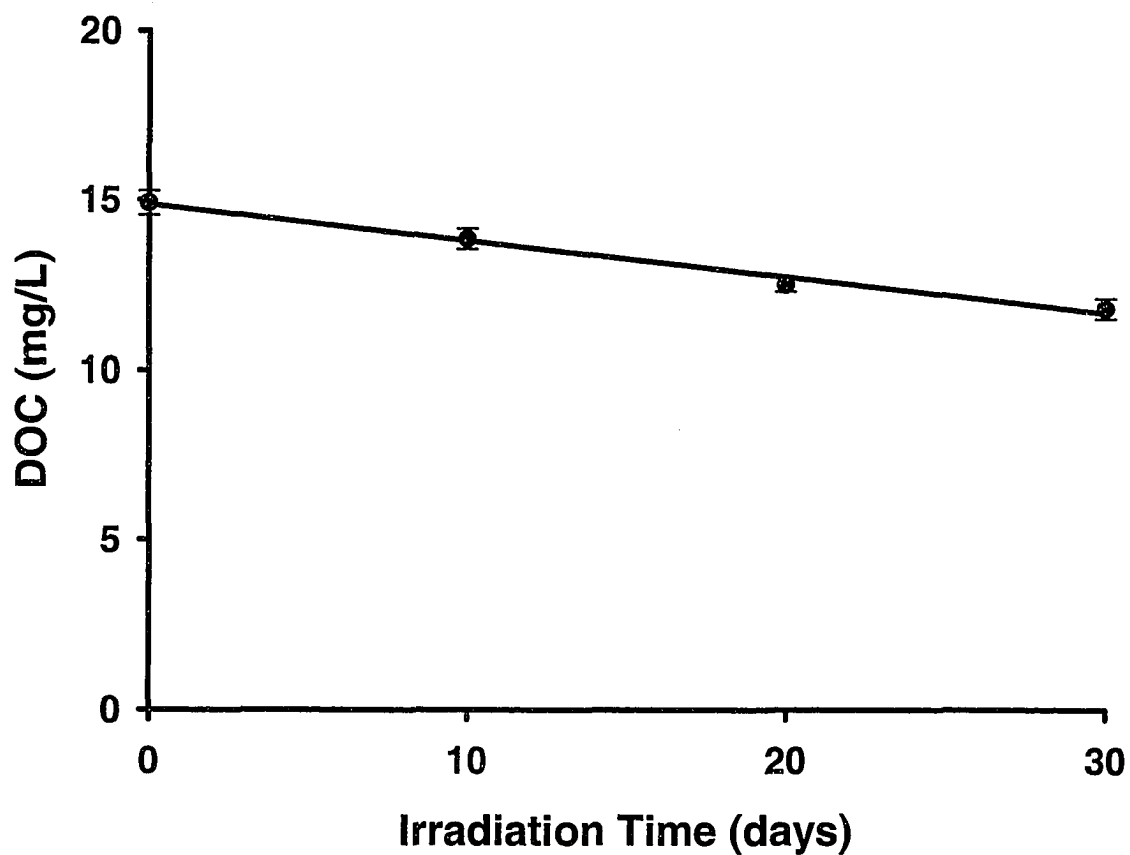


Figure 35 Changes in the concentration of DOC as the function of the duration of the exposure to sunlight for Grand River surface water sample. pH = 7.9 ± 0.1 .

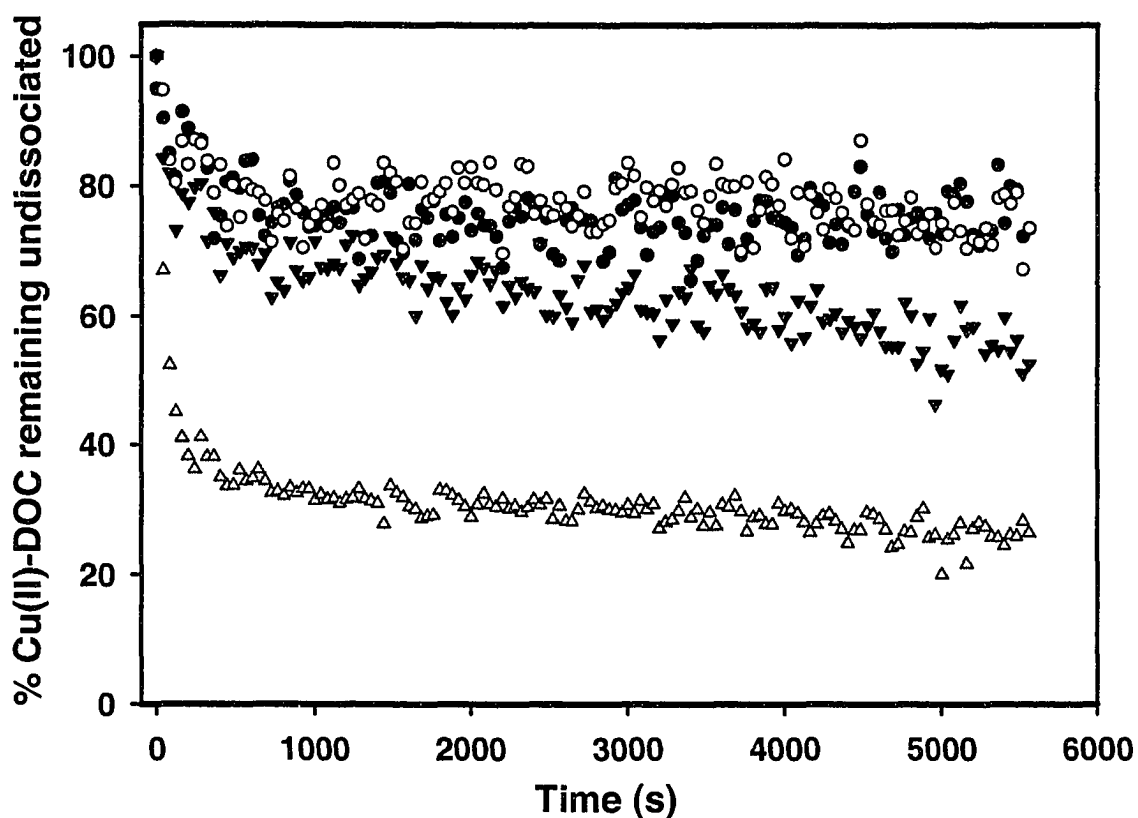


Figure 36 The influence of solar radiation on the lability of Cu(II)-DOC complexes in a freshwater sample collected from Grand River on June 23, 2002, determined by CLEM/ ICP-MS, using Chelex 100 as the competing ligand. DOC 14.9 ± 0.4 mg/L, pH 7.9 ± 0.1 , ionic strength 6×10^{-3} mol/L, temperature 23 ± 2 °C. (●), 0 days; (○), 10 days; (△), 20 days; (▼), 30 days.

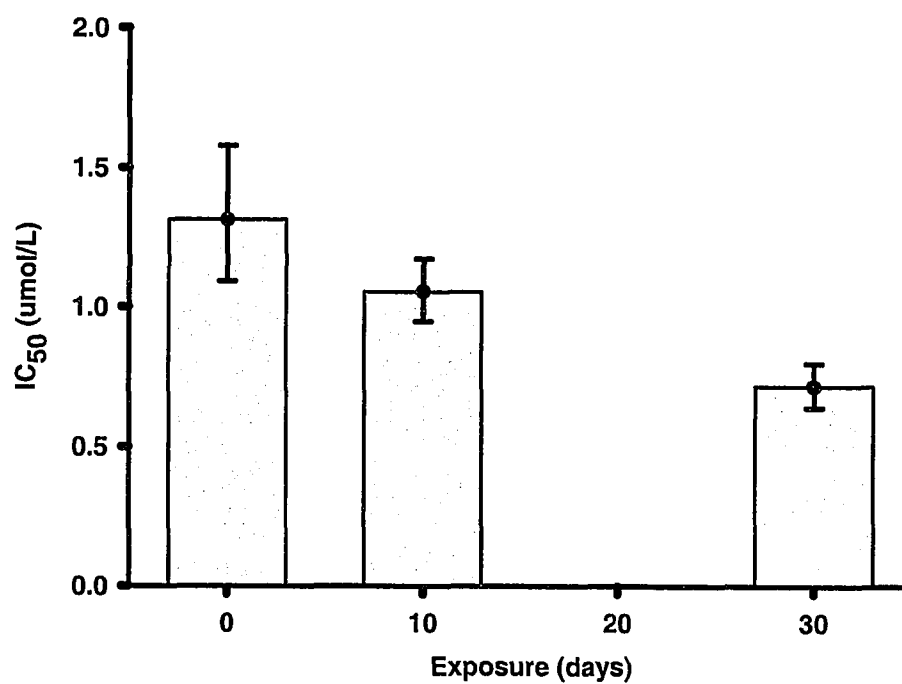


Figure 37 IC₅₀ values at 95% confidence levels, determined from bioassays using Grand River water samples, which were spiked with Cu and exposed to solar radiation for 0, 10, and 30 days [184].

Cu(II)-DOC complexes. By contrast, no significant change was observed for the kinetic speciation of Pb(II)-DOC complexes on exposure to sunlight, as shown in Figure 39. A small increase in lability was observed for Ni(II)-DOC complexes, as shown in Figure 40.

The results for the kinetic speciation of Cd(II)-DOC complexes suggest a gradual increase in lability from 0 to 10 to 20 days of exposure to sunlight, but a decrease in the lability after 30 days of exposure—just as was observed for Cu(II)-DOC complexes, as shown in Figure 41. There was no significant change in the lability of Co(II)-DOC complexes from 0 to 20 days of exposure to sunlight, but a decrease in the lability after 30 days of exposure—just as was observed for Cu(II)-DOC complexes, as shown in Figure 42.

These results suggest that solar radiation had different effects on the binding of these six metals by DOC in freshwater samples collected from Grand River. The greatest change in the lability of the complexes of Ni, Zn and Cd occurred from 0 days to 10 days of exposure to sunlight, and of the complexes of Cu occurred from 10 days to 20 days of exposure to sunlight, whereas no significant increase in the lability was observed for the complexes of Pb from 0 days to 30 days.

As reported by other workers, photochemical formation of reactive intermediates, such as singlet oxygen ($^1\text{O}_2$), OH radicals ($\cdot\text{OH}$), DOM-derived peroxy radicals ($\text{ROO}\cdot$), [182] as well as low-molecular-weight carboxyl acids [186] may lead to the degradation of DOC.

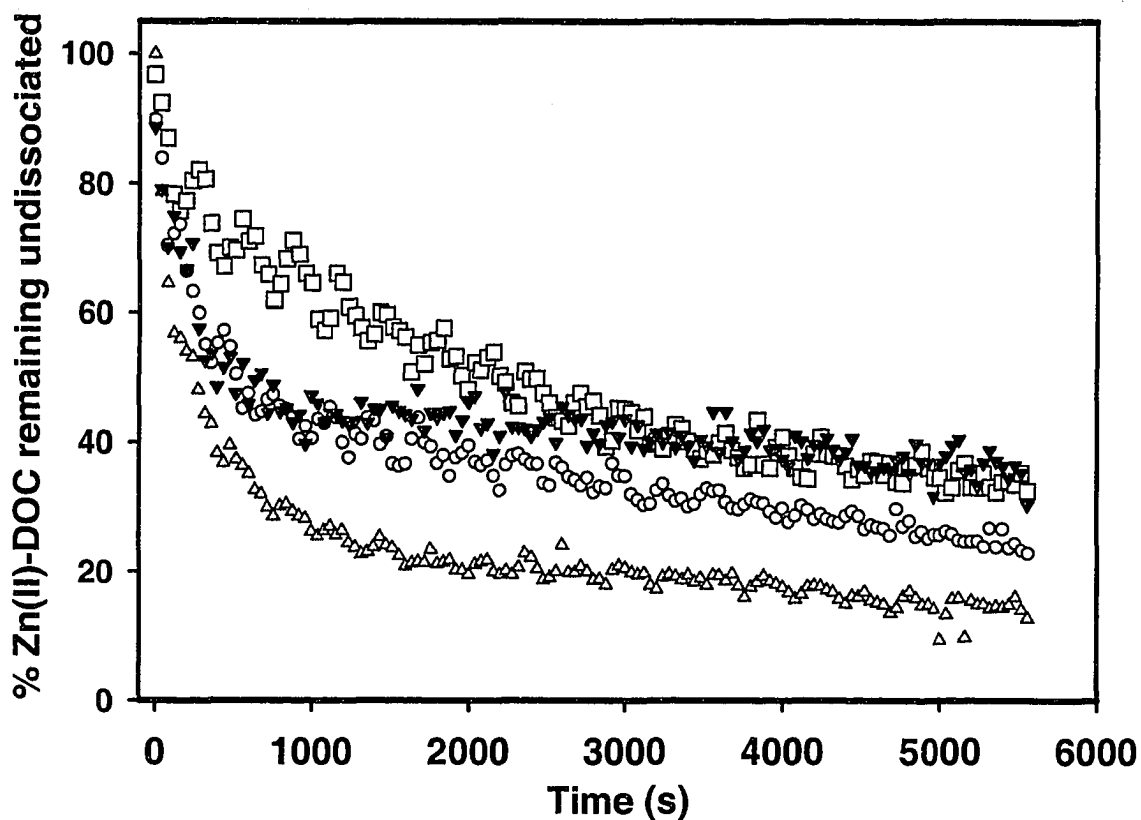


Figure 38 The influence of solar radiation on the lability of Zn(II)-DOC complexes in a freshwater sample collected from Grand River on June 23, 2002, determined by CLEM/ ICP-MS, using Chelex 100 as the competing ligand. DOC 14.9 ± 0.4 mg/L, pH 7.9 ± 0.1 , ionic strength 6×10^{-3} mol/L, temperature 23 ± 2 °C. (□), 0 days; (▼), 10 days; (Δ), 20 days; (○), 30 days.

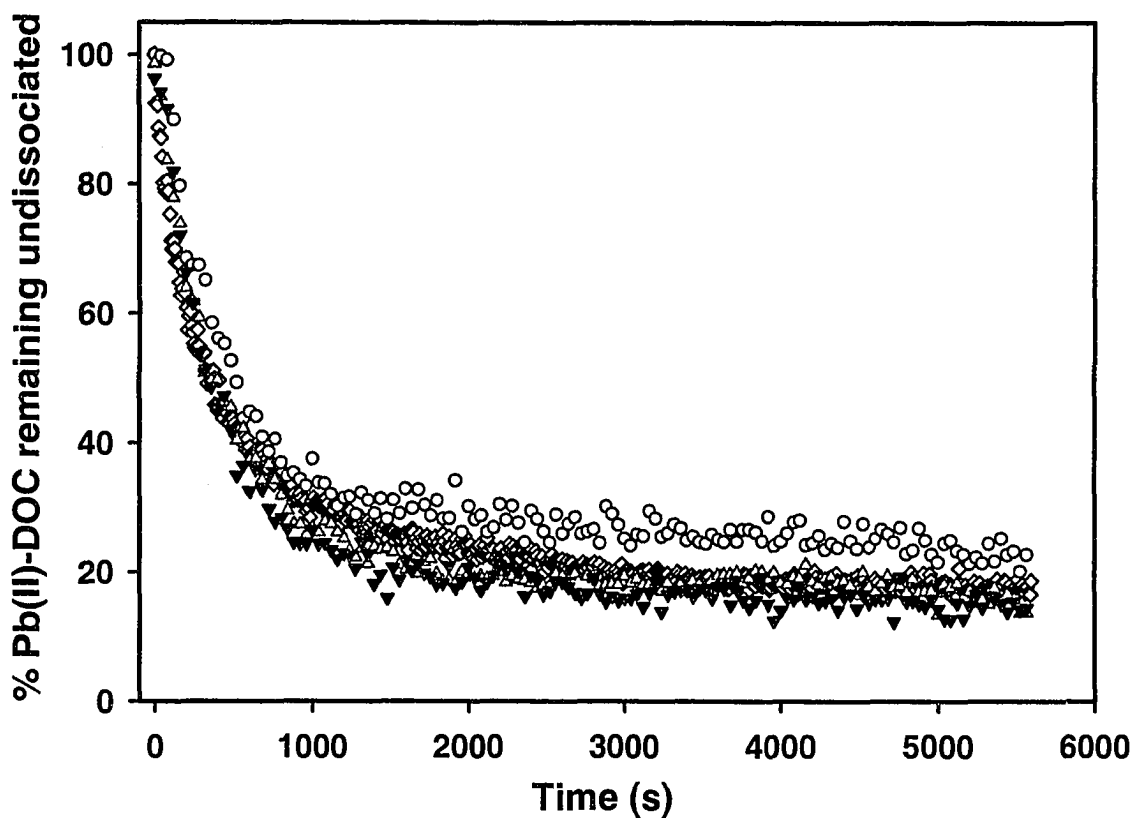


Figure 39 The influence of solar radiation on the lability of Pb(II)-DOC complexes in a freshwater sample collected from Grand River on June 23, 2002, determined by CLEM/ ICP-MS, using Chelex 100 as the competing ligand. DOC 14.9 ± 0.4 mg/L, pH 7.9 ± 0.1 , ionic strength 6×10^{-3} mol/L, temperature 23 ± 2 °C. (\diamond), 0 days; (\circ), 10 days; (Δ), 20 days; (\blacktriangledown), 30 days.

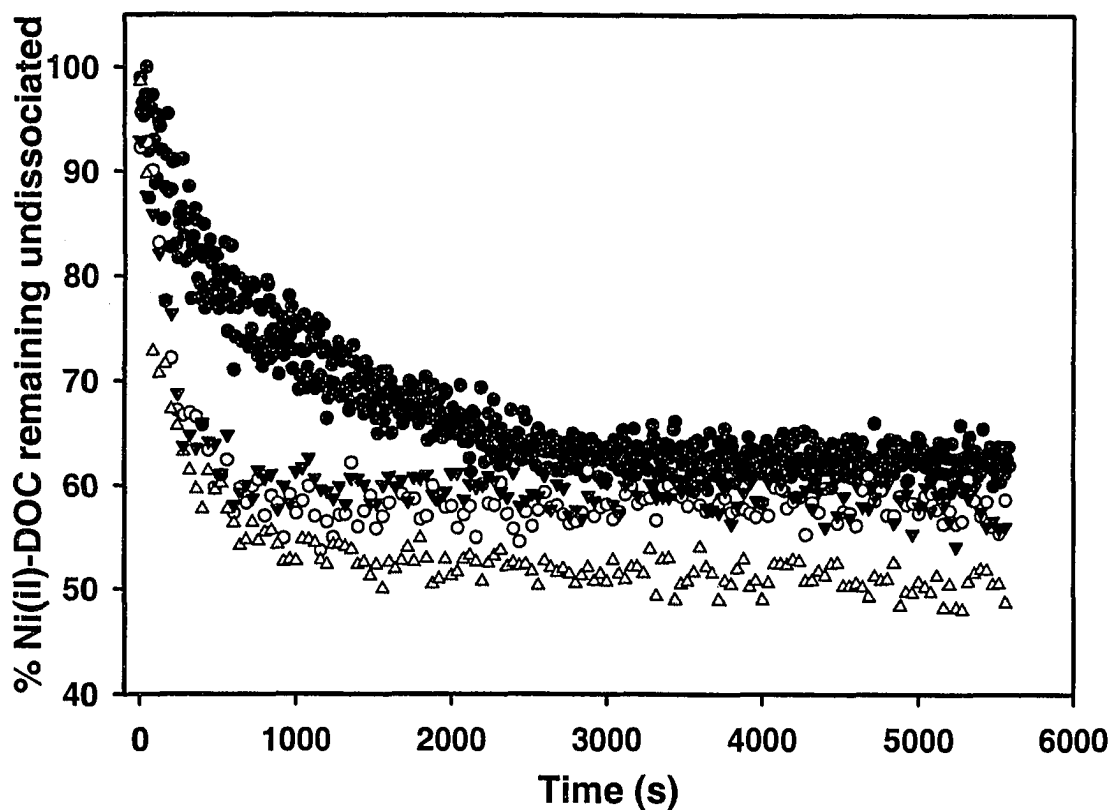


Figure 40 The influence of solar radiation on the lability of Ni(II)-DOC complexes in a freshwater sample collected from Grand River on June 23, 2002, determined by CLEM/ ICP-MS, using Chelex 100 as the competing ligand. DOC 14.9 ± 0.4 mg/L, pH 7.9 ± 0.1 , ionic strength 6×10^{-3} mol/L, temperature 23 ± 2 °C. (●), 0 days; (○), 10 days; (Δ), 20 days; (▼), 30 days.

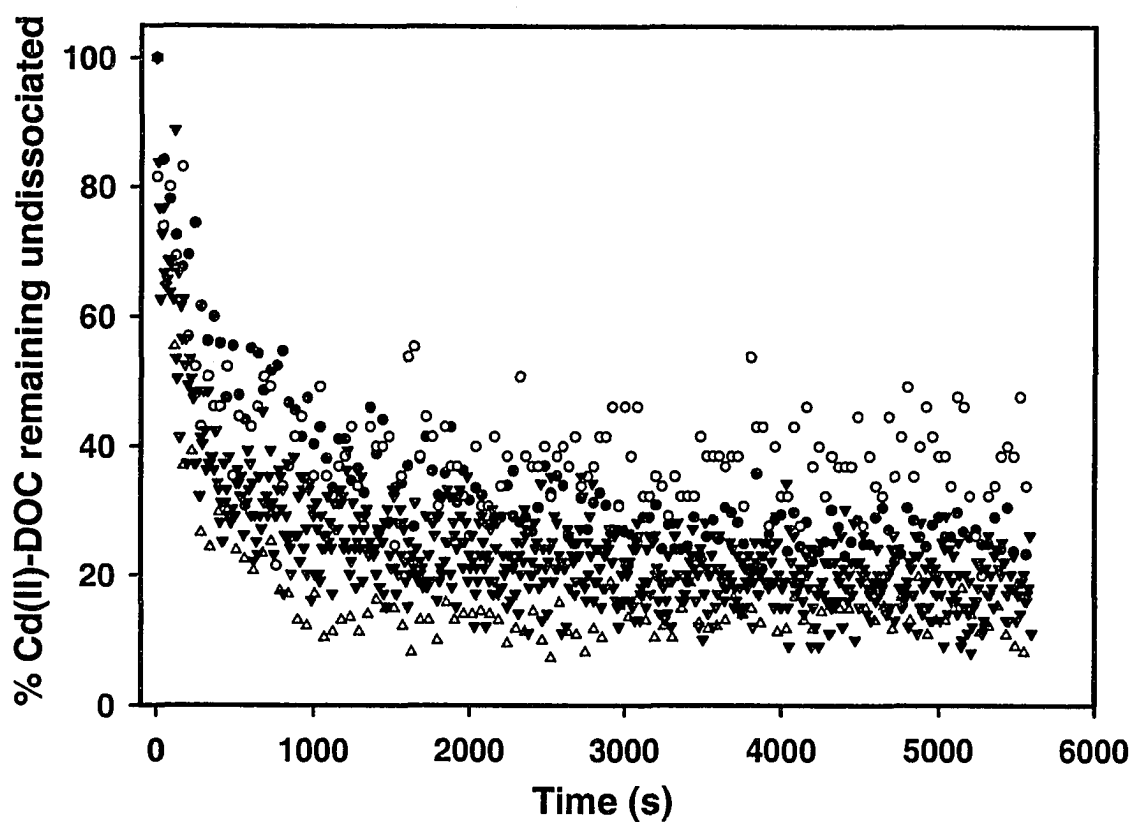


Figure 41 The influence of solar radiation on the lability of Cd(II)-DOC complexes in a freshwater sample collected from Grand River on June 23, 2002, determined by CLEM/ ICP-MS, using Chelex 100 as the competing ligand. DOC 14.9 ± 0.4 mg/L, pH 7.9 ± 0.1 , ionic strength 6×10^{-3} mol/L, temperature 23 ± 2 °C. (●), 0 days; (○), 10 days; (Δ), 20 days; (▼), 30 days.

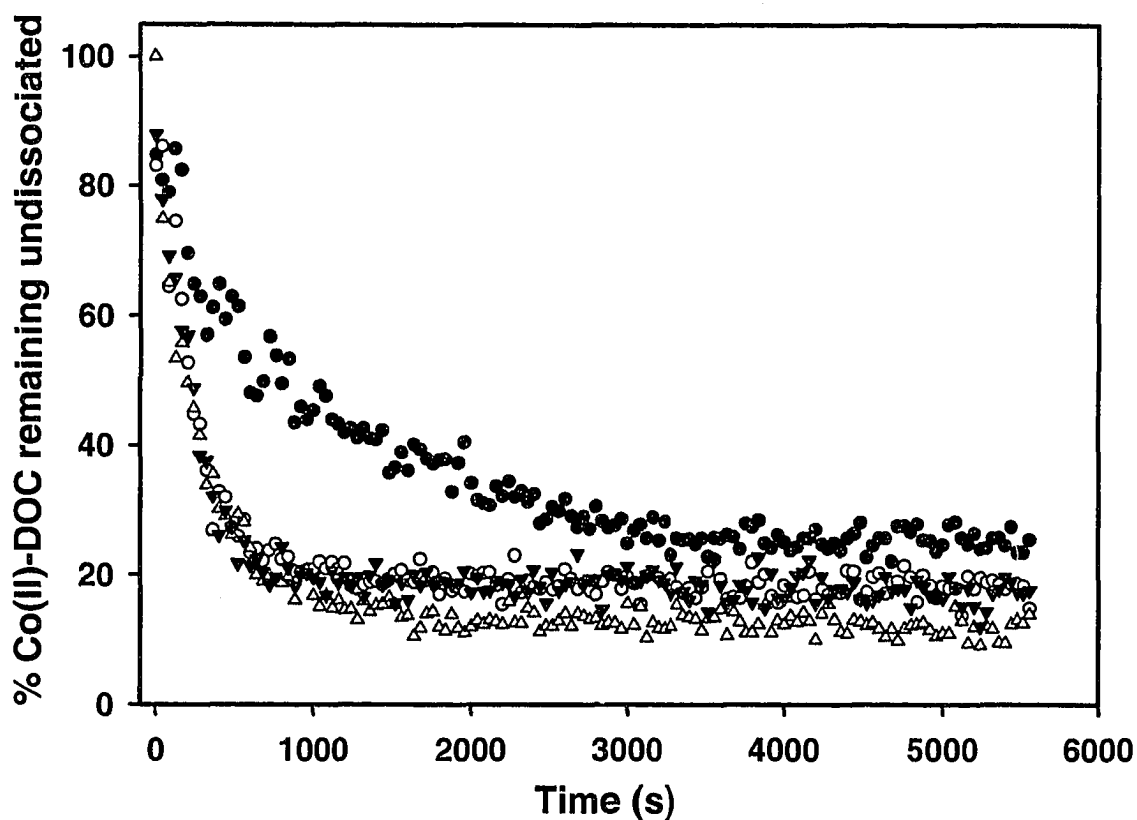


Figure 42 The influence of solar radiation on the lability of Co(II)-DOC complexes in a freshwater sample collected from Grand River on June 23, 2002, determined by CLEM/ ICP-MS, using Chelex 100 as the competing ligand. DOC 14.9 ± 0.4 mg/L, pH 7.9 ± 0.1 , ionic strength 6×10^{-3} mol/L, temperature 23 ± 2 °C. (●), 0 days; (○), 10 days; (△), 20 days; (▼), 30 days.

The interactions of solar radiation with DOC, and their effects on the binding characteristics of the DOC in the euphotic zone of fresh waters (i.e. the surface layer) for metals is probably a major controlling factor in the geochemistry of metals in the freshwater environment.

6.5 Conclusions

With increasing time of exposure to sunlight from 0 days to 30 days, DOC concentrations in natural freshwaters decline, and toxicity of metals to *Selenastrum capricornutum* increases.

Exposure to sunlight significantly reduces the metal binding properties of “fresh” DOC in freshwaters, suggesting that the metal-binding protective effects of DOM depend on the length of the time the DOC is exposed to sunlight. This research shows the importance of exposure time of DOC to sunlight in the chemical speciation and metal bioavailability of metals in the freshwater environment.

This Chapter presents the results of studies on the effects of solar UV-B radiation on some metal-DOC complexes in freshwaters, as revealed by the Competing Ligand Exchange Method (CLEM), using Chelex as the competing ligand and ICP-MS. The results of this study are in sharp contrast with those of an earlier worker from this laboratory [186], who used simulated UV-B radiation and Anodic Stripping Voltammetry-Rotating Disk Electrode (ASV-RDE) technique and reported significantly different results. The originality of this study lies in exposing the danger of accepting the results of a single speciation technique blindly without testing their validity. The reasons

for this difference between the results of the two speciation techniques need to be subjected to further study by future workers. The ASV-RDE technique, with its critical dependence on the essential requirement of equilibration of the added metal-spikes with the native metals, must demonstrate that the metal-spikes are equilibrated. The originality of this work lies in exposing the above problem, which is presented for the first time.

-- Chapter 7 --

Kinetic Speciation of Ni, Cu and Pb in Lake Surface Waters.

**Comparison of Labile Metal Concentrations Obtained by
Competing Ligand Exchange Method/Adsorptive Cathodic
Stripping Voltammetry with those Predicted by a Computer
Speciation Code, Windermere Humic Aqueous Model
(WHAM), V and VI, for Free Metal Ion Concentrations**

7.1 Introduction

Adsorptive Cathodic Stripping Voltammetry (AdCSV) with 8-hydroxyquinoline (oxine), with dimethylglyoxime (DMG), has been previously discussed for kinetic speciation of copper and nickel in chapters 3 and 4, respectively. AdCSV with 8-hydroxyquinoline was used before for lead determination [187] in natural waters. Chakrabarti et al. [110-113] have studied the kinetic speciation of Pb(II)-FA complexes using Competing Ligand Exchange Method (CLEM) with Chelex-100 as the competing ligand and Graphite Furnace Atomic Absorption Spectrometry (GFAAS) or Inductively Coupled Plasma Mass Spectrometry (ICP-MS) for quantification of the lead that has remained bound to the fulvic acid complexes at different measurement times.

It has been reported that the free-metal ion concentration is often related to metal toxicity and bioavailability and freshwaters [5,188]; however, determination of free-metal ion concentration in freshwaters is a difficult task to accomplish at environmentally relevant concentrations, which can be lower than, sometimes much lower than, 10^{-9} M [198]. One approach that has recently received increasing acceptance in predicting free metal concentration is the use of equilibrium-based, computer speciation codes [190-196]. Windermere Humic Aqueous Model (WHAM) developed by Tipping et al. [190,193-195], is an equilibrium-based, computer speciation code for waters, sediments, and soils, and assumes discrete-site electrostatic binding. There are two models of WHAM: WHAM V and its improved version WHAM VI. The main difference between these two models is that Model VI has high-affinity tridentate sites for metals present in small amounts. Besides Model VI also accounts for competition and ionic strength effects, and

for proton-metal exchange [198]. A more detailed description of WHAM V and VI can be found in the literature [192,193].

In order to evaluate the applicability of WHAM for freshwater samples, WHAM predictions must be compared with measured concentrations. WHAM is able to predict the free metal ion concentration, given some easily determined input parameters such as pH and concentrations of total metals, dissolved anions and cations, and DOC [198].

The kinetic speciation technique using CLEM/AdCSV [12,115,140,141,188] gives an analytical signal that represents the total concentration of all labile complexes including metal aqua complex. In order to have a measured concentration of labile metal complexes, the percentage of the labile fraction is multiplied by the total metal concentration of the sample [198]. The WHAM prediction is used as a “check” against the measured concentration of labile metal complexes containing the metal aqua complex.

The objectives of the study presented in this chapter are: (1) to investigate the kinetic speciation of Ni, Cu, and Pb, using CLEM/AdCSV in freshwater samples collected from Rouyn-Noranda (Québec) area; (2) to compare the WHAM predictions with measured concentrations of labile metal complexes by CLEM/AdCSV, in order to appraise the applicability of WHAM for freshwater samples.

7.2 Theory

The theory for Adsorptive Cathodic Stripping Voltammetry (AdCSV) has been presented earlier in Chapter 3. The Pb(II)-oxine complexes have 1:1 and 1:2 stoichiometries, $Pb(ox)^+$ and $Pb(ox)_2$, with stability constants $\beta_{Pb(ox)^+} = 10.03$ and $\beta_{Pb(ox)_2} = 17.34$, respectively [197]. The structure of the complex is shown in Figure 43.

As discussed in chapter 3, in the presence of a large excess of a competing ligand, such as oxine for the determination of Pb^{2+} , eqn (3.3) can be rewritten as

$$[Pb^{2+}]_t = [Pb(Ox)_2]_t = \sum_{i=1}^n [PbL_i]_0 [1 - \exp(-k_i t)] \quad (7.1)$$

The concentration of “free” metal ion, $[Pb^{2+}]_t$, at any time, t , is described by an exponential function that rises to a limiting value.

7.3 Experimental

7.3.1 Materials and reagents

Standard solutions (1000 mg/mL) nickel, copper, and lead were purchased from SCP Science (ICP grade). A 2 M stock solution of pure KNO_3 was prepared by dissolving an

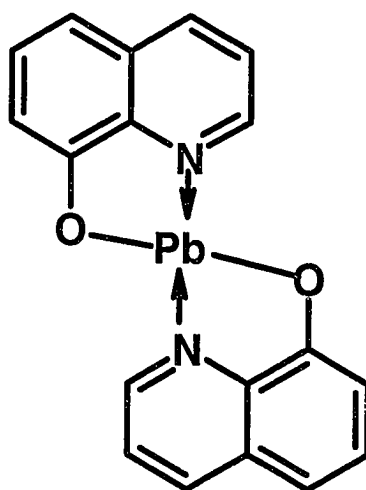


Figure 43 The structure of bis(8-hydroxyquinolinato)lead(II) used in CLEM/AdCSV

appropriate quantity of pure KNO_3 (Aldrich) in ultrapure water. Working standard solutions were prepared daily by dilution of the stock solutions with ultrapure water, which had been acidified to 1% (v/v) with ultrapure nitric acid (Seastar, Canada) to prevent the metal loss by adsorption on the container wall. A stock solution of 0.1M dimethylglyoxime (DMG) was prepared by dissolving an appropriate amount of the solid DMG (Fisher Scientific, certified) in ethanol (Spectro grade). 0.01M stock solution of 8-hydroxyquinoline (oxine) was prepared by dissolving an appropriate amount of the solid oxine (Fisher Scientific, certified) in pure methanol (HPLC grade). The HEPES [N-2-hydroxyethylpiperazine-N-2-ethanesulfonic acid] (BDH, ACS grade) and sodium hydroxide (ACS reagent grade, BDH) were used to prepare the aqueous stock solutions of 2 M HEPES, and 2 M sodium hydroxide, respectively. Nitric acid (Seastar, Canada) and sodium hydroxide were used in order to adjust the pH to the desired value. The pH was checked before and after each experiment. Stock solutions were prepared with ultrapure water of resistivity 18.2 $\text{M}\Omega\text{-cm}$, which was obtained direct from an ultrapure water system, Milli-Q-Academic (Millipore Corporation). All solutions were prepared by dilution of the stock solutions with ultrapure water immediately prior to determination unless otherwise specified. Because the oxine solutions could undergo photolytic decomposition, fresh solutions of oxine were prepared weekly.

7.3.2 Containers and their cleaning procedure

Containers and their cleaning procedure were the same as presented in section 3.3.3 (chapter 3).

7.3.3 Method optimization

Method optimization for kinetic speciation of Cu and Ni using the CLEM/AdCSV method was clearly discussed in chapters 3 and 4. In this section, method optimization for kinetic speciation of lead using CLEM/ AdCSV with oxine as a competing ligand will be addressed. The parameters of the AdCSV method were optimized to study the dissociation kinetics of Pb(II)-DOC complexes in freshwater samples.

7.3.3.1 Effect of deposition time

The effect of increasing adsorption time on the AdCSV/square wave voltammetry (SWV) peak-height current is shown in Figure 44, which shows that the peak-height current increased linearly with time up to 16 min.; an increase in the deposition time causes a decrease in the slope of the peak-height current versus adsorption time curve. The optimum deposition time of 20 seconds was chosen to determine dissociation kinetics of lead in freshwaters.

7.3.3.2 Effect of deposition potential

Pb(Ox)₂ accumulation onto mercury drop was studied as a function of potentials applied in the range between -0.0 and -0.9 V as shown in Figure 45. The reduction in peak-height current with more negative deposition potentials may be due to the saturation of the drop surface by the adsorbed lead-oxine complex [126,127]. The lead-oxine complex accumulation onto mercury drop was found to be optimum at a potential of -0.3 V.

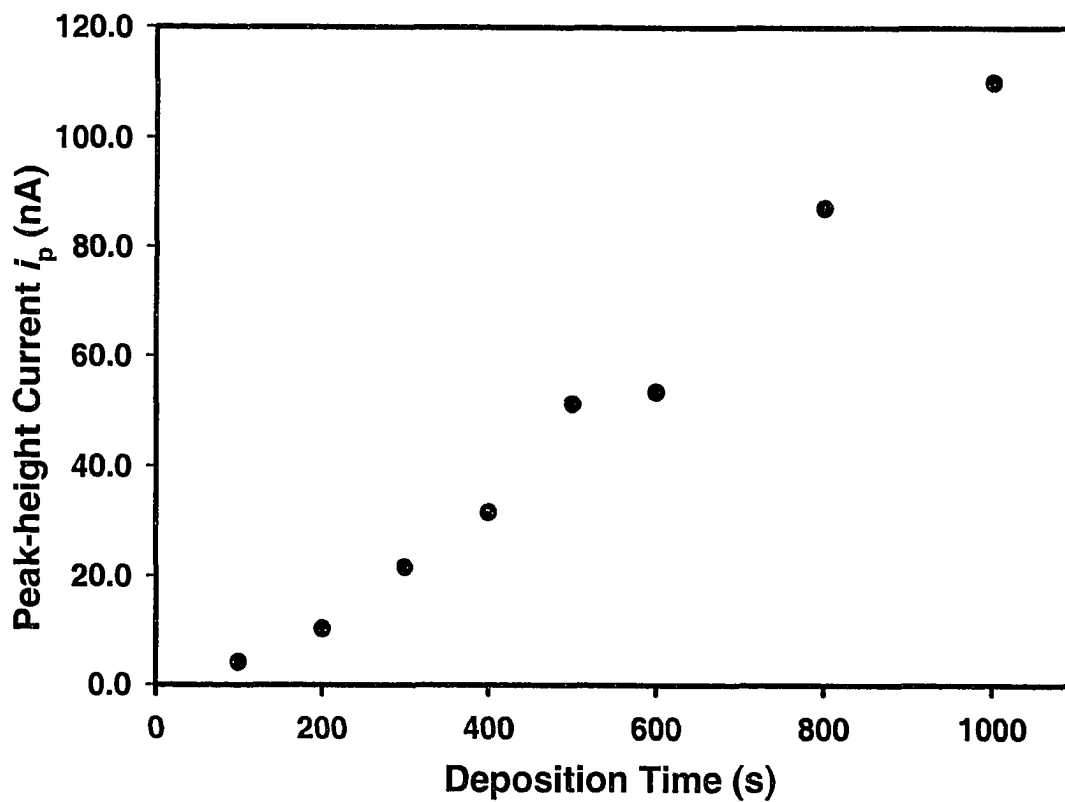


Figure 44 Effect of variation of the deposition time on the AdCSV/SWV peak-height current obtained (i_p , nA) in a model solution containing 0.01M HEPES, Pb(II) 4.8×10^{-9} M, oxine 1×10^{-6} M, pH 7.5 ± 0.1 , ionic strength 1×10^{-2} M, temperature 23 ± 2 °C.

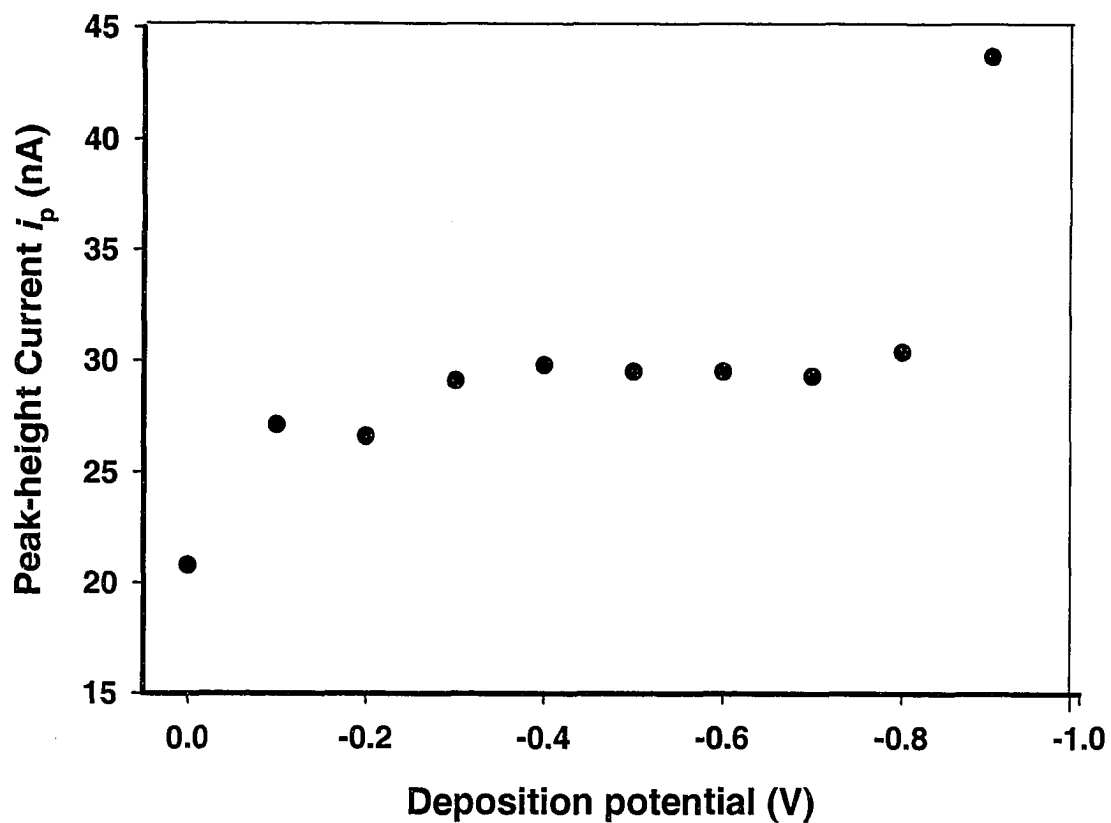


Figure 45 Effect of variation of the deposition potential on the AdCSV/SWV peak-height current obtained (i_p , nA) in a model solution containing 0.01M HEPES, Pb(II) 4.8×10^{-9} M, oxine 1×10^{-6} M, pH 7.5 ± 0.1 , ionic strength 2×10^{-2} M, temperature 23 ± 2 °C.

7.3.3.3 *Effect of the SWV-frequency*

The AdCSV/SWV peak-height current was measured as a function of the SWV frequency (Hz) as shown in Figure 46. The peak-height current increases with increasing SWV frequency; the background current of each scan also increases, but the peak-height current increases more rapidly. The background current can be subtracted from the sample current, as it is relatively smooth and constant during a scan. It was also found that the peak potential shifted in a negative direction with increasing SWV frequency. The increasing peak-height current and increasingly negative shift in the peak potential with increasing oxine concentration were probably caused by increased stability of the adsorbed copper-oxine complex. A frequency of 75 Hz was selected as the optimum frequency for the remaining optimization experiments and determination of dissociation kinetics of lead in freshwaters.

7.3.3.4 *Effect of oxine concentration*

The effect of the variation of oxine concentration on the AdCSV/SWV peak-height current is presented in Figure 47. Figure 47 shows that the peak-height current for lead-oxine complex is almost constant with the oxine concentration around 5×10^{-6} M, and then decreases at higher oxine concentrations, whereas the sample peak-height current decreases and the background current increases at oxine concentrations higher than 5×10^{-6} M probably because of competitive adsorption of free oxine onto the mercury electrode surface. An oxine concentration of 1×10^{-6} M was therefore selected as the optimum oxine concentration for the remaining optimization experiments and the determination of dissociation kinetics of lead in freshwaters. It was also found that the

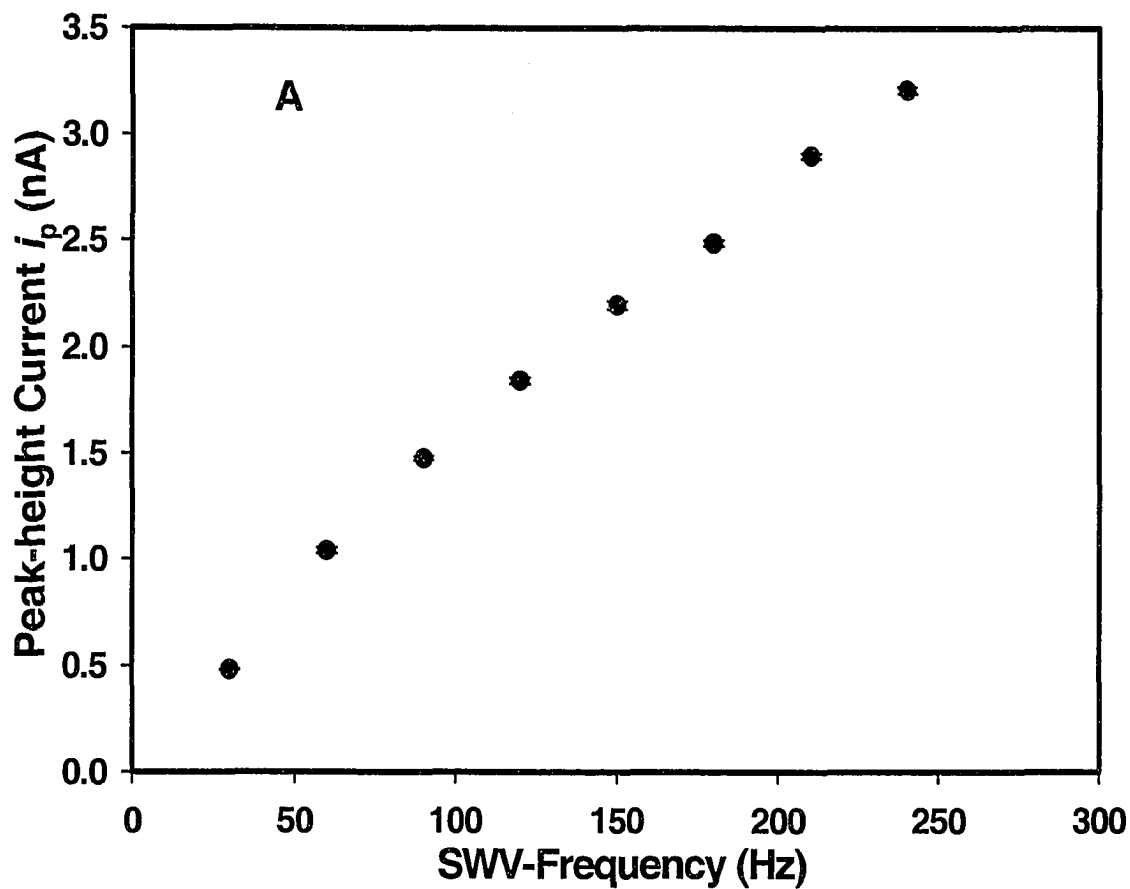


Figure 46 Effect of SWV-frequency on the AdCSV/SWV peak-height current (i_p , nA) obtained in a model solution containing 0.01 M HEPES, Pb(II) 4.8×10^{-9} M, oxine 1×10^{-6} M, pH 7.5 ± 0.1 , ionic strength 1×10^{-2} M, temperature 23 ± 2 °C.

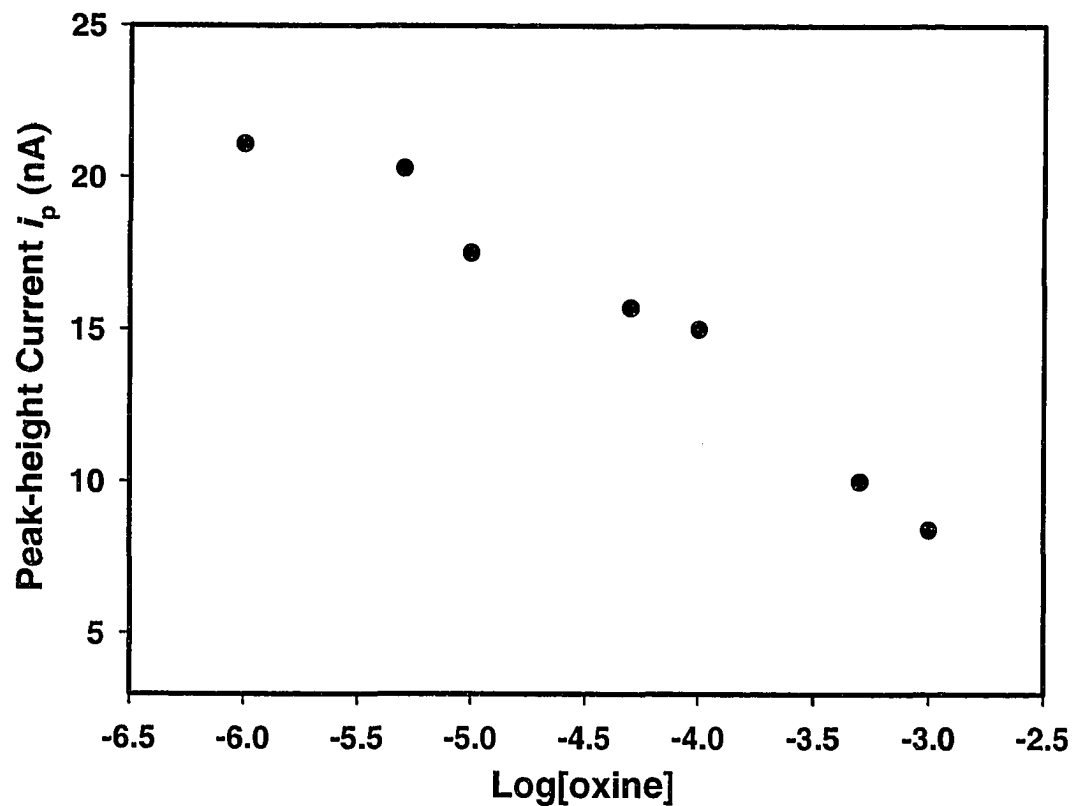


Figure 47 Effect of variation in the oxine concentration on the AdCSV/SWV peak-height current (i_p , nA) obtained in a model solutions containing 0.01 M HEPES, Pb(II) 4.8×10^{-9} M, oxine 1×10^{-6} M, pH 7.5 ± 0.1 , ionic strength 1×10^{-2} M, temperature 23 ± 2 °C.

potential of the peak shifted in a negative direction with increasing oxine concentrations. This was probably due to increased stability of the adsorbed lead-oxine complex.

7.3.4 *Sampling sites and sampling protocol*

Freshwater samples were collected from Rouyn-Noranda, Québec as shown in Figure 48. The lakes in the area of Rouyn-Noranda were impacted by acids and metals from current metal mining operations, abandoned mines, and atmospheric deposition from a large, nearby copper smelter that had been in operation since 1927 [198]. Lake Opasatica was upwind from the smelter, and was less affected by atmospheric fallout from the smelter [199]. Lake Dufault was the most highly contaminated lake based on the data from previous reported studies [198,200,201].

Teflon bottles of 500 mL, 2 L and 2.2 L capacity were used for collecting and storing of water samples and reagents. These bottles were pre-cleaned following the procedure described by Chakrabarti et al. [202].

Samples of surface waters were collected in 2.2 L Teflon bottles (screw-capped) in July and August of 2002 from lakes Opasatica and Dufault. The water samples were filtered through 0.45 μm membrane filters (Gelman Material No. 63077) in our laboratory within 24 h of the sample collection to filter out the particulate matter. These filters, made of mixed cellulose esters, had the advantage of providing filtrates having low blanks for the metals. Each 0.45 μm filter was able to filter approximately 500 mL of water sample before it was clogged. The DOC concentration of the filtered water samples was measured using a Total Organic Carbon (TOC) Analyzer (O I Analytical Model 1010). A

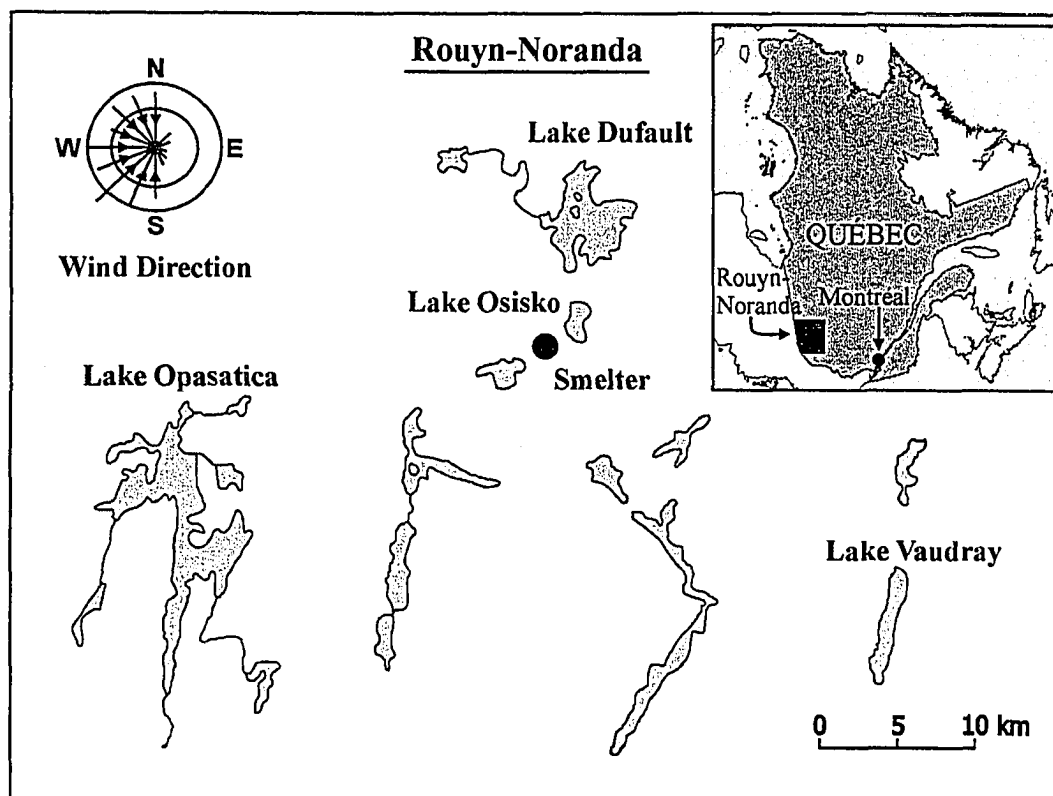


Figure 48 Map of the sampling area in Rouyn-Noranda, Québec, and the lakes studied. The filled circle is the location of the smelter. Adapted from J.C. Brodeur [198].

Table 16 Some properties of the surface-waters of the lakes in Rouyn-Noranda, Québec. Blank spaces refer to metals that were not determined.

	Samples collected in July 2002		Samples collected in August 2002	
	Lake Dufault	Lake Opasatica	Lake Dufault	Lake Opasatica
pH of samples (± 0.1)	7.2	7.7	7.3	7.6
Conductivity (mS/m)*	15.4	11.0	14.8	9.8
DOC (mg/L) ^a	10.9	10.4	6.7	6.9
[M] ^b				
Ni	1.6×10^{-8}	1.4×10^{-8}	3.1×10^{-8}	1.5×10^{-8}
Zn	8.3×10^{-7}	5.7×10^{-8}	5.8×10^{-7}	4.6×10^{-8}
Cd	3.1×10^{-9}	1.8×10^{-10}	2.6×10^{-9}	4.5×10^{-11}
Cu	1.5×10^{-7}	4.2×10^{-8}	2.4×10^{-7}	4.6×10^{-8}
Fe	3.5×10^{-7}	3.5×10^{-7}	1.5×10^{-6}	1.1×10^{-6}
Al	2.3×10^{-7}	1.2×10^{-6}	5.6×10^{-7}	1.1×10^{-7}
Co		N/D		8.5×10^{-10}
Pb	1.4×10^{-9}	7.2×10^{-10}	2.3×10^{-10}	1.9×10^{-10}
Mn		1.4×10^{-8}	3.6×10^{-9}	6.7×10^{-9}
Major Cations (M) ^c				
Mg	1.4×10^{-4}	1.4×10^{-4}	1.6×10^{-4}	1.3×10^{-4}
Ca	4.9×10^{-4}	3.5×10^{-4}	5.1×10^{-4}	2.9×10^{-4}
Na	1.7×10^{-4}	2.2×10^{-4}	1.7×10^{-4}	1.6×10^{-4}
K	1.7×10^{-5}	2.0×10^{-5}	1.6×10^{-5}	1.9×10^{-5}
Major Anions (M) ^c				
F	N/D	N/D	N/D	1.1×10^{-6}
Cl	1.1×10^{-4}	1.2×10^{-4}	1.2×10^{-4}	1.1×10^{-4}
SO ₄	3.8×10^{-4}	1.6×10^{-4}	3.8×10^{-4}	1.0×10^{-4}
NO ₃	8.4×10^{-3}	1.3×10^{-3}	4.7×10^{-6}	1.1×10^{-8}

*Conductivity is not an input parameter for calculating free-metal ion concentrations in these lakes using WHAM

^a Determined by OI Analytical Model 1010 TOC Analyzer.

^b Determined by ICP-MS

^c Determined by Thermo Jarrel Ash IRIS Radial Inductively Coupled Plasma Optical Emission Spectrometer (ICP-OES).

^d Determined by Dionex Series 4000i Ion Chromatograph

N/D: Not Detectable

subsample (30 mL) of the filtered samples was acidified with nitric acid (Seastar, Canada) to pH 1.5. The acidified sample was used to determine the total concentrations of nickel, copper, and lead, using ICP-MS. The remaining filtered samples were stored in the dark at 4 °C until the kinetic experiments, and were used for the kinetic studies within 72 h of filtration. Table 16 presents some characteristics of surface water samples collected from Rouyn-Noranda, Québec in July 2002 and August 2002.

7.3.5 Apparatus

As presented in section 3.3.6 (chapter 3).

7.3.6 Kinetic experiments

Kinetic experiments for Ni and Cu were done as described in chapters 3 and 4 respectively. Briefly, a 10 mL sample of surface water from Lake Dufault (July 2002), buffered to pH 7.2 with 2M HEPES/NaOH, was de-gassed with ultra high-purity nitrogen (UHP, Praxair) for 15 min. Just before the stirring of the test solution was initiated, 10 μ L of 0.001 M oxine was added to this freshwater sample and a potential of -0.3 V was immediately applied to the SMDE to start a 20 s accumulation step by adsorption. Table 17 presents the electrochemical parameters for the determination of metal speciation: nickel, copper, and lead in surface water of the lakes in Rouyn-Noranda, Québec. Similar experiments were performed for other lake water samples. The pH change in the test solution was found to be < 0.5 pH units between the beginning and the end of the experiment. "

Table 17 Parameters of the electrochemical techniques used for the determination of metal speciation: nickel, copper, and lead in surface water samples from the in lakes in Rouyn-Noranda, Québec.

Parameter	Nickel^a	Copper^b	Lead^b
Method	CLEM/ AdCSV	CLEM/ AdCSV	CLEM/ AdCSV
Deposition Potential (V)	0.60	-0.3	-0.3
Deposition Time (s)	10	10	20
Equilibration Time (s)	5	5	10
Initial Potential (V)	-0.60	0.10	-0.20
Final Potential (V)	-1.30	-0.60	-0.60
Step Potential (mV)	5	10	20
Frequency (Hz)	100	75	75
Amplitude (mV)	15	20	50

^a Using kinetics-based CLEM/AdCSV with dimethylglyoxime as the competing ligand.

^b Using kinetics-based CLEM/AdCSV with 8-hydroxyquinoline as the competing ligand.

7.3.7 Data analysis

As discussed in the chapter 3, the overall reaction is treated as pseudo-first-order and the dissociation rate coefficients and their associated kinetically distinguishable components were calculated by fitting the experimental data to a two-component exponential-growth model by non-linear regression analysis using the Marquardt-Levenberg algorithm. The calculations were performed using SIGMAPLOT 8 computer program (SPSS Science).

7.4 Results and Discussion

7.4.1 Nickel speciation in freshwater samples collected from Rouyn-Noranda, Québec, in August 2002

Table 16 presents some properties of the freshwater samples. Dissociation kinetics of Ni(II)-DOC complexes in Rouyn-Noranda samples determined by CLEM/AdCSV using dimethylglyoxime (DMG) as the competing ligand are presented in Figure 49. The experimental data were fitted to the kinetic model (equation 7.1) with a non-linear regression analysis [203]. The results of regression analysis are presented in Table 18. Two kinetically distinguishable components were observed in the freshwater samples. These two kinetically distinguishable components do not mean that the system under study has two distinct metal complexes but it represents the minimum number of the components required to describe the kinetic data. Sekaly et al. [154,155] have reported on kinetic speciation using CLEM/ICP-MS: the binding sites of humic substances probably exist as distributions of sites, but they can be described by recognizable groups that have small distribution of dissociation rate coefficients.

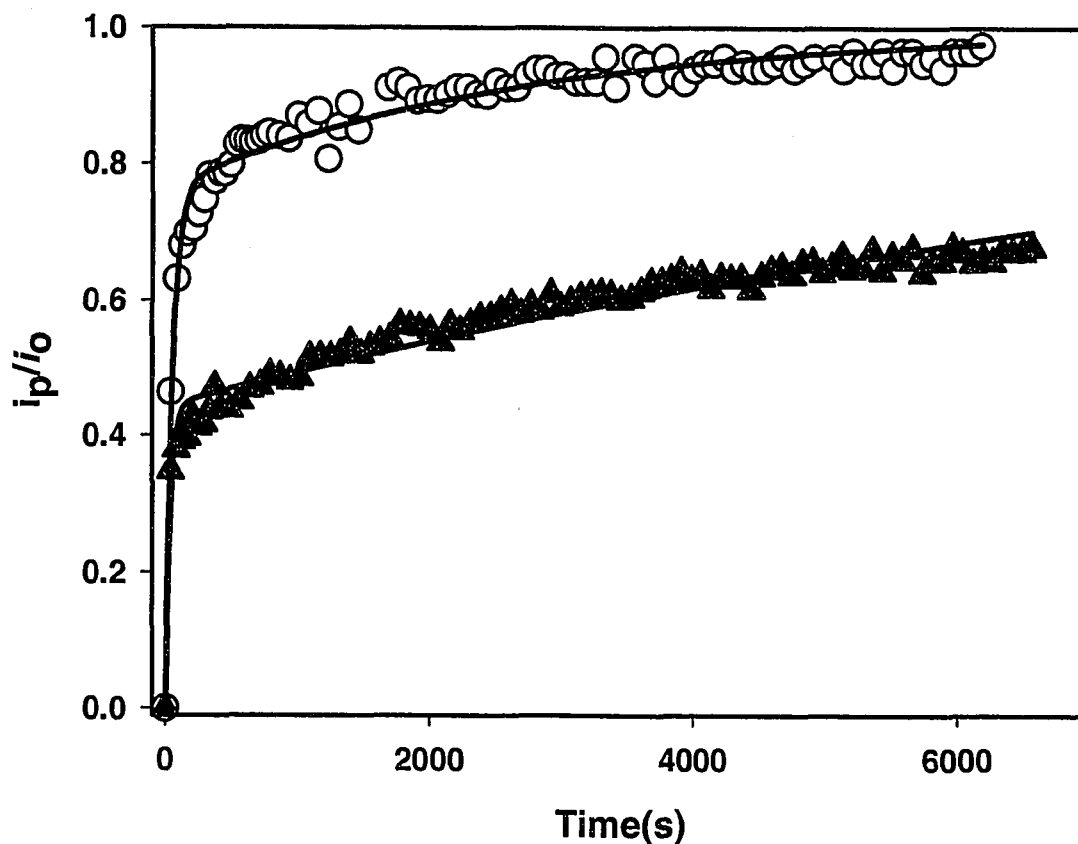


Figure 49 Lability (i_p/i_o) of Ni(II)-DOC complexes in complexes in freshwater samples collected from Rouyn-Noranda, Québec, in August 2002, determined by CLEM/AdCSV, using DMG as the competing ligand; (○), Lake Dufault August 2002, [Ni(II) 3.1×10^{-8} M] + [DOC 6.7 mg/L], pH 7.3 ± 0.1 , ionic strength $\sim 2 \times 10^{-2}$ M, temperature 23 ± 2 °C; (▲), Lake Opasatica August 2002, [Ni(II) 1.5×10^{-8} M] + [DOC 6.9 mg/L], pH 7.6 ± 0.1 , ionic strength $\sim 2 \times 10^{-2}$ M, temperature 23 ± 2 °C.. Solid lines represent non-linear curve-fitting.

Table 18 Ligand exchange kinetics of Ni(II)-DOC in the lake-water samples, determined by CLEM/AdCSV, using DMG as the competing ligand. DMG 1×10^{-3} M, HEPES 0.01 M, ionic strength $\sim 2 \times 10^{-2}$ M, temperature 23 ± 2 °C.

Sample	${}^a[\text{Ni}]_t$ (M)	$C_1(\%)$	$C_2(\%)$	$k_1, (\text{s}^{-1}, 10^{-2})$	$k_2, (\text{s}^{-1}, 10^{-5})$	R^2
Lake Dufault	3.1×10^{-8}	76 ± 4	24 ± 1	1.9 ± 0.4	37 ± 4	0.974
August 2002						
Lake Opasatica	1.5×10^{-8}	44 ± 4	56 ± 0	2.9 ± 0.5	9.5 ± 0.5	0.962
August 2002						

k_1 and k_2 are dissociation rate coefficients of the kinetically distinguishable components. $\%C_1$ and $\%C_2$ are the percentage concentrations of the first and the second component, respectively. The uncertainties represent 95.5% confidence limits of non-linear regression analysis, for an individual value.

${}^a[\text{Ni}]_t$ is total dissolved nickel, determined by ICP-MS.

The dissociation rate coefficient of $1.7 \times 10^{-2} \text{ s}^{-1}$ for the sample from Lake Dufault August 2002 is probably attributable to the dissociation of metal aqua complex and highly labile metal complexes. Total binding sites on humic substances present in freshwater is not known. However, a rough estimate can be obtained from the concentration of DOC, which was in the range of $\sim 7\text{-}11 \text{ mg/L}$ in each of the samples. Thus, the results suggest that the lability of the Ni(II)-complexes increases with increasing [Ni]/[DOC] ratio, as the strong binding sites (which are few) were first occupied, and after they were saturated then numerous weaker binding sites were occupied. The Ni(II)-DOC complex in the surface-water sample from Lake Dufault August 2002 was more labile because the lake had a high [Ni]/[DOC] mole ratio. As shown in Figure 48, the lake Dufault was located directly downwind and close to the smelter, and hence, most likely received the highest amount of nickel through atmospheric deposition. The nickel-DOC complexes in the surface-water sample from Lake Opasatica were more non-labile because the lake had a [Ni]/[DOC] mole ratio and was located upwind from the smelter and hence, received little atmospheric depositions from the smelter. These results agree with those reported by Mandal et al. [146] for the kinetic speciation and toxicity of Ni(II) in freshwaters from the Sudbury (Canada) area, and by N. M Hassan [204], who has reported that lability of Ni(II)-DOC complexes in freshwater samples collected from lakes Dufault and Opasatica in July 2001 is higher than the lability in the current samples. This may be attributed to higher concentrations of Ca^{2+} and Mg^{2+} in samples collected in July 2001 relative to the samples reported in this study.

7.4.2 Copper speciation in lake-water samples collected from Rouyn-Noranda, Québec in July 2002 and August 2002

Dissociation kinetics of Cu(II)-DOC complexes in surface-water samples collected from Rouyn-Noranda, Québec in July 2002 and August 2002 were investigated. Figure 50 presents the results of the above investigation. The results in Figure 50 and Table 19 were obtained by AdCSV using oxine as the competing ligand. In Figure 50, the sharply rising section at the beginning of each curve was due to uptake of Cu-aqua complex and highly labile Cu(II)-DOC complexes. The slowly-rising section of each curve was probably due to the slow dissociation of strong Cu(II)-DOC complexes. Figure 50 suggests the presence of two kinetically distinguishable components. The solid lines in Figure 50 represent data that were fitted to the Kinetic Model (equation 7.1) by non-linear regression analysis. The concentration of total dissolved copper in Lake Dufault was relatively high because it was located close to the smelter at Rouyn-Noranda (Québec), and hence, most likely received the highest amount of copper through atmospheric deposition. The Cu(II)-DOC complexes in the surface water sample from Lake Dufault August 2002 was the most labile because it had the highest [Cu]/[DOC] mole ratio as shown in Table 21a. Fasfous et al. [178] have reported on the dissociation kinetics of Cu(II)-FA complexes that there is a progressive increase in the dissociation rate coefficients with increasing metal-to-FA mole ratio, suggesting that the observed dissociation rate coefficients are associated with progressively weaker sites as the metal loading of the system is increased.

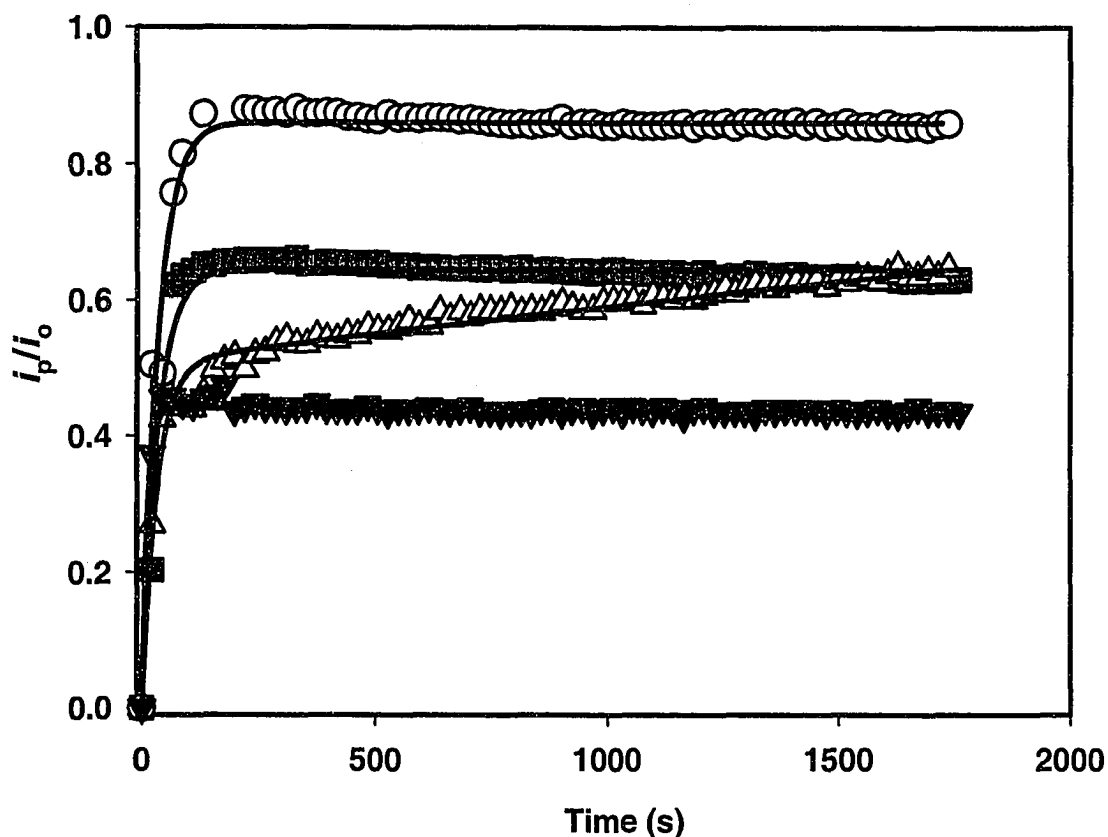


Figure 50 Lability (i_p/i_o) of Cu(II)-DOC complexes in complexes in lake-water samples collected from Rouyn-Noranda, Québec, in July 2002 and August 2002, determined by CLEM/AdCSV, using oxine as the competing ligand; (▼), Lake Dufault July 2002, [Cu(II) 1.5×10^{-7} M] + [DOC 10.9 mg/L], pH, 7.2 ± 0.1 , ionic strength $\sim 2 \times 10^{-2}$ M, temperature 23 ± 2 °C; (Δ), Lake Opasatica July 2002, [Cu(II) 4.2×10^{-8} M] + [DOC 10.4 mg/L], pH 7.7 ± 0.1 , ionic strength $\sim 2 \times 10^{-2}$ M, temperature 23 ± 2 °C; (O), Lake Dufault August 2002, [Cu(II) 2.4×10^{-7} M] + [DOC 6.7 mg/L], pH 7.3 ± 0.1 , ionic strength $\sim 2 \times 10^{-2}$ M, temperature 23 ± 2 °C; (■), Lake Opasatica August 2002, [Cu(II) 4.6×10^{-8} M] + [DOC 6.9 mg/L], pH 7.6 ± 0.1 , ionic strength $\sim 2 \times 10^{-2}$ M, temperature 23 ± 2 °C. Solid lines represent non-linear curve-fitting.

Table 19 Ligand exchange kinetics of Cu(II)-DOC in lake-water samples from Rouyn-Noranda, Québec, determined by CLEM/AdCSV, using 8-hydroxyquinoline (oxine) as the competing ligand. Oxine 1×10^{-5} M, HEPES 0.01 M, ionic strength $\sim 2 \times 10^{-2}$ M, temperature 23 ± 2 °C.

Sample	$^a[\text{Cu}]_t$ (M)	C_1 (%)	C_2 (%)	k_1 (s^{-1} , 10^{-2})	k_2 (s^{-1} , 10^{-4})	R^2
Lake Dufault July 2002	1.5×10^{-7}	51 ± 2	49 ± 1	2.4 ± 0.3	1.4 ± 0.1	0.931
Lake Opasatica July 2002	4.2×10^{-8}	44 ± 1	56 ± 0	8.9 ± 0.3	$< 10^{-6}$ (Inert)	0.935
Lake Dufault August 2002	2.4×10^{-7}	86 ± 4	14 ± 1	2.9 ± 0.2	$< 10^{-6}$ (Inert)	0.981
Lake Opasatica August 2002	4.6×10^{-8}	64 ± 3	36 ± 1	2.9 ± 2.3	$< 10^{-6}$ (Inert)	0.982

k_1 and k_2 are dissociation rate coefficients of the kinetically distinguishable components. $\%C_1$ and $\%C_2$ are the percentage concentrations of the first and second, respectively. The uncertainties represent 95.5% confidence limits of non-linear regression analysis, for an individual value.

$^a[\text{Cu}]_t$ is total dissolved copper, determined by ICP-MS.

7.4.3 Lead speciation in lake-water samples collected from Rouyn-Noranda, Québec in July 2002 and August 2002

Figure 51 and Table 20 present the results of the dissociation kinetics of lead complexes in freshwater samples collected from Rouyn-Noranda, Québec in July 2002 and August 2002. The results suggest that the lability of the lead(II)-complexes increases with increasing $[Pb]/[DOC]$ mole ratio, as the less abundant strong binding sites were first occupied, after they were saturated and then the numerous weak binding sites were occupied. For Pb as well as for Ni and Cu, the concentration of dissolved lead in Lake Dufault was found to be the highest because it was located upwind and close to the smelter, and hence, most likely received the highest amount of lead through atmospheric deposition.

The lead-DOC complexes in the surface water sample from Lake Dufault July 2002 was the most labile because it had the highest $[Pb]/[DOC]$ mole ratio as shown in Table 21b. The above results agree with those reported by Sekaly et al. [157] for the kinetic speciation of Ni(II), Pb(II), and Cu(II) in model solutions of Armadale fulvic acid.

A unique property of naturally occurring complexants, such as humic acid, is that their metal binding properties change with the metal/DOC mole ratio [158,164]. The decrease of the observed dissociation rate coefficients with decreasing $[M(II)]/DOC$ mole ratio, can be attributed to the heterogeneous characteristics of humic substances, such as polyfunctional, polyelectrolytic and conformational properties. This suggests that humic acid has closely spaced binding energies that enable metals to be buffered over a large

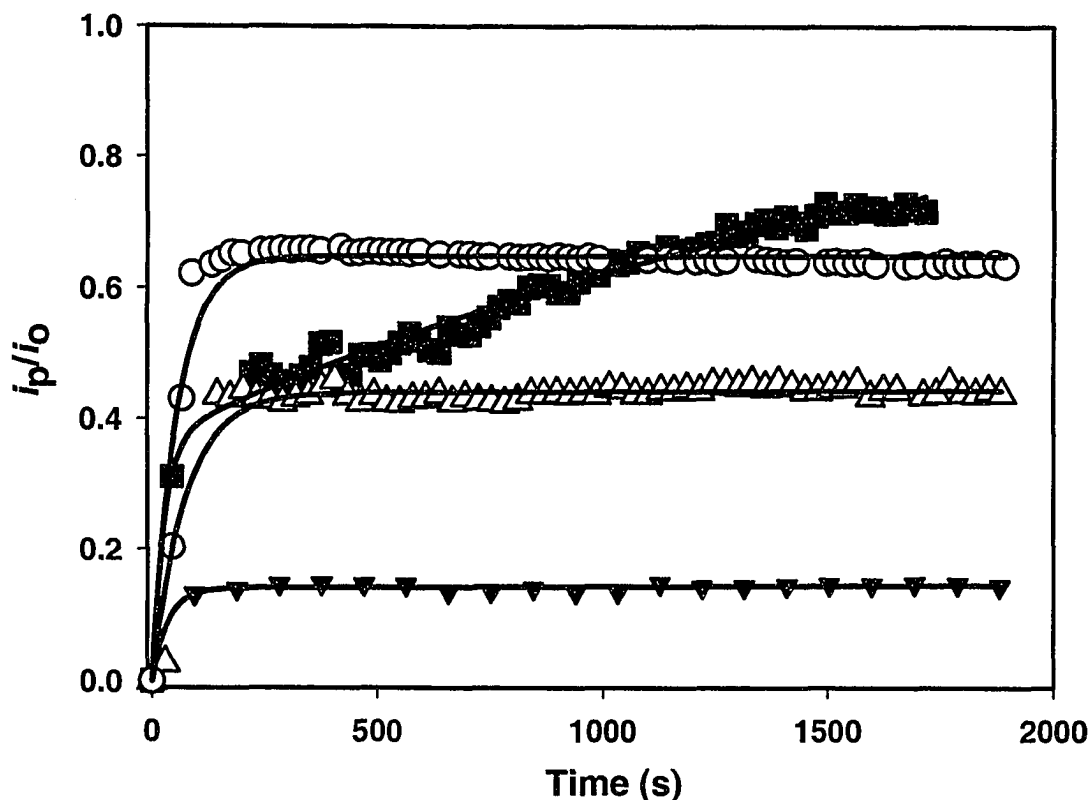


Figure 51 Lability (i_p/i_o) of Pb(II)-DOC complexes in complexes in lake-water samples collected from Rouyn-Noranda, Québec, in July 2002 and August 2002, determined by CLEM/AdCSV, using oxine as the competing ligand; (O), Lake Dufault July 2002, [Pb(II) 1.4×10^{-9} M] + [DOC 10.9 mg/L], pH, 7.2 ± 0.1 , ionic strength $\sim 2 \times 10^{-2}$ M, temperature 23 ± 2 °C; (■), Lake Opasatica July 2002, [Pb(II) 7.2×10^{-10} M] + [DOC 10.4 mg/L], pH 7.7 ± 0.1 , ionic strength $\sim 2 \times 10^{-2}$ M, temperature 23 ± 2 °C; (Δ), Lake Dufault August 2002, [Pb(II) 2.3×10^{-10} M] + [DOC 6.7 mg/L], pH, 7.3 ± 0.1 , ionic strength $\sim 2 \times 10^{-2}$ M, temperature 23 ± 2 °C; (▼), Lake Opasatica August 2002, [Pb(II) 1.9×10^{-10} M] + [DOC 6.9 mg/L], pH 7.6 ± 0.1 , ionic strength $\sim 2 \times 10^{-2}$ M, temperature 23 ± 2 °C. Solid lines represent non-linear curve-fitting.

Table 20 Ligand exchange kinetics of Pb(II)-DOC in freshwaters, determined by CLEM/AdCSV, using 8-hydroxyquinoline (oxine) as the competing ligand. Oxine 1×10^{-6} M, HEPES 0.01 M, ionic strength $\sim 2 \times 10^{-2}$ M, temperature 23 ± 2 °C.

Sample	${}^a[\text{Pb}]_t$ (M)	C_1 (%)	C_2 (%)	k_1 (s^{-1} , 10^{-1})	k_2 (s^{-1} , 10^{-6})	R^2
Lake Dufault July 2002	1.4×10^{-9}	65 ± 5	35 ± 1	1.8 ± 0.3	$<10^{-6}$ (Inert)	0.931
Lake Opasatica July 2002	7.2×10^{-10}	44 ± 4	56 ± 1	1.3 ± 0.3	3.3 ± 20	0.935
Lake Dufault August 2002	2.3×10^{-10}	37 ± 4	63 ± 1	1.8 ± 1.0	512 ± 20	0.981
Lake Opasatica August 2002	1.9×10^{-10}	14 ± 1	86 ± 0	2.9 ± 1.0	2.9 ± 5	0.982

k_1 and k_2 are dissociation rate coefficients of the kinetically distinguishable components. $\%C_1$ and $\%C_2$ are the percentage concentrations of the first and second, respectively. The uncertainties represent 95.5% confidence limits of non-linear regression analysis, for an individual value.

${}^a[\text{Pb}]_t$ is total dissolved lead, determined by ICP-MS.

concentration range (several orders of magnitude) with only gradual changes in free metal ion concentration.

Competition of major cations (Ca^{2+} and Mg^{2+}) is an important factor controlling the lability of the metal-DOC complexes in freshwaters. Since the concentrations of major cations are several order of magnitude (about 5) greater than the concentrations of trace metals. Thus, presence of large amount of Ca^{2+} in electrical double layer and diffuse layer can screen the negative charges imparted on the DOC [158] leading to a significant decrease in the total binding energy. Mandal et al. [12] have reported on influence of major cations (e.g. Ca^{2+} and Mg^{2+}) on metal speciation in model solution and freshwaters: large excess amounts of Ca^{2+} and/or Mg^{2+} promote the release of large fractions of Ni(II)-DOC, as free Ni^{2+} ions. Competition of major cations (e.g Ca^{2+} and Mg^{2+}) with Cu(II) for the binding sites on humic acid is comprehensively discussed in chapter 3.

7.4.4 A comparison of results of the kinetic speciation method with those of the computer speciation code: WHAM V and VI

Tables 21a and Table 21b present WHAM model predictions of the speciation of Ni, Cu, and Pb in the lake water samples based on 65% of the DOC as “active”, and the measured concentrations of labile Ni(II)-, Cu(II)-, Pb(II)-complexes in the lake waters, collected from Rouyn-Noranda, Québec, in July 2002 and August 2002. The experimental pH of all the lake waters was, however, set to pH ~7.3 using the buffer HEPES; this made the ionization of the acid groups of the DOC in all lake waters roughly the same and facilitated comparison of the results of all four lakes [189].

WHAM modelling was done in several different ways to minimize the difference between the measured concentration of labile metal complexes (including free-metal-ion) and the free-metal-ion concentration predicted by WHAM. It has been suggested by other workers [133,205-210] that only a portion of the [DOC] is “active” with respect to metal-binding since the DOC is not entirely composed of HA and FA [55]. WHAM was run using 3 different concentrations of “active” DOC: 50, 65 and 80% of the total [DOC] as FA in order minimize the differences between measured and predicted free metal ion concentrations [189]. The measured concentrations of labile Metal-complexes were compared with those predicted by WHAM using the three concentrations of “active” DOC, and it was found that in most cases, the measured free-metal ion concentrations were satisfactorily modelled by assuming between 65 and 80% of the DOC as “active”. In order to determine which version (V or VI) of WHAM was better suited for modelling the above lake surface waters, the results of WHAM V were compared with those of WHAM VI [189]. Input parameters used for calculating free-metal ion concentrations in the four lakes using WHAM have been presented earlier in Table 16.

Nickel modelling

Figure 52 shows the results of the modelling and the experimental results for nickel. It is important to note here that for the nickel speciation using CLEM/AdCSV method gives total concentration of all labile complexes included small organic and inorganic complexes of the nickel as well as nickel aqua complex. Whereas the predicted value from WHAM also included the inorganic complexes such as NiCl_2 and NiSO_4 as well as the free-nickel-ion, although in most cases, the concentrations of the inorganic

components were negligible compared to the free-nickel-ion concentration [189]. Consequently, it was expected that the measured $[\text{Ni}^{2+}]$ by the CELM/AdCSV analytical method would be higher than the WHAM-predicted $[\text{Ni}^{2+}]$ [189].

The concentration of nickel aqua complex depends on the $[\text{Ni}]/[\text{DOC}]$ ratio as shown in Table 21a. The general expectations is for Lake Dufault to have the highest $[\text{Ni}^{2+}]$ since it has the highest $[\text{Ni}]/[\text{DOC}]$ mole ratio, and Lake Opasatica to have the lowest $[\text{Ni}^{2+}]$. Figures 53A and 53B show that the free Ni^{2+} ion concentration predicted by WHAM V and VI compared reasonably well with the measured concentrations. The predictions of both WHAM V and VI were nearly equal for Lake Opasatica. For Lake Dufault, WHAM VI prediction would have the lowest $[\text{Ni}^{2+}]$, whereas the predictions of WHAM V would have the highest $[\text{Ni}^{2+}]$. The predictions of WHAM V for free Ni^{2+} ion concentrations were in closer agreement with the measured concentrations (which, however, represented labile nickel complexes) for Lake Dufault [189].

Copper modelling

It has been reported in the literature [211] and also by our laboratory [173] that Cu and Pb form strong complexes with HS. This strong binding is reflected in WHAM – the $\log K_{\text{MA}}$ values for Cu and Pb reflect the strongest modeled metal-binding (Table 22) of the six metals investigated in this thesis. The default values for the constant $\log K_{\text{MA}}$ values of FA in both WHAM V [192] and VI [193] control the strength of metal-binding to FA. Figure 53 shows the results of the measured concentrations of $[\text{Cu}^{2+}]$ using CLEM/AdCSV (see Table 19 and Figure 50), and those predicted by WHAM V and VI.

Table 21a WHAM model predictions of the speciation of Ni, Cu, and Pb in the lake water samples based on 65% of the DOC as “active”, and the measured concentrations of labile Ni(II)-, Cu(II)-, and Pb(II)-complexes in the lake waters collected from Rouyn-Noranda, Quebec, in July 2002 and August 2002.

Nickel

Sample	[Ni] ^a (M)	DOC ^b (mg/L)	[Ni] ^a /DOC (mol/g)	WHAM V [Ni ⁺²] (M)	WHAMVI [Ni ⁺²] (M)	Measured concentration of labile Ni-complexes (M)
Lake Dufault August 2002	3.1 x 10 ⁻⁸	6.7	4.7 x 10 ⁻⁶	2.6 x 10 ⁻⁸	1.36 x 10 ⁻⁸	2.4 x 10 ⁻⁸
Lake Opasatica August 2002	1.5 x 10 ⁻⁸	6.9	2.1 x 10 ⁻⁶	9.5 x 10 ⁻⁹	9.8 x 10 ⁻⁹	6.4 x 10 ⁻⁹

^a[Ni]_t is total dissolved nickel, determined by ICP-MS.

^b Determined by OI Analytical Model 1010 TOC Analyzer.

Copper

Sample	[Cu] ^a (M)	DOC ^b (mg/L)	[Cu] ^a /DOC (mol/g)	WHAM V [Cu ⁺²] (M)	WHAMVI [Cu ⁺²] (M)	Measured concentration of labile Cu-complexes (M)
Lake Dufault July 2002	1.5 x 10 ⁻⁷	10.9	1.4 x 10 ⁻⁵	4.8 x 10 ⁻¹⁰	1.4x 10 ⁻¹⁰	7.9 x 10 ⁻⁸
Lake Opasatica July 2002	4.2 x 10 ⁻⁸	10.4	4.0 x 10 ⁻⁶	2.1 x 10 ⁻¹¹	2.3 x 10 ⁻¹²	1.8 x 10 ⁻⁸
Lake Dufault August 2002	2.4 x 10 ⁻⁷	6.7	3.5 x 10 ⁻⁵	5.4 x 10 ⁻⁹	1.0 x 10 ⁻⁹	2.0 x 10 ⁻⁷
Lake Opasatica August 2002	4.6 x 10 ⁻⁸	6.9	6.6 x 10 ⁻⁶	1.2 x 10 ⁻¹⁰	5.0 x 10 ⁻¹²	2.9 x 10 ⁻⁸

^a[Cu]_t is total dissolved copper, determined by ICP-MS.

^b Determined by OI Analytical Model 1010 TOC Analyzer.

Table 21b WHAM model predictions of the speciation of Ni, Cu, and Pb in the lake water samples based on 65% of the DOC as “active”, and the measured concentrations of labile Ni(II)-, Cu(II)-, and Pb(II)-complexes in the lake waters collected from Rouyn-Noranda, Quebec, in July 2002 and August 2002.

Lead

Sample	[Pb] ^a (M)	DOC ^b (mg/L)	[Pb] ^a /DOC (mol/g)	WHAM V [Pb ⁺²] (M)	WHAMVI [Pb ⁺²] (M)	Measured concentration of labile Pb-complexes (M)
Lake Dufault July 2002	1.4×10^{-9}	10.9	1.2×10^{-7}	1.3×10^{-11}	1.6×10^{-12}	8.8×10^{-10}
Lake Opasatica July 2002	7.2×10^{-10}	10.4	7.0×10^{-8}	1.3×10^{-12}	2.7×10^{-13}	3.2×10^{-10}
Lake Dufault August 2002	2.3×10^{-10}	6.7	3.4×10^{-8}	1.5×10^{-11}	8.9×10^{-13}	8.4×10^{-11}
Lake Opasatica August 2002	1.9×10^{-10}	6.9	2.8×10^{-8}	1.7×10^{-12}	7.6×10^{-14}	2.7×10^{-11}

^a[Pb]_t is total dissolved lead, determined by ICP-MS.

^b Determined by OI Analytical Model 1010 TOC Analyzer.

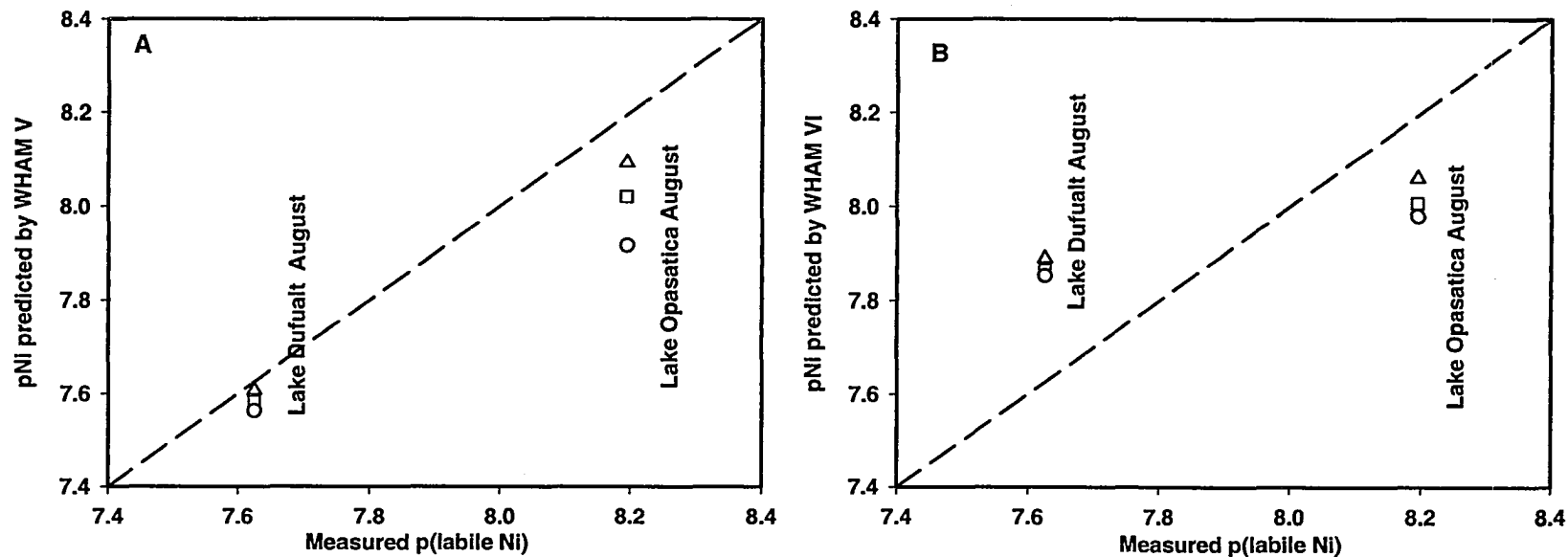


Figure 52 Comparison of WHAM predicted pNi with the measured concentrations of labile Ni(II)-complexes in lake-water samples collected from Rouyn-Noranda, Québec, in July 2002 and August 2002. Input parameters used for calculating free-metal ion concentrations in the four lakes using WHAM have been presented in Table 16. Each lake was modelled using 3 different active DOC concentrations. (---) 1:1 line; (O), 50% active DOC; (\square), 65% active DOC; (\triangle), 80% active DOC. A) WHAM V predictions ; B) WHAM VI predictions.

Table 22 Default values of the constant $\log K_{MA}$ in Model V [192] and VI [193].

Metal	$\log K_{MA}$ for FA WHAM V	$\log K_{MA}$ for FA WHAM VI	Standard deviation
Ni	1.4	1.4	0.3 (4)
Zn	1.3	1.6	0.2 (4)
Cd	1.5	1.6	0.1 (3)
Cu	0.8	2.1	0.2 (9)
Pb	0.9	2.2	0.2 (4)
Co	1.7	1.4	0.2 (2)

Standard deviations are for the $\log K_{MA}$ values for WHAM VI, which are based on the number of measurements shown in parentheses.

The lowest [Cu] was in Lake Opasatica, and the highest [Cu] was in Lake Dufault. Since the $[\text{Cu}^{2+}]$ would depend on [Cu]/[DOC] ratios (see Table 21a), and the [Cu]/[DOC] ratio of Lake Dufault was much higher than that of Lake Opasatica, it was expected that Lake Dufault would have the highest $[\text{Cu}^{2+}]$ concentration. Both the measured $[\text{Cu}^{2+}]$ and the WHAM predictions agreed with the expectation. The results of the CLEM/AdCSV method represented the sum of labile Cu(II) complexes including the Cu-aqua complex ($[\text{Cu}(\text{H}_2\text{O})_6]^{2+}$); hence, the measured results were expected to be equal to or greater than those predicted by WHAM. The WHAM V predicted values of $[\text{Cu}^{2+}]$ were only 2 order of magnitude lower than the measured $[\text{Cu}^{2+}]$, whereas WHAM VI prediction for Lake Opasatica, was 3 orders of magnitude lower than the measured $[\text{Cu}^{2+}]$.

Lead modelling

Figure 54 shows the results of the modelling and experimental results for lead. The concentration of lead aqua complex depends on the [Pb]/[DOC] mole ratio. Table 21b shows that the highest [Pb]/[DOC] mole ratio was for the water sample of Lake Dufault, and the lowest ratio was for the water sample of Lake Opasatica. Both the measured concentrations of labile Pb(II)-DOC complexes and the WHAM predictions agreed with the expectation. The measured concentrations of labile Pb(II)-DOC complexes did not agree that well with the predictions of WHAM— both versions V and VI. The WHAM V predicted values of $[\text{Pb}^{2+}]$ were only 1-2 order of magnitude lower than the measured labile lead concentrations, whereas WHAM VI prediction for all lakes was 2-3 orders of magnitude lower than the measured labile lead concentrations. This result, however, was reasonable, considering the assumptions and uncertainties of WHAM. WHAM V had

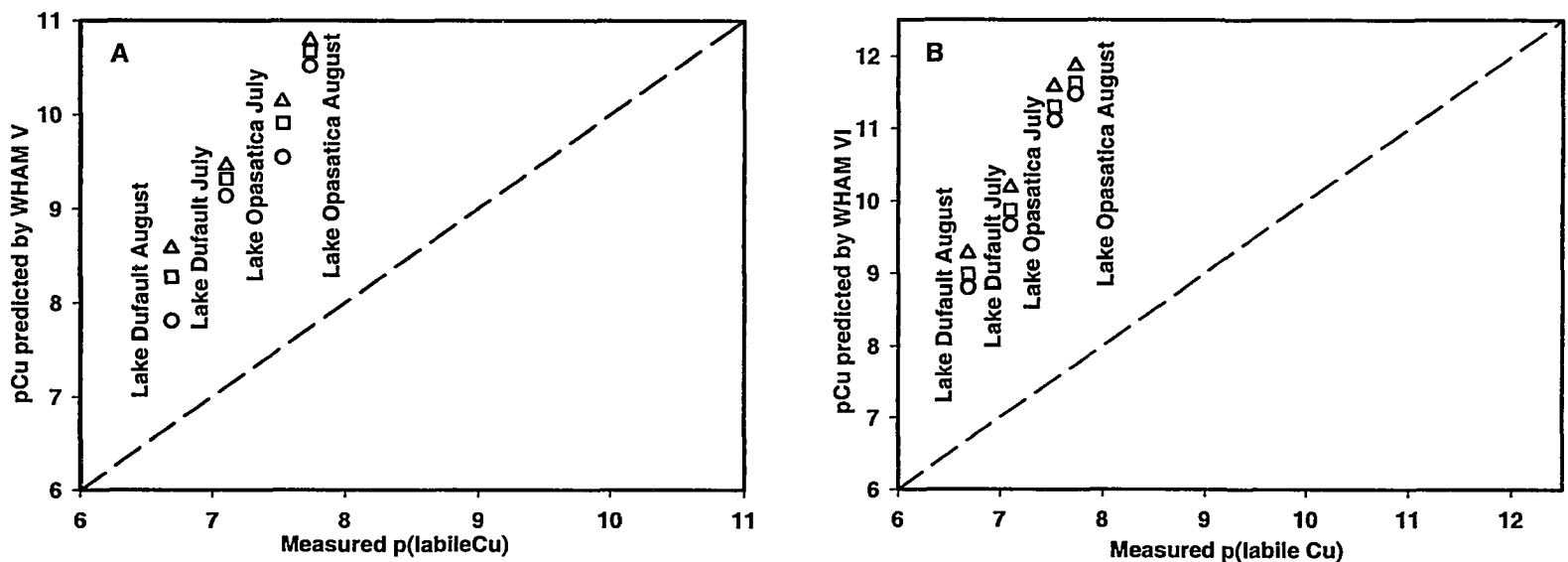


Figure 53 Comparison of WHAM predicted pCu with the measured concentrations of labile Cu(II)-complexes in lake-water samples collected from Rouyn-Noranda, Québec, in July 2002 and August 2002. Input parameters used for calculating free-metal ion concentrations in the four lakes using WHAM have been presented in Table 7.1. Each lake was modelled using 3 different active DOC concentrations. (---) 1:1 line; (O), 50% active DOC; (□), 65% active DOC; (△), 80% active DOC. A) WHAM V predictions ; B) WHAM VI predictions.

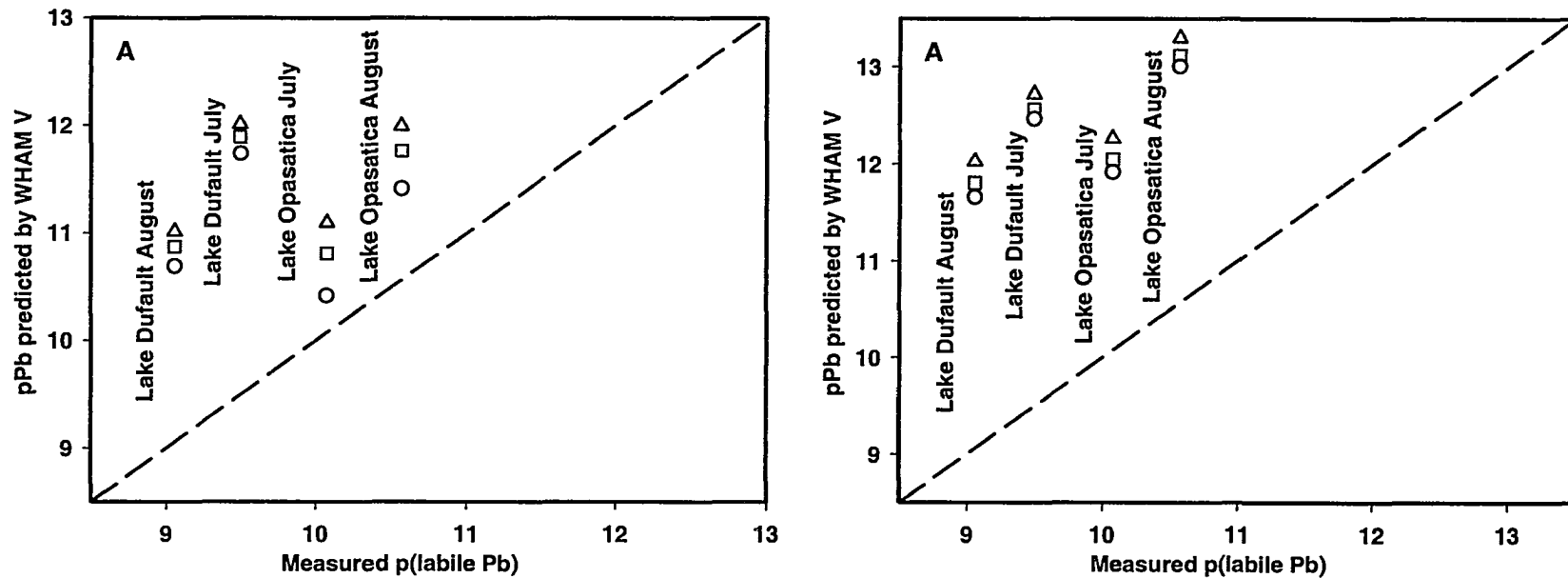


Figure 54 Comparison of WHAM predicted pPb with the measured concentrations of labile Pb(II)-complexes in lake-water samples collected from Rouyn-Noranda, Québec, in July 2002 and August 2002. Input parameters used for calculating free-metal ion concentrations in the four lakes using WHAM have been presented in Table 16. Each lake was modelled using 3 different active DOC concentrations. (---), 1:1 line; (O), 50% active DOC; (□), 65% active DOC; (△), 80% active DOC. A) WHAM V predictions; B) WHAM VI prediction

a slightly better agreement with the measured labile lead concentration than WHAM VI (see Table 22).

7.5 Conclusions

This Chapter has presented the results of CLEM/AdCSV of Pb(II), Ni(II), and Cu(II) complexes of DOC in freshwaters. This study is original in concept and in experimentation.

Total metal concentration was found to be highest in Lake Dufault because it was located upwind and close to the smelter, and hence, most likely received the highest amount of lead through atmospheric deposition. Therefore, the most labile Ni(II)-DOC, Cu(II)-DOC and Pb(II)-DOC complexes were found to be in Lake Dufault because of the relatively high [metal]/[DOC] mole ratio and competition by major cations (e.g., Ca^{2+} and Mg^{2+}).

The results showed that for most metals, WHAM V provided reasonable estimates for $[\text{Ni}^{2+}]$, $[\text{Cu}^{2+}]$, and $[\text{Pb}^{2+}]$ in lake surface waters having different conditions of pH and DOC concentrations. In comparing the measured labile metal concentrations (including free-metal ion concentrations) with the WHAM predictions, one should bear in mind that the kinetics-based CLEM/AdCSV provided the concentration of labile metal complexes including metal-aqua complexes whereas the WHAM-predicted concentrations were only those of the free-metal ion, M^{2+} [189]. Hence, in the case of copper and lead, it was not unreasonable to expect that the measured concentrations were greater than the WHAM-predicted $[\text{Cu}^{2+}]$ and $[\text{Pb}^{2+}]$. Indeed, the measured concentrations of the labile Cu(II) and Pb(II) complexes were larger than the WHAM-predicted concentrations. However, for

nickel, the agreement between the measured concentrations of the labile Ni(II)-DOC complexes (including Ni²⁺ ion) and the WHAM-predicted concentrations was reasonable estimates of free-metal ion concentrations in comparison with the measured concentrations of labile complexes of the above three metals [189].

This study has shown that an active DOC concentration between 65% and 80% is adequate to model the lake waters studied. Comparing WHAM V with WHAM VI, this study has found that WHAM V is equal to or better than WHAM VI for most of the lake waters studied. Both WHAM V and WHAM VI have been tested extensively by others against several data sets and have been found to perform adequately when modeling freshwaters [189].

-- Chapter 8 --

**Kinetic Speciation of Trace Metals in Some Metal-Impacted
Freshwater Lakes: a Comparison of Results of Distribution
Analysis Method with those of a Non-linear Regression
Method. Comparison of above results with the predictions of
WHAM V and VI**

8.1 Introduction

The interactions of trace metals with Dissolved Organic Matter (DOM), which is ubiquitous in freshwaters, sediments and soils, play an important role in trace metal transport, fate and bioavailability. The competition of major cations with trace metals is a phenomenon in freshwaters. However, trace metals also compete with one another for the binning sites on the naturally-occurring complexants [13,14].

From a modelling perspective, simple ligands of known structure have reactions of well-defined stoichiometry and can be dealt with using the mass action approach. In contrast, humic substances which are both physically and chemically heterogeneous, such as humic and fulvic acids, have been reported to have a continuous distribution of binding sites [28,155]. Hence, dissociation rate coefficients and equilibrium constants of metal-humate complexes cannot be interpreted by classical molecular models that are based on the existence of a very limited number of coordinating sites in a given complexant (e.g. hexadentate ligand, EDTA) [212].

A number of modelling approaches have been developed in recent years to describe some of the observed behaviour of humic substances. The Discrete Multi-Ligand Model has been used to model humic substances; it assumes that different independent or discrete complexant sites are present on humic substances [213], in other words as a mixture of simple homogenous complexants [212]. An alternative to the above approach that attempts to address the problem of chemical heterogeneity of acidic functional groups and the numerical spread of their associated equilibrium constants is the Continuous Distribution Model. This statistical concept has been used now for some time and it is

physically more realistic since humic substances have continuous distribution binding sites [213-214]. The Distribution Analysis Methods can be used to characterize binding under equilibrium conditions [215-217] and non-equilibrium conditions [70,218-219]. Several models have been developed for analysis of kinetic data: the Discrete Multi-Component Model [26,66-67] the Discrete Kinetic Spectra Model [69], the Continuous Kinetic Spectra Model [66], and the Log-Normal Distribution Model [69,71].

Based on the kinetic model proposed in this thesis, dissociation of metal-DOC is essentially a multi-exponential decay. The question then arises whether the overall decay is a sum of a limited number of exponentials or a continuous distribution. Non-linear regression analysis method analyzes the data assuming first that the decay is a sum of two exponential terms. If the quality of the fit is unsatisfactory, a third exponential term is added. It has been found that in most cases, the addition of a fourth component does not improve further the quality of the fit (artefacts). A satisfactory fit with a sum of two (three or four) exponential terms does not mean that the system under study has two (three or four) distinct metal complexes [220]. To answer the question whether the overall decay consists of a few distinct exponentials or should be interpreted in terms of a continuous distribution, it is advantageous to use an approach that does have a *priori* assumption about the number of components, initial estimates of the values of the rate coefficient, or shape of the distribution (e.g. Gaussian). The Distribution Analysis Method provides such an approach [221].

The objectives of the work presented in this chapter were i) to investigate some of the factors that influence the kinetics of dissociation of some transition metal complexes in freshwater lakes in Canada within the context of freshwaters as dynamic systems; ii) to investigate the chemical significance of speciation parameters based on non-linear regression analysis and on distribution analysis; iii) to compare the predictions of Windermere Humic Aqueous Model (WHAM) with the measured concentrations of labile metal complexes based on the two methods of data analysis. The trace metals investigated were Co, Ni, Cu, Zn, Cd, and Pb in samples of lake surface-water collected from Rouyn-Noranda, Quebec.

8.2 The Kinetic Model

The Kinetic Model was the same as presented in section 5.2. (chapter 5).

8.3 Experimental

8.3.1 Materials and reagents

Stock solutions (1000 mg/mL) of cobalt, nickel, copper, zinc, cadmium and lead were purchased from SCP Science (Montreal, Canada grade). Working standard solutions were prepared daily by dilution of the stock solutions with ultrapure water (of resistivity 18.2 M Ω -cm) which had been acidified to contain 1% (v/v) ultrapure nitric acid (Seastar, Canada) to prevent loss of analyte metals by adsorption on the container walls.. Analytical grade (minimum 99% pure) Chelex 100 resin, 100-200 mesh, sodium form, (Bio-Rad) was pre-cleaned following the method of Morel et al. [160]. The wet capacity of Chelex 100 resin was 0.61 meq/g [161].

8.3.2 Containers and their cleaning procedure

Containers and cleaning procedure were the same as presented in section 5.3.2 (chapter 5).

8.3.3 Freshwater samples

Figure 48 shows a map of the sampling area of Rouyn-Noranda, Québec, from where the freshwater samples were collected. The lakes in the area of Rouyn-Noranda were impacted by acids and metals from current metal mining operations, abandoned mines, and atmospheric deposition from a large, nearby copper smelter that had been in operation since 1927 [198]. Lakes Opasatica and Vaudray were upwind from the smelter, and were the least affected by atmospheric fallout from the smelter. Lakes Dufault and Osisko were the most highly contaminated lakes based on data from previous studies [198, 200-201]. Lake Osisko also received liquid effluents from the smelting operations in the past. Samples of surface waters were collected in 2.2 L Teflon bottles (screw-capped) from the four lakes in June 2003. Immediately after the receipt of the water samples at our laboratories, they were filtered through 0.45 μm Versapore membrane capsule filters (Pall) using a peristaltic pump (in our laboratory) within 24 h of the sample collection. Each 0.45 μm filter was able to filter approximately 500 mL of water sample before it was clogged. The pH and conductivity of the samples were measured using an Accumet 20 pH/conductivity meter (Fisher). The DOC concentration of the filtered water samples was measured using a Shimadzu Total Organic Carbon Analyzer, Model TOC-VCSH. A subsample (30 mL) of the filtered samples was acidified with nitric acid (Seastar, Canada) to pH 1.5. The acidified sample was used to determine the total nickel

concentrations using ICP-MS. The remaining filtered samples were stored in the dark at 4 °C until the kinetic experiments, and were used for the kinetic studies within 72 h of filtration. Table 23 presents some properties of surface-water samples collected from Rouyn-Noranda, Québec, in June 2003.

The ionic strength (IS) was calculated from electrical conductivity (EC) using an empirical relationship (eqn. 8.1) [222]:

$$IS = 0.014 \times EC - 4 \times 10^{-4} \quad (8.1)$$

where units for IS and EC are mol L⁻¹ and mS cm⁻¹, respectively. Calculated ionic strengths using eqn. 8.1 were in good agreement with those determined from complete elemental analysis. The conductivity measurements were used to calculate the ionic strength of the samples.

8.3.4 Kinetic experiments

The simultaneous (rapid, sequential) dissociation kinetics of Co(II), Ni(II), Cu(II), Zn(II), Cd(II) and Pb(II) complexes was studied using Chelex 100 as the competing ligand and an Agilent 7500cs ICP-MS. Three grams (1% w/v, w stands for the wet weight) of Chelex 100 was added to 300 mL of the sample solution in a cylindrical Teflon Reactor (500 mL volume); the sample solution was stirred continuously with a Teflon-coated stirring bar, and was filtered with an online 0.40 µm polycarbonate membrane filter (Corning) to separate the Chelex 100 resin before introducing the filtrate into the plasma torch by solution nebulization at a flow rate of approximately 1 mL/min as shown in Figure 32.

Table 23 Some properties of the surface-water samples of the selected lakes in Rouyn-Noranda, Québec.

	Lake Opasatica	Lake Dufault	Lake Osisko	Lake Vaudray
pH of samples	6.9	7.0	7.3	6.1
Conductivity (mS/m)	13.9	16.5	34.6	3.47
DOC (mg/L) ^a	9.0	15.7	6.0	11.0
[M] ^b				
Ni	1.1×10^{-8}	1.2×10^{-8}	1.9×10^{-8}	1.5×10^{-8}
Zn	2.8×10^{-8}	9.6×10^{-7}	1.1×10^{-7}	6.9×10^{-8}
Cd	4.4×10^{-11}	4.9×10^{-9}	2.7×10^{-10}	7.1×10^{-10}
Cu	4.4×10^{-8}	1.8×10^{-7}	5.4×10^{-8}	4.2×10^{-8}
Fe	2.8×10^{-5}	3.7×10^{-5}	2.8×10^{-5}	6.8×10^{-6}
Al	4.5×10^{-7}	1.6×10^{-7}	1.4×10^{-7}	2.9×10^{-6}
Co	6.3×10^{-10}	1.6×10^{-9}	8.3×10^{-10}	9.5×10^{-10}
Pb	5.8×10^{-10}	2.9×10^{-9}	1.0×10^{-9}	6.7×10^{-10}
Mn	1.3×10^{-8}	2.3×10^{-6}	2.7×10^{-8}	2.1×10^{-7}
Major Cations (M) ^c				
Mg	1.3×10^{-4}	1.3×10^{-4}	1.9×10^{-4}	1.4×10^{-4}
Ca	3.8×10^{-4}	4.9×10^{-4}	6.1×10^{-4}	1.1×10^{-4}
Na	3.7×10^{-3}	2.6×10^{-3}	2.8×10^{-2}	3.9×10^{-4}
K	N/D	N/D	2.0×10^{-5}	N/D
Major Anions (M) ^d				
F	2.5×10^{-4}	7.1×10^{-5}	1.7×10^{-4}	9.0×10^{-5}
Cl	1.9×10^{-4}	1.4×10^{-4}	5.1×10^{-4}	1.7×10^{-5}
SO ₄	1.7×10^{-4}	3.7×10^{-4}	3.1×10^{-4}	4.3×10^{-5}
NO ₃	4.7×10^{-6}	7.0×10^{-6}	7.4×10^{-6}	5.7×10^{-6}
PO ₄	N/D	N/D	N/D	N/D

pH of the samples had an uncertainty of ± 0.1 .

*Conductivity was not an input parameter for calculating free-metal ion concentrations in these lakes using WHAM.

^a Determined by Shimadzu Total Organic Carbon Analyzer, Model TOC-VCSH.

^b Determined by ICP-MS.

^c Determined by Thermo Jarrel Ash IRIS Radial Inductively Coupled Plasma Optical Emission Spectrometer (ICP-OES).

^d Determined by Dionex Series 4000i Ion Chromatograph.

N/D: Not Detectable.

Table 24 Instrumental operating conditions and data acquisition protocol for ICP-MS

ICP-MS	
RF power (kW)	1.4
Cooling argon flow rate (L min ⁻¹)	16
carrier argon flow rate (L min ⁻¹)	1.1
Data acquisition parameters	
dwel time (ms)	100
scan mode	peak hop
signal measurement	counts s ⁻¹
points/spectral peak	1
resolution	normal

The data acquisition was initiated 60 seconds before the resin was added to the Teflon Reactor in order to check if there is any contamination from the pre-treatment of the resin [221].

8.3.5 Data analysis

Analyzing experimental data to obtain speciation parameters is a crucial point in the kinetic speciation method. Two methods of data analysis have been used for these experiments.

8.3.5.1 Non-linear regression analysis

The experimental data were analyzed for discrete values of the dissociation rate coefficients by a non-linear regression method based on the Marquardt-Levenberg algorithm [202]. The minimum number of kinetic parameters (no of the exponential terms) required to accurately fit the data was determined by finding the number of components in which the sum of the square of the weighted residuals achieved a minimum value [221].

$$\text{Sum of squares of the weighted residuals} = \sum \left[\frac{C(t) - C_T(t)}{C(t)^{1/2}} \right]^2 \quad (8.2)$$

In the above equation, $C(t)$ is the experimental value and $C_T(t)$ is the calculated value using the parameters obtained from the regression analysis. The non-linear regression analysis gave up to two components in metal-DOC complexes with specific values of the rate coefficients for dissociation of each component.

8.3.5.2 Distribution Analysis Method

Kinetic spectra were obtained by fitting the kinetic data to equation (5.4) (chapter 5) using the distribution analysis feature (Level 2) of the FLA-900 (Edinburgh Analytical Instruments, UK) fluorescence lifetime analysis program, as described previously [150-151]. The Distribution Analysis Method requires no *a priori* assumption about the number of components, initial estimates of the values of the rate coefficient, or shape of the distribution (e.g. Gaussian).

Figure 55 shows an example of the output file of the program (this figure quoted from [223]). Experimental decay curve and the fitted data plus the plot of the residuals are presented in the left-hand side of the figure. The right hand-side of Figure 55 shows a kinetic spectrum of dissociation rate coefficients and a table of the mean lifetime and percentage of the relative weight for each peak in the kinetic spectrum. Standard deviation of the mean lifetime represents the width of the distribution [245].

Under the experimental conditions used in the work, the analytical time scale of measurement is 13 s to 8000 s, which corresponds to $k_d \sim 10^{-2} \text{ s}^{-1}$ to 10^{-5} s^{-1} . Complexes with $k_d > 10^{-2} \text{ s}^{-1}$ cannot be experimentally resolved from the metal aqua complex because the latter has very nearly the same dissociation rate coefficients. This represents the upper limit of the rate coefficients that can be experimentally determined within the experimental time scale of the method. This limitation arises from the time required for Chelex 100 to mix with the sample solution. The lower limit is simply

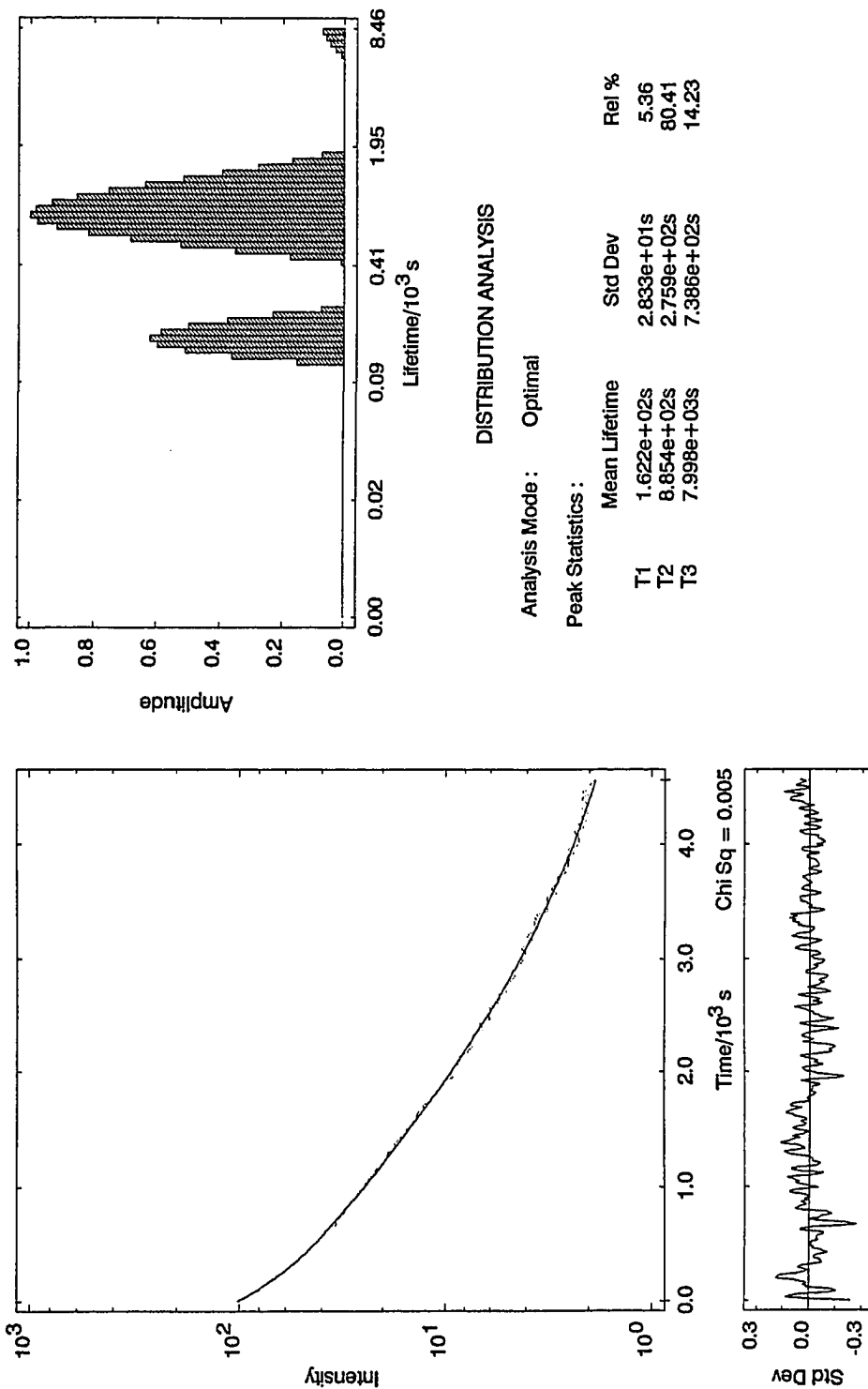


Figure 55 Example of an output file from Distribution Analysis Method software [223].

defined by the time taken to complete the kinetic run. Metal species with $k_d < 10^{-5}$ (i.e., k_{ft} and $k_{dt} \ll 1$) are defined as inert [163].

8.4 Results and Discussion

Kinetic data for the dissociation of Co(II), Ni(II), Cu(II), and Zn(II) complexes in lake-water samples are presented in Figures 56-59. The steeply falling section at the beginning of the curve can be attributed to uptake of the M^{2+} aqua complex and/or rapidly-dissociating M(II)-DOC complexes that cannot be experimentally distinguished from the aqua complex (*dynamic*). The very slowly-falling section of the Pb(II)-DOC curve is probably due to the very slow rate of dissociation ($k_d < 10^{-5} \text{ s}^{-1}$) of strong metal complexes (*inert*), which represent the lower limit of rate coefficients that can be measured under the experimental conditions (i.e. an analytical window of 3 h) used in this study.

The dissociation rate coefficients of M(II)-DOC, determined using non-linear regression, are presented in Tables 25-28. The dissociation rate coefficient was an average value of a group of closely related rate coefficients. The analysis showed that a minimum of two components was required to describe the dissociation kinetics of the metal-DOC complexes.

The kinetic data in Figures 56-59 were also analyzed with the Distribution Analysis Method and the results are presented in Tables 29-32. Each kinetically distinguishable component probably reflects a range of chemically related, but not identical metal complexes with similar dissociation rate coefficients [27]. As shown in Tables 29-32,

the observed dissociation rate coefficients from the distribution analysis range from 10^{-2} to 10^{-5} s^{-1} . The uncertainties, which are represented by the standard deviations of the distributions, are simply a measure of the width of the distributions. The widest range of dissociation rate coefficients was observed for the slowest kinetically distinguishable component. This is a reflection of the relatively high concentration of this component. The shape and size of the distribution probably arises from the colloidal nature of humic substances.

An important limitation of Distribution Analyses based on numerical methods, such as equation (5.4) (chapter 5) is that they are sensitive to artefacts, which result in peak broadening [67,154]. The importance of testing the observed speciation parameters by non-linear regression and the Distribution Analysis Method for their chemical significance [28] is therefore emphasized to determine whether the results are simply a mathematical solution to the time-dependent concentration data, or if the complex chemistry of trace metal speciation in freshwaters can be approximated by a small set of rate coefficients. The theory for metal complexation in aqueous solutions suggests that three factors are expected to influence metal exchange reactions with DOM: i) metal-to-ligand mole ratio, ii) Ligand Field Stabilization Energy (LFSE) for transition metals, and iii) ionic potential (z^2/r).

8.4.1 *Metal-to-Ligand Mole Ratio*

As presented in Table 23, the four lake-water samples had different metal-to-DOC mole ratios for the metals under discussion, resulting in different concentrations of labile

metal-complexes, including free metal ion (aqua complex) being present in the samples of the lake waters. The measured values of $[M^{2+}]$ plus labile M(II)–DOC complexes depend on the affinity of metal for the binding sites, and at a given pH and ionic strength. The percentage of labile M(II)–DOC complexes, including free metal ion (aqua complex) present in the water samples, will be determined by the $[M]/[DOC]$ mole ratio and on the competition of the other metals with the target metal.

8.4.2 Ligand Field Stabilization Energy

The effects of Ligand Field Stabilization Energy (LFSE) are usually significant in the chemistry of the first-row transition metals. Kinetic speciation of the metal complexes of Co(II) d^7 , Ni(II) d^8 , Cu(II) d^9 , and Zn(II) d^{10} in lake-water samples are presented in Figures 56-59. Dissociation rate coefficients based on non-linear regression analysis are presented in Tables 25-28. The influence of the d -electron configuration on the dissociation rate coefficients of Co(II) d^7 , Ni(II) d^8 , Cu(II) d^9 , and Zn(II) d^{10} in the lake-water samples is presented in Figure 60. Even though the metals were not present in equimolar concentrations, the results suggest that, with the exception of Cu(II) which can be attributed to Jahn Teller Effect, the dissociation rate coefficients fall into the similar trend predicted from the LFSEs (strong field) (i.e. $k_{d,Co(II) d^7} < k_{d,Ni(II) d^8} > k_{d,Cu(II) d^9} < k_{d,Zn(II) d^{10}}$), and indicate that inert complexes are those with large LFSEs. A similar trend was reported by Sekaly et al. [31] for the dissociation rate coefficients of Ni(II) d^8 , Cu(II) d^9 and Zn(II) d^{10} in model solutions of Laurentian fulvic acid and in freshwaters collected from the Sudbury (Canada) area. These results on the slow dissociation kinetics of Cu(II) complexes also agree with those of Achterberg et al.

[174], who reported that equilibrium between organically complexed copper and suspended particulate matter was reached only after 4 to 15 h. The particularly slow dissociation kinetics of Ni(II) and Cu(II) complexes suggest that the usual equilibrium assumption for freshwaters may not be valid for these metals.

Distribution Analysis Method has been applied (equation 5.4) (chapter 5) to analyze the kinetic data and the results are presented in Tables 29-32. Figure 61 shows a trend in the dissociation rate coefficients similar to that presented above (i.e. $k_{d,Co(II)} d^7 < k_{d,Ni(II)} d^8 > k_{d,Cu(II)} d^9 < k_{d,Zn(II)} d^{10}$) in the four lake-water samples .

8.4.3 Ionic Potential

Since the ionic potential (z^2/r) determines the electrostatic component of the total metal-ligand binding energy [26], the metals for which the binding energy is expected to be dependent on ionic potential are Zn(II), Cd(II) and the post-transition metal, Pb(II) (Figures 62-65 and Tables 25-28). Kinetic results based on non-linear regression analysis of Pb(II) ($z^2/r = 0.030 \text{ pm}^{-1}$), Cd(II) ($z^2/r = 0.037 \text{ pm}^{-1}$) and Zn(II) ($z^2/r = 0.046 \text{ pm}^{-1}$) in Lake Dufault ($R^2 = 0.391$), Lake Osisko ($R^2 = 0.941$), Lake Opasatica ($R^2 = 0.0963$) and Lake Vaudray ($R^2 = 0.737$) are shown in Figure 66. Interestingly, the results for Zn(II), Cd(II) and Pb(II) indicate a reversal in the trend predicted from the ionic potential, suggesting that for Cd(II) and Pb(II) the metal binding is not electrostatic. Similar discussion was made in chapter 5. An inverse relationship between the dissociation rate coefficients and the ionic potential was also observed in dissociation rate coefficients based on the Distribution Analysis Method in lake water

samples: Lake Dufault ($R^2 = 1.00$), Lake Osisko ($R^2 = 0.916$), Lake Opasatica ($R^2 = 0.0.959$) and Lake Vaudray ($R^2 = 0.795$), as presented in Figure 67 and Tables 29-32.

The distribution of the rate coefficients for the dissociation for the M(II)-DOC complexes was for all the metals broader than the distribution obtained with the aqua ligand complexes [155]. The rate coefficients of metal-DOC complexes had a broader distribution at lower $[M]/[DOC]$ mole ratios. The width of the peaks was probably due to the heterogeneity of the complexing ligand (DOC). The distribution of the rate coefficients was not the same for all the metals. Suggesting that DOC has intrinsic binding properties that may vary from one metal to another. Similar results have reported by Sekaly et al [151-152] on applying distribution method on simulated data and real data. In general, good agreement was obtained between the rate coefficients retrieved by these two methods. Dissociation rate coefficients obtained by the Distribution Analysis Method showed a better chemical significance than those obtained by the non-linear regression analysis.

8.4.4 WHAM modelling

Tables 33a and 33b present WHAM predictions, based on 65% of the $[DOC]$ as “active”. Tables 33a and 33b show measured $[M^{2+}]$, and labile inorganic- and organic-metal complexes in the surface waters of the four lakes in the Rouyn-Noranda area, Québec. The samples of the lake surface waters contained varying concentrations of metals because of their different proximities to the copper smelter (see Figure 48). Lakes Vaudray and Opasatica had the lowest $[M]/[DOC]$ mole ratios and were

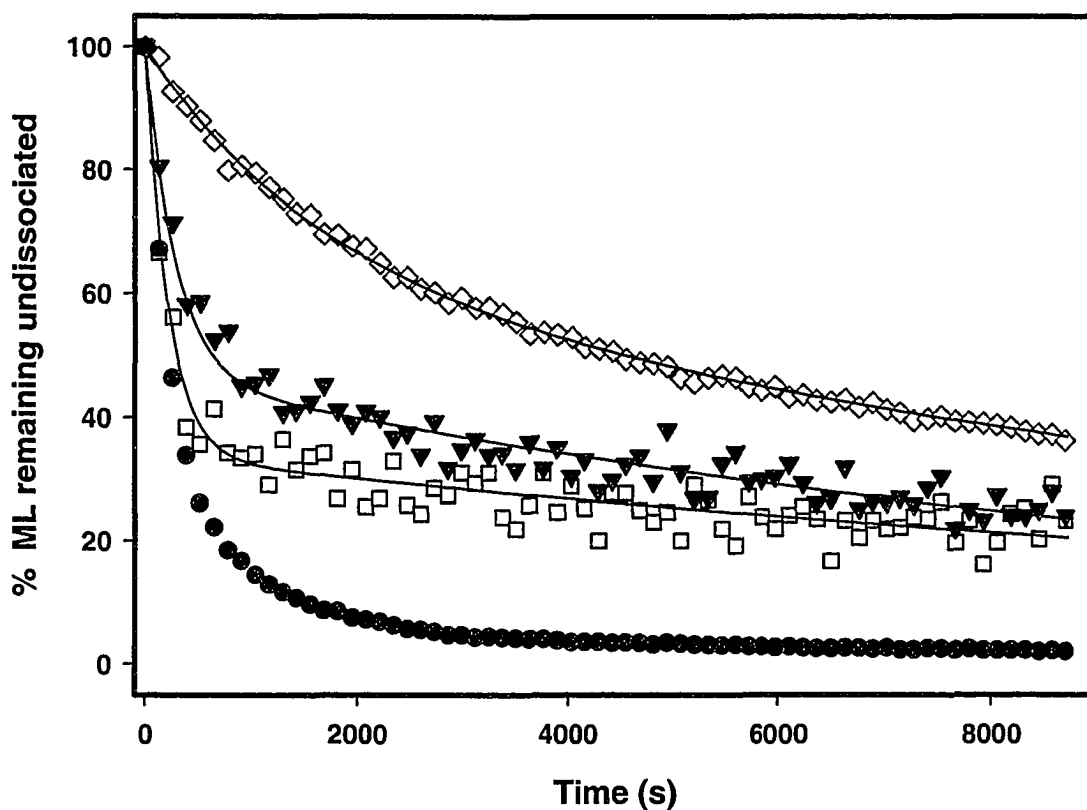


Figure 56 Dissociation kinetics of M(II)-DOC complexes in Lake Dufault water samples collected from the Rouyn-Noranda area, Québec, in June 2003, determined by CLEM/ICP-MS, using Chelex 100 as the competing ligand. DOC = 15.7 ± 1.5 , pH 6.1 ± 0.1 , ionic strength 1.9×10^{-3} mol/L, temperature 23 ± 2 °C. (\diamond), Cu(II)-DOC; (\blacktriangledown), Ni(II)-DOC; (\square), Co(II)-DOC; (\bullet), Zn(II)-DOC complexes. Solid lines represent non-linear curve-fitting.

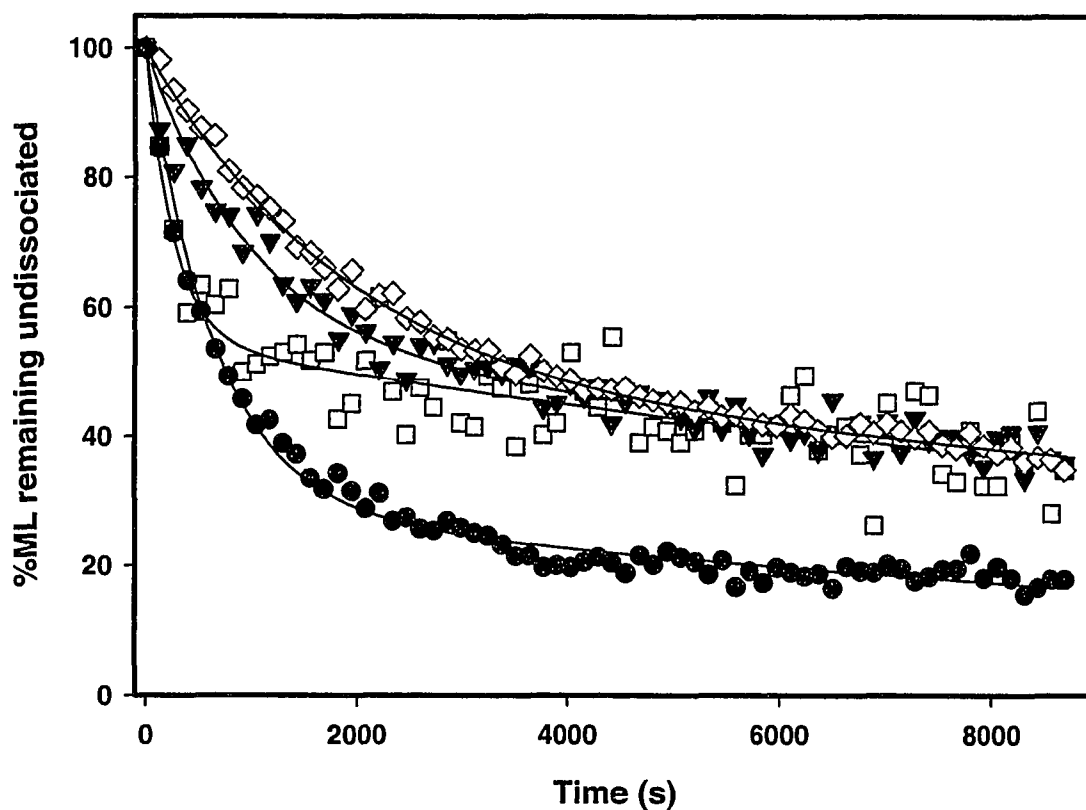


Figure 57 Dissociation kinetics of M(II)-DOC complexes in Lake Osisko water samples collected from the Rouyn-Noranda area, Québec, in June 2003, determined by CLEM/ICP-MS, using Chelex 100 as the competing ligand. DOC = 6.0 ± 1.3 , pH 7.3 ± 0.1 , ionic strength 4.4×10^{-3} mol/L, temperature 23 ± 2 °C. (\diamond), Cu(II)-DOC; (\blacktriangledown), Ni(II)-DOC; (\square), Co(II)-DOC; (\bullet), Zn(II)-DOC complexes. Solid lines represent non-linear curve-fitting.

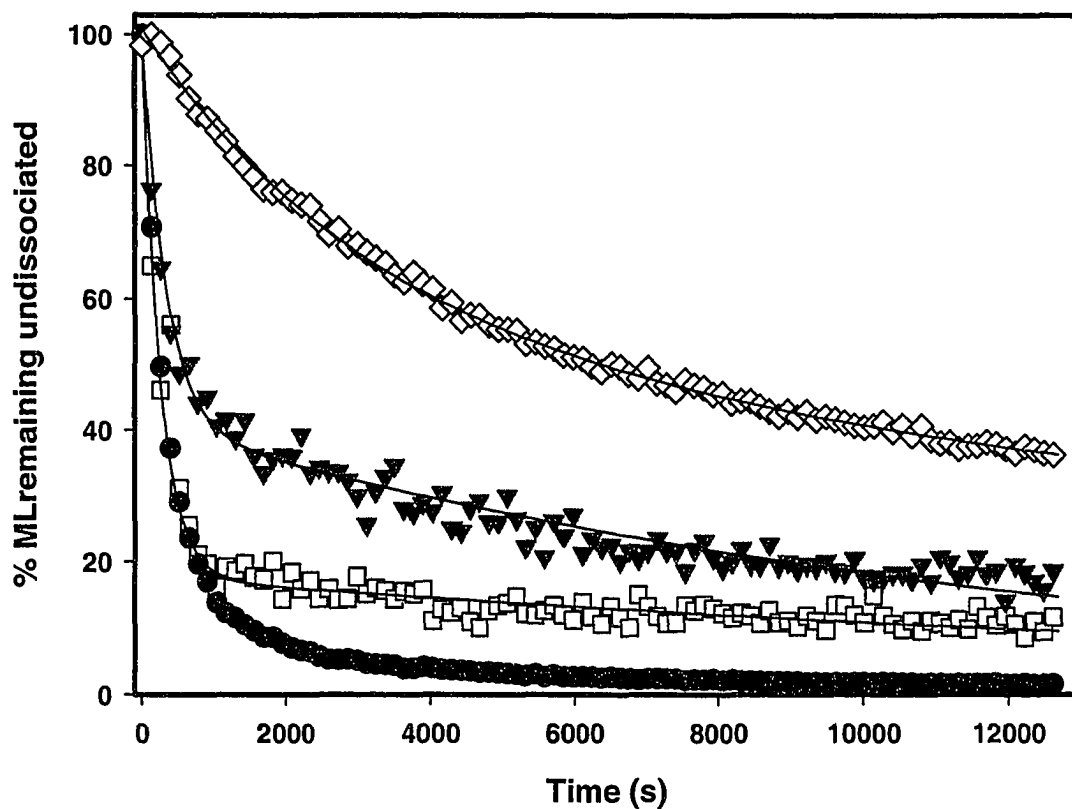


Figure 58 Dissociation kinetics of M(II)-DOC complexes in Lake Opasatica water samples collected from the Rouyn-Noranda area, Québec, in June 2003, determined by CLEM/ICP-MS, using Chelex 100 as the competing ligand. DOC = 9.0 ± 0.4 , pH 6.9 ± 0.1 , ionic strength 1.5×10^{-3} mol/L, temperature 23 ± 2 °C. (\diamond), Cu(II)-DOC; (\blacktriangledown), Ni(II)-DOC; (\square), Co(II)-DOC; (\bullet), Zn(II)-DOC complexes. Solid lines represent non-linear curve-fitting.

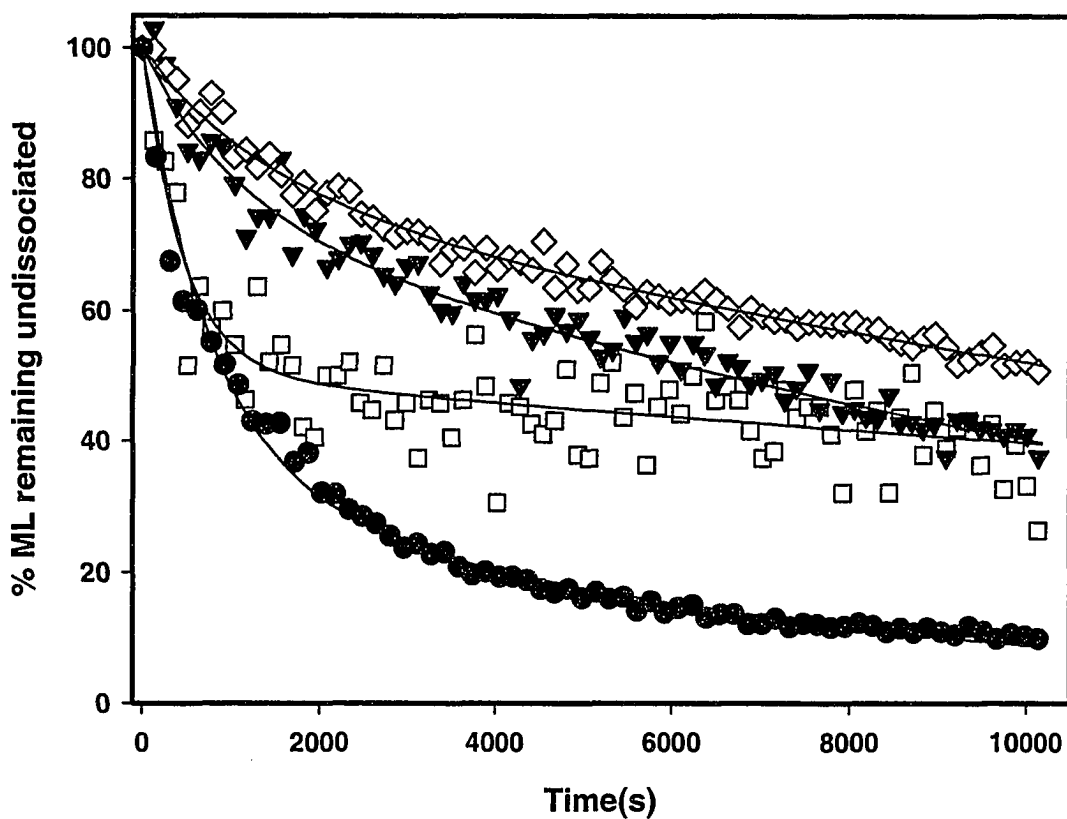


Figure 59 Dissociation kinetics of M(II)-DOC complexes in Lake Vaudray water samples collected from the Rouyn-Noranda area, Québec, in June 2003, determined by CLEM/ICP-MS, using Chelex 100 as the competing ligand. DOC = 11.0 ± 0.6 , pH 6.1 ± 0.1 , ionic strength 8.6×10^{-5} mol/L, temperature 23 ± 2 °C. (\diamond), Cu(II)-DOC; (\blacktriangledown), Ni(II)-DOC; (\square), Co(II)-DOC; (\bullet), Zn(II)-DOC complexes; complexes. Solid lines represent non-linear curve-fitting.

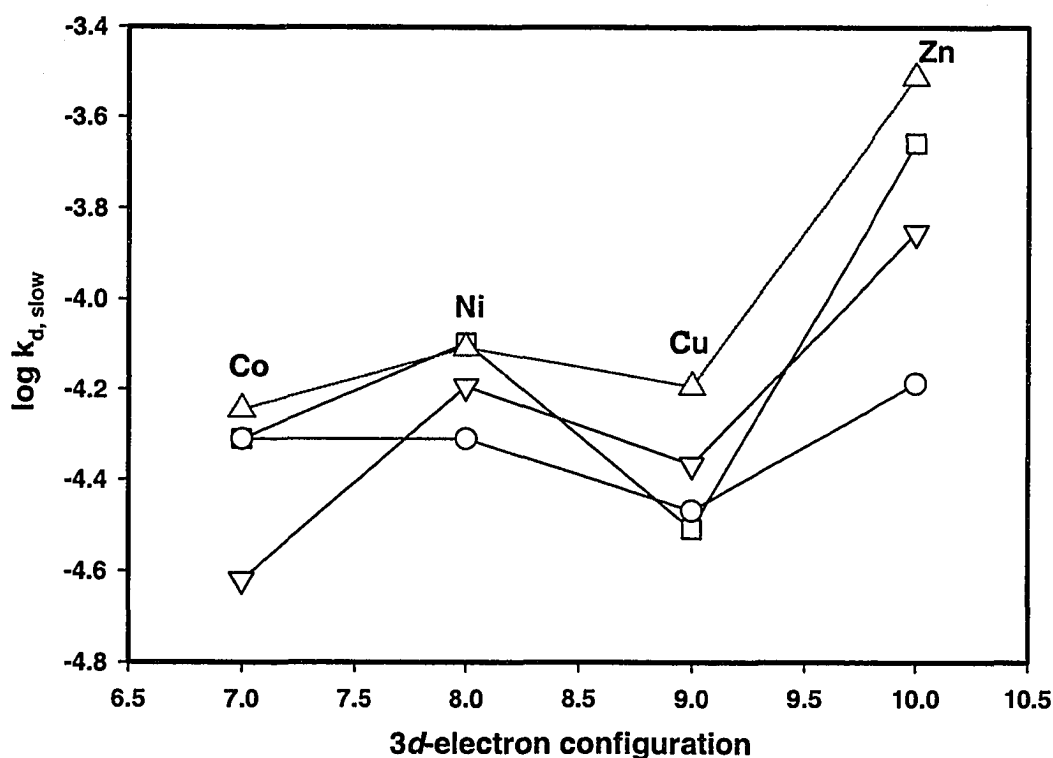


Figure 60 Influence of the *d*-electron configuration on dissociation rate coefficient of the slowest kinetically distinguishable component, $k_{d,slow}$ in freshwater samples collected from the Rouyn-Noranda area, received on June 26, 2003, determined by CLEM/ICP-MS, using Chelex 100 as the competing ligand. (Tables 25-28). Temperature 23 ± 2 °C. (□), Lake Opasatica, pH 6.9 ± 0.1 , DOC 9.0 ± 0.4 mg/L, ionic strength 1.5×10^{-3} mol/L; (Δ), Lake Dufault, pH 7.0 ± 0.1 , DOC 15.7 ± 2.9 mg/L, ionic strength 1.9×10^{-3} mol/L; (○), Lake Osisko, pH 7.3 ± 0.1 , DOC 6.0 ± 1.3 mg/L, ionic strength 4.4×10^{-3} mol/L; (▽), Lake Vaudray, pH 6.1 ± 0.1 , DOC 11.0 ± 0.6 mg/L, ionic strength 8.6×10^{-5} mol/L. The non-linear regression analysis was used to fit the kinetic data.

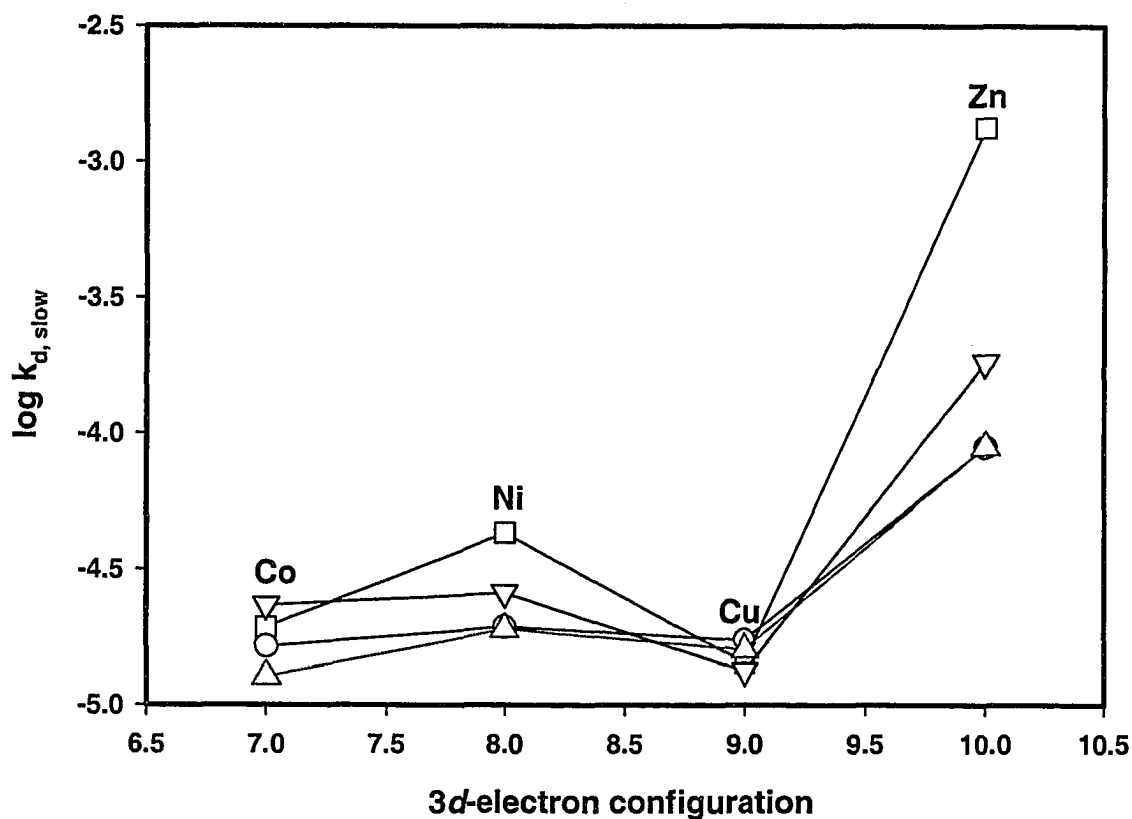


Figure 61 Influence of the d -electron configuration on mean dissociation rate coefficient of the slowest kinetically distinguishable component, $k_{d,slow}$ in freshwater samples collected from the Rouyn-Noranda area, received on June 26, 2003, determined by CLEM/ICP-MS, using Chelex 100 as the competing ligand. (Tables 29-32). Temperature 23 ± 2 °C. (□), Lake Opasatica, pH 6.9 ± 0.1 , DOC 9.0 ± 0.4 mg/L, ionic strength 1.5×10^{-3} mol/L; (○), Lake Dufault, pH 7.0 ± 0.1 , DOC 15.7 ± 2.9 mg/L, ionic strength 1.9×10^{-3} mol/L; (Δ), Lake Osisko, pH 7.3 ± 0.1 , DOC 6.0 ± 1.3 mg/L, ionic strength 4.4×10^{-3} mol/L; (▽), Lake Vaudray, , pH 6.1 ± 0.1 , DOC 11.0 ± 0.6 mg/L, ionic strength 8.6×10^{-5} mol/L. The Distribution Analysis Method was used to fit the kinetic data.

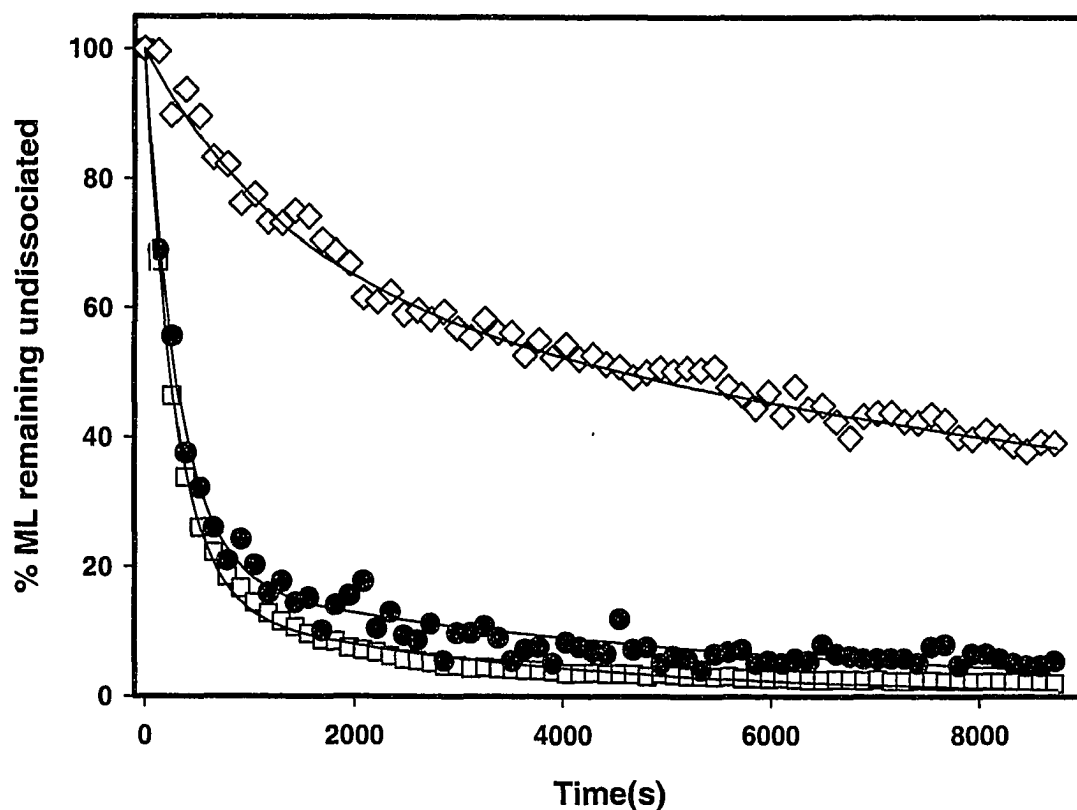


Figure 62 Dissociation kinetics of M(II)-DOC complexes in Lake Dufault water samples collected from the Rouyn-Noranda area, Québec, in June 2003, determined by CLEM/ICP-MS, using Chelex 100 as the competing ligand. DOC = 15.7 ± 2.9 , pH 6.1 ± 0.1 , ionic strength 1.9×10^{-3} mol/L, temperature 23 ± 2 °C. (\diamond), Pb(II)-DOC; (\bullet), Cd(II)-DOC; (\square), Zn(II)-DOC complexes. Solid lines respresent non-linear curve-fitting.

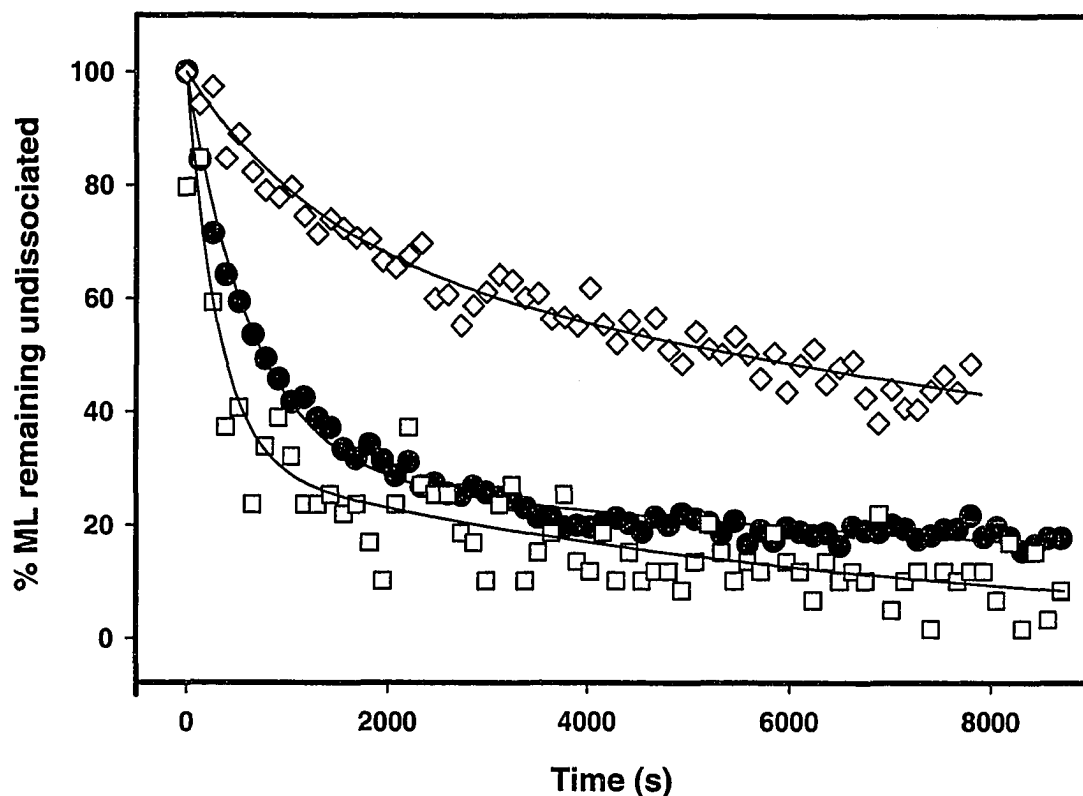


Figure 63 Dissociation kinetics of M(II)-DOC complexes in Lake Osisko water samples collected from the Rouyn-Noranda area, Québec, in June 2003, determined by CLEM/ICP-MS, using Chelex 100 as the competing ligand. DOC = 6.0 ± 1.3 ; pH 7.3 ± 0.1 , ionic strength 4.4×10^{-3} mol/L, temperature 23 ± 2 °C. (\diamond), Pb(II)-DOC; (\square), Cd(II)-DOC; (\bullet), Zn(II)-DOC complexes. Solid lines represent non-linear curve-fitting.

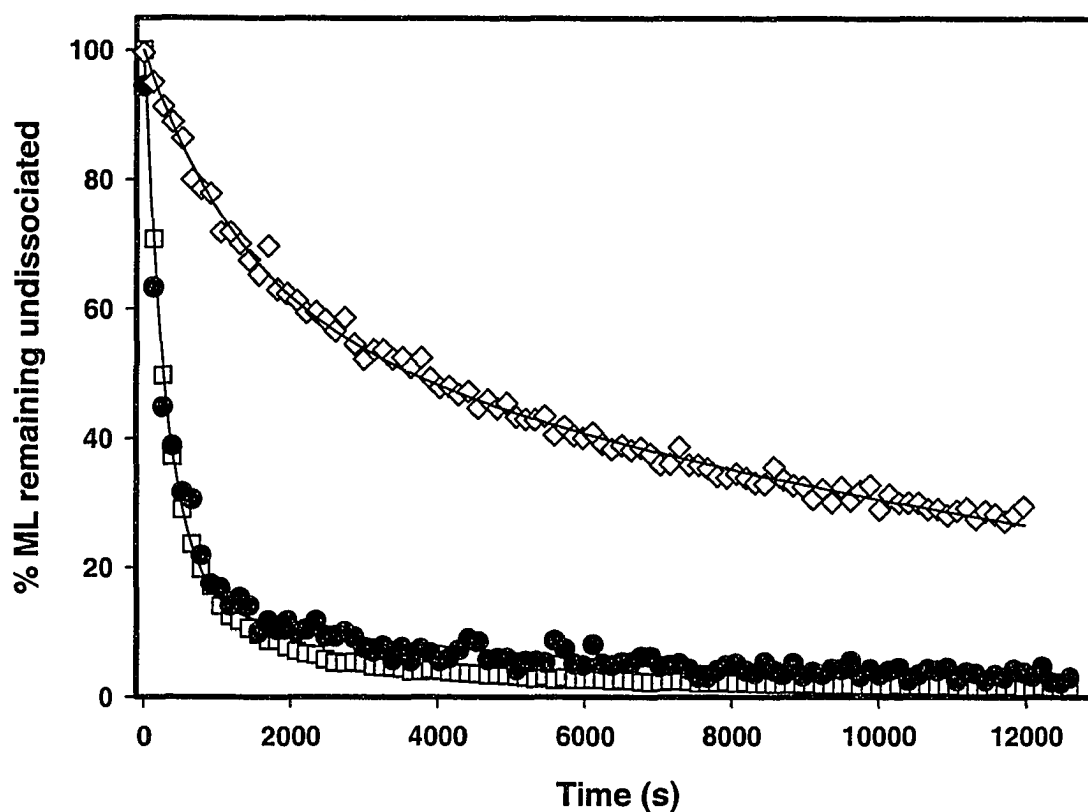


Figure 64 Dissociation kinetics of M(II)-DOC complexes in Lake Opasatica water samples collected from the Rouyn-Noranda area, Québec, in June 2003, determined by CLEM/ICP-MS, using Chelex 100 as the competing ligand. DOC = 9.0 ± 0.4 , pH 6.9 ± 0.1 , ionic strength 1.5×10^{-3} mol/L, temperature 23 ± 2 °C. (\diamond), Pb(II)-DOC; (\bullet), Cd(II)-DOC; (\square), Zn(II)-DOC complexes. Solid lines represent non-linear curve-fitting.

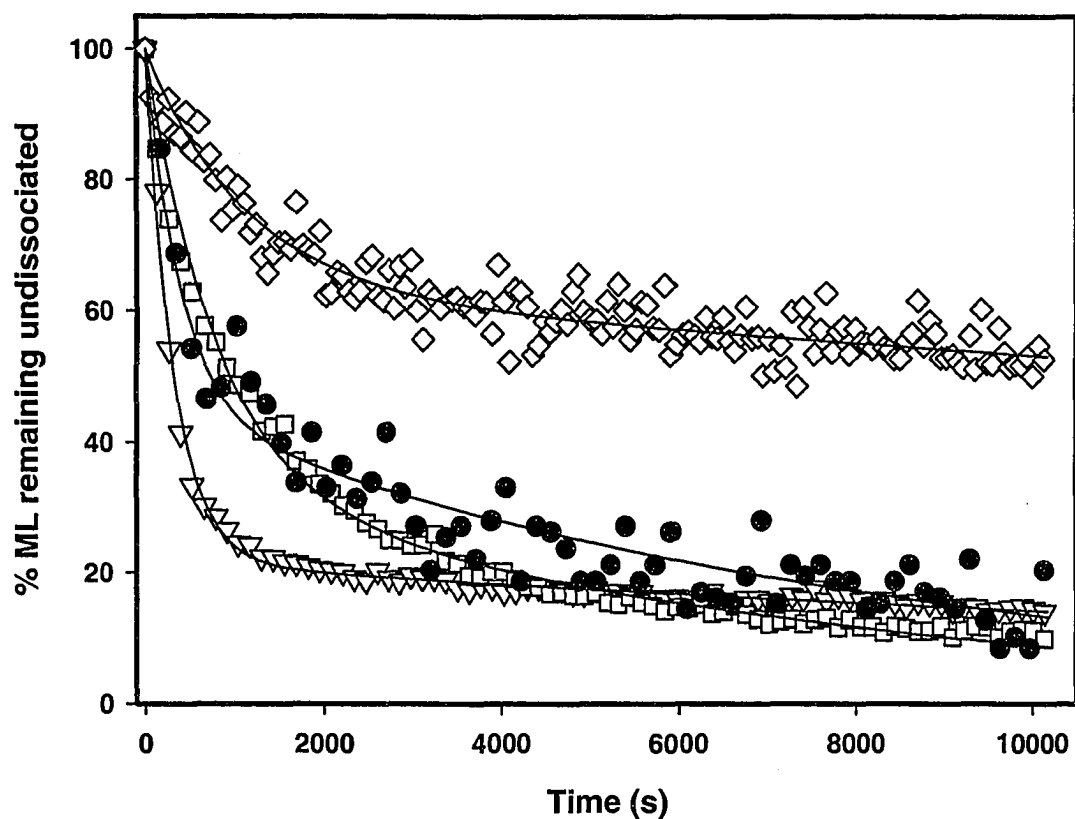


Figure 65 Dissociation kinetics of M(II)-DOC complexes in Lake Vaudray water samples collected from the Rouyn-Noranda area, Québec, in June 2003, determined by CLEM/ICP-MS, using Chelex 100 as the competing ligand. DOC = 11.0 ± 0.6 , pH 6.1 ± 0.1 , ionic strength 8.6×10^{-3} mol/L, temperature 23 ± 2 °C. (●), Cd(II)-DOC; (◇), Pb(II)-DOC; (□), Zn(II)-DOC; (▽), Mn(II)-DOC complexes. Solid lines represent non-linear curve-fitting.

Table 25 Ligand exchange kinetics of M(II)-DOC in Lake Dufault-water samples collected from the Rouyn-Noranda area, determined by CLEM/ICP-MS, using Chelex 100 as the competing ligand. The water samples were received on June 26, 2003. Ionic strength 1.9×10^{-3} mol/L; temperature 23 ± 2 °C. The non-linear regression analysis was used to fit the kinetic data.

Analyte	^a [M] _t (mol/L)	<u>Kinetically distinguishable components</u>		<u>Dissociation rate coefficients</u>		R ²
		C ₁ (%)	C ₂ (%)	k ₁ (s ⁻¹ , 10 ⁻³)	k ₂ (s ⁻¹ , 10 ⁻⁵)	
Co	1.6×10^{-9}	66±3	34±1	0.5±0.0	5.7±0.4	0.903
Ni	1.2×10^{-8}	53±2	47±1	3.5±0.3	7.8±0.3	0.947
Cu	1.8×10^{-7}	36±2	64±2	0.63±0.05	6.4±0.4	0.994
Zn	9.6×10^{-7}	85±1	15±1	3.5±0.1	30.8±1.4	0.996
Pb	2.9×10^{-9}	36±2	64±1	0.74±0.08	5.8±0.5	0.982
Cd	4.9×10^{-9}	82±2	18±2	3.5±0.1	17±1	0.972

^a[M]_t is total dissolved metals, determined by ICP-MS.

The uncertainties represent 95.5 % confidence limits in the non-linear regression analysis, for an individual measurement.

Table 26 Ligand exchange kinetics of M(II)-DOC in Lake Opasatica-water samples collected from the Rouyn-Noranda area, determined by CLEM/ICP-MS, using Chelex 100 as the competing ligand. The water samples were received on June 26, 2003. Ionic strength 1.5×10^{-3} mol/L; temperature 23 ± 2 °C. The non-linear regression analysis was used to fit the kinetic data.

Analyte	^a [M] _t (mol/L)	<u>Kinetically distinguishable components</u>		<u>Dissociation rate coefficients</u>		R ²
		C ₁ (%)	C ₂ (%)	k ₁ (s ⁻¹ , 10 ⁻³)	k ₂ (s ⁻¹ , 10 ⁻⁵)	
Co	6.3×10^{-10}	82±1	18±0	4.0±0.1	4.9±0.3	0.996
Ni	1.1×10^{-8}	59±2	41±1	3.0±0.2	8.0±0.2	0.961
Cu	4.4×10^{-8}	47±2	53±2	3.0±0.1	3.1±0.3	0.997
Zn	2.6×10^{-8}	89±1	11±0	2.9±0.0	22±1	0.996
Pb	5.8×10^{-10}	39±1	61±1	0.8±0.0	7.0±0.2	0.996
Cd	4.4×10^{-11}	86±1	14±0	3.2±0.1	13.9±0.1	0.981

^a[M]_t is total dissolved metals, determined by ICP-MS.

The uncertainties represent 95.5 % confidence limits in the non-linear regression analysis, for an individual measurement.

Table 27 Ligand exchange kinetics of M(II)-DOC in Lake Osisko-water samples collected from the Rouyn-Noranda area, determined by CLEM/ICP-MS, using Chelex 100 as the competing ligand. The water samples were received on June 26, 2003. Ionic strength 4.4×10^{-3} mol/L; temperature 23 ± 2 °C. The non-linear regression analysis was used to fit the kinetic data.

Analyte	^a [M] _t (mol/L)	<u>Kinetically distinguishable components</u>		<u>Dissociation rate coefficients</u>		R ²
		C ₁ (%)	C ₂ (%)	k ₁ (s ⁻¹ , 10 ⁻³)	k ₂ (s ⁻¹ , 10 ⁻⁵)	
Co	8.3×10^{-10}	45±4	55±1	3.8±0.8	4.9±0.5	0.715
Ni	1.9×10^{-8}	44±2	56±2	1.1±0.1	4.9±0.4	0.960
Cu	5.4×10^{-8}	51±2	49±2	5.4±0.3	3.4±0.5	0.995
Zn	1.1×10^{-7}	71±1	29±1	1.5±0.0	6.5±0.5	0.984
Pb	1.0×10^{-9}	32±4	68±5	7.5±0.2	5.8±1.1	0.925
Cd	2.7×10^{-10}	69±5	31±2	3.2±0.4	14.9±0.2	0.814

^a[M]_t is total dissolved metals, determined by ICP-MS.

The uncertainties represent 95.5 % confidence limits in the non-linear regression analysis, for an individual measurement.

Table 28 Ligand exchange kinetics of M(II)-DOC in Lake Vaudray-water samples collected from the Rouyn-Noranda area, determined by CLEM/ICP-MS, using Chelex 100 as the competing ligand. The water samples were received on June 26, 2003. Ionic strength 8.6×10^{-3} mol/L; temperature 23 ± 2 °C. The non-linear regression analysis was used to fit the kinetic data.

Analyte	^a [M] _t (mol/L)	<u>Kinetically distinguishable components</u>			<u>Dissociation rate coefficients</u>			R ²
		C ₁ (%)	C ₂ (%)	C ₃ (%)	k ₁ (s ⁻¹ , 10 ⁻³)	k ₂ (s ⁻¹ , 10 ⁻⁴)	k ₃ (s ⁻¹ , 10 ⁻⁵)	
Co	9.5×10^{-10}	50±4	---	50±1	2.2±0.3	---	2.4±0.4	0.741
Ni	1.5×10^{-8}	23±2	---	77±2	1.0±0.2	---	6.4±0.3	0.955
Cu	4.2×10^{-8}	---	20±1	80±1	---	3.8±0.8	4.3±0.3	0.983
Zn	6.9×10^{-8}	66±1	34±1	---	1.3±0.0	1.4±0.0	---	0.988
Pb	7.2×10^{-10}	---	37±2	63±1	---	9.1±0.8	1.7±0.3	0.920
Cd	6.6×10^{-10}	55±4	45±2	---	2.6±0.3	1.2±0.1	---	0.878

^a[M]_t is total dissolved metals, determined by ICP-MS.

The uncertainties represent 95.5 % confidence limits in the non-linear regression analysis, for an individual measurement.

Table 29 Ligand exchange kinetics of M(II)-DOC in Lake Dufault-water samples collected from the Rouyn-Noranda area, determined by CLEM/ICP-MS, using Chelex 100 as the competing ligand. The water samples were received on June 26, 2003. Ionic strength 1.9×10^{-3} mol/L; temperature 23 ± 2 °C. The Distribution Analysis Method was used to fit the kinetic data.

Analyte	^a [M] _t (mol/L)	<u>Kinetically distinguishable components</u>			<u>Dissociation rate coefficients</u>			χ^2
		C ₁ (%)	C ₂ (%)	C ₃ (%)	k ₁ (s ⁻¹ , 10 ⁻³)	k ₂ (s ⁻¹ , 10 ⁻⁴)	k ₃ (s ⁻¹ , 10 ⁻⁵)	
Co	6.3×10^{-10}	2.87	--	97.13	3.5±2.3	---	1.9±2.8	0.15
Ni	1.1×10^{-8}	0.54	---	99.46	17.9±26.0	---	4.3±10.8	0.39
Cu	4.4×10^{-8}	---	2.2	97.80	---	3.5±1.3	1.4±3.9	0.01
Zn	2.6×10^{-8}	100.0	---	---	1.3±3.5	---	---	0.01
Pb	5.8×10^{-10}	0.03		99.97	55.9±41.9	---	3.8±12.8	0.16
Cd	4.4×10^{-11}	0.21	20.91	78.88	123±56	26.5±17.2	9.1±8.9	0.24

^a[M]_t is total dissolved metals, determined by ICP-MS.

--- Not observed from the distribution analysis.

χ^2 is goodness of fit.

The values after the ± sign are measures of the widths of the distributions.

Table 30 Ligand exchange kinetics of M(II)-DOC in Lake Opasatica-water samples collected from the Rouyn-Noranda area, determined by CLEM/ICP-MS, using Chelex 100 as the competing ligand. The water samples were received on June 26, 2003. Ionic strength 1.5×10^{-3} mol/L; temperature 23 ± 2 °C. The Distribution Analysis Method was used to fit the kinetic data.

Analyte	$[M]_t^a$ (mol/L)	<u>Kinetically distinguishable components</u>			<u>Dissociation rate coefficients</u>			χ^2
		$C_1(\%)$	$C_2(\%)$	$C_3(\%)$	$k_1 (s^{-1}, 10^{-3})$	$k_2 (s^{-1}, 10^{-4})$	$k_3 (s^{-1}, 10^{-5})$	
Co	9.5×10^{-10}	0.49	0.71	98.80	6.7 ± 3.1	12.6 ± 4.3	1.6 ± 2.8	0.41
Ni	1.5×10^{-8}	0.28	1.09	98.63	6.4 ± 2.4	10.0 ± 4.9	5.2 ± 19.4	0.00
Cu	4.2×10^{-8}	0.01	2.29	97.70	2.3 ± 0.3	4.7 ± 2.0	1.9 ± 4.2	0.31
Zn	6.9×10^{-8}	44.69	---	55.31	2.4 ± 2.2	---	8.9 ± 3.5	0.05
Pb	7.2×10^{-10}	---	0.95	99.05	---	9.3 ± 3.6	2.1 ± 6.1	0.08
Cd	6.6×10^{-10}	16.13	---	83.87	2.1 ± 2.2	---	3.9 ± 5.0	0.41

^a $[M]_t$ is total dissolved metals, determined by ICP-MS.

--- Not observed from the distribution analysis.

χ^2 is the goodness of fit.

The values after the \pm sign are measures of the widths of the distributions.

Table 31 Ligand exchange kinetics of M(II)-DOC in Lake Osisko-water samples collected from the Rouyn-Noranda area, determined by CLEM/ICP-MS, using Chelex 100 as the competing ligand. The water samples were received on June 26, 2003. Ionic strength 4.4×10^{-3} mol/L; temperature 23 ± 2 °C. The Distribution Analysis Method was used to fit the kinetic data.

Analyte	^a [M] _t (mol/L)	<u>Kinetically distinguishable components</u>			<u>Dissociation rate coefficients</u>			χ^2
		C ₁ (%)	C ₂ (%)	C ₃ (%)	k ₁ (s ⁻¹ , 10 ⁻³)	k ₂ (s ⁻¹ , 10 ⁻⁴)	k ₃ (s ⁻¹ , 10 ⁻⁵)	
Co	8.3×10^{-10}	0.17	3.5	96.33	6.6±1.5	9.6±3.3	1.3±1.9	0.65
Ni	1.9×10^{-8}	0.01	1.30	98.70	87.5±8.1	8.9±3.2	1.9±3.7	0.14
Cu	5.4×10^{-8}	---	2.24	97.76	---	5.9±2.0	1.6±3.5	0.03
Zn	1.1×10^{-7}	44.69	---	55.31	2.4±2.2	---	8.9±3.5	0.02
Pb	1.0×10^{-9}	0.07	---	99.93	74.4±46.0	---	4.7±12.0	0.98
Cd	2.7×10^{-10}	---	100	--	---	1.5±7.8	---	0.03

^a[M]_t is total dissolved metals, determined by ICP-MS.

--- Not observed from the distribution analysis.

χ^2 is goodness of fit.

The values after the ± sign are measures of the widths of the distributions.

Table 32 Ligand exchange kinetics of M(II)-DOC in Lake Vaudray-water samples collected from the Rouyn-Noranda area, determined by CLEM/ICP-MS, using Chelex 100 as the competing ligand. The water samples were received on June 26, 2003. Ionic strength 8.6×10^{-3} mol/L; temperature 23 ± 2 °C. The Distribution Analysis Method was used to fit the kinetic data.

Analyte	^a [M] _t (mol/L)	<u>Kinetically distinguishable components</u>			<u>Dissociation rate coefficients</u>			χ^2
		C ₁ (%)	C ₂ (%)	C ₃ (%)	k ₁ (s ⁻¹ , 10 ⁻³)	k ₂ (s ⁻¹ , 10 ⁻⁴)	k ₃ (s ⁻¹ , 10 ⁻⁵)	
Co	9.5×10^{-10}	0.05	0.41	99.55	1090±55.1	32.8±12.3	2.3±4.3	1.42
Ni	1.5×10^{-8}	0.12	---	99.88	7.1±2.9	---	2.6±7.8	0.31
Cu	4.2×10^{-8}	---	0.26	99.74	---	9.9±2.5	1.3±4.0	3.00
Zn	6.9×10^{-8}	---	100	---	---	1.8±6.6	---	0.20
Pb	7.2×10^{-10}	---	---	100	---	---	8.1±31.9	1.1
Cd	6.6×10^{-10}	---	---	100	---	---	9.2±38.9	1.23

^a[M]_t is total dissolved metals, determined by ICP-MS.

--- Not observed from the distribution analysis.

χ^2 is the goodness of fit.

The values after the ± sign are measures of the widths of the distributions.

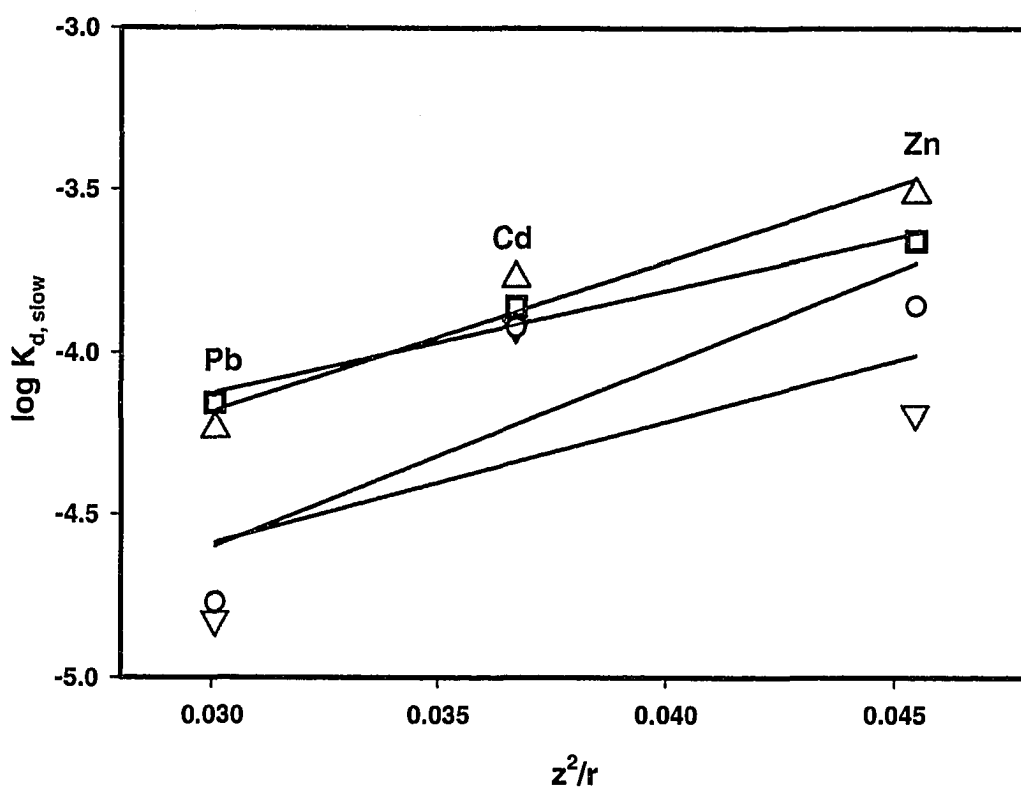


Figure 66 Influence of the ionic potential (z^2/r) on dissociation rate coefficient of the slowest kinetically distinguishable component, $k_{d,slow}$ in freshwater samples collected from the Rouyn-Noranda area, received on June 26, 2003, determined by CLEM/ICP-MS, using Chelex 100 as the competing ligand. (Tables 25-28). Temperature 23 ± 2 °C. (□), Lake Opasatica, pH 6.9 ± 0.1 , DOC 9.0 ± 0.4 mg/L, ionic strength 1.5×10^{-3} mol/L; (▽), Lake Dufault, pH 7.0 ± 0.1 , DOC 15.7 ± 2.9 mg/L, ionic strength 1.9×10^{-3} mol/L; (△), Lake Osisko, pH 7.3 ± 0.1 , DOC 6.0 ± 1.3 mg/L, ionic strength 4.4×10^{-3} mol/L; (○), Lake Vaudray, pH 6.1 ± 0.1 , DOC 11.0 ± 0.6 mg/L, ionic strength 8.6×10^{-5} mol/L. The non-linear regression analysis was used to fit the kinetic data.

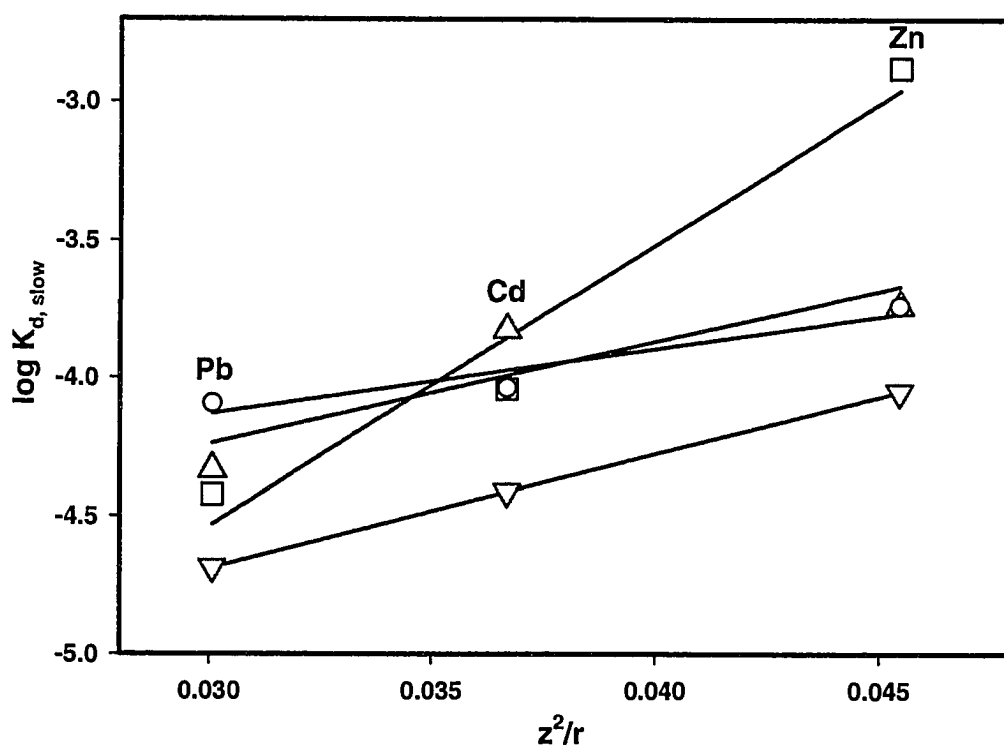


Figure 67 Influence of the ionic potential (z^2/r) on mean dissociation rate coefficient of the slowest kinetically distinguishable component, $k_{d,slow}$, in freshwater samples collected from the Rouyn-Noranda area, received on June 26, 2003, determined by CLEM/ICP-MS, using Chelex 100 as the competing ligand. (Tables 29-32). Temperature 23 ± 2 °C. □, Lake Opasatica, pH 6.9 ± 0.1 , DOC 9.0 ± 0.4 mg/L, ionic strength 1.5×10^{-3} mol/L; ▽, Lake Dufault, pH 7.0 ± 0.1 , DOC 15.7 ± 2.9 mg/L, ionic strength 1.9×10^{-3} mol/L; △, Lake Osisko, pH 7.3 ± 0.1 , DOC 6.0 ± 1.3 mg/L, ionic strength 4.4×10^{-3} mol/L; ○, Lake Vaudray, pH 6.1 ± 0.1 , DOC 11.0 ± 0.6 mg/L, ionic strength 8.6×10^{-5} mol/L. The Distribution Analysis Method was used to fit the kinetic data.

expected to have the lowest $[M^{2+}]$ since the metals were probably bound to the DOC. Lakes Osisko and Dufault had much higher $[M]/[DOC]$ mole ratios, and were expected to have higher $[M^{2+}]$ than the other two lakes since the strong binding sites on the DOC were all probably occupied by the metals, leaving the remaining metals to be bound by weaker sites, resulting in the formation of labile metal complexes, including free metal ion (metal aqua complex). However, the experimental results did not conform to this expectation probably because of the competition by other major metal cations such as those of Al, Fe, Ca, Mg, and trace metals. The experimental pHs of all the lake-water samples were the same as those of the samples (Table 23). WHAM modelling was done in several different ways to minimize the difference between the measured $[M^{2+}]$ and the $[M^{2+}]$ predicted by WHAM, as discussed in chapter 6. The measured free-metal ion concentration plus labile fraction were compared with those predicted by WHAM using 65% of “active” DOC, and it was found that in most cases, increasing the percentage of the active DOC from 65% to 80% corresponding to an decrease in the predicted free-metal-ions by ~ 5-25% in lake-water samples. The predictions of WHAM V were compared with those of WHAM VI in order to determine which version (V or VI) of WHAM was better suited for modelling the above lake-water samples.

Nickel modelling

The labile (i.e. rapidly-dissociating) nickel complexes are distinguished from the non-labile (or very slowly-dissociating) nickel complexes by their dissociation rate coefficients. In order to compare the measured concentrations with the WHAM predictions, the percentage of the labile fraction is multiplied by the total metal

concentration of the sample. This gives a value that represents the dissociation rate coefficients of a mixture of very labile complexes, e.g. for nickel, small organic and inorganic complexes of nickel as well as the free-nickel ion (i.e. $\text{Ni}(\text{H}_2\text{O})_6^{2+}$). Since the measured value was for the labile-nickel concentration, and the predicted values from WHAM also included the inorganic complexes such as NiCl_2 and NiSO_4 as well as the free-nickel-ion, although in most cases, the concentrations of the inorganic components were negligible compared to the free-nickel-ion concentration; hence, the measured values are expected to be equal to, or greater than, those predicted by WHAM [189].

The measured values of $[\text{Ni}^{2+}]$ plus labile Ni(II)–DOC complexes depend on the affinity of nickel for the binding sites, and at a given pH and ionic strength, $[\text{Ni}^{2+}]$ will be determined by the $[\text{Ni}]/[\text{DOC}]$ mole ratio and on the competition of the other metals with nickel [189]. Table 33a presents the experimentally measured concentrations of labile Ni(II) complexes, and the WHAM-predicted $[\text{Ni}^{2+}]$. The general expectation was for Lake Osisko to have the highest $[\text{Ni}^{2+}]$ since it had the highest $[\text{Ni}]/[\text{DOC}]$ mole ratio (Table 33a), and Lake Dufault to have the lowest $[\text{Ni}^{2+}]$. The measured labile nickel complexes did not follow the trend expected from the $[\text{Ni}]/[\text{DOC}]$ mole ratio. This was probably because the $[\text{Ni}^{2+}]$ does not depend only on the $[\text{Ni}]/[\text{DOC}]$ mole ratio as explained earlier. WHAM predictions were a two-factor of magnitude higher than the measured labile Ni(II)–DOC complexes (relative non-linear regression analysis). The values of $\log K_{\text{MA}}$ used in the WHAM model (Table 22) (chapter 7) are simple averages of values obtained from different data sets. Variations in $\log K_{\text{MA}}$ among the data sets may be due to errors in the data, and to errors in the model, arising from its application to

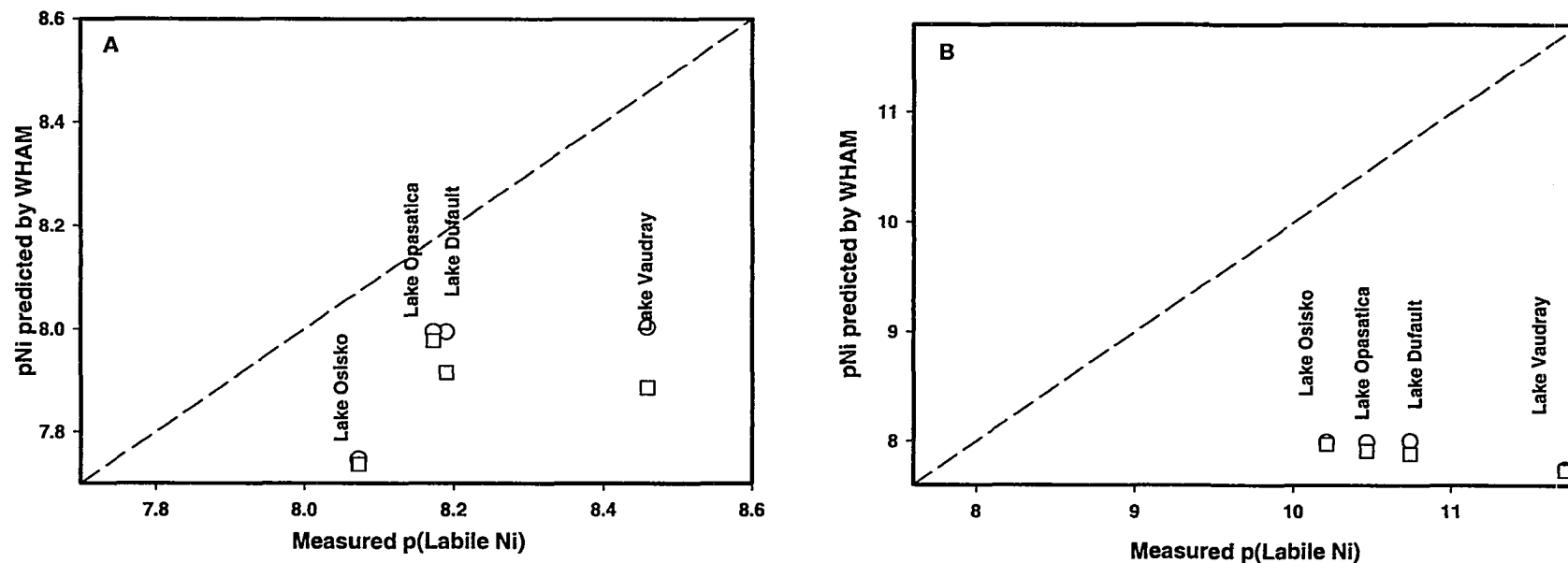


Figure 68 Comparison of the pNi predicted by WHAM V and WHAM VI, with the measured concentrations of labile Ni(II)-complexes in lake-water samples collected from the Rouyn-Noranda area, Québec, (received on June 26, 2003). (---) 1:1 line, (o) WHAM V predictions, (□) WHAM VI predictions. Input parameters used for calculating free-metal ion concentrations in four lakes using WHAM have been presented in Table 23. WHAM predictions based on 65% of the DOC as a ‘active’. Free metal ion plus labile metal complexes, were measured by CLEM/ICP-MS, using Chelex 100 as the competing ligand. A) Kinetic data were analyzed by non-linear regression analysis; B) Kinetic data were analyzed by Distribution Analysis Method.

Table 33a WHAM model predictions of the speciation of Co, Ni, Cu, Zn, Cd, and Pb in the lake water samples based on 65% of the DOC as “active”, and the measured concentrations of labile Co(II)-, Ni(II)-, Cu(II)-, Zn(II)-, Cd(II)-, and Pb(II)-complexes in the lake water samples collected from the Rouyn-Noranda area, Quebec, in June 2003.

Analyte	Sample	^a [M] _t (M)	^b DOC (mg/L)	^a [M] _t /DOC (mol/g)	WHAM V [M ⁺²] (M)	WHAMVI [M ⁺²] (M)	Measured concentration of labile Cu-complexes (M) by non-linear regression	Measured concentration of labile Cu-complexes (M) by distribution analysis
Co	Lake Dufault	1.6 x 10 ⁻⁹	10.9	1.0 x 10 ⁻⁷	1.44 x 10 ⁻⁹	1.6 x 10 ⁻⁹	1.1 x 10 ⁻⁹	7.8 x 10 ⁻¹²
	Lake Opasatica	6.3 x 10 ⁻¹⁰	10.4	7.0 x 10 ⁻⁸	5.9 x 10 ⁻¹⁰	5.9 x 10 ⁻¹⁰	5.2 x 10 ⁻¹⁰	1.8 x 10 ⁻¹¹
	Lake Osisko	8.3 x 10 ⁻¹⁰	6.7	1.4 x 10 ⁻⁷	8.0 x 10 ⁻¹⁰	8.0 x 10 ⁻¹⁰	3.7 x 10 ⁻¹⁰	1.4 x 10 ⁻¹²
	Lake Vaudray	9.5 x 10 ⁻¹⁰	6.9	8.6 x 10 ⁻⁸	7.9 x 10 ⁻¹⁰	8.4 x 10 ⁻¹⁰	4.8 x 10 ⁻¹⁰	4.8 x 10 ⁻¹³
Ni	Lake Dufault	1.2 x 10 ⁻⁸	10.9	7.8 x 10 ⁻⁷	1.0 x 10 ⁻⁸	1.2 x 10 ⁻⁸	6.5 x 10 ⁻⁹	3.4 x 10 ⁻¹¹
	Lake Opasatica	1.1 x 10 ⁻⁸	10.4	1.3 x 10 ⁻⁶	1.0 x 10 ⁻⁸	1.1 x 10 ⁻⁸	6.7 x 10 ⁻⁹	6.1 x 10 ⁻¹¹
	Lake Osisko	1.9 x 10 ⁻⁸	6.7	3.2 x 10 ⁻⁶	1.8 x 10 ⁻⁸	1.8 x 10 ⁻⁸	8.5 x 10 ⁻⁹	1.9 x 10 ⁻¹²
	Lake Vaudray	1.5 x 10 ⁻⁸	6.9	1.4 x 10 ⁻⁶	9.9 x 10 ⁻⁹	1.3 x 10 ⁻⁸	3.5 x 10 ⁻⁹	1.8 x 10 ⁻¹¹
Cu	Lake Dufault	1.9 x 10 ⁻⁷	10.9	1.2 x 10 ⁻⁵	5.7 x 10 ⁻⁸	1.9 x 10 ⁻⁷	6.7 x 10 ⁻⁸	1.8 x 10 ⁻¹¹
	Lake Opasatica	4.4 x 10 ⁻⁸	10.4	4.9 x 10 ⁻⁶	1.8 x 10 ⁻⁸	2.2 x 10 ⁻⁹	2.1 x 10 ⁻⁸	9.8 x 10 ⁻¹⁰
	Lake Osisko	5.4 x 10 ⁻⁸	6.7	9.0 x 10 ⁻⁶	2.5 x 10 ⁻⁸	3.6 x 10 ⁻⁹	2.8 x 10 ⁻⁸	1.2 x 10 ⁻⁹
	Lake Vaudray	4.2 x 10 ⁻⁸	6.9	3.8 x 10 ⁻⁶	6.1 x 10 ⁻⁹	2.4 x 10 ⁻⁹	8.3 x 10 ⁻⁹	1.1 x 10 ⁻¹⁰

^a[M]_t is total dissolved metals, determined by ICP-MS.

^b Determined by Shimadzu Total Organic Carbon Analyzer, Model TOC-VCSH.

Table 33b WHAM model predictions of the speciation of Co, Ni, Cu, Zn, Cd, and Pb in the lake water samples based on 65% of the DOC as “active”, and the measured concentrations of labile Co(II)-, Ni(II)-, Cu(II)-, Zn(II)-, Cd(II)-, and Pb(II)- complexes in the lake water samples collected from the Rouyn-Noranda area, Quebec, in June 2003.

Analyte	Sample	^a [M] _t (M)	^b DOC (mg/L)	^a [M] _t /DOC (mol/g)	WHAM V [M ⁺²] (M)	WHAMVI [M ⁺²] (M)	Measured concentration of labile Cu-complexes (M) by non-linear regression	Measured concentration of labile Cu-complexes (M) by distribution analysis
Zn	Lake Dufault	9.6 x 10 ⁻⁷	10.9	6.1 x 10 ⁻⁵	7.4 x 10 ⁻⁷	9.6 x 10 ⁻⁷	8.1 x 10 ⁻⁷	4.3 x 10 ⁻⁷
	Lake Opasatica	2.6 x 10 ⁻⁸	10.4	2.9 x 10 ⁻⁶	2.2 x 10 ⁻⁸	2.2 x 10 ⁻⁸	2.3 x 10 ⁻⁸	2.6 x 10 ⁻⁸
	Lake Osisko	1.1 x 10 ⁻⁷	6.7	1.8 x 10 ⁻⁵	9.5 x 10 ⁻⁸	9.7 x 10 ⁻⁸	7.5 x 10 ⁻⁸	4.7 x 10 ⁻⁸
	Lake Vaudray	6.9 x 10 ⁻⁸	6.9	6.3 x 10 ⁻⁶	4.0 x 10 ⁻⁸	5.4 x 10 ⁻⁸	4.6 x 10 ⁻⁸	6.9 x 10 ⁻⁸
Cd	Lake Dufault	4.9 x 10 ⁻⁹	10.9	3.1 x 10 ⁻⁷	4.1 x 10 ⁻⁹	4.9 x 10 ⁻⁹	1.8 x 10 ⁻⁹	4.7 x 10 ⁻¹¹
	Lake Opasatica	4.5 x 10 ⁻¹¹	10.4	4.9 x 10 ⁻⁹	4.0 x 10 ⁻¹¹	3.7 x 10 ⁻¹¹	1.7 x 10 ⁻¹¹	1.3 x 10 ⁻¹⁴
	Lake Osisko	2.7 x 10 ⁻¹⁰	6.7	4.4 x 10 ⁻⁸	2.4 x 10 ⁻¹⁰	2.4 x 10 ⁻¹⁰	8.5 x 10 ⁻¹¹	1.9 x 10 ⁻¹³
	Lake Vaudray	7.1 x 10 ⁻¹⁰	6.9	6.5 x 10 ⁻⁸	5.2 x 10 ⁻¹⁰	5.4 x 10 ⁻¹⁰	2.6 x 10 ⁻¹⁰	2.7 x 10 ⁻¹⁰
Pb	Lake Dufault	2.9 x 10 ⁻⁹	10.9	1.8 x 10 ⁻⁷	1.1 x 10 ⁻⁹	2.9 x 10 ⁻⁹	2.3 x 10 ⁻⁹	4.6 x 10 ⁻¹⁰
	Lake Opasatica	5.8 x 10 ⁻¹⁰	10.4	6.5 x 10 ⁻⁸	2.9 x 10 ⁻¹⁰	2.4 x 10 ⁻¹¹	5.0 x 10 ⁻¹⁰	1.2 x 10 ⁻¹²
	Lake Osisko	1.0 x 10 ⁻⁹	6.7	1.7 x 10 ⁻⁷	5.6 x 10 ⁻¹⁰	5.7 x 10 ⁻¹¹	6.9 x 10 ⁻¹⁰	1.0 x 10 ⁻⁹
	Lake Vaudray	6.7 x 10 ⁻¹⁰	6.9	6.1 x 10 ⁻⁸	1.4 x 10 ⁻¹⁰	4.5 x 10 ⁻¹¹	3.7 x 10 ⁻¹⁰	6.7 x 10 ⁻¹⁰

^a[M]_t is total dissolved metals, determined by ICP-MS.

^b Determined by Shimadzu Total Organic Carbon Analyzer, Model TOC-VCSH.

data covering different experimental conditions. However, the main reason for the variation was probably that different samples of HS were used to obtain the data. Such differences may arise from differences in isolation procedures, or they may reflect variability in the natural materials. As a result, WHAM is unable to fit the binding data of Nickel with DOC in freshwaters. It is informative to consider errors in the prediction of binding that might arise from the use of the model with its default parameter set [189]. Table 22 (chapter 7) shows standard deviations of the $\log K_{MA}$ value for each metal. The effect on the WHAM prediction of the $[M^{n+}]$ by adding or subtracting one standard deviation of $\log K_{MA}$ can be large. For Co, the WHAM-predicted values can vary by about 1.0 log units, whereas for Cu, the WHAM-predicted values can vary by about 1.5 log units [8]

Figure 68A shows that the results predicted by WHAM V and VI compared reasonably well (within a factor of two) with the measured concentrations of labile nickel complexes by non-linear regression analysis, whereas, Figure 68B shows that results predicted by WHAM V and VI were 2-3 orders of magnitude higher than the measured nickel labile complexes obtained by Distribution Analysis Method.

Cobalt modelling

The predictions of both WHAM V and VI were nearly the same for all the lakes. Figure 69A shows that the results predicted by WHAM V and VI compared reasonably well with the measured concentrations of labile cobalt complexes by non-linear regression analysis for all the lakes (within a factor of two), whereas, Figure 69B shows that the results predicted by WHAM V and VI were 1-3 orders of magnitude higher than the

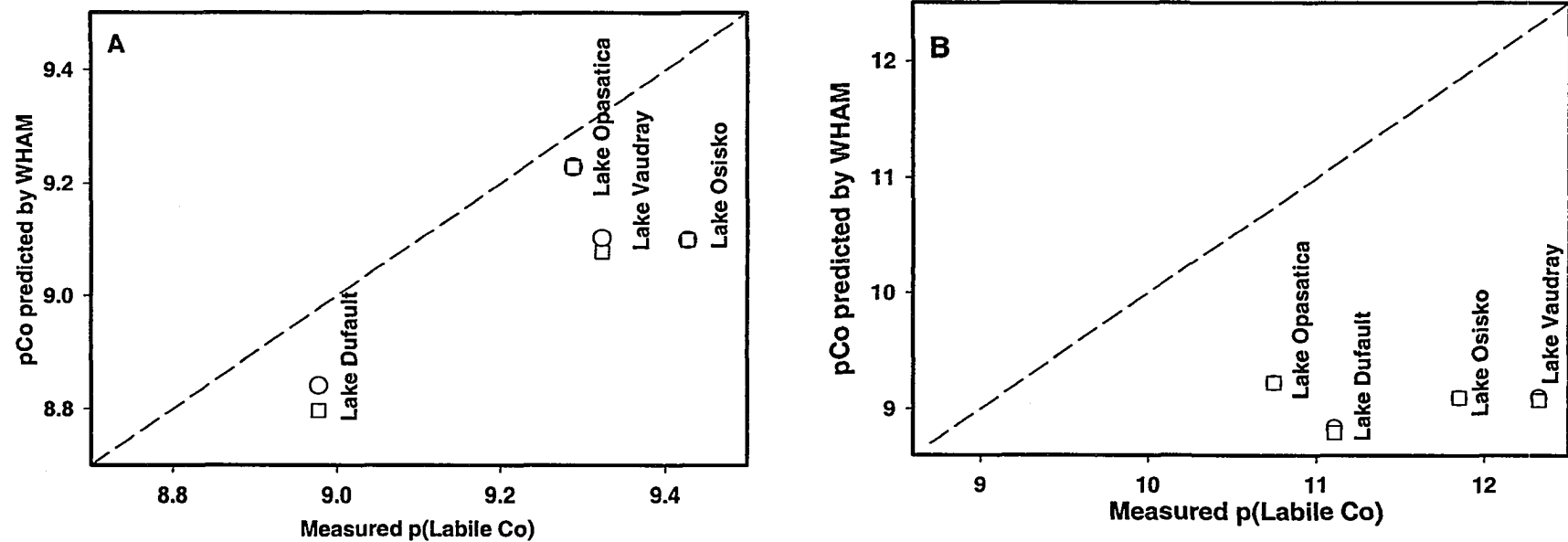


Figure 69 Comparison of the pCo predicted by WHAM V and WHAM VI, with the measured concentrations of labile Co(II)-complexes in lake-water samples collected from the Rouyn-Noranda area, Québec, (received on June 26, 2003). (---) 1:1 line, (o) WHAM V predictions, (□) WHAM VI predictions. Input parameters used for calculating free-metal ion concentrations in four lakes using WHAM have been presented in Table 23. WHAM predictions based on 65% of the DOC as a 'active'. Free metal ion plus labile metal complexes, were measured by CLEM/ICP-MS, using Chelex 100 as the competing ligand. A) Kinetic data were analyzed by non-linear regression analysis; B) Kinetic data were analyzed by Distribution Analysis Method.

measured concentrations of labile cobalt complexes by Distribution Analysis Method for all the lakes. This result, however, is reasonable, considering the assumptions and uncertainties of WHAM (relative to non-linear regression).

Copper modelling

The prediction of WHAM V was 1 order of magnitude closer to the measured concentrations of labile copper complexes by both non-linear regression analysis and Distribution Analysis Method than that of WHAM VI. Figure 70A shows that the results predicted by WHAM V compared reasonably well with the measured concentrations of labile copper complexes by non-linear regression analysis for all the lakes, whereas, Figure 70B shows that the results predicted by WHAM V were 1-2 orders of magnitude higher than the measured concentrations of labile copper complexes by Distribution Analysis Method for all the lakes except Lake Dufault. This result, however, is reasonable, considering the assumptions and uncertainties of WHAM (relative to non-linear regression).

Zinc modelling

The predictions of both WHAM V and VI were nearly the same for all the lakes. Figures 71A and 71B show that the results predicted by WHAM V and VI compared reasonably well (within one order of magnitude) with the measured concentrations of labile zinc complexes by non-linear regression analysis and by Distribution Analysis Method for all the lakes.

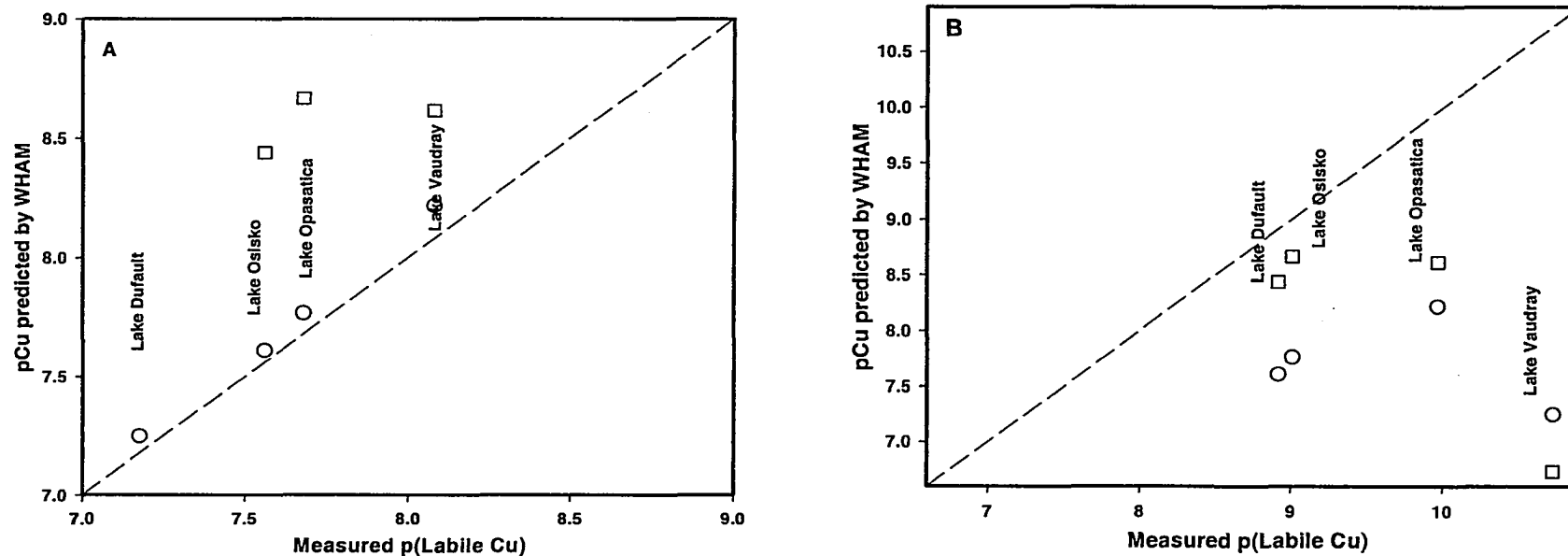


Figure 70 Comparison of the pCu predicted by WHAM V and WHAM VI, with the measured concentrations of labile Cu(II)-complexes in lake-water samples collected from the Rouyn-Noranda area, Québec, (received on June 26, 2003). (---) 1:1 line, (o) WHAM V predictions, (□) WHAM VI predictions. Input parameters used for calculating free-metal ion concentrations in four lakes using WHAM have been presented in Table 23. WHAM predictions based on 65% of the DOC as a 'active'. Free metal ion plus labile metal complexes, were measured by CLEM/ICP-MS, using Chelex 100 as the competing ligand. A) Kinetic data were analyzed by non-linear regression analysis; B) Kinetic data were analyzed by Distribution Analysis Method.

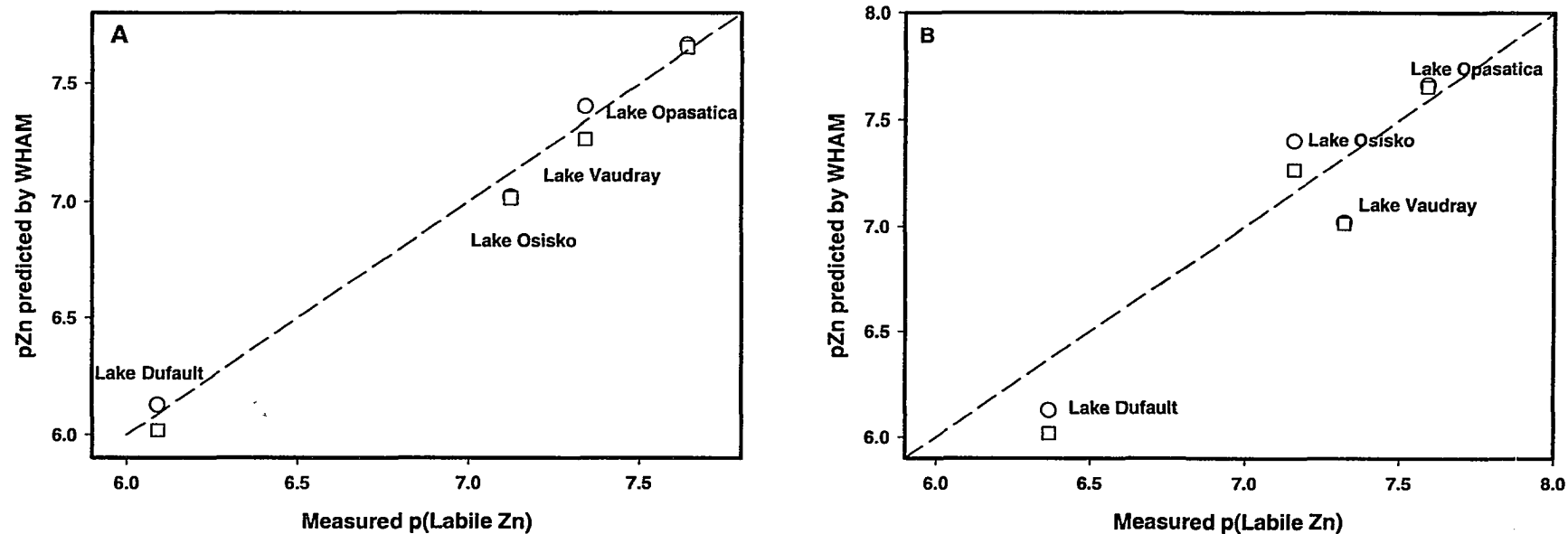


Figure 71 Comparison of the pZn predicted by WHAM V and WHAM VI, with the measured concentrations of labile Zn(II)-complexes in lake-water samples collected from the Rouyn-Noranda area, Québec, (received on June 26, 2003). (---) 1:1 line, (o) WHAM V predictions, (□) WHAM VI predictions. Input parameters used for calculating free-metal ion concentrations in four lakes using WHAM have been presented in Table 23. WHAM predictions based on 65% of the DOC as a ‘active’. Free metal ion plus labile metal complexes, were measured by CLEM/ICP-MS, using Chelex 100 as the competing ligand.. A) Kinetic data were analyzed by non-linear regression analysis; B) Kinetic data were analyzed by Distribution Analysis Method.

Cadmium modelling

The predictions of both WHAM V and VI were nearly the same for all the lakes. The highest [Cd]/[DOC] mole ratio was for the water sample of Lake Dufault, and the lowest mole ratio was for the water sample of Lake Opasatica (Table 33b). The measured labile Cd(II)-DOC complexes showed the same trend expected from the [Cd]/[DOC] mole ratio. The WHAM predictions were almost two factor of magnitude higher than measured labile Cd(II)-DOC complexes by non-linear regression analysis. WHAM has been parameterized mainly for high metal loading conditions, which may result in the model being unable to adequately model lakes under low metal loading conditions [189].

Figure 72A shows that the results predicted by WHAM V and VI compared reasonably well with the measured concentrations of labile cadmium complexes by non-linear regression analysis for all the lakes, whereas Figure 72B shows that results predicted by WHAM V and VI are higher by 2-3 orders of magnitudes than results obtained using Distribution analysis method.

Lead modelling

Figure 73 shows the results of the modelling by WHAM and the measured values for lead. The $[Pb^{2+}]$ depends on the [Pb]/[DOC] ratio. Table 33b shows that the highest [Pb]/[DOC] ratio was for the water sample of Lake Dufault, and the lowest ratio was for the water sample of Lake Vaudray. Therefore, the expectation was that Lake Dufault would have the highest and Lake Vaudray would have the lowest labile lead complexes. Both the measured concentrations of labile Pb-complexes and the WHAM predictions

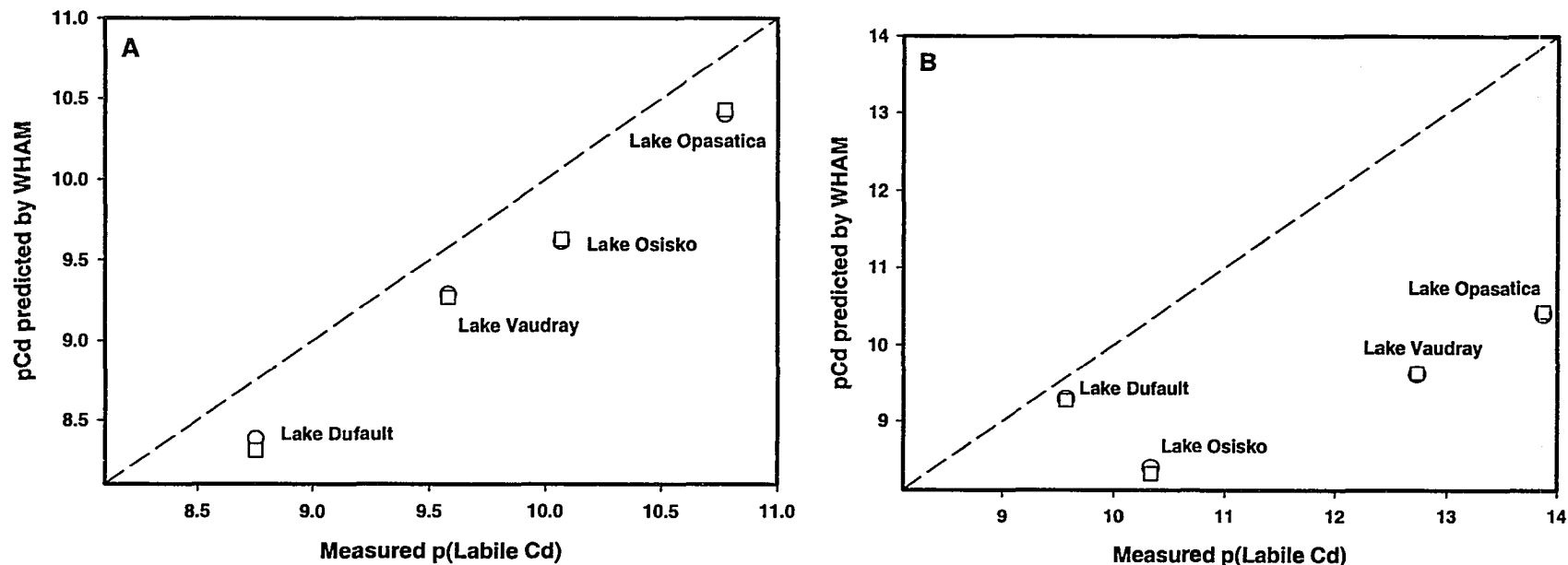


Figure 72 Comparison of the pCd predicted by WHAM V and WHAM VI, with the measured concentrations of labile Cd(II)-complexes in lake-water samples collected from the Rouyn-Noranda area, Québec, (received on June 26, 2003). (---) 1:1 line, (o) WHAM V predictions, (□) WHAM VI predictions. Input parameters used for calculating free-metal ion concentrations in four lakes using WHAM have been presented in Table 23. WHAM predictions based on 65% of the DOC as a ‘active’. Free metal ion plus labile metal complexes, were measured by CLEM/ICP-MS, using Chelex 100 as the competing ligand. A) Kinetic data were analyzed by non-linear regression analysis; B) Kinetic data were analyzed by Distribution Analysis Method.

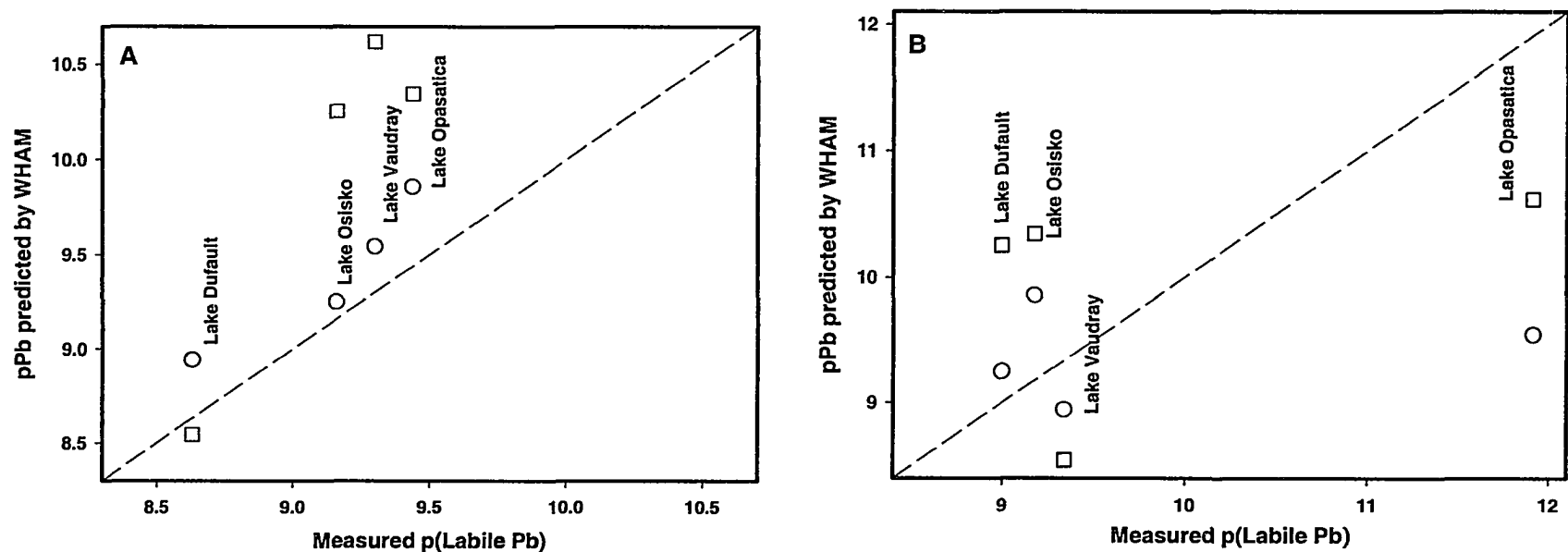


Figure 73 Comparison of the pPb predicted by WHAM V and WHAM VI, with the measured concentrations of labile Pb(II)-complexes in lake-water samples collected from the Rouyn-Noranda area, Québec, (received on June 26, 2003). (---) 1:1 line, (o) WHAM V predictions, (□) WHAM VI predictions. Input parameters used for calculating free-metal ion concentrations in four lakes using WHAM have been presented in Table 23. WHAM predictions based on 65% of the DOC as a ‘active’. Free metal ion plus labile metal complexes, were measured by CLEM/ICP-MS, using Chelex 100 as the competing ligand.. A) Kinetic data were analyzed by non-linear regression analysis; B) Kinetic data were analyzed by Distribution Analysis Method.

agree with the expectation. Figure 73A shows that the results predicted by WHAM V and VI compared reasonably well with the measured concentrations of labile lead complexes by non-linear regression analysis for all lakes. The predictions of WHAM V are in closer agreement with the measured concentrations (which, however, represent labile lead complexes) for all the lakes (see Table 22), whereas Figure 73B shows results predicted by WHAM V and VI and the measured concentrations of lead complexes by Distribution Analysis Method.

The results of the WHAM comparison have confirmed that WHAM most likely describes the differences in the solution composition such as pH and ionic strength and DOC that WHAM effectively acts as a probe for comparing the past data on metal-binding with the results and conditions of the present work [189].

For Ni(II), Cu(II), and Zn(II), the agreement between the measured concentrations of labile Ni(II)-, Cu(II)-, and Zn(II) complexes (including free metal ion), and the WHAM-predicted concentrations of free Ni²⁺, Cu⁺² and Zn⁺² ions were not satisfactory. This was probably due to the measured labile M(II) complexes being mostly composed of free Ni²⁺, Cu⁺² and Zn⁺² ions, respectively. The WHAM-predicted results for [Co²⁺], [Ni²⁺] and [Cd²⁺] were two factors of magnitude higher than the measured labile Co(II)-, Ni(II)- and Cd(II)-DOC complexes, probably because the default parameters in WHAM did not correctly describe the binding of these metals to the binding sites on the DOC. However, the difference was not large enough to impugn the validity of the WHAM. Comparing

WHAM V with WHAM VI, this study has found that the models are very similar, but WHAM VI is equal to or better than WHAM V for all metals except for Cu and Pb. The general conclusions are that WHAM provided reasonable estimates of the free-metal-ion fractions for the six metals in the surface waters of the four lakes.

Measured labile fraction of metal complexes by non-linear regression analysis is reasonably well correlated with the WHAM (V, VI) predictions of the free metal concentrations, suggesting that non-linear regression analysis provides a better estimate of the labile complexes of the metals reported above than Distribution Analysis Method does for these lake-water samples.

8.5 Conclusion

Total metal concentration was found to be highest in Lake Dufault because it was located upwind and close to the smelter, and hence, most likely received the highest amount of lead through atmospheric deposition. Therefore, the most labile Co(II)-, Ni(II)-, Cu(II), Zn(II), Cd(II), Pb(II)-DOC complexes were found to be in Lake Dufault because of the relatively high [metal]/[DOC] mole ratio and competition by major cations (e.g., Ca²⁺ and Mg²⁺).

The results showed that for most metals, WHAM V provided reasonable estimates for [Ni²⁺], [Cu²⁺], and [Pb²⁺] in lake surface waters having different conditions of pH and DOC concentrations. In comparing the measured labile metal concentrations (including free-metal ion concentrations) with the WHAM predictions, one should bear in mind that the kinetics-based CLEM/AdCSV provided the concentration of labile metal complexes

including metal-aqua complexes whereas the WHAM-predicted concentrations were only those of the free-metal ion, M^{2+} . Hence, in the case of copper and lead, it was not unreasonable to expect that the measured concentrations were greater than the WHAM-predicted $[Cu^{2+}]$ and $[Pb^{2+}]$. Indeed, the measured concentrations of the labile Cu(II) and Pb(II) complexes were larger than the WHAM-predicted concentrations. However, for nickel, the agreement between the measured concentrations of the labile Ni(II)-DOC complexes (including free Ni^{2+} ion) and the WHAM-predicted. The ability of the Kinetic Model to correctly predict the influence of the metal-to-ligand ratio, ionic potential, and LFSE on the relative rates of metal complex dissociation supports the conclusion that the Kinetic Model provides a chemically significant description of the kinetics of metal-DOM interactions in freshwaters. The observed trends suggest that these trace metals compete for the same binding sites of DOM and emphasize the importance of considering the valence-shell electron configuration for predicting the competition of trace metals in the freshwater environment.

A satisfactory fit of the experimental data indicates only that the values obtained are compatible with the Kinetic Model, and does not prove the actual existence of certain metal complex or a particular distribution. Therefore, valid interpretation of the results requires a good knowledge of the physico-chemical characteristics of the samples and of the reliability of the data [223]

In comparing the measured free-metal ion concentrations with the WHAM predictions, one should bear in mind the metal species actually measured by the speciation technique

employed. Kinetics-based CLEM/ICP-MS (the speciation techniques employed) provided the concentrations of labile metal complexes including metal-aqua complexes, whereas the WHAM-predicted concentrations were only those of the free-metal ion, M^{2+} . Hence, it is not unreasonable to expect the measured concentrations of labile metal complexes to be greater than the WHAM-predicted $[M^{2+}]$. However, for all metals, WHAM-predicted $[M^{2+}]$ were in reasonable agreement with the measured concentrations of labile metal complexes by non-linear regression analysis. Both WHAM V and WHAM VI have been tested extensively by others against several data sets and have been found to perform adequately when modelling freshwaters. Comparing WHAM V with WHAM VI, this study has found that the agreement of WHAM V with the measured concentrations of labile metal complexes by non-linear regression analysis is equal to or better than that of WHAM VI for all the lake waters studied. The general conclusions are that WHAM provides overestimates of free-metal ion fractions, which are not in reasonable agreement with measured labile metal complexes in the surface waters of the four lakes. Hence, WHAM is still a valuable tool for metal speciation studies, especially when good estimates of $[M^{2+}]$ are not readily available [189].

In general, good agreement was found between the dissociation rate coefficients determined by the two data analysis methods: non-linear regression analysis and Distribution Analysis Method. However, relative proportions of kinetically distinguishable components obtained by non-linear regression analysis are more reasonable than those obtained by Distribution Analysis Method for the lake-water

samples studied. These two methods of data analysis are, however, complementary rather than competitive because of their different statistical basis.

-- Chapter 9 --

**Heterogeneity of Humic Substances. Differential Equilibrium
Functions of Pb(II)-Complexes in Model Solutions of a Well-
Characterized Humic Acid Determined by Pseudopolarography
using a Static Mercury Drop Electrode**

9.1 Introduction

Heterogeneity here refers to both the physical and chemical properties of naturally-occurring organic complexants, such as humic substances in natural waters. In unpolluted natural waters, most metals are present at trace or ultratrace levels, typically 10^{-8} – 10^{-12} M [224], even below 10^{-12} M [225]. In freshwaters and soils, it is often difficult to determine the identity and concentration of metal complexes, some of which are transient. It is however possible to characterize these metal species by speciation parameters, which are quantitative measures of their chemical characteristics. It often requires a number of speciation parameters to characterize a system fully. Some important speciation parameters of a metal complex are dissociation rate coefficient (which is a measure of its kinetic lability), diffusion coefficient (which is a measure of its mobility), and stability constant (which is a measure of the availability of free metal ion at equilibrium).

Voltammetric methods are well suited for investigation of speciation of trace elements in natural waters. Because of their high sensitivity and the relative simplicity and compactness of the apparatus, voltammetric methods are easily applicable in the field. More importantly, voltammetric signals are strongly linked to the physico-chemical characteristics of the electroactive species. Voltammetric methods are sensitive to stability of metal-ligand complex, rate of association and dissociation of a metal-ligand complex (kinetic lability), and diffusion coefficient (mobility) of a metal complex [226]. Thus, in principle, information on speciation of the element of interest can be obtained by voltammetric methods [227-231].

9.2 Theory

9.2.1 Pseudopolarography

Metal speciation studies analogous to those performed by d.c. polarography at a dropping mercury electrode can be carried out at much lower concentrations ($10^{-7} - 10^{-9}$ M) by pseudopolarography (stripping polarography) [231-234]. Pseudopolarography involves repeating the anodic stripping voltammetric step using a series of deposition potentials. The relationship between the stripping (oxidation) current and the corresponding reduction potential for the metal of interest is an s-shaped, polarogram-like curve, known as a pseudopolarogram. It has been shown that for simple, labile complexes, the half-wave potential for the pseudopolarographic curve is shifted to a more negative potential relative to that for the free metal ion, in a way that is analogous to conventional d.c. polarography [235-236]. Hence, stability constants for complexes can be calculated from pseudopolarographic data using methods developed for conventional d.c. polarography. The advantages of pseudopolarography over polarography are its increased sensitivity and much lower limits of detection, which enable electrochemical investigations at environmentally relevant concentrations.

The polarographic wave for a solution containing “simple”, homogenous ligands is described by the DeFord and Hume equation [237-238].

$$E = E^{\circ} + \frac{RT}{nF} \ln \left[\frac{1}{\alpha} \left(\frac{D_R}{D_{ML}} \right)^{1/2} \right] + \frac{RT}{nF} \ln \left(\frac{1 - i/i_{lim}}{i/i_{lim}} \right) \quad (9.1)$$

where E° is the normal redox potential (V) of the redox couple, R is the Gas Constant ($8.314 \text{ J K}^{-1} \text{ mol}^{-1}$), T is the absolute temperature in kelvin (K), n is the number of electrons exchanged, F is Faraday Constant ($96,485 \text{ C mol}^{-1}$), α is the degree of

complexation of the metal, D_R is the diffusion coefficient of reduced form of M, M^o in mercury, D_{ML} is the diffusion coefficient of ML in the solution, i_{lim} is the diffusion-limited limiting current and i is the measured current.

Heterogeneous organic complexants (such as fulvic acid) have a continuous distribution of complexing sites which results in the formation of metal complexes having closely-spaced stability constants, spreading the polarographic wave. In this case, stronger sites become active in controlling the free metal ions concentration as M is progressively depleted. Increasingly negative applied potentials are required to drive the dissociation of the remaining metal complexes, and the polarographic wave becomes asymmetrical, elongated and shifted towards negative potentials [84], as shown in Figure 74. An important consequence is that the Deford and Hume equation cannot be applied to determine conditional stability constants of metal complexes of heterogeneous complexants based on shifts in the half-wave potential.

An equation to describe the shape of a polarographic wave in the presence of heterogeneous complexants was derived by Filella et al. [84]:

$$E = E_0 + \frac{RT}{nF} \ln \left[\frac{1}{A^{1/\Gamma} c_L} \left(\frac{c_M}{c_L} \right)^{(1-\Gamma)/\Gamma} \left(\frac{D_R}{D_{ML}} \right)^{1/2} \right] + \frac{RT}{nF} \ln \left[\frac{(1 - i/i_{lim})^{1/\Gamma}}{i/i_{lim}} \right] \quad (9.2)$$

In equation 9.2, A is Freundlich constant; c_M and c_L are the concentrations of M and L in the bulk solution, respectively. Γ is a parameter that reflects the degree of heterogeneity

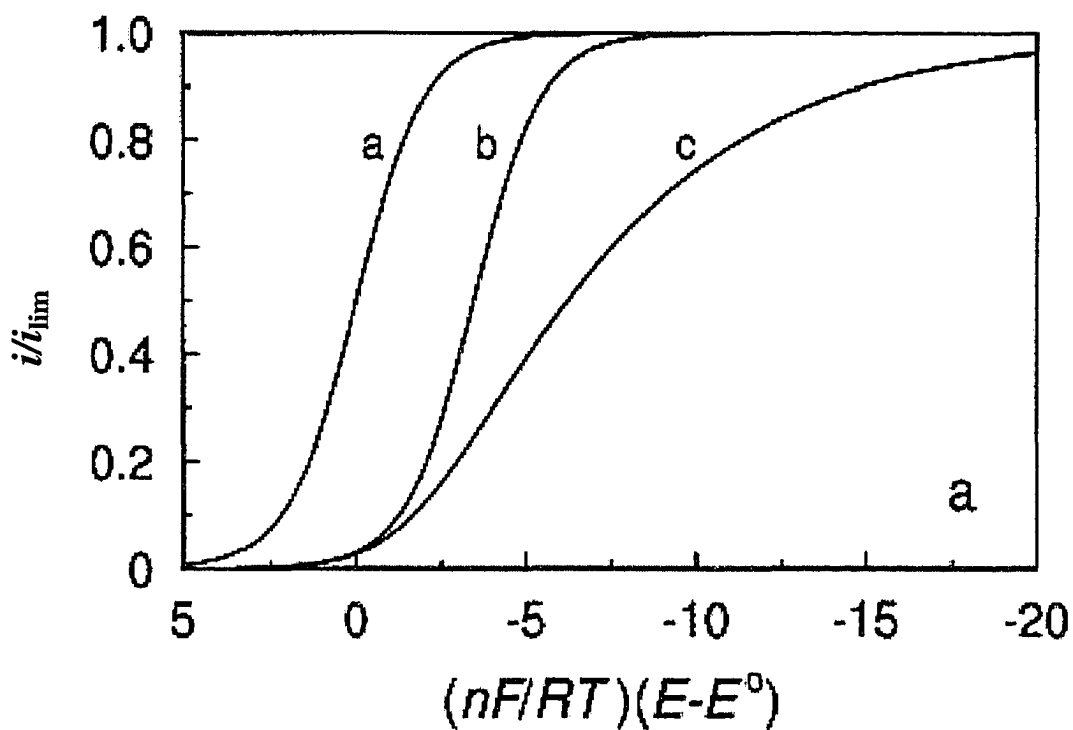


Figure 74 Simulated polarographic curves for the reduction of M a) under non-complexing conditions; b) in the presence of a simple, homogeneous ligand (equation 9.1), $\Gamma = 1$; c) in the presence of a heterogeneous complexant (equation 9.2), $\Gamma = 0.3$. [239].

of the system and is independent of experimental conditions; all other terms have been defined previously. For $[M]_b \gg [M]$, Γ may be used as another means of expressing the complexation buffer intensity of the system, β [10]:

$$\Gamma = \frac{1}{[M]_b} \cdot \frac{d[M]_b}{d \log[M]} = \frac{\beta}{[M]_b} \quad (9.3)$$

where $[M]_b$ and $[M]$ stand for the concentrations of the bound and the free metal ion, respectively, and β is the complexation buffer intensity of the system (which is indicative of the natural-water's capacity to buffer the effect of sudden addition of metals [164]). The meaning of Γ (equation 9.3) and its constancy make it a very important parameter for describing the properties of heterogeneous complexant, especially as regards to interpretation of the voltammetric signals.

The advantage of equation (9.2) is that the heterogeneous properties of the complexant (i.e., Γ) is explicitly considered. Comparison of equations (9.1) and (9.2.) reveals that the Deford and Hume equation is simply a special case of equation (9.2) for the condition of a homogeneous, simple complexant (i.e. $\Gamma = 1$).

9.2.2 Differential Equilibrium Function

Using equation (2.8), the polarographic wave can be used to define the Differential Equilibrium Function (DEF) [85-86,240], and hence, the thermodynamic binding properties of naturally-occurring, heterogeneous complexants, such as humic and fulvic acids.

$$\log \theta = \Gamma \log K_0^* - \Gamma \log K^* \quad (2.24)$$

where θ is the degree of site occupation, i.e. the fraction of all sites occupied. Γ is the slope of a linear DEF curve, and gives a measure of the heterogeneity of the system ($\Gamma = 1$ correspond to a homogenous system; Γ values range form 0.2 to 0.8). K^* is the Differential Function Parameter. K_0^* is the value of K^* for $\theta = 1$ and is a constant, with arbitrary physical meaning.

9.2.3 Diffusion coefficients

The weighted average diffusion coefficient (\bar{D}) of the metal complexes in the water samples can be estimated using the following equation:

$$i_L = \frac{n F A \bar{D}^{-1/2} c_{M,T} \omega^{1/2}}{g} \quad (9.4)$$

where i_L is the diffusion-limited limiting current, n is the number of electrons involved in the electrode reaction, A is the electrode surface area exposed to the analyte, \bar{D} is the weighted average diffusion coefficient, ω is the angular velocity (rad s^{-1}) of the rotating electrode, $c_{M,T}$ is the total metal concentration in the bulk solution, and g is a constant that depends on the cell geometry [240].

9.3 Experimental

9.3.1 Materials and reagents

Standard solutions (1000 $\mu\text{g/mL}$) of Cu(II), Ni(II), Zn(II) and Pb(II) were purchased from SCP Science, Montreal, Canada. Ultrapure water of resistivity 18.2 $\text{M}\Omega\cdot\text{cm}$ was obtained direct from a Milli-Q-Plus water purification system (Millipore Corporation). A 2 M stock solution of sodium acetate was prepared by dissolving an appropriate quantity of

sodium acetate trihydrate (ACS grade/BDH) in ultrapure water. The sodium acetate solution was then purified of metals by electrolysis at -1.5 V vs. E_{SCE} for at least 48 h. immediately prior to its use. The electrolysis was continued while the sodium acetate aqueous solution was drained from the electrolysis cell in order to make sure that the impurity metals removed by electrolysis did not go back into the sodium acetate aqueous solution on the termination of electrolysis. A 2 M stock solution of acetic acid was prepared by diluting glacial acetic acid (ACS grade/Anachemia) with ultrapure water. The humic acid was supplied by Dr. Les Evans (University of Guelph, Guelph, Ontario), who purified the HA and characterized it according to the procedure recommended by the International Humic Substances Society [124]. Since the actual molar mass was not directly ascertainable for naturally-occurring, heterogeneous complexants such as HA, the molar mass of the HA was estimated by using its bidentate complexing capacity of 4.88 mmol/g [124]. A stock solution of approximately 1.00 g L⁻¹ HA was prepared by dissolving a suspension of approximately 0.100 g of the HA in 100 mL of ultrapure water by adding to it (electrolytically-purified) NaOH aqueous solution – the pH of HA solution was found to be 10 [189]. The pH of the HA solution was adjusted to 8.0 with ultrapure HNO₃ using an Accumet 20 pH/conductivity meter (Fisher Scientific), fitted with an Accuplast combination glass electrode. The HA solution was stored in the dark at 4 °C until used.

9.3.2 Containers and their cleaning procedure

All containers used were made of Teflon. After cleaning with ultrapure water, the containers were completely filled with pure water containing 10% (v/v) nitric acid (AR

grade) and allowed to stand at the room temperature for one week. They were then rinsed five times with ultrapure water. Finally, they were filled with ultrapure water, and allowed to stand until they were used. The filling water was renewed periodically to ensure continued contact with clean water.

9.3.3 *Model solutions and pseudopolarography*

A series of model solutions (100 mL volume) of lead in HA were prepared by adding known amounts of the HA stock solution to a 1.0×10^{-7} M lead solution to make [Pb(II)]/[HA] mole ratios 0.1, 0.01, and 0.001. The [HA] in each model solution was 0.2, 2.0, 20 mg/L, respectively, which was chosen to model a wide range of freshwater samples. The model solutions were buffered to pH 4.8 (using AcOH/NaOAc), and were allowed to equilibrate overnight. KNO_3 was used to fix the ionic strength of all the model solutions at 0.05 M. The effect of metal competition on the Differential Equilibrium Functions of the Pb(II)-HA complexes in model systems was investigated using pseudopolarography/Differential Pulse Anodic Stripping Voltammetric (DPASV) at pH 4.8, ionic strength 0.05 and fixed [Pb(II)]/[HA] mole ratio 0.01. Metal competition in model solutions was investigated by adding the HA to an aqueous solution containing a fixed concentration of the Pb(II) (10^{-7} M) and varying concentrations of one of the competing trace metals, Cu(II), Ni(II), and Zn(II). A 30.00 g aliquot of the model solution was weighed and used as the model solution. The pH of the model solution was again checked immediately prior to analysis.

9.3.4 Apparatus

Voltammetric measurements were made with a computer-controlled Autolab PGSTAT30 potentiostat/galvanostat (Eco Chemie BV, The Netherlands), equipped with a Metrohm 663 VA stand (Metrohm, Switzerland). The working electrode was a static mercury drop electrode (Metrohm, Switzerland). The reference electrode was a Ag/AgCl electrode in a glass tube filled with 4 M KCl and fitted with a porous Vycor tip (Bioanalytical Systems, Inc., USA). The counter electrode was made of a platinum rod (Metrohm, Switzerland). Analysis of voltammetric peaks was done using the General Purpose Electrochemical Software v4.8 (Eco Chemie BV, The Netherlands). The data were transferred to a Pentium computer and saved for processing.

9.3.5 Electrochemical parameters

Each sample was purged with nitrogen gas for 10 min. prior to use. Differential pulse anodic stripping voltammetry (DPASV) was applied. The electrode-stirring rate was set at 2000 rpm. For DPASV, the following operating conditions were used: deposition time 120 s, equilibration time 15 s, initial potential -0.6 V, end potential -0.1 V, step potential 2.5 mV, modulation amplitude 25 mV, modulation time 50 ms, interval time 50 ms. The deposition time was chosen to avoid surface saturation effects during the stripping step.

9.3.6 Data analysis

The experimental data were fitted to equation (9.2) using a commercial software program, NLREG v5.2 (Phillip H. Sherrod, Brentwood, TN, USA).

9.4 Results and Discussion

Typical pseudopolarograms for three solutions of Pb(II) are presented in Figure 75. The top curve is that for a solution of Pb^{2+} buffered with HOAc/NaOAc, and is the pseudopolarogram for the Pb^{2+} aqua complex: a sharp, well-defined wave with a flat plateau, indicating a fully reversible electrode process. The lower curve was for the same concentration of Pb(II), which had been equilibrated for 12 hours in a model solution of humic acid. From equation 9.4, it was expected that there would be a reduction in the limiting current of the Pb(II)-HA complexes relative to that for the Pb^{2+} aqua complex corresponding to a decrease in \bar{D} of the Pb(II)-HA complexes relative to that of Pb^{2+} aqua complex. Additionally, the wave was elongated (broadened and flattened), reflecting a decrease in Γ (i.e., greater heterogeneity). The spreading and flattening of the polarographic wave in the presence of heterogeneous complexants results from the fact that stronger sites became free and therefore active in controlling the free metal ion concentration as the total metal concentration was depleted at the electrode surface. The overall result was that the metal complexes that were available at the electrode surface were more stable than those in the bulk solution. With increasingly greater depletion of the metal at the electrode surface, this effect became progressively pronounced, resulting in greater flattening and elongation of the polarographic wave along the ordinate axis.

The parameters Γ , K^* and i_{lim} (and hence \bar{D}_{ML}) can be determined by fitting the experimental data to equation (9.2) [17]. The difficulty in applying equation (9.2) is that there is no closed-form solution for the measured current, i (the independent variable). Equation (9.5) has been proposed for the determination of Γ and i_{lim} [84]:

$$\frac{1}{(d\chi_E/d\ln i)+1} = \Gamma - \Gamma \frac{i_{\text{lim}}}{i} \quad (9.5)$$

where $\chi_E = nF(E - E^0)/RT$. However, numerous attempts to apply equation (9.5) using both real and simulated data were unsuccessful. The experimental data were fitted to equation (9.2) using a commercial software program, NLREG v5.2 (Phillip H. Sherrod, Brentwood, TN, USA).

The solid lines in Figure 75 represent the experimental data that were fitted to equation (9.2). The open circles, squares, triangles and diamonds were the experimental points that were not included in the regression analysis. Experimental data points at the baseline and at the plateau of the polarographic wave of Figure 75 caused the non-linear regression curve to “blow up”. The regression analyses typically rely on data points only from the rising portion of the polarographic wave. Since only a small section (the rising portion) of the polarographic wave was utilized in the regression analysis, it was important to ensure that a sufficient number of measurements (e.g. 10 – 15) were made on the rising section of the polarographic wave.

The results obtained by applying equation (9.2) to analyze polarographic data of Pb^{2+} aqua complex were in good agreement with those obtained from the Deford and Hume equation, which had been rearranged as shown in equation (9.6). In addition, values of Γ obtained by applying equation (9.2) were close to the theoretical value of $\Gamma = 1$ expected for homogeneous systems such as metal aqua complexes.

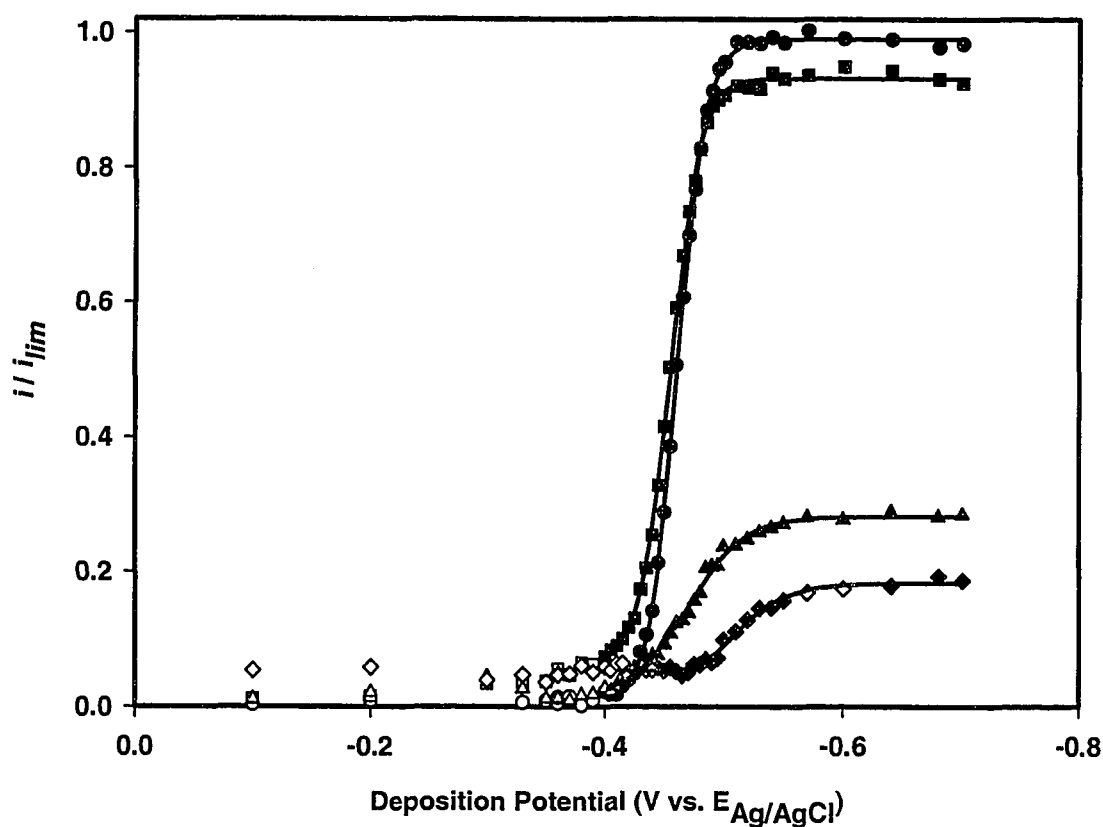


Figure 75 Typical pseudopolarogram for Pb(II)-HA in model solutions of humic acid. $c_{\text{Pb}} = 1.0 \times 10^{-7}$ mol/L; (●), Pb(II) + nil HA; (■), Pb(II) + $c_{\text{HA}} (1 \times 10^{-6}$ mol/L); (▲), Pb(II) + $c_{\text{HA}} (1 \times 10^{-5}$ mol/L); (◆), Pb(II) + ($c_{\text{HA}} 1 \times 10^{-4}$ mol/L); (○), no humic acid (data omitted from the non-linear regression analysis); (□), $c_{\text{HA}} 1 \times 10^{-6}$ mol/L (data omitted from the non-linear regression analysis); (△), $c_{\text{HA}} = 1 \times 10^{-5}$ mol/L (data omitted from the non-linear regression analysis); (◇), $c_{\text{HA}} 1 \times 10^{-4}$ mol/L (data omitted from the non-linear regression analysis). HOAc/NaOAc buffer, pH 4.8 ± 1.0 , ionic strength = 0.05 M, temperature = 23 ± 2 °C.

$$i = \frac{i_{lim}}{1 + \frac{nF}{RT} \exp(E - E_{1/2})} \quad (9.6)$$

The constant, K_o^* , was determined from the shift of the polarographic wave relative to the pseudopolarogram of the metal aqua complex using equations (9.7) [237] and (9.8) [84].

$$\ln \alpha = \frac{nF}{RT} (E_{1/2} - E_{1/2}^L) + \ln \left(\frac{i_{lim}}{i_{lim}^L} \right) \quad (9.7)$$

where $E_{1/2}$ is the half-wave potential in the absence of ligand, $E_{1/2}^L$ is the half-wave potential in the presence of ligand, i_{lim} is the limiting current in the absence of ligand, i_{lim}^L is the limiting current in the presence of ligand, and α (degree of complexation) is related to K_o^* by equation (9.8) [84].

$$\alpha = c_L \frac{K_o^* \Gamma}{1 - \Gamma} \left(\frac{c_L}{c_M} \right)^{(1-\Gamma)/\Gamma} \quad (9.8)$$

Influence of metal-to-ligand mole ratio on Differential Equilibrium Function

Since Differential Equilibrium Function (K_o^*) explicitly accounts for θ , the degree of occupation of all sites by the metals, K_o^* is relatively independent of the experimental conditions. However, the determination of Γ and K_o^* still may be influenced by the limitations of anodic stripping voltammetry used.

9.4.1 *The effect of [Pb(II)]/[HA] mole ratio on the Differential Equilibrium Function of Pb(II)-HA complexes.*

Table 34 shows that decreasing mole ratio of [Pb(II)]/[HA] increases the heterogeneity of the system— Γ value decreases from the homogenous case of 0.91 at the mole ratio of 1.0×10^{-1} to the heterogeneous case of $\Gamma = 0.35$ at the mole ratio of 1.0×10^{-3} . Not shown is that θ , the degree of site occupation, also decreases down the Table. K^* increases because stronger sites are free at the electrode surface compared with the bulk solution; i_{lim} decreases greatly because stronger sites form stronger Pb(II)-HA complexes, which are less labile, and hence, form much less free Pb^{2+} ion, resulting in a greatly decreased concentration of free Pb^{2+} ion at the electrode surface. Since \bar{D} is the weighted average diffusion coefficient, a decrease in its value (down the last column of Table 34) reflects the same trend as seen in the column of i/i_{lim} —the smaller concentrations of free Pb^{2+} ion down the column results in a smaller value in the i_{lim} and in the weighted average diffusion coefficient—free Pb^{2+} ion is smaller in size than the Pb(II)-HA complexes, and hence has a larger $D_{M^{n+}}$ value; Pb(II)-HA complexes are larger in size, and hence, have smaller D_{Pb-HA} values. The weighted arithmetic mean of all the individual diffusion coefficients (D values) is the \bar{D} value. The heterogeneity results agree with that of Pinherio et al. [241], who have reported that Pb(II) complexation by Irish moss-peat-derived humic acid is heterogeneous ($\Gamma = 0.43$).

An important requirement for applying equations (9.2) and (9.8) to ASV is that the ligand, L, must be present at the electrode surface in large excess relative to the total

Table 34 Effect of decreasing the mole ratio of [Pb(II)]/[HA] on the Differential Equilibrium Functions of Pb(II)-HA system in model solutions of humic acid (HA). $c_{Pb} = 1.0 \times 10^{-7}$ mol/L. HOAc/NaOAc buffer, pH 4.8 ± 1.0 , ionic strength 0.05 M, temperature = 23 ± 2 °C.

$c_{Pb,T}/c_{HA}$	Γ	$\log K_0^*$	i/i_{lim}	\bar{D} ($m^2 s^{-1}$)
1.0×10^{-1}	0.91	5.6	0.95	7.4×10^{-10}
1.0×10^{-2}	0.48	7.4	0.28	2.4×10^{-11}
1.0×10^{-3}	0.35	8.7	0.19	8.7×10^{-12}

metal concentration during the reduction step [240] to ensure that L is present in large excess at the electrode surface during the oxidation (stripping) step too. Town et al. [87] reported using in their ASV work a 400- to 2800-fold excess of FA ligand.

Plot of the $\log \theta$ versus $\log K^*$ (Differential Equilibrium Parameter) is a straight-line, as shown in Figure 76. Since the stronger sites of the heterogeneous ligands are occupied first when they bind the metal, as the degree of occupation of all site types, θ , increases, the averaging of the apparent equilibrium between M and the site L_i is carried out with an increasing number of weaker sites; hence, K^* (Differential Equilibrium Parameter), decreases.

In the presence of a sufficient excess of complexing ligand, L, the Γ values are independent of the metal-to-ligand mole ratio. The polarographic waves are asymmetrical and consequently shifts in the half-wave potential cannot be directly related to differences in stability constants as in the case of simple (homogenous) labile complexes. The site occupation by the metals at the electrode surface depends on the applied potential. Hence, the spreading of the polarographic wave is due to a change in the metal-to-ligand mole ratio in the diffusion layer and is specific for heterogeneous complexants. As a consequence, the lability of metal complexes may also vary along the polarographic wave.

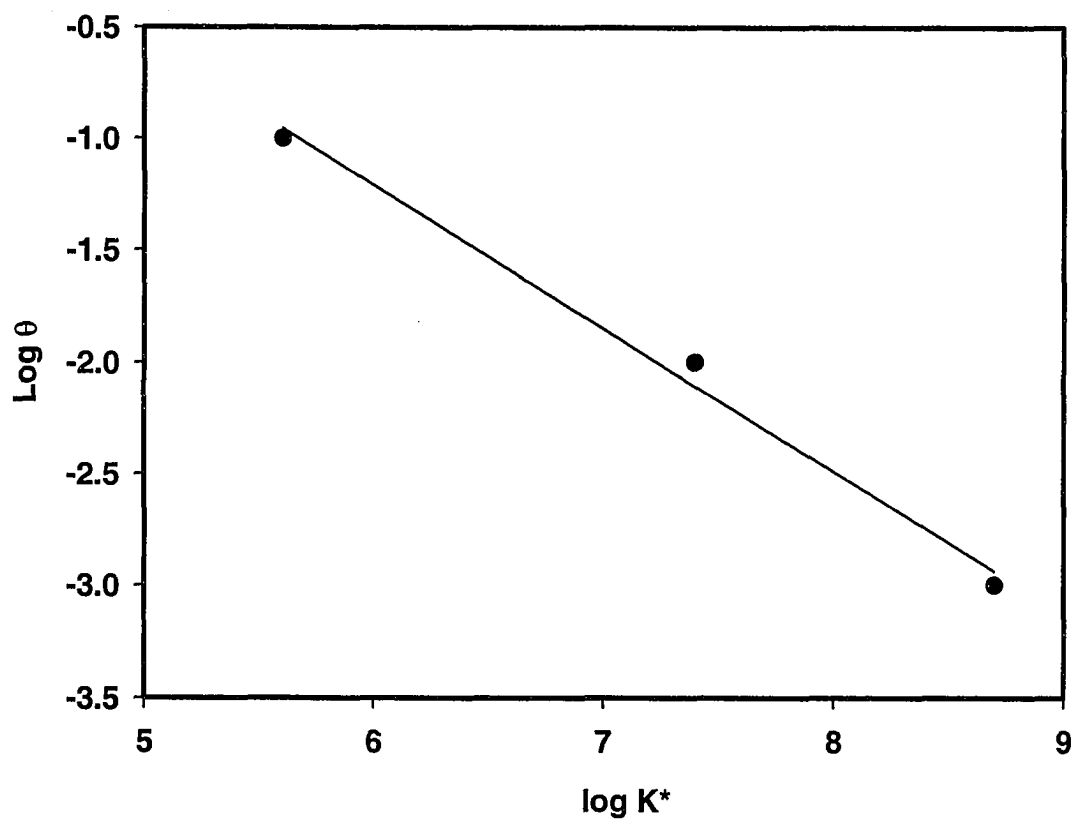


Figure 76 Differential Equilibrium Function of Pb(II)-HA complex. $c_{Pb} = 1.0 \times 10^{-7}$ mol/L. HOAc/NaOAc buffer, pH $4.8.0 \pm 0.1$, ionic strength 5.0×10^{-2} mol/L, temperature 23 ± 2 °C.

9.4.2 *Kinetic lability of Pb(II)-HA complexes*

In natural systems, interpretation of the voltammetric signal is often further complicated by the loss of lability at some stage of the polarographic wave. At increasingly negative potentials more stable (less labile) complexes are encountered until the polarographic wave is characterized by a partially kinetic limiting current—the surface concentration of ML is still finite, but it does not decrease as increasingly negative potentials are applied because of the limitations imposed by the very low dissociation rate coefficients.

Numerical simulations have been developed by Filella et al. [242] to investigate the influence of non-labile complexes on the shape of the polarographic wave (Figure 77). Although a detailed investigation of lability using the numerical methods of Filella et al. is beyond the scope of this work, the lability of metal complexes can be studied by varying the analytical timescale of measurement. In anodic stripping voltammetry with a Static Mercury Drop Electrode that uses an electro-mechanical stirrer, a convective-diffusive mass transport regime is established using forced convection, and analytical timescale can be controlled by varying the thickness of the diffusion layer.

In pseudopolarography using a Static Mercury Drop Electrode (SMDE), the important variable to define the kinetic properties of the metal complexes is the timescale of measurement, which is related to the stirring rate used in this technique. Figure 78 shows the effect of the stirring rate on the shape of pseudopolarograms. The stirring rate directly affects the analytical timescale of measurement by controlling the thickness of the diffusion layer. The top curve in Figure 78 is that for a solution of Pb(II) buffered with

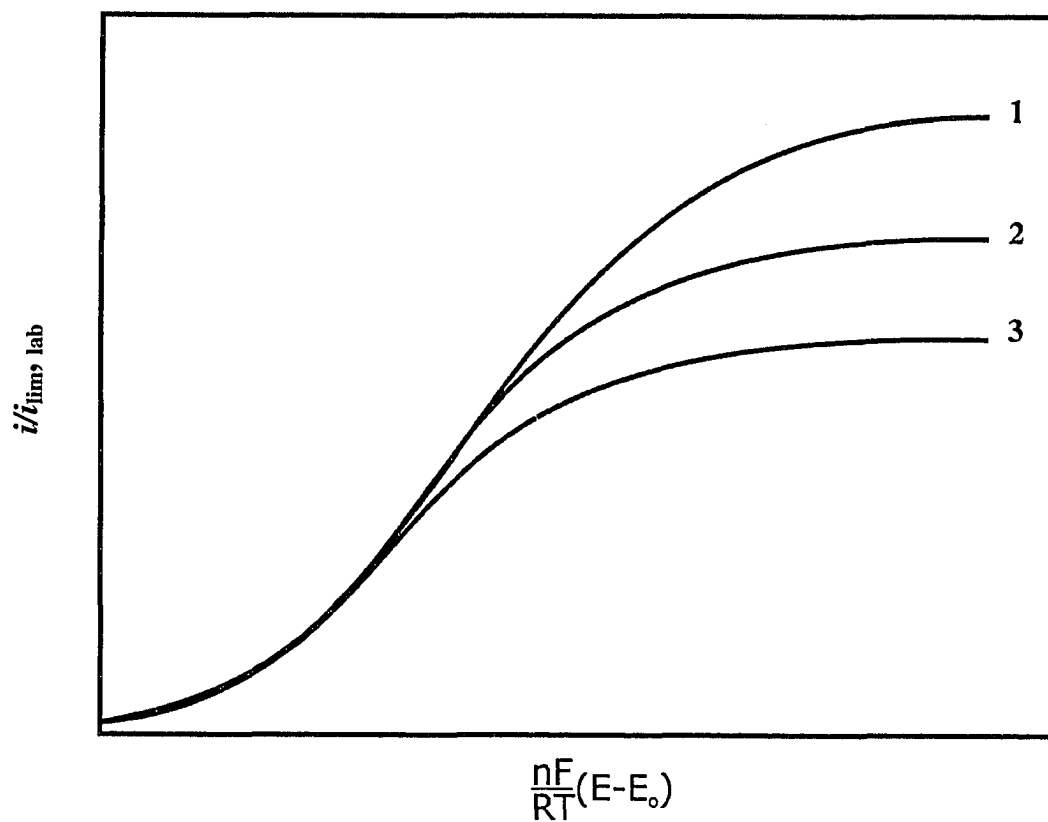


Figure 77 Numerical simulations of the influence of lability (i/i_{lim}) on the shape of the polarographic wave [84]. Changes in the shape of the d.c. polarographic waves when passing from a fully labile system (curve 1) to a partly labile system (curves 2 and 3). $i_{lim,lab}$ = limiting current obtained for the fully labile system.

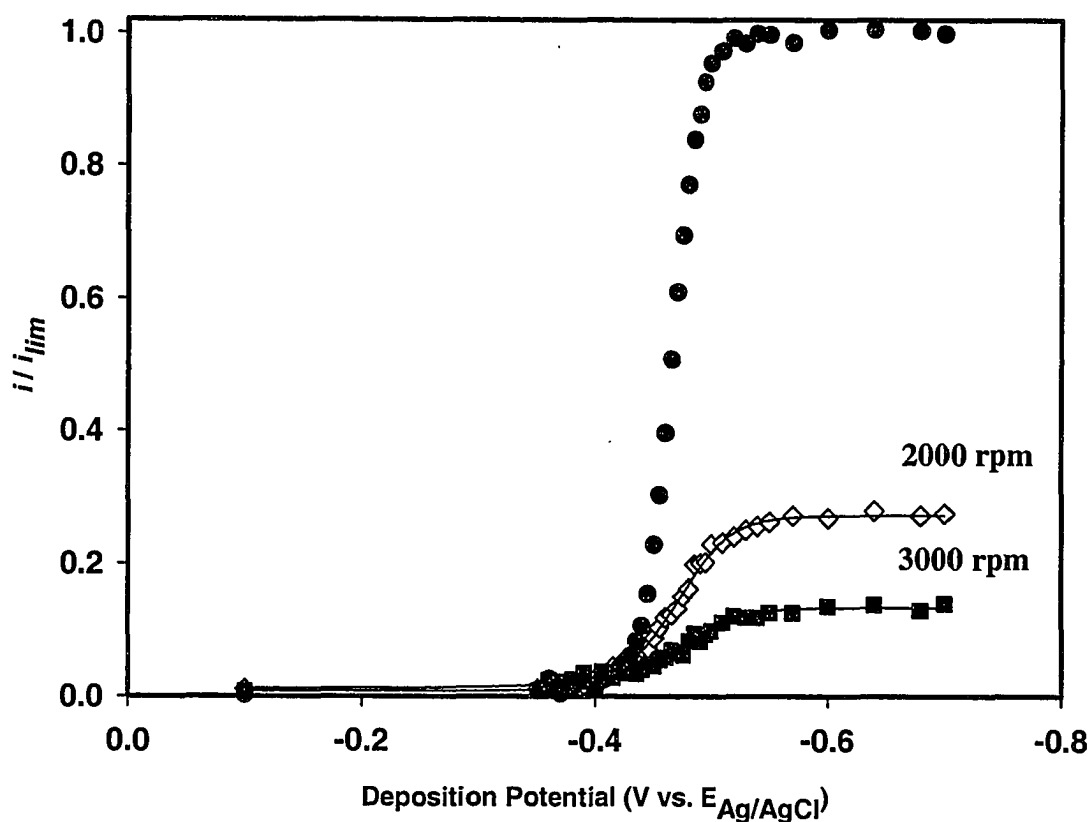


Figure 78 Influence of the stirring rate (timescale of measurement) on the lability (i/i_{lim}) of the Pb(II)-HA complexes. $c_{Pb} = 1.0 \times 10^{-7}$ mol/L. $c_{HA} = 1.0 \times 10^{-5}$ mol/L. HOAc/NaOAc buffer, pH 4.8 ± 1.0 , ionic strength 0.05 M, temperature 23 ± 2 °C. (●), Pb(II) + HA; (◇), 2000 rpm; (■), 3000 rpm.

HOAc/NaOAc and can be attributed to the Pb^{2+} aqua complex. Figure 78 shows that the limiting current decreases as the stirring rate is increased probably because with increasing rates of stirring, fewer time is allowed for the metal complex to dissociate and be reduced at the SMDE; hence, less free-metal-ions are available for reduction at the electrode surface. Table 35 shows the influence of the stirring rate on Differential Equilibrium Functions of Pb(II)-HA complexes in model solutions of humic acid (HA). With increased the stirring rates, K_0^* increases, i_{lim} decreases, \bar{D} (weighted average diffusion coefficient) decreases, and Γ decreases slightly from 0.48 to 0.43, which is probably not significant. The above observation can be explained as follows [84]. Because free metal ion is consumed at the electrode surface, $[\text{M}]_b$ and therefore θ , decreases through the diffusion layer from $x = \infty$ to $x = 0$; consequently, K^* increases, stronger sites being free at the electrode surface compared with the bulk solution. \bar{D} decreases because the concentration of free Pb^{2+} (which has a larger diffusion coefficient than Pb(II)-HA complexes) decreases. However, the stirring rate mechanism used for the Stationary Mercury Drop Electrode (SMDE) voltammetry gives a rather ill-defined convective-diffusive mass transfer regime at the SMDE surface, with a more diffuse and wider diffusion layer than that given by Rotating Disk Electrode Voltammetry. This lack of a well-defined, thinner diffusion layer at the SDME surface precludes more a rigorous generalization of the effects of measurement timescale on the SDME voltammetric signal.

Table 35 Influence of the stirring rate on Differential Equilibrium Functions of Pb(II)-HA complexes in model solutions of humic acid (HA). $c_{\text{Pb}} = 1.0 \times 10^{-7}$ mol/L. $c_{\text{HA}} = 1.0 \times 10^{-5}$ mol/L. HOAc/NaOAc buffer, pH 4.8 ± 1.0 , ionic strength 0.05 M, temperature = 23 ± 2 °C.

Stirring Rate (rpm)	Γ	$\log K_0^*$	i/i_{lim}	\bar{D}_{ML} ($\text{m}^2 \text{s}^{-1}$)
2000	0.48	7.4	0.28	2.4×10^{-11}
3000	0.43	8.0	0.14	1.6×10^{-12}

9.4.3 *Effect of various concentrations of other trace metals, Cu(II), Ni(II) and Zn(II), on the heterogeneity of Pb(II)-HA complexes*

The Differential Equilibrium Functions of the Pb(II)-HA complexes have been investigated at constant pH and fixed ionic strength, in the presence of various concentrations of the following trace metals: Cu(II), Ni(II), or Zn(II). Figure 79 shows the pseudopolarographic waves for the effect of various concentrations of Cu(II) on Pb(II)-HA complexes at pH 4.8 (fixed with HOAc/NaOAc buffer), and at ionic strength 0.05 M (fixed with KNO₃). Two concentrations of the competing trace metal, Cu(II), were used: one was the same concentration as that of Pb(II) (1.0×10^{-7} M), and the other concentration was one order of magnitude higher than that of Pb(II) (1.0×10^{-6} M). At the fixed mole ratio of $[Pb(II)]/[HA] = 0.01$, the increasing concentration of Cu(II) results in higher i_{lim} values and shifts the half-wave potential towards more a positive direction, indicating an increase in the mean diffusion coefficient of Pb-HA complexes, and decreasing stability of the Pb(II)-HA complexes (lower K_0^*), respectively. This suggests that trace metal, Cu(II), competes with Pb(II) for binding sites of the HA. The data of the pseudopolarographic curves in Figure 78 were analyzed according to eq. (9.2) and (9.8) and the resulting Differential Equilibrium Functions of the Pb(II)-HA complexes are presented in Table 36. In agreement with the qualitative information obtained from the shape of the pseudopolarographic curves, K_0^* of the Pb(II)-HA complexes decreases with the equal or greater concentration of Cu(II). The log K-values of the Pb(II)-HA complexes decreases slightly from 7.4 to 7.1 in the presence of increasing concentrations of Cu(II) from 0 to 1.0×10^{-6} M. The results can be rationalized by hypothesizing progressive displacement of Pb(II) by Cu(II) from the binding sites of HA, resulting in

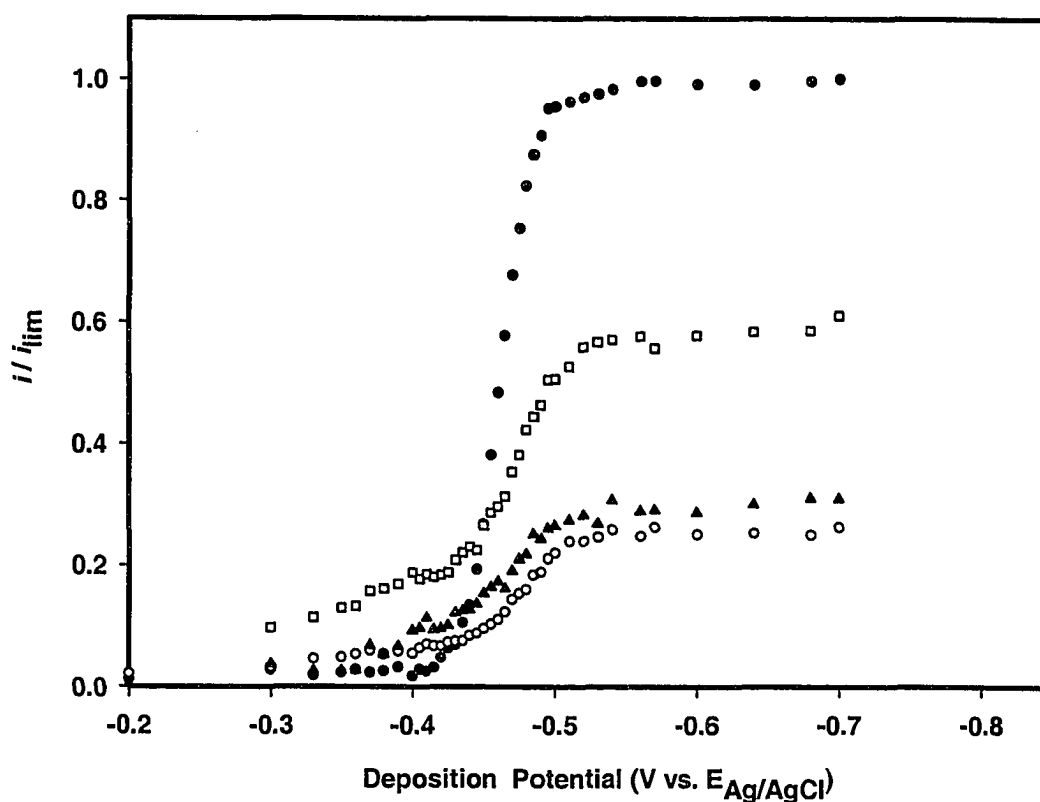


Figure 79 Effect of various concentrations of Cu(II) on the pseudopolarographic waves of Pb(II)-HA complexes in model solutions, using DPASV at a SMDE. $[\text{Pb(II)}] = 1.0 \times 10^{-7} \text{ M}$, $c_{\text{HA}} = 1.0 \times 10^{-5} \text{ M}$, $\text{pH } 4.8 \pm 0.1$ (AcOH / NaOAc), ionic strength 0.05 M (KNO_3), temperature $23 \pm 2 \text{ }^\circ\text{C}$. Concentration of Pb(II) is the same for all curves. (●), Pb(II) + nil HA; (O), Pb(II)-HA + nil Cu(II); (▲), Pb(II)-HA + Cu(II) $1.0 \times 10^{-7} \text{ M}$; (□), Pb(II)-HA + Cu(II) $1.0 \times 10^{-6} \text{ M}$.

the formation of more free Pb^{2+} ions, which enhances the limiting currents, i_{lim} . If this hypothesis is true, then Cu(II) and Pb(II) are competing for the same binding sites of the HA. This effect was also observed for similar concentrations of Ni(II) or Zn(II) added to a fixed concentration of Pb(II) (1.0×10^{-7} M) as shown in Table 36. Table 36 shows that at a fixed mole ratio of $[\text{Pb(II)}]/[\text{HA}] = 0.01$, similar to what has been observed for Cu(II), increasing concentration of Ni(II) or Zn(II) results in higher i_{lim} . The results are compatible with the hypothesis that trace metals, Ni(II) and Zn(II), also compete with Pb(II) for binding sites of HA.

As reported by Fillela et al. [243], the stability of Pb(II) complexation by humic substances depends on metal loading, with stronger sites being utilized at lower Pb(II) loadings. Thus, the DEF, or any data interpretation method that takes these characteristics into account provides a more appropriate description of Pb(II)-HA binding. In particular, the DEF enables the heterogeneity of the Pb(II)-HA complexes formed to be quantified by the variable Γ . Table 34 shows that at the highest Pb(II) loading (the $[\text{Pb(II)}]/[\text{HA}]$ mole ratio of 1.0×10^{-1}), the Pb(II)-HA complexation is homogeneous ($\Gamma = 0.91$), whereas with lower mole ratios of $[\text{Pb(II)}]/[\text{HA}]$ of 1.0×10^{-2} and 1.0×10^{-3} , the system becomes progressively more heterogeneous.

Table 36 presents the effects of various concentrations of Zn(II) on Differential Equilibrium Functions of Pb(II)-HA complexes at pH 4.8 and at ionic strength 0.05 M; Γ values are clustered around 0.5, which is typical of heterogeneous systems. As shown earlier in Table 34, at the [Pb] concentration of 1.0×10^{-7} M, with the mole ratio of

Table 36 Differential Equilibrium Functions of Pb(II) in model solutions of humic acid in the presence of various concentrations of Ni(II), Cu(II), or Zn(II). $c_{Pb} = 1.0 \times 10^{-7}$ mol/L. $c_{HA} = 1.0 \times 10^{-5}$ mol/L, and their lability (i/i_{lim}). HOAc/NaOAc buffer, pH 4.8 ± 1.0 , I = 0.05 M, temperature = 23 ± 2 °C.

Competing Metal, M(II)	[M(II)]	Γ	$\log K_0^*$	i/i_{lim}	\bar{D}_{ML} (m ² s ⁻¹)
Ni	1.0×10^{-7}	0.45	7.4	0.27	5.9×10^{-11}
Ni	1.0×10^{-6}	0.55	7.2	0.45	1.0×10^{-10}
Cu	1.0×10^{-7}	0.47	7.2	0.31	7.9×10^{-11}
Cu	1.0×10^{-6}	0.58	7.1	0.58	1.6×10^{-10}
Zn	1.0×10^{-7}	0.50	7.4	0.29	7.1×10^{-11}
Zn	1.0×10^{-6}	0.57	7.3	0.51	1.3×10^{-10}

$[\text{Pb(II)}]/[\text{HA}] = 0.01$, the i/i_{lim} is 0.28; in this case, a ten-fold greater concentration of Zn(II) than that of the Pb(II) results in higher i_{lim} , indicating decreasing stability of the Pb(II)-HA complexes. The results may be rationalized by hypothesizing that at the mole ratio of $[\text{Pb(II)}]/[\text{HA}] = 0.01$, if the $[\text{Zn(II)}]$ is 1.0×10^{-6} M, and $[\text{Pb(II)}]$ is 1.0×10^{-7} M, then only Zn(II) competes with Pb(II) for the binding sites of HA. At a $[\text{Zn(II)}]$ concentration equal to that of $[\text{Pb(II)}]$, Zn(II) does not compete with Pb(II) for the binding sites of HA. The data for Cu(II), which is reported to have the strongest affinity for the binding sites of HA, however, parallel those of Zn(II), which is rather surprising in view of the reportedly much weaker binding affinity of Zn(II) for the binding sites of HA.

Table 36 shows that the increasing order of competing effects on the K_0^* values of the Pb(II)-HA complexes are: Cu(II) > Ni(II) > Zn(II). This can be rationalized as follows: for 3d transition metals in octahedral substitution reactions, Ligand Field Stabilization Energy (LFSE) is a contributory factor in the ability of the 3d transition metal complexes to undergo ligand substitution reactions. The kinetic inertness of some transition metals is related to unfavourable changes in LFSE during complex formation [158]. A large LFSE in the initial octahedral complex results in a large sacrifice on going to a transition state of lower symmetry. Thus, the ease of ligand substitution in octahedral complexes may be expected to parallel the magnitude of the LFSE. Those metals that have high LFSE form strong complexes. The stability of Cu(II) complexes is enhanced by the Jahn Teller effect, which is responsible for the stability in the stability order: Cu(II) > Ni(II) > Zn(II). Because of the Jahn Teller effect, in the tetragonally distorted Cu(II)L₆ complex, the four

equatorial bonds are shortened (and strengthened), and two axial bonds are lengthened (and weakened) compared with the undistorted octahedral Cu(II)L₆ complex.

9.4.4 Diffusion coefficients

There is a lack of data on diffusion coefficients for heterogeneous complexants in natural waters [244-245]. Diffusion coefficients reflect the mobility of the metal species, and hence, have important effects on the transport and bioavailability of the metals in the aquatic environment. As a rough approximation, the metal complexes of individual molecules of a given group of heterogeneous complexants (e.g. fulvic compounds) are often assumed to have similar sizes and a single diffusion coefficient [242]. Tables 34-35 present average diffusion coefficients of Pb-HA complexes. The experimentally determined diffusion coefficient was obtained by fitting the observed current to equation (9.4). D_{ML} has much lower values than the corresponding D_M , indicating that the lead complexes with the humic acid are significantly larger than the Pb²⁺ aqua complex ($D_{Pb} = 8.28 \times 10^{-10} \text{ m}^2 \text{ s}^{-1}$ [246]).

9.5 Conclusion

Pseudopolarography has two main advantages over normal extraction of metal-complexation parameters of heterogeneous freshwater systems: one is the avoidance of the problems associated with changes in the individual peak potential band widths caused by the metal-to-ligand mole ratio at the electrode surface; the other is that by doing a single experiment, the polarographic wave can be used to completely extract Differential Equilibrium Functions.

DEF- K_0^* and Γ are not affected by experimental conditions, and thus have predictive values, allowing K^* to be calculated for any metal-to-ligand mole ratio.

The Differential Equilibrium Function is a useful predictive tool to describe the metal-ligand binding properties that is independent of the experimental conditions. The main advantage of the Differential Equilibrium Functions is that it can be applied to predict the stability constants for a wide range of metal binding conditions. When the spreading of the polarographic wave is due only to the presence of labile, heterogeneous complexes, equation (9.2) can be used to describe the shape of the polarographic wave. Nevertheless, valid interpretation requires careful consideration of the lability effects.

-- Chapter 10 --

**Differential Equilibrium Functions and Differential Kinetic
Functions of Heterogeneous Systems. Pseudopolarography of
Cu(II), Zn(II), Cd(II) and Pb(II) complexes in Model Solutions
of a Well-Characterized Fulvic Acid using a Static Mercury
Drop Electrode: Kinetics versus Equilibrium**

10.1 Theory

Theory of pseudopolarography has been presented in chapter 9.

10.1.1 Differential Equilibrium Function

A plot of $\log \theta$ versus $\log K^*$ (equation 2.24 in chapter 2) is Differential Equilibrium Function (DEF).

$$\log \theta = \Gamma \log K_0^* - \Gamma \log K^* \quad (2.24)$$

10.1.2 Kinetic Differential Function

The influence of naturally-occurring heterogeneous complexants, such as fulvic acid, on the dissociation rate coefficients of the metal complexes will be studied by the Differential Kinetic Function (equation 2.27) (chapter 2).

$$\log \theta = \Gamma \log K_o^* - \Gamma \log k_a + \Gamma \log k_d^* \quad (2.27)$$

10.2 Experimental

10.2.1 Materials and reagents

Stock solutions (1000 mg/mL) of manganese, cobalt, nickel, copper, zinc, cadmium and lead were purchased from SCP Science (Montreal, Canada). Working standard solutions were prepared daily by dilution of the stock solutions with ultrapure water (of resistivity 18.2 M Ω -cm) and acidified to contain 1% (v/v) ultrapure nitric acid (Seastar, Canada). A 2 M sodium acetate stock solution was prepared by dissolving an appropriate quantity of sodium acetate trihydrate (ACS grade/BDH) in ultrapure water. The sodium acetate (NaOAc) solution was purified of metals by electrolysis at -1.5 V vs. E_{SCE} for at least 48 h. A 2 M stock solution of acetic acid was prepared by diluting glacial acetic acid

(HOAc) (Seastar Chemicals, Vancouver, BC) with ultrapure water. The Laurentian FA was obtained from Fredriks Research Products (Amsterdam, The Netherlands). The concentration of carboxylic and phenolic groups in the Laurentian fulvic acid is 11.6 mmol/g [162]. A stock solution of Laurentian FA was prepared by dissolving 1.0000 g of freeze-dried Laurentian FA in 1.00 L of ultrapure water. All test solutions were prepared daily by serial dilution of the above stock solutions with ultrapure water immediately prior to determination unless otherwise specified. Ultrapure water (18.2 M Ω ·cm) was obtained direct from a Milli-Q Academic water purification system (Millipore Corporation, USA), fitted with an organic purification column to remove organic matter.

10.2.2 Fulvic acid model solutions

Two model solutions were prepared in ultrapure water to contain varying concentrations of Laurentian fulvic acid (4.00×10^{-3} g/L to 4.00×10^{-2} g/L) and equimolar concentrations of Mn(II), Co(II), Ni(II), Cu(II), Zn(II), Cd(II) and Pb(II). The concentration of each metal was 7.0×10^{-7} mol/L. The pH of the fulvic acid model solutions was adjusted to 5.0 ± 0.1 with HOAc/NaOAc buffer, and the samples left to equilibrate overnight (12 h). The pH and conductivity of the samples were measured using an Accumet 20 pH/conductivity meter (Fisher). The changes in the pH between the beginning and the end of the experiment were found to be < 0.1 pH units.

10.2.3 Apparatus

The apparatus has been described in section 9.3.4 (chapter 9).

10.2.3 Electrochemical parameters

Each sample solution was purged with nitrogen gas for 10 min prior to use. Differential pulse anodic stripping voltammetry (DPASV) was applied. The electrode-stirring rate was set at 2000 rpm. For DPASV, the following operating conditions were applied: deposition time 120 s, equilibration time 15 s, initial potential -1.2 V, end potential 0 V, step potential 2.5 mV, modulation amplitude 25 mV, modulation time 50 ms, interval time 50 ms. The deposition time was chosen to avoid surface saturation effects during the stripping step.

10.2.4 Data analysis

The experimental data were fitted to equation (9.2) using a commercial software program, NLREG v5.2 (Phillip H. Sherrod, Brentwood, TN, USA).

10.3 Results and Discussion

Pseudopolarography was used to investigate the physiochemical properties of Cu(II), Zn(II), Cd(II) and Pb(II) in model solutions of fulvic acid. The model solutions were prepared to contain all the above metals in equimolar concentrations, and two fixed concentration of FA for the two sets of experiments (see Table 37). The pseudopolarograms of the above systems are presented in Figures 80-83. The data from these Figures have been subjected to non-linear regression analysis to extract the Differential Equilibrium Functions of the metal-FA systems, which are presented Table 37. Table 37 shows that Zn(II) and Pb(II) behave as a homogenous systems under the metal-binding conditions of the experiment. Cd(II) also behaves as homogenous system under the higher metal loading condition: [Cd(II)]/[FA] mole ratio of 5.6×10^{-2} , but as a

heterogeneous system at the lower metal loading condition: $[\text{Cd(II)}]/[\text{FA}]$ mole ratio of 5.6×10^{-3} . This can be rationalized as follows. At the lower loading condition of Cd(II), there is one order of magnitude fewer Cd(II) present, which are bound to the strong sites of the FA, forming stable Cd(II)-FA complexes, which are non-labile ($i/i_{\text{lim}} = 0.57$). Such non-labile metal-complexation makes the Cd(II)-FA system more heterogeneous. Values of $\Gamma < 1$ reflect heterogeneous system. Cu(II) is unique among metals for its strong affinity for binding with humic substances (in this case, with FA), and has been reported by other workers to form heterogeneous systems with fulvic acids.

It is interesting to note that the values of Γ for Pb(II) in model solutions of Laurentian fulvic acid are virtually indistinguishable from a homogeneous complexant ($\Gamma \approx 1$) for the two Pb(II) loading conditions used. However, it has been reported that at low lead loadings, Laurentian fulvic acid behaves as a heterogeneous ($\Gamma = 0.59$) complexant towards Pb(II) [87].

10.3.1 Influence of metal loading on the Differential Equilibrium Functions (DEF)

Figure 81 can be rationalized as follows. At the lower $[\text{Zn(II)}]/[\text{FA}]$ mole ratio (5.6×10^{-3}), most of the Zn(II) was bound by the small number (< 10%) of strong sites of FA, forming stable Zn(II)-FA complexes which were non-labile. At the higher $[\text{Zn(II)}]/[\text{FA}]$ mole ratio (5.6×10^{-2}), there were 10 times more Zn(II) for the same number of binding sites of HA as in the previous case—the result was that more Zn(II) ions were bound to weak sites of the FA, forming weak Zn(II)-FA complexes which were

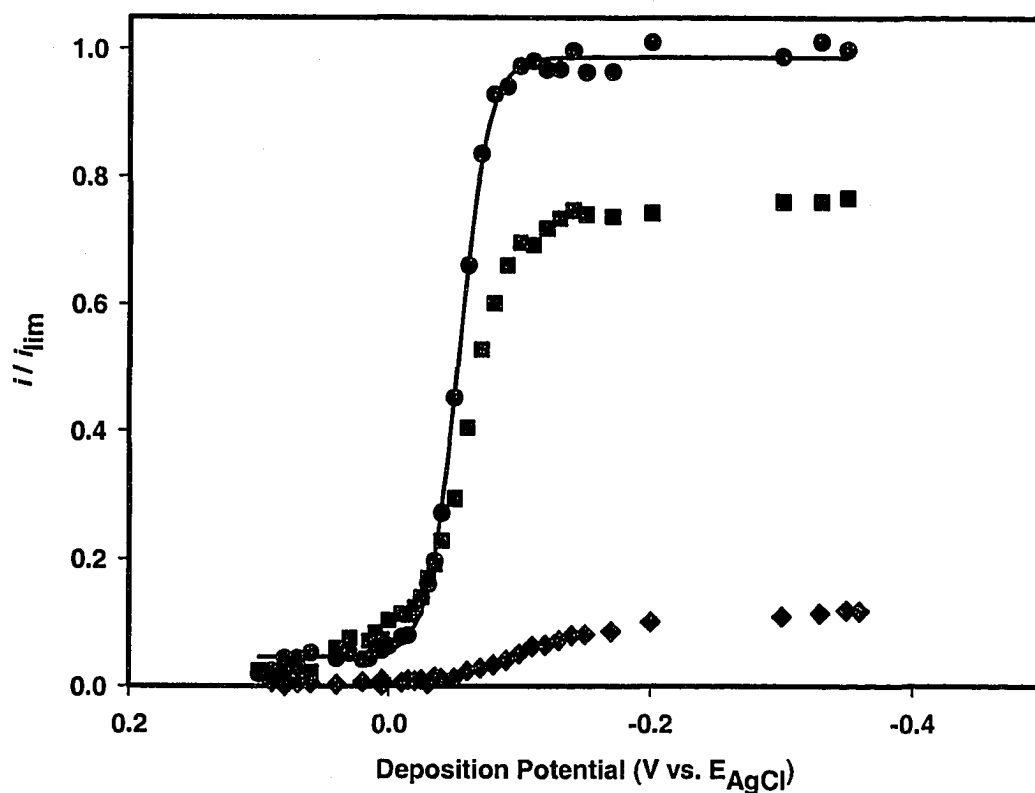


Figure 80 Pseudopolarogram for Cu(II)-FA in model solutions of Laurentian fulvic acid. $c_{Cu} = 7.0 \times 10^{-7}$ mol/L; (●), Cu(II) + nil FA; (■), $c_{Cu}/c_{FA} = 5.6 \times 10^{-2}$; (◆), $c_{Cu}/c_{FA} = 5.6 \times 10^{-3}$. HOAc/NaOAc buffer, pH 5.0 ± 1.0 , ionic strength = 0.05 M, temperature = 23 ± 2 °C.

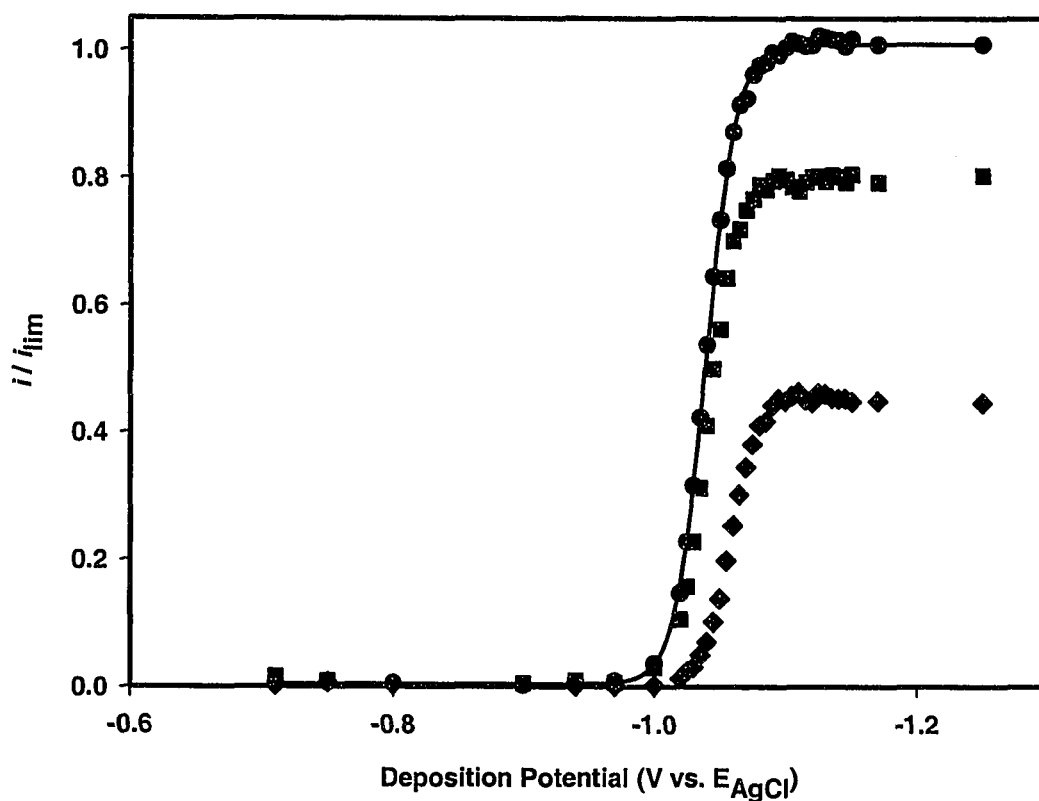


Figure 81 Pseudopolarogram for Zn(II)-FA in model solutions of Laurentian fulvic acid. $c_{Zn} = 7.0 \times 10^{-7}$ mol/L; (●), Zn(II) + nil FA; (■), $c_{Zn}/c_{FA} = 5.6 \times 10^{-2}$; (◆), $c_{Zn}/c_{FA} = 5.6 \times 10^{-3}$. HOAc/NaOAc buffer, pH 5.0 ± 1.0 , ionic strength = 0.05 M, temperature = 23 ± 2 °C.

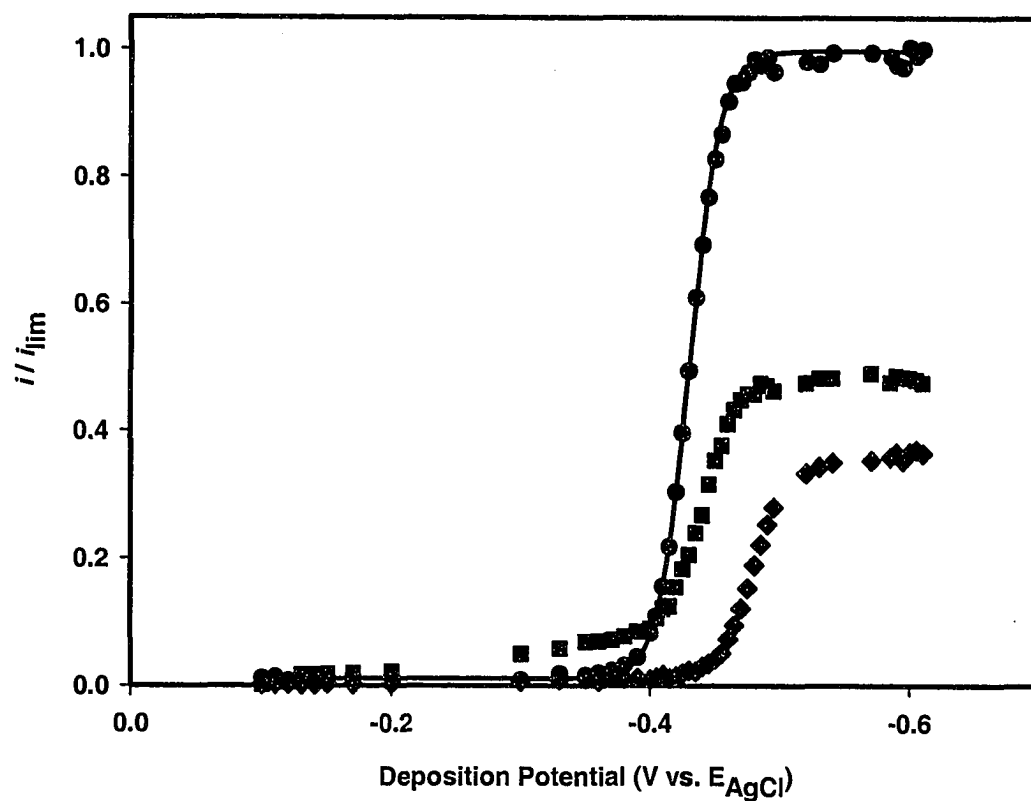


Figure 82 Pseudopolarogram for Pb(II)-FA in model solutions of Laurentian fulvic acid. $c_{\text{Pb}} = 7.0 \times 10^{-7}$ mol/L; (●), Pb(II) + nil FA; (■), $c_{\text{Pb}}/c_{\text{FA}} = 5.3 \times 10^{-2}$; (◆), $c_{\text{Pb}}/c_{\text{FA}} = 5.6 \times 10^{-3}$. HOAc/NaOAc buffer, pH 5.0 ± 1.0 , ionic strength = 0.05 M, temperature = 23 ± 2 °C.

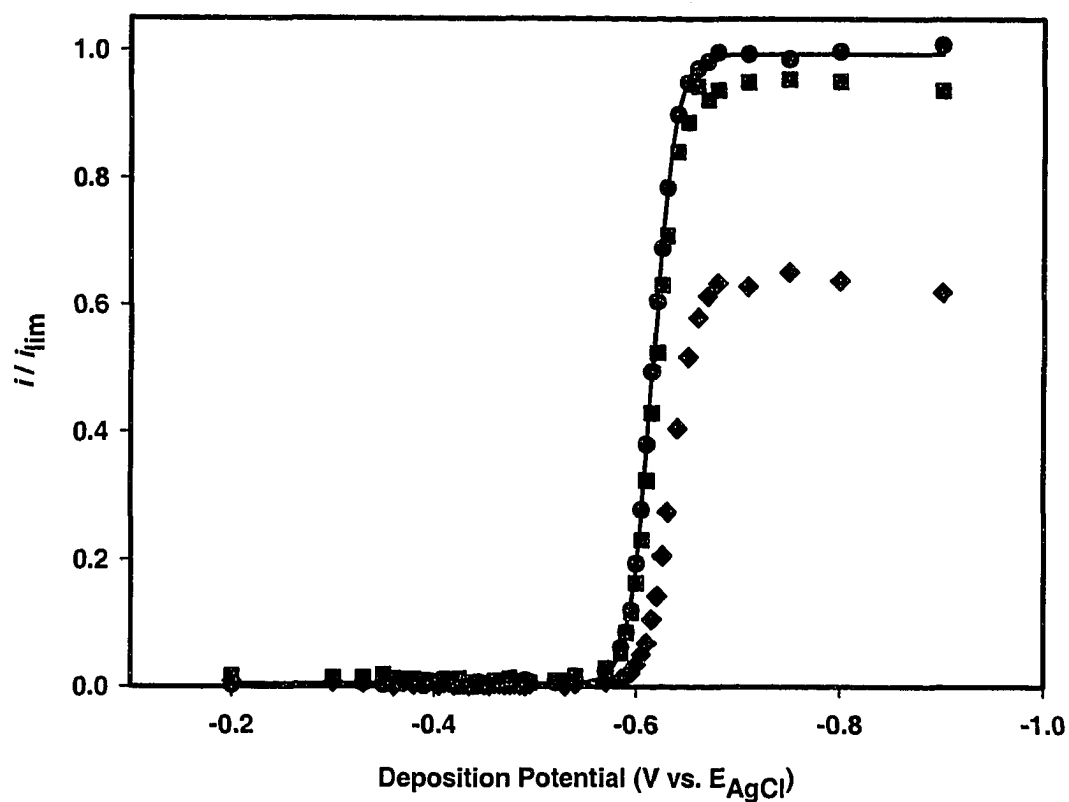


Figure 83 Pseudopolarogram for Cd(II)-FA in model solutions of Laurentian fulvic acid. $c_{\text{Cd}} = 7.0 \times 10^{-7}$ mol/L; (●), Cd(II) + nil FA; (■), $c_{\text{Cd}}/c_{\text{FA}} = 5.6 \times 10^{-2}$; (◆), $c_{\text{Cd}}/c_{\text{FA}} = 5.6 \times 10^{-3}$. HOAc/NaOAc buffer, pH 5.0 ± 1.0 , ionic strength = 0.05 M, temperature = 23 ± 2 °C.

more labile. The result was that more free Zn^{2+} were available for reduction at the electrode, giving a higher limiting currents, i_{lim} . Also, at the higher metal-to-fulvic acid mole ratio 5.6×10^{-2} , with the exception of Cu(II), the value of Γ was indistinguishable from that for a homogeneous system, whereas at lower metal loading conditions with the lower metal-to-fulvic acid mole ratio 5.6×10^{-3} , Γ was lower, indicating heterogeneity of the systems. The case of copper is different from the other metals, primarily because Cu(II) forms stronger and less labile metal complexes with FA than the other metals. At the lower [Cu(II)]/[FA] mole ratio of 5.6×10^{-3} , the fewer [Cu(II)] present was probably bound to the strong sites (< 10%) of the FA. These insights into the metal-ligand binding show the power of Differential Equilibrium Functions to provide hitherto-unavailable understanding of the metal complexes of heterogeneous humic substances.

10.3.2 Ionic Potential

The metals for which the binding energy is expected to depend on ionic potential (z^2/r) of metal ion [27] include Zn(II), Cd(II) and the post-transition metal, Pb(II). The ionic potentials are: Pb(II) ($z^2/r = 0.030 \text{ pm}^{-1}$), Cd(II) ($z^2/r = 0.037 \text{ pm}^{-1}$), Mn(II) ($z^2/r = 0.041 \text{ pm}^{-1}$) and Zn(II) ($z^2/r = 0.046 \text{ pm}^{-1}$). Figure 84 presents the relationship between Differential Equilibrium Parameter, K^* , and the ionic potential of the metals, at two metal-to-fulvic acid mole ratios: 0.056, 0.0056. The Figure shows an inverse correlation between K^* and the ionic potential. Since K^* represents a Differential Equilibrium Function, the above inverse correlation suggests that with the increasing ionic potential a metal's binding to fulvic acid has a lesser electrostatic component, i.e., the metal-FA

Table 37 Differential Equilibrium Functions of Zn(II), Cd(II), Pb(II) and Cu(II) in model solutions of Laurentian fulvic acid. $c_M = 7.0 \times 10^{-7}$ mol/L, and the lability (i/i_{lim}) of these systems. HOAc/NaOAc buffer, pH 5.0 ± 0.1 , ionic strength = 0.05 M, temperature = 23 ± 2 °C.

Analyte	[M(II)]/[FA]	Γ	$\log K_0^*$	i/i_{lim}	\bar{D}_{ML} ($m^2 s^{-1}$)
Cu	5.6×10^{-2}	0.64	6.5	0.76	4.2×10^{-10}
Cu	5.6×10^{-3}	0.20	8.5	0.12	1.0×10^{-11}
Zn	5.6×10^{-2}	0.98	4.7	0.79	4.0×10^{-10}
Zn	5.6×10^{-3}	0.90	5.7	0.45	1.3×10^{-10}
Cd	5.6×10^{-2}	0.97	5.2	0.95	6.3×10^{-10}
Cd	5.6×10^{-3}	0.79	6.3	0.57	2.3×10^{-10}
Pb	5.6×10^{-2}	0.94	5.7	0.49	2.0×10^{-10}
Pb	5.6×10^{-3}	0.95	7.1	0.36	1.1×10^{-10}

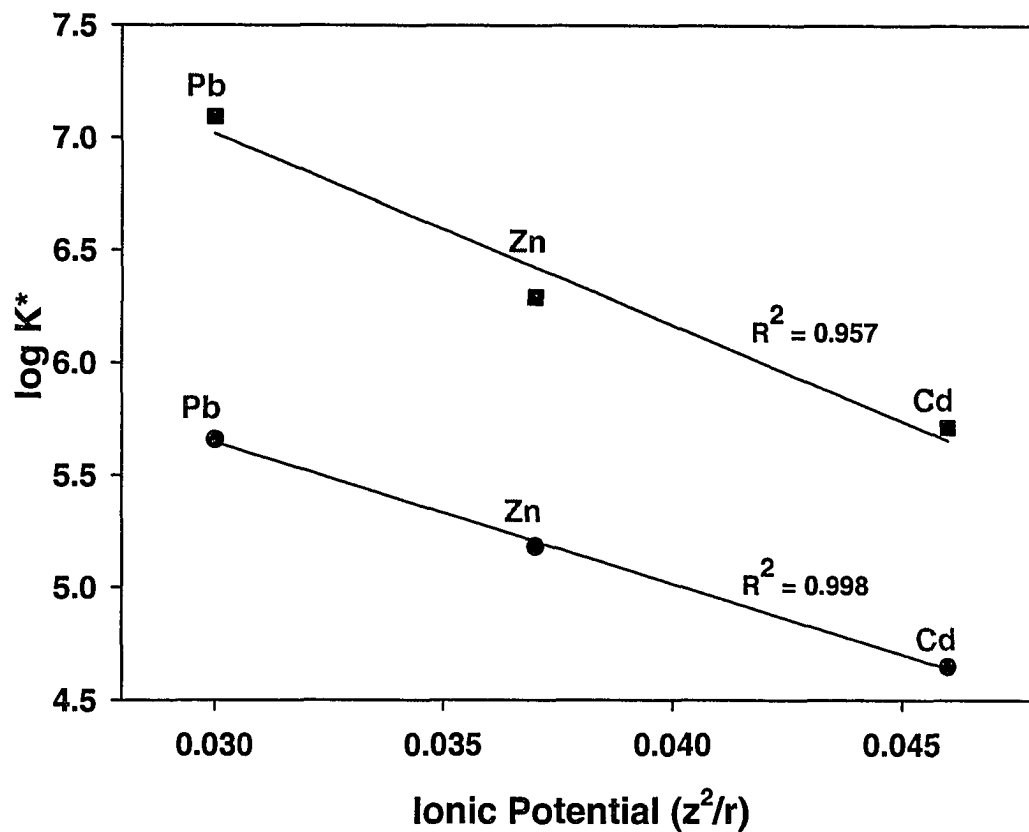


Figure 84 Influence of the ionic potential (z^2/r) on the Differential Equilibrium Parameter, K^* , of metal (Pb(II), Zn(II), Cd(II)) complexes in model solutions of Laurentian fulvic acid, measured by pseudopolarography. pH 5.0 ± 0.1 , ionic strength 0.05 mol/L, temperature 23 ± 2 °C. (●), $c_M / c_{FA} = 5.6 \times 10^{-2}$; (■), $c_M / c_{FA} = 5.6 \times 10^{-3}$.

bond becomes more covalent. Mattock [167] attributed the reversal in the trend expected from electrostatic effects to greater metal-ligand bond stabilization in systems with partial covalent character. This effect probably results from mutual cation and anion polarization, which favours combination of large, polarizable metal ions, such as Pb^{2+} , which has a large, effective nuclear charge, with soft (polarizable) ligands, such as nitrogen-containing (e.g. amino acids), sulphur-containing (e.g. sulphahydryl) minor binding sites. Since increasing ionic potential results in greater electrostatic interactions, and hence, greater electrostatic binding energy, the covalent character is expected to decrease with increasing ionic potential of the metal cation. This was observed by Fasfous et al. [178] for Zn(II), Cd(II), and Pb(II) complexes in FA. The exception to the trend is Cu(II), which has shortened (and strengthened) equatorial bonds and lengthened (and weakened) axial bonds in octahedrally coordinated aqua complex, $[\text{Cu}(\text{H}_2\text{O})_6]^{2+}$, as a result of the Ligand Field Stabilization Energy (LFSE) combined with the Jahn-Teller effect [147]. This exceptional behaviour of copper was also experimentally observed by Sekaly et al. [157], who studied the Cu(II)-complex dissociation kinetics using Cu^{2+} aqua complex, $[\text{Cu}(\text{H}_2\text{O})_6]^{2+}$, and was also observed by Achterberg et al. [174], who studied dissolved copper species in freshwaters, employing adsorptive cathodic stripping voltammetry and radiotracers, and also by Town and Filella [87], who studied the speciation of Cu (II)- and Pb(II)- fulvic acid complexes using pseudopolarography.

10.3.3 *Differential Kinetic Function (DKF)*

The Differential Kinetic Functions of Mn(II), Co(II), Ni(II), Cu(II), Cd(II) and Pb(II) in model systems of Laurentian fulvic acid (LFA) containing equimolar concentrations of

all of the above metals were determined as shown Table 38. Because equation (2.27) is strictly defined for the Differential Kinetic Parameter, k_d^* , Table 38 was prepared by replacing k_d^* with the weighted average dissociation rate coefficient, \bar{k}_d , by analogy with equations (2.26) and (2.27). The DEF is described by equation (10.1).

$$\log \theta = \Gamma \log K_o^* - \Gamma \log k_a + \Gamma \log \bar{k}_d \quad (10.1)$$

where,

$$\bar{k}_d = \frac{\sum_i k_{d,i} c_{ML_i}}{\sum_i c_{ML_i}} = \frac{\sum_i k_{d,i} c_{ML_i}}{\bar{K}_{CM} \sum_i c_{L_i}} \quad (10.2)$$

Table 38 shows that Γ was about the same ($\Gamma \sim 0.8$ to 1.0) for Mn(II), Co(II), Pb(II) and Cd(II), indicating that these systems were homogenous; whereas Ni(II) and Cu(II) systems were heterogeneous. The results are in reasonably good agreement with those obtained by pseudopolarography ($\Gamma_{Pb} = 0.95$ and $\Gamma_{Cu} = 0.20$), suggesting that the Differential Kinetic Function and the Differential Equilibrium Function are independent of the analytical technique used to measure them. The slightly lower values of Γ obtained for the Differential Equilibrium Function by Anodic Stripping Voltammetry was probably due to a loss in lability, as discussed in chapter 9.

10.3.4 Linear Free Energy Relationship

Kinetic data on metal-complex dissociation reactions in natural systems are scarce, which has hampered research in aquatic chemical kinetics. Despite the absence of any universal relationship between the thermodynamics and kinetics of reactions, Linear Free Energy

Table 38 Differential Kinetic Functions for M(II)-FA complexes in model solutions of Laurentian fulvic acid. $c_M 7.0 \times 10^{-7}$ M. HOAc/NaOAc buffer, pH 5.0 ± 1.0 , ionic strength = 0.05 M, temperature = 23 ± 2 °C.

Metal	Γ	$\log \theta = \Gamma \log K_o^* - \Gamma \log k_a + \Gamma \log k_d^*$	R^2
Mn	0.82	$\text{Log } \theta = -1.50 + 0.82 \log k_d^*$	0.951
Co	0.84	$\text{Log } \theta = -2.07 + 0.84 \log k_d^*$	0.913
Ni	0.27	$\text{Log } \theta = -4.20 + 0.27 \log k_d^*$	0.971
Cu	0.16	$\text{Log } \theta = -4.53 + 0.16 \log k_d^*$	0.992
Cd	0.92	$\text{Log } \theta = -1.60 + 0.92 \log k_d^*$	0.988
Pb	1.00	$\text{Log } \theta = -1.46 + 1.01 \log k_d^*$	0.994

Relationships (LFERs) between the energetics and rates of reactions for many sets of related compounds have been empirically established [244]. Although they began as empirical relationships, most have an underlying theoretical basis. Linear relationship between rate coefficient k_i and equilibrium constant, K_i can be expressed [247] as

$$\ln k_i = \alpha \ln K_i + C \quad (10.3)$$

where α (its value between 0 and 1) and C are constants. The LFER correlation is often used to predict either kinetic or thermodynamic parameters by interpolations [247].

For reactions based on the disjunctive pathway, Hammond's postulate [166] suggests that the LFER between the standard Gibbs free energy change (ΔG°) and the free energy of activation (ΔG^\ddagger) results from a transition state and an intermediate near on the energy surface having similar energies. Hence, a simple inverse relationship between $\log k_d$ and $\log K$ is expected for a series of complexes of a particular metal. Here it is important to consider the contributions of both enthalpy and entropy to stability constants and rate coefficients, as shown in equations (5.5) and (5.6).

It should be mentioned that K determined by pseudopolarography is for formation reaction of metal complexes (ML_i), whereas k_d determined by CELM/ICP-MS is for dissociation of metal complexes. So to be able to correlate them, they have to be described in either dissociation or formation reaction. For dissociation reaction of metal complex, the instability constant is the inverse of the stability constant for formation reaction of metal complex.

Figures 85-86 show a straight-line relationship between $\log k_d$ and $-\log K_0^*$, indicating a LFER between ΔG^\ddagger and ΔG° , which suggests that the ML_i and its transition state have similar geometry.

10.4 Conclusion

The advantage of LFERs is that kinetic parameters, which tend to be difficult to determine, can be estimated from thermodynamic parameters, for which the tabulated values are often available.

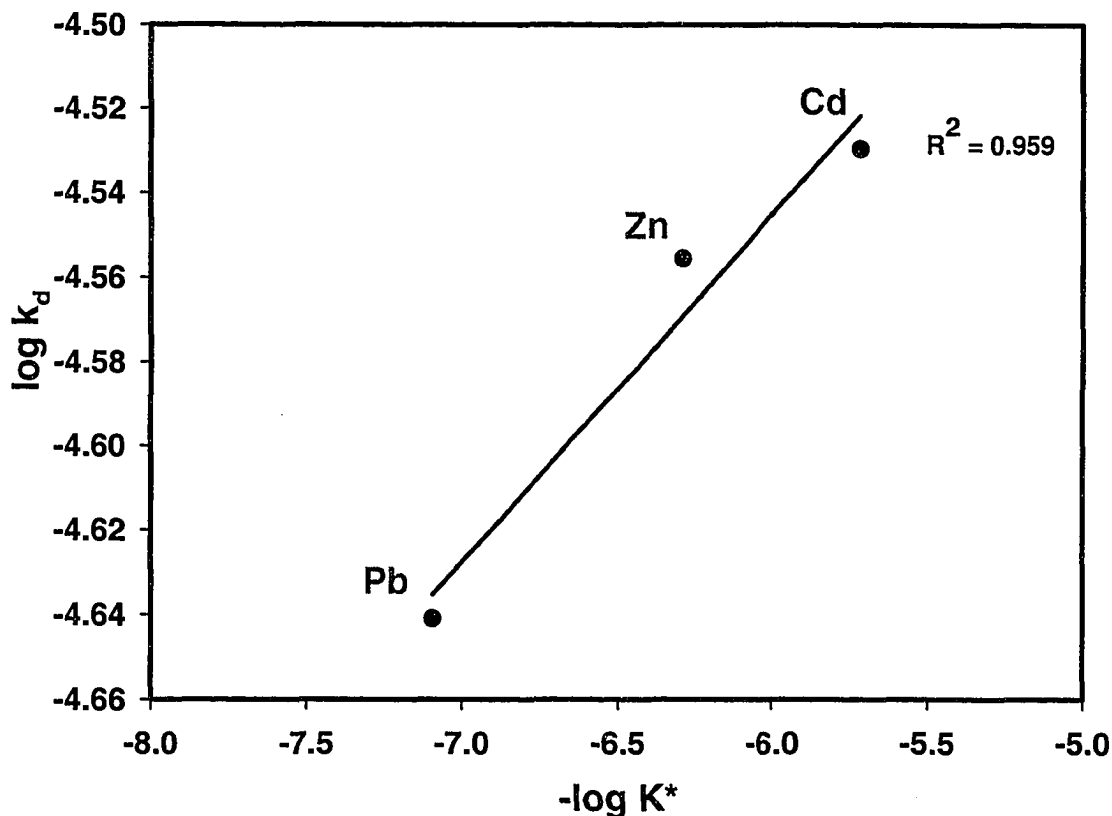


Figure 85 Linear free energy relationship between the dissociation rate coefficient (k_d) of Zn(II), Cd(II), and Pb(II) complexes with Laurentian fulvic acid and Differential Equilibrium Parameter (K^*). $c_M / c_{FA} = 5.6 \times 10^{-3}$. HOAc/NaOAc buffer, pH 5.0 ± 1.0 , ionic strength = 0.05 M, temperature = 23 ± 2 °C.

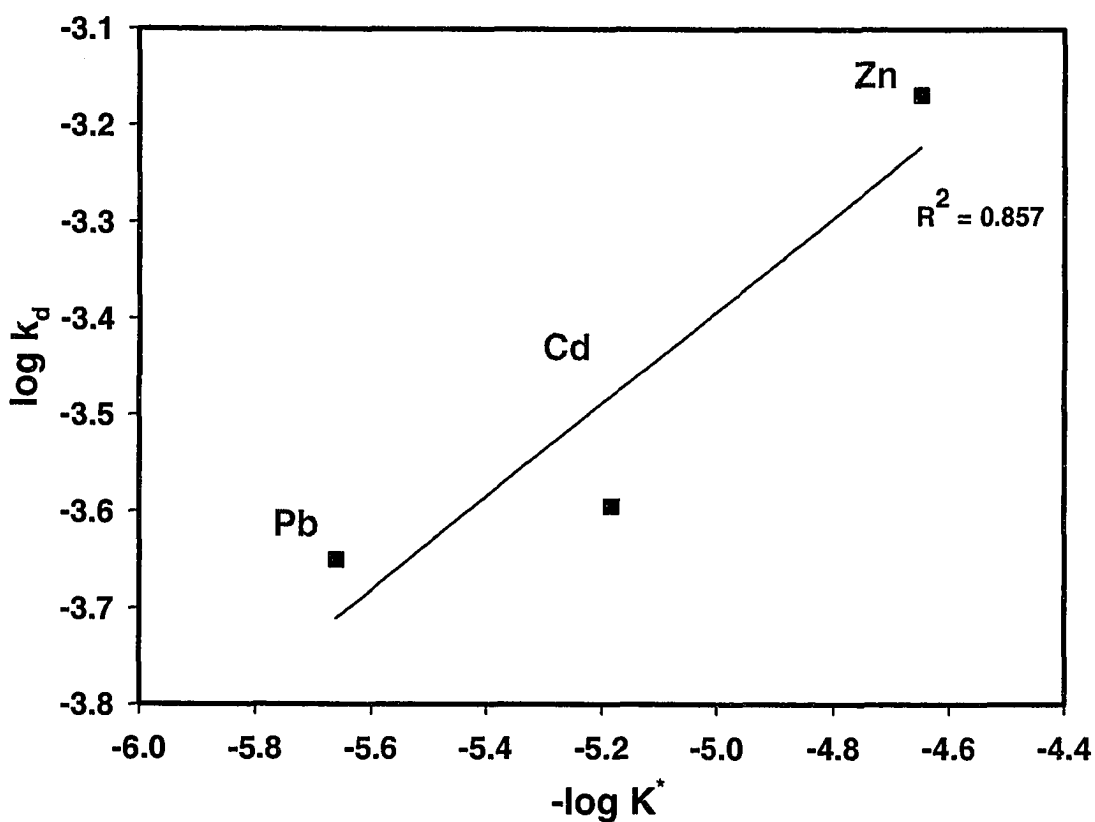


Figure 86 Linear free energy relationship between the dissociation rate coefficient (k_d) of Zn(II), Cd(II), and Pb(II) complexes with Laurentian fulvic acid and Differential Equilibrium Parameter (K^*). $c_M / c_{FA} = 5.6 \times 10^{-2}$. pH 5.0 ± 0.1 , ionic strength 0.05 mol/L, temperature 23 ± 2 °C.

References

1. D.M. Templeton, F. Ariese, R. Cornelis, L-G. Danielelsson, H. Munta, H. Van Leeuwen and L. Lobinski, *Pure Appl Chem.*, **2000**, 72, 1453.
2. J. Buffle, *Complexation Reactions in Aquatic Systems: An Analytical Approach*, Ellis Horwood Limited, Chichester, UK, **1990**, pp. 2-15, 37.
3. W. Stumm and J.J. Morgan, *Aquatic Chemistry: Chemical Equilibria and Rates in Natural Waters*, 3rd Ed., John Wiley and Sons, Inc., New York, USA, **1996**, pp. 257, 284, 301, 614-616, 625-628, 632-635, 668.
4. A. Caroline and R. Stone, *Science.*, **2003**, 300, 925.
5. P.G.C. Campbell, *Metal Speciation and bioavailabilty of aquatic systems.*, John Wiley & Sons Ltd, Chichester, England, **1995**, 45-102.
6. K. Hughes, M.E. Meek, R. Newhook and P.K.L. Chan, *Regulatory Toxicology and Pharmacology.*, **1995**, 22, 213.
7. R. Mandal, *Competitive Binding of Metal Ions By Humic Substances in Model Systems and in Freshwaters*, Ph.D. Thesis, Carleton University, Ottawa, Canada, **2001**, pp. 1-2, 97,
8. E. Tipping, *Cation Binding by Humic Substances.*, 1st Ed, Cambridge University Press, Cambridge, UK, **2002**, pp. 28, 324-325.
9. J.G. Hering and F.M.M. Morel, *Environ. Sci. Technol.*, **1988**, 22, 1234.
10. J. Buffle, R.S. Altmann and M. Filella, *Anal. Chim. Acta.*, **1990**, 232, 225.
11. F.M.M. Morel and J.G. Hering, *Principles and Applications of Aquatic Chemistry*, John Wiley and Sons, New York, USA, **1993**, Chapter 6, 322.

12. R. Mandal, M.S.A. Salam, J. Murimboh, N.M. Hassan, C.L. Chakrabarti, M.H. Back and D.C. Grégoire, *Environ. Sci. Technol.*, **2000**, 34, 2201.
13. H.B. Xue, D. Kistler and L. Sigg, *Limnol. Oceanogr.*, **1995**, 40, 1142.
14. R. Mandal, A.L.R. Sekaly, J. Murimboh, N.M. Hassan, C.L. Chakrabarti, M.H. Back, D.C. Grégoire and W.H. Schroeder, *Anal. Chim. Acta.*, **1999**, 395, 323.
15. M.M. Nederlof, W.H. van Riemsdijk and L.K. Koopal, *Environ. Sci. Technol.*, **1994**, 28, 1048.
16. J. Buffle and M. Filella, *Anal. Chim. Acta*, **1995**, 313, 144.
17. M. Schnitzer, *Soil Sci Soc. Am. Proc.*, **1969**, 33, 75.
18. D.S. Gamble, M. Schnitzer and I. Hoffman, *Can. J. Chem.*, **1970**, 48, 3197.
19. F.J. Stevenson, "Binding of Metal Ions by Humic Substances", in *Environmental Biogeochemistry.*, Ed. J.O. Nriagu, Ann Arbor, MI: Ann Arbor Science, **1976**, Vol. 2, pp. 519-540.
20. Y. Chen and F.J. Stevenson, "Soil Organic Matter Interactions with Trace Elements", in *Role of Organic Matter in Modern Agriculture*, Eds. Y. Chen and Y. Avnimelech, Dordrecht: Nijhoff, **1986**, pp. 73-116.
21. Johannes, M.C. De Wit, W.H. Van Riemsdijk, N.M. Nederlof, D.G. Kinniburgh and L.K. Koopal, *Anal. Chim. Acta.*, **1990**, 232, 189.
22. J.A. Marinsky, in *Aquatic Surface Chemistry: Chemical Processes at the Particle-Water Interface.*, W. Stumm (Ed.), Wiley Interscience, New York, USA, **1987**, Chapter 3.
23. E. Tipping, C.A. Bakes and M.A. Hurley, *Wat. Res.*, **1988**, 22, 597.

24. B.M. Bartschat, S.E. Cabaniss and F.M.M. Morel, *Environ. Sci. Technol.*, **1992**, 26, 284.
25. S.A. Green, F.M.M. Morel and N.V. Blough, *Environ. Sci. Technol.* **1992**, 26, 294.
26. F. Helfferich, *Ion Exchange*, McGraw-Hill, New York, **1962**.
27. C.H. Langford and D.W. Gutzman, *Anal. Chim. Acta.*, **1992**, 256, 183.
28. C.H. Langford and R.L. Cook, *Analyst.*, **1995**, 120, 591.
29. G.D. Templeton III, and N.D. Chasteen, *Geochim. Cosmochim. Acta.*, **1980**, 44, 741.
30. E. Tipping and D. Cooke, *Geochim. Cosmochim. Acta.*, **1982**, 46, 75.
31. O. C. Zafiriou, J. Jousset-Dubien, R. G. Zepp and R. G. Zika. *Environ. Sci. Technol.*, **1984**, 18, 358A.
32. C. E. Williamson, D. P. Morris, L. Pace and O. G. Olson., *Limnol. Oceanogr.*, **1999**, 44, 795-803.
33. R. G. Zika, Marine organic photochemistry. In: Duursma, E. and R. Dawson (eds.). *Marine organic chemistry: Evolution, composition, interactions, and chemistry of organic matter in seawater*. Elsevier Sci. Publ. **1981**. Vol. 31, pp. 299-325.
34. K. B. Beauclerc and J. M. Gunn. *J. Environ. Monitor.* 3(6): 575.
35. S. Bertilsson and L. J. Tranvik, *Limnol. Oceanogr.*, **1998**, 43, 885.
36. M. A Moran and R. G. Zepp, *Limnol. Oceanogr.*, **1997**, 42, 1307.
37. D. Lean, *Aquatic Humic Substances—Ecology and Biogeochemistry*, Springer, Berlin, **1998**, pp.109-124.
38. F. H Frimmel, *Impact of light on the properties of aquatic natural organic matter*. *Environ. Int.* **1998**, 24, 559-571.

39. M. A. Moran, W. M. Sheldon, Jr. and R. G. Zepp. *Limnol. Oceanogr.*, 45(6), 2000, 1254.
40. W. L. Miller and R. G. Zepp. *Geophys. Res. Lett.*, 1995, 22(4), 417.
41. Gao, Huizhen and R. G. Zepp. *Environ. Sci. Technol.*, 1998, 32(19), 2940.
42. K. Salonen and A. Vähätalo, *Environ. Int.*, 1994, 20, 373.
43. W. Granéli, M. Lindell and L. Tranvi, *Limnol. Oceanogr.*, 1996, 41, 698.
44. R. M. W. Amon and R. Benner, *Geochim. Cosmochim. Acta.*, 1996, 60, 1783.
45. Vodacek, A., N. A. Bough, M. D. DeGrandpre, E. T. Peltzer and R. K. Nelson, *Limnol. Oceanogr.*, 1997, 43, 674-686.
46. N. D. Yan, W. Keller, N. M. Scully, D. R. S. Lean and P. J. Dillon, *Nature*, 1996, 381(6578): 141-143.
47. H. Xue and L. Sigg, *Limnol. Oceanogr.*, 1993, 38(6), 1200.
48. H. Xue and L. Sigg, in *Environmental Electrochemistry: Analyses of Trace Element Biogeochemistry*, M. Tallefert and T.F. Rozan (Eds.), ACS Symposium Series 811, American Chemical Society, Washington, DC, USA, 2002, Chapter 18.
49. K.W. Bruland, E.L. Rue, J.R. Donat, S.A. Skrabal and J.W. Moffett, *Anal. Chim. Acta.*, 2000, 405, 99.
50. J.R. Donat, K.A. Lao and K.W. Bruland, *Anal. Chim. Acta.*, 1994, 284, 547.
51. H. Xue and W.G. Sunda, *Environ. Sci. Technol.*, 1997, 31, 1902.
52. T.M. Florence. *Analyst.*, 1986, 111, 489.
53. M.S. Shuman and L.C. Michael, *Environ. Sci. Technol.*, 1978, 12, 1069.
54. P.M.V. Nirel and F.M.M. Morel., *Wat Res.*, 1990, 24 (8), 1055.

55. J. Buffle, *Complexation Reactions in Aquatic Systems: An Analytical Approach*, Ellis Horwood Limited, Chichester, UK, **1990**, pp. 3-6, 77, 81-89.
56. F. M. M. Morel and J. G. Hering, *Principles and Applications of Aquatic Chemistry*, John Wiley: New York, USA, **1993**, pp. 319-420.
57. D.R. Turner, in *Metal Speciation and Bioavailability in Aquatic Systems*, A. Tessier and D.R. Turner (Eds.), IUPAC series on Analytical and Physical Chemistry of Environmental Systems, John Wiley and Sons, Inc., Chichester, UK, **1995**, pp. 150-154.
58. D.M. Anderson and F.M.M. Morel, *Limnol. Oceanogr.*, **1978**, 23, 283.
59. M.A. Anderson and F.M.M. Morel, *Limnol. Oceanogr.*, **1982**, 27, 789.
60. W.G. Sunda and R.R. Guillard, *J. Mar. Res.*, **1976**, 34, 511.
61. J.G. Hering and F.M.M. Morel, in W. Stumm, *Aquatic Chemical Kinetics*, John Wiley & Sons, Inc., New York, **1990**, pp. 145-171.
62. S.E. Cabaniss, *Environ. Sci. Technol.*, **1990**, 24, 583.
63. J. Buffle, *Complexation Reactions in Aquatic Systems: An Analytical Approach*, Chichester: Ellis Horwood, **1990**, p. 81.
64. M.R. Hoffmann, *Environ. Sci. Technol.*, **1981**, 15, 345.
65. C.H. Langford and T.R. Khan, *Can. J. Chem.*, **1975**, 53, 2979.
66. L.E. Sojo and H. de Haan, *Environ. Sci. Technol.*, **1991**, 25, 935.
67. J.A. Lavigne, C.H. Langford and M.K.S. Mak, *Anal. Chem.*, **1987**, 59, 2616.
68. B.J. Plankey and H.H. Patterson, *Environ. Sci. Technol.*, **1987**, 21, 595.
69. A.W. Rate, R.G. McLaren and R.S. Swift, *Environ. Sci. Technol.*, **1992**, 26, 2477.
70. D.L. Olson and M.S. Shuman, *Anal. Chem.*, **1983**, 55, 1103.

71. A.W. Rate, R.G. McLaren and R.S. Swift, *Environ. Sci. Technol.*, **1993**, 27, 1408.
72. J.G. Hering and F.M.M. Morel, *Environ. Sci. Technol.*, **1990**, 24, 242.
73. N.M. Hassan, *Metal Speciation Dynamics in Freshwaters: A Kinetic Exploration*, Ph.D. Thesis, Carleton University, Ottawa, Canada, **2003**, pp. 10-31, 63-95, 195,
74. F.M.M. Morel and J.G. Hering, *Principles and Applications of Aquatic Chemistry*, John Wiley & Sons, Inc., New York, USA, **1993**, pp. 319-320, 400-401.
75. M. Eigen and R.G. Wilkins, in *Mechanisms of Inorganic Reactions*, ACS Symposium Series No. 49, American Chemical Society, Washington, DC, USA, **1965**, 55-80.
76. D.W. Margerum, G.R. Cayley, D.C. Weatherburn and G.K. Pagenkopf, in *Coordination Chemistry*, Vol 2, A.E. Martell, Ed., ACS Monograph 174, Washington, DC, USA, **1978**, pp. 1-220.
77. J. Wang, *Stripping Analysis: Principles, Instrumentation, and Applications*, VCH Publishers, Inc., Deerfield Beach, Florida, USA, **1985**, pp. 1-34, 65-66, 81-82, 116-125.
78. H.P. van Leeuwen, in *In Situ Monitoring of Aquatic Systems: Chemical Analysis and Speciation*, J. Buffle and G. Horvai (Eds.), John Wiley and sons Ltd., New York, USA, **2000**, Chapter 8.
79. H.P. van Leeuwen and J. Pinheiro, *J. Electroanal. Chem.*, **1999**, 471, 55.
80. H.G. De Jong and H.P van Leeuwen, *J. Electroanal. Chem.*, **1987**, 234, 1.
81. H.G. De Jong and H.P van Leeuwen, *J. Electroanal. Chem.*, **1987**, 234, 17.
82. J. D. Murimboh, *Speciation Dynamics in the freshwater Environment: Unifying Concepts in Metal Speciation Bioavailability*, Ph.D. Thesis, Carleton University, Ottawa, Canada, **2001**, pp. 11-18.

83. R.S. Altmann and J. Buffle, *Geochim. Cosmochim. Acta.*, **1988**, 52, 1505.
84. M. Filella, J. Buffle and H.P. van Leeuwen, *Anal. Chim. Acta.*, **1990**, 232, 209.
85. D.S. Gamble, *Can. J. Chem.*, **1970**, 48, 2662.
86. D.S. Gamble and C.H. Langford, *Environ. Sci. Technol.*, **1988**, 22, 1325.
87. R.M. Town and M. Filella, *J. Electroanal. Chem.*, **2000**, 488, 1.
88. F.M.M. Morel, *Principles of Aquatic Chemistry*, John Wiley and Sons, Inc., New York, USA, **1983**, pp. 300-304.
89. P.G.C. Campbell, O. Errécalde, C. Fortin, V.P. Hiriart-Baer and B. Vigneault, *Comparative Biochemistry and Physiology.*, **2002**, Part C 133, 189.
90. J. Buffle and R.R. De Vitre, in *Chemical and Biological Regulation of Aquatic Systems*, CRC Press, Inc., Boca Raton, USA, **1994**, pp. 210-211.
91. J.R. Donat, K.A. Lao and K.W. Bruland, *Anal. Chim. Acta.*, **1984**, 284, 547.
92. B.L. Lewis, G.W. Luther III, H. Lane and T.M. Church, *Electroanalysis.*, **1995**, 7, 166.
93. J. Buffle and F.L. Greter, *J. Electroanal. Chem.*, **1979**, 101, 231.
94. M. Filella, R. Town and J. Buffle, in *Chemical Speciation in the Environment*, Eds. A.M. Ure and C.M. Davidson, Blackie Academic & Professional, London, **1995**, pp. 167-200.
95. H.P. van Leeuwen, *Journal of Radioanalytical and Nuclear Chemistry.*, **2000**, 246(3), 487.
96. D.W. Gutzman and C.H. Langford, *Environ. Sci. Technol.*, **1993**, 27, 1388.
97. J. G. Hering and F. M. M. Morel, *Environ. Sci. Technol.*, **1988**, 22, 1469.
98. F.M.M. Morel, *Principles of Aquatic Chemistry*, J. Wiley, New York, **1983**, p. 267.

99. D.M.J. Tubbing, W. Admiraal, R.F.M.J. Cleven, M. Iqbal, D. van de Meent and W. Verweij, *Water Res.*, **1994**, 28, 37.
100. R.J.M. Hudson, *Sci. Total Environ.*, **1998**, 219, 95.
101. H.P. van Leeuwen, *Environ. Sci. Technol.*, **1999**, 33, 3743.
102. J.G. Hering and F.M.M. Morel, *Geochim. Cosmochim. Acta.*, **1989**, 53, 611.
103. J. Labuda, M. Buckova and L. Halamova, *Electroanalysis.*, **1997**, 9, 1129.
104. R.A.G. Jansen, H.P. van Leeuwen, R.F.M.J. Cleven and M.A.G.T. van den Hoop, *Environ. Sci. Technol.*, **1998**, 32, 3882.
105. J. van Doornmalen, J.T. van Elteren and J.J.M. de Goeij, *Anal. Chem.*, **2000**, 72, 3043.
106. P. Figura and B. McDuffie, *Anal. Chem.*, **1979**, 51, 120.
107. P. Figura and B. McDuffie, *Anal. Chem.*, **1980**, 52, 1433.
108. M.L. Lann, C. Elleouet, F. Quenel, C.L. Madec, *Environ Chem Lett*, **2003**, 1, 98.
109. C.M.G Van Den Berg and M. Nimmo, *The Science of The Total Environment.*, **1987**, 60, 185.
110. Y. Lu, C.L. Chakrabarti, M.H. Back, A.L.R. Sekaly, D.C. Grégoire, W.H. Schroeder, *J. Anal. Atom. Spec.*, **1996**, 11, 1189.
111. Y. Lu, C.L. Chakrabarti, M.H. Back, D.C. Grégoire, W.H. Schroeder, *Int. J. Environ. Anal. Chem.*, **1995**, 60, 313.
112. A.L.R. Sekaly, C.L. Chakrabarti and D.C. Grégoire, In Proceedings of the Second Biennial International Conference on Chemical Measurement and Monitoring of the Environment, Ottawa, Canada; Clement, R.C.; Burk, B., Eds.; **1998**; pp. 611-618.

113. M.T. Lam, J. Murimboh and C.L. Chakrabarti, In Proceedings of the Second Biennial International Conference on Chemical Measurement and Monitoring of the Environment, Ottawa, Canada; Clement, R.C.; Burk, B., Eds.; **1998**; pp. 589-594.
114. D.L. Olson and M.S. Shuman, *Geochim. Cosmochim. Acta.*, **1985**, 49, 1371.
115. C.L. Chakrabarti, M.H. Back, D.C. Gregoire and W.H. Schroeder, *Anal. Chim. Acta.*, **1994**, 293, 95.
116. F. M. M. Morel and J. G. Hering, *Principles and Applications of Aquatic Chemistry*, John Wiley: New York, **1993**; pp. 323-325, 398-403, 405.
117. Z. Marina and C. Marine Res, *Electroanalysis.*, **1995**, 7(4), 350.
118. C.M.G van den Berg and J.R. Donat., *Anal. Chim. Acta.*, **1992**, 257, 281.
119. M.L.A.M. Campos and C.M.G van den Berg, *Anal. Chim. Acta.*, **1994**, 284, 481.
120. C. Colombo and C.M.G. van den Berg, *Anal Chim Acta.*, **1997**, 337, 29.
121. T. Fujinaga, K. Izutka, S. Ckazaki and H. Sawameto. *J. Electroanal. Chem.*, **1969**, 21, 187.
122. F. Garay, V. Solis and M. Lovric, *J. Electroanal. Chem.*, **1999**, 478, 17.
123. F. Garay and V. Solis , *J. Electroanal. Chem.*, **2001**, 505, 109.
124. K.A. Bolton, S. Sjöberg and L.J. Evans, *Soil Sci. Soc. Am. J.*, **1996**, 60, 1064.
125. J. W. Guthrie, *A Multi-Technique Approach For The Study Of Speciation Of Ni, Cd, Cu, Pb, And Zn In Freshwaters*, Ph.D. Thesis, Carleton University, Ottawa, Canada, **2004**, pp. 47, 72, 82.
126. J.R. Donat and C.M.G. van den Berg, *Mar. Chem.*, **1992**, 38, 69.
127. M.L.A.M. Campos and C.M.G. van den Berg, *Anal. Chim. Acta.*, **1994**, 284, 481.
128. C. Muller, J. Claret, J. Feliu and J. Virgili, *Collect. Czech. Chem.*, **1984**, 49, 481.

129. L. Jin and N.J. Gogan, *Anal. Chim. Acta.*, **2000**, 412, 77.
130. M. M Ortiz Viana, M. P. Da Silva, R. Agraz, J. R. Procopio and M. T. Sevilla., *Anal. Chim. Acta.*, **1999**, 382,179.
131. R. M. Town and M. Filella, *Limnol. Oceanogr.*, **2000**, 45, 1341.
132. Y. Cao, M. Conklin and E. Betterton, *Environ. Health Persp.*, **1995**, 103, 29.
133. S.E. Cabaniss and M.S. Shuman, *Geochim. Cosmochim. Acta.*, **1988**, 52 , 185.
134. W.G. Sunda and P.J. Hanson, in *Chemical Modelling in Aqueous Systems*, Eds. E.A. Jenne, ACS Symposium Series 93, American Chemical Society, Washington, D.C., **1979**, pp. 147-180.
135. J. Buffle, P. Deladoey, F.L. Greter and W. Haerdi, *Anal. Chim. Acta.*, **1980**, 16 255.
136. M.A.G.T. van den Hoop, H.P. van Leeuwen, J.P. Pinheiro, A.M. Mota and M.de L.S. Goncalves, *Colloids and Surfaces.*, **1995**, 95, 305.
137. A.S. Mathuthu and J.H. Ephraim, *Talanta.*, **1993**, 40, 521.
138. F.M.M. Morel and J.G. Hering, *Principles and Applications of Aquatic Chemistry*, John Wiley & Sons, New York, USA, **1993**, pp. 358-360, 378-391, 398, 400-403.
139. H.B. Xue, S. Jansen, A. Prasch and L. Sigg, *Environ. Sci. Technol.*, **2001**, 35, 539.
140. B. Pihlar, P. Valenta and H.W. Nürnberg, *J. Electroanal. Chem.*, **1986**, 214, 157.
141. F. Ma, D. Janger and L. Renman, *Anal. Chem.*, **1997**, 69, 1782.
142. C.M.G. van den Berg and M. Nimmo, *Sci. Total Environ.*, **1987**, 60, 185.
143. C.M.G. van den Berg, *Analyst.*, **1989**, 114, 1527.
144. E.P. Achterberg and C.M.G. van den Berg, *Deep-Sea Research.*, **1997**, 44, 693.
145. M.T. Lam, J. Murimboh, N.M. Hassan and C.L. Chakrabarti, *Anal. Chim. Acta.*, **1999**, 402, 195.

146. R. Mandal, N.M. Hassan, J. Murimboh, C.L. Chakrabarti, M.H. Back, U. Rahayum and D.R.S. Lean, *Environ. Sci. Technol.*, **2002**, 36, 1477.9
147. B. Douglas, D. McDaniel and J. Alexandar, *Concepts and Models of Inorganic Chemistry*, 3rd Ed., John Wiley & Sons, Inc., New York, **1994**, pp. 751-752.
148. F.A. Cotton and G. Wilkinson, *Advanced Inorganic Chemistry*, 4th Ed., John Wiley & Sons, Inc., New York, **1980**, p. 790.
149. R. Kalvoda and M. Kopanica, *Pure App. Chem.*, **1989**, 61, 97.
150. B. Cosovic, in *Aquatic Chemical Kinetics: Reaction Rates of Processes in Natural Waters*, W. Stumm (Ed.), John Wiley & Sons, New York, **1990**, p. 294.
151. V. Celo, J. Murimboh, M.S.A. Salam and C.L. Chakrabarti, *Environ. Sci. Technol.*, **2001**, 35, 1084.
152. C.M.G. van den Berg, *Anal. Chim. Acta.*, **1991**, 250, 265.
153. M.M.G.S. Rocha, M.M.P.M. Neto, M.O. Torres and A. de Varennes, *Electroanalysis*, **1997**, 9, No.2, 145.
154. A.L.R. Sekaly, M.H. Back, C.L. Chakrabarti, D.C. Grégoire, J.Y. Lu and W.H. Schroeder, *Spectrochim. Acta.*, **1998**, 53B, 837.
155. A.L.R. Sekaly, M.H. Back, C.L. Chakrabarti, D.C. Grégoire, J.Y. Lu and W.H. Schroeder, *Spectrochim. Acta.*, **1998**, 53B, 847.
156. S. Jansen, R. Blust, H. P. van Leeuwen, *Environ. Sci. Technol.*, **2002**, 36, 2164.
157. A. L. R. Sekaly, R. Mandal, N. M. Hassan, C. L. Chakrabarti, M. H. Back, D. C. Grégoire and W. H. Schroeder, *Anal. Chim. Acta.*, **1999**, 402, 211.
158. F.M.M. Morel and J.G. Hering, *Principles and Applications of Aquatic Chemistry*, John Wiley: New York, USA, **1993**, pp. 398-403.

159. D. M. Gakamsky, A. A. Goldin, E. P. Petrov and A. N. Rubinov, *Biophys. Chem.*, **1992**, *44*, 47.
160. N. M. Price, G. I. Harrison, J. G. Hering, R. J. Hudson, P. M. V. Nirel, B. Palenik and F. M. M. Morel, *Biol. Oceanogr.*, **1988/1989**, *6*, 443.
161. Chelex 100 and Chelex 20 Chelating Ion Exchange Resin Instruction Manual. Bio-Rad: Hercules, CA; p. 13.
162. Tramonti, V. M.Sc. Thesis, Concordia University: Montréal, Canada, **1988**.
163. H. P. Van Leeuwen, *Electroanalysis.*, **2001**, *13*, 826.
164. J. Buffle, R. S. Altmann, M. Filella and A. Tessier, *Geochim. Cosmochim. Acta.*, **1990**, *54*, 1535.
165. P. L. Brezonik, In *Aquatic Chemical Kinetics, Reaction Rates of Processes in Natural Waters*; Stumm, W. (Ed.); John Wiley: New York, **1990**; pp. 113-143.
166. G. S. Hammond, *J. Am. Chem. Soc.*, **1955**, *77*, 334. *54*, 1535.
167. G. Mattock, *Acta Chim. Scand.*, **1954**, *8*, 777.
168. D. S. Gamble, A. W. Underdown, and C. H. Langford, *Anal. Chem.* **1980**, *52*, 1901.
169. J. Buffle, *Complexation Reactions in Aquatic Systems: an Analytical Approach*, Horwood, Chichester, UK, **1988**; pp. 195-200.
170. C. H. Langford, D. S. Gamble, A. W. Underdown and S. Lee, In *Aquatic and Terrestrial Humic Substances*, Christman, R. F.; Giessing, E. T. (Eds.); Ann Arbor Science: Ann Arbor, MI, **1983**; Ch 4.
171. I. S. Butler and J. F. Harrod, *Inorganic Chemistry Principles and Applications*; Benjamin/Cummings: Redwood City, **1989**; p. 422.

172. R. J. C. Rossotti, In *Modern Coordination Chemistry*, Lewis, J.; Wilkins, R. G. (Eds.); Interscience: New York, **1960**; pp. 1-77.
173. A. L. R. Sekaly, J. Murimboh, N. M. Hassan, R. Mandal, M. E. Ben Younes, C. L. Chakrabarti, M. H. Back, and D. C. Grégoire, *Environ. Sci. Technol.*, **2003**, *37*, 68.
174. Achterberg, E. P.; van Elteren, J. T.; Kolar, Z. I. *Environ. Sci. Technol.* **2002**, *36*, 914.
175. K. Deczky, and C. H. Langford, *Can. J. Chem.*, **1978**, *56*, 1947.
176. G. R. Aiken, D.M. McKnight, R. L. Wershaw and P. MacCathy (eds.), *Humic substances in soil, sediment and water*. **1985**, Wiley, New York, USA.
177. W.J. Cooper, Sunlight-induced photochemistry of humic substances in natural waters: Major reactive species. In: Suffet, I. H. and P. MacCarthy (eds.). *Aquatic Humic Substances: Influence on Fate and Treatment of Pollutants*. Advances in Chemistry Series, **1989**, 219. American Chemical Society: Washington, DC, USA. pp. 333-362.
178. I. I. Fasfous, T. Yapici, C. L. Chakrabarti, N. M. Hassan, M. H. Back, J. Murimboh, D. R. S. Lean and D. C. Grégoire. *Environ. Sci. Technol.*, **2004**, *38*, 4979-4986.
179. H. De Haan, *Limnol. Oceanogr.*, **1993**, *38*: 1072-1076.
180. R. G. Wetzel, P. G. Hatcher and T. Bianchi. *Limnol. Oceanogr.*, **1995**, *40*, 1369.
181. R. J. Kieber, X. Zhou and K. Mopper. *Limnol. Oceanogr.*, **1990**, *35*(7), 1503.
182. W. Stumm and J.J. Morgan, *Aquatic Chemistry Chemical*, John Wiley: New York, USA, **1996**, pp. 726-737.
183. F.M.M. Morel and J.G. Hering, *Principles and Applications of Aquatic Chemistry*, John Wiley: New York, USA, **1993**, pp. 482-491.
184. F.M.M. Morel and J.G. Hering, *Principles and Applications of Aquatic Chemistry*, John Wiley: New York, USA, **1993**, pp. 370.

185. J. Murimboh, N.M. Hassan, I.I. Fasfous, T. Yapici, L. Si., C.L. Chakrabarti, D.R.S. Lean. IUPAC Congress and 86th Canadian Society for Chemistry Conference and Exhibition, Ottawa, Ontario, August 10-15, **2003**.
186. N.M. Hassan, *Metal Speciation Dynamics in Freshwaters: A Kinetic Exploration*, Ph.D. Thesis, Carleton University, Ottawa, Canada, **2003**, pp. 195-215.
187. B. Nowack, H.B. Xue and L. Sigg, *Environ. Sci. Technol.*, **1997**, 31, 866.
188. J.M. Wood, in *Metal Ions in Biological Systems*, Vol. 18. H. Sigel (Ed.), Dekker, New York, USA, **1984**, Chapter 7.
189. J.W. Guthrie, N.M. Hassan, M.S.A, M. Salam, I. I. Fasfous, C. A. Murimboh, J.; Murimboh. C.L. Chakrabarti, D.C. Gregior, *Analytica Chimica Acta.*; **2005**, 528 (2), 205-218.
190. S.V. Mattigod and G. Sposito, in E.A. Jenne (Ed), *Chemical Modeling in Aqueous Systems*, ACS Symp. **1979**, 837, 856.
191. J.A. Allison and E.M. Perdue, in N. Senesi, T.M. Miano (Eds.) *Humic Substances in the Global Environment and Implication on Human Health*. Elsevier Science, Amsterdam, **1994**, 927-942.
192. E. Tipping, *Comp. Geosci.*, **1994**, 20, 973.
193. E. Tipping, *Aquatic Geochem.*, **1998**, 4, 3.
194. E. Tipping, *Colloids Surf. A.*, **1993**, 73, 117.
195. E. Tipping and M.A. Hurley, *Geochim. Chosmochim. Acta.*, 1992, 56, 3627.
196. M.F. Benedetti, W.H. van Riemsdijk, L.K. Koopal, D.G. Kinneburgh, D.C. Goody, and C.J. Milne, *Geochim. Cosmochim. Acta.*, **1996**, 60, 448.

197. Sillen, Lars Gunnar. Stability constants of metal-ion complexes. Supplement No. 1. The Chemical Society Burlington House, London, W1V 0BN, pp 720.
198. J.C. Brodeur, G. Sherwood, J.B. Rasmussen, and A. Hontela, *Can. J. Fish. Aquat. Sci.*, **1997**, 54, 2752
199. J. W. Guthrie, *A Multi-Technique Approach For The Study Of Speciation Of Ni, Cd, Cu, Pb, And Zn In Freshwaters*, Ph.D. Thesis, Carleton University, Ottawa, Canada, **2004**, pp. 48-51.
200. Y. Couillard, P.G.C. Campbell, and A. Tessier, *Limnol. Oceanogr.*, **1993**, 38, 299.
201. A. Tessier, Y. Couillard, P.G.C. Campbell, and J.C. Auclair, *Limnol. Oceanogr.*, **1993**, 38, 1.
202. C.L. Chakraborti, Y. Lu, J. Cheng, M.H. Back and W.H. Schroeder, *Anal. Chim. Acta*, **1993**, 267, 47.
203. D.W. Marquardt, *Journal of the Society for Industrial and Applied Mathematics*, **1963**, 11, 431.
204. N.M. Hassan, *Metal Speciation Dynamics in Freshwaters: A Kinetic Exploration*, Ph.D. Thesis, Carleton University, Ottawa, Canada, **2003**, pp. 108-120.
205. G.C. Dwane and E. Tipping, *Environ. Int.*, **1998**, 24, 609.
206. S.E. Bryan, E. Tipping, and J. Hamilton-Taylor, *Comp. Biochem. Physiol. C: Pharmacol. Toxicol.*, **2002**, 133, 37-49.
207. A.L. Nolan, M.J. McLaughlin, and S.D. Mason, *Environ. Sci. Technol.*, **2003**, 37, 90.
208. E. Tipping, S. Lofts and A.J. Lawlor, *Sci. Tot. Environ.*, **1998**, 210/211, 63.
209. S. Lofts and E. Tipping, *Sci. Tot. Environ.*, **2000**, 251/252, 381.

210. E. Tipping, C. Rey-Castro, S.E. Bryan, and J. Hamilton-Taylor, *Geochim. Cosmochim. Acta.*, **2002**, 66, 3211.
211. H. Xue, and L. Sigg, *Aquatic Geochem.*, **1999**, 5, 313.
212. A.L.R. Sekaly, *Trace Metal Binding to fulvic acids in model systems and freshwaters*, Ph.D. Thesis, Carleton University, Ottawa, Canada, **2000**, pp. 13.
213. W. Fish, D.A. Dzombak and F.M.M. Morel, *Environ. Sci. Technol.*, **1986**, 20, 669.
214. E.M. Perdue and C.R. Lytle, in *Aquatic and Terrestrial Humic Materials*; edited by R.F. Christman and E.T. Gjessing and Ann Arbor Science, Michigan, **1983**, pp. 295-313.
215. M.M. Nederlof, W.H. van Riemsdijk and L.K. Koopal, *Environ. Sci. Technol.*, **1992**, 26, 763.
216. M.M. Nederlof, W.H. van Riemsdijk and L.K. Koopal, *J. Colloid Interface Sci.*, **1990**, 135, 410.
217. M.M. Nederlof, W.H. van Riemsdijk and L.K. Koopal, in *Heavy Metals in the Environments.*, edited by J.P. Vernet, Elsevier, Amsterdam, **1991**, pp. 365-396.
218. B.J. Stanley, K. Topper and D.B. Marshall, *Anal. Chim. Acta.*, **1994**, 287, 25.
219. M.S. Shuman, B.J. Collins, P.J. Fitzgerald and D.L. Olson, in *Aquatic and Terrestrial Humic Materials*, edited by R.F. Christman and E.T. Gjessing, Ann Arbor Science, Ann Arbor, Michigan, **1983**, pp. 349-370.
220. Jean-Claude Brochon, Alastair K. Livesey, Jacques Pouget and Bernard Valeour, *Chemical Physics Letters.*, **1990**, 174, 517.
221. A.L.R. Sekaly, *Trace Metal Binding to fulvic acids in model systems and freshwaters*, Ph.D. Thesis, Carleton University, Ottawa, Canada, **2000**, pp. 31-45, 93-95.

222. M.J. McLaughlin, K.G. Tiller and M.K. Smart, *Aust. J. Soil Res.*, **1997**, 35, 183.
223. A.L.R. Sekaly, *Trace Metal Binding to fulvic acids in model systems and freshwaters*, Ph.D. Thesis, Carleton University, Ottawa, Canada, **2000**, pp. 9.
224. J. Buffle, K.J. Wilkinson, M.L. Tercier and N. Parthasarathy, *Annali di Chimica.*, **1997b**, 87, 67.
225. J. Buffle, M.L. Tercier, N. Parthasarathy and K.J. Wilkinson, *Chimia.*, **1997a**, 51, 690.
226. H.P. van Leeuwen and R.M. Town, *J. Electroanal. Chem.*, **2002**, 523, 16-25.
227. J. Heyrovsky and J. Kuta, *Principals of Polarography*, Academic, New York, **1966**.
228. M. Whitfield and D. Jagner (Eds.), *Marine Electrochemistry. A Practical Introduction*, Wiley, New York, **1981**.
229. J. Buffle, *Complexation Reactions in Aquatic Systems: an Analytical Approach.*, Horwood, Chichester, **1988**, p. 304-380.
230. W. Davidson and M. Whitfield, *J. Electroana., Chem.*, **1977**, 75, 763.
231. M.A.G.T. van den Hoop and H.P. van Leeuwen, *Anal. Chim. Acta.*, **1993**, 273, 275
232. S. Bubić and M. Branica, *Thalassia Jugosl.*, **1973**, 9, 47.
233. S. Komorsky-Lovrić, M. Lovrić and M. Branica, *J. Electroanal. Chem.*, **1986**, 214, 37.
234. B.L. Lewis, G.W. Luther III, H. Lane and T.M. Church, *Electroanalysis.*, **1995**, 7, 166.
235. A. Zirino and S.P. Kounaves, *Anal. Chem.*, **1977**, 49, 56.
236. M.S. Shuman and J.L. Cromer, *Anal. Chem.*, **1979**, 51, 1546.
237. D. DeFord and N. Hume, *J. Am. Chem. Soc.*, **1951**, 73, 5321.

238. D.R. Crow, *Polarography of Metal Complexes*, Academic Press, London, **1964**, pp. 1-18.
239. M. Filella and R.M. Town, *J. Electroanal. Chem.*, **2000**, 485, 21.
240. J. Buffle, *Complexation Reactions in Aquatic Systems: An Analytical Approach*, Ellis Horwood Limited, Chichester, UK, **1988**, pp. 118, 473, 541.
241. J.P. Pinheiro, A.M. Mota, and M.L. Simões Gonçalves, *Anal. Chim. Acta.*, **1994**, 284, 525.
242. M. Filella, H.P. van Leeuwen, J. Buffle and K. Holub, *J. Electroanal. Chem.*, **2000**, 485, 144.
243. M. Filella and R.M. Town, *Fresenius J. Anal. Chem.*, **2001**, 370, 413.
244. J. Buffle, *Complexation Reactions in Aquatic Systems: An Analytical Approach*, Ellis Horwood Limited, Chichester, UK, **1988**, p. 10.
245. J. Buffle, K. Wilkinson, S. Stoll, M. Filella and J. Zhang, *Env. Sci. Technol.*, **1998**, 32, 2887.
246. K.B. Oldham and J.C. Myland, *Fundamentals of Electrochemical Science*, Academic Press, Inc., San Diego, USA, **1994**, p. 233.
247. F. M. M. Morel and J. G. Hering. *Principles and Applications of Aquatic Chemistry*, John Wiley: New York, **1993**; pp. 79.

GLOSSARY

Symbol	Definition	Symbol	Definition
A	Freundlich constant	K	thermodynamic equilibrium constant (L mol ⁻¹)
A	Electrode surface area (m ²)	\bar{K}	mean equilibrium constant (L mol ⁻¹)
c	concentration (mol/L)	K*	differential equilibrium parameter (L mol ⁻¹)
c _L	concentration of ligand, L (mol/L)	K _o *	constant (= value of K* for θ = 1) (L mol ⁻¹)
c _{FA}	concentration of fulvic acid (mol/L)	k _a	association rate coefficient (L mol ⁻¹ s ⁻¹)
c _M	free metal ion concentration (mol/L)	k _a '	= k _a c _L (s ⁻¹)
c _{M,T}	total metal concentration (mol/L)	k _d	dissociation rate coefficient (s ⁻¹)
c _{ML}	concentration of complex ML (mol/L)	\bar{k}_d	mean dissociation rate coefficient (s ⁻¹)
c _{ML(t)}	concentration of complex ML at any time, t (mol/L)	k _w	rate coefficient for water exchange
c _{ML_i}	concentration of complex formed by site i (mol/L)	M	free metal ion (metal aqua complex)
c ^o _{ML_i}	concentration of complex ML _i at time zero (mol/L)	ML	metal complex formed by M with ligand, L
D	diffusion coefficient (m ² s ⁻¹)	ML _i	metal complex formed by M with site type i
\bar{D}	mean diffusion coefficient (m ² s ⁻¹)	t	time (s)
D _M	diffusion coefficient of free metal ion, M (m ² s ⁻¹)	T	temperature (K)
D _{ML}	diffusion coefficient of complex, ML (m ² s ⁻¹)	Γ	slope of the Differential Equilibrium Function and the Differential Kinetic Function (0 < Γ ≤ 1)
E	potential (V)	δ	thickness of the Nernstian diffusion layer
E _{1/2}	half-wave potential (V)	ε	= D _{ML} /D _M
i _{lim}	limiting current (A)	θ	Degree of site occupation of the ligands in a heterogeneous system (=c _{ML} /c _L)
i _p	peak current (A)	Λ	lability parameter
J	flux	Λ _{ss}	steady state lability parameter
J _{kin}	kinetically controlled flux	μ	Reaction layer thickness = (D _M /k _a ') ^{1/2}
J _{diff}	diffusion-controlled flux		